

## 4 Crystallographic basis of Polytypism and Twinning in Micas

**Massimo Nespolo**

*LCM3B, UMR, CNRS 7036  
Université Henri Poincaré Nancy 1, BP 239  
F54506 Vandoeuvre-les-Nancy cedex, France*

nespolo@lcm3b.uhp-nancy.fr

**Slavomil Ďurovič**

*Slovak Academy of Sciences  
Institute of Inorganic Chemistry; Department of Theoretical Chemistry  
Dúbravská cesta, 9; SK-842 36 Bratislava, Slovakia*

uachduro@savba.sk

### INTRODUCTION

Although the investigation of micas dates back to the pre-scientific era (see Cipriani, this volume), the idea of polytypism (originally not distinguished from “polymorphism”) in the micas did not ensue until 1934, when Pauling proposed it in a private conversation quoted by Hendricks and Jefferson (1939). The existence of several structural types was however known from goniometric measurements and morphological analysis performed in the 19<sup>th</sup> century (e.g., Marignac 1847; Baumhauer 1900) and collected in the 4<sup>th</sup> volume of the *Atlas der Krystallformen* (Goldschmidt 1918; for a comparative review and later measurements see Peacock and Ferguson 1943) and appears also in the different axial settings introduced to describe the unit cell of micas (e.g., Brooke and Miller 1852; Des Cloizeaux 1862; Koksharov 1875; Tschermak 1878).

The systematic investigation by X-ray diffraction (XRD) started with Mauguin (1927, 1928), who pointed out that the *c* axis of phlogopite was half that of muscovite. Pauling (1930) was the first to solve the structure of a mica, a fuchsite (now termed “chromian muscovite”, according to Rieder et al. 1998), by visual comparison of a subset of intensities from photographs, and introduced the first model of the structure of phyllosilicates on the basis of the coordination theory. Jackson and West (1931) were the first to perform a complete structure determination, investigating a muscovite- $2M_1$ . Hendricks and Jefferson (1939) investigated one hundred samples of micas and discovered several “polymorphs”, many of which were however twins of simpler structural types (shorter-period polytypes). The symmetry of the 2:1 mica layer was not fully recognized until Pabst (1955) showed that the correct space-group type of  $1M$  polytype was  $C2/m$  instead than  $Cm$ , as previously assumed by Hendricks and Jefferson (1939) and reported also by Peacock and Ferguson (1943). Since the accomplishment of such an apparently easy task as the determination of the structure of the single-layer polytype took so long time and so much effort, it is not surprising that the whole phenomenon of polytypism in micas occupied several researchers from different countries for a long run of time, and still keeps undisclosed some of its most interesting and challenging points.

Although the causes of the complexity of the phenomenon of polytypism in micas are multifaceted, they can be simplified to “magic words”, *local (partial) symmetry*, and a “magic number”, 3. As shown hereafter, each atomic plane in mica has an *ideal* symmetry of at least trigonal, which is preserved in each of the two kinds of sheets (tetrahedral and octahedral), but it is reduced to monoclinic when considering the layer as

a unit. The two  $T$  sheets of a layer are staggered along  $c$  and the amount of the stagger in the (001) projection is ideally  $|a|/3$ . For each non-orthogonal polytype an ideally orthogonal multiple cell can always be chosen, with 3-times the periodicity of the polytype in the stacking direction. In the *real* structure, some of the atoms move slightly from the positions corresponding to the ideal symmetry, but each atomic plane still preserves a trigonal *pseudo-symmetry*. Then, the (001) projection of the layer stagger deviates more or less from  $|a|/3$ , and the multiple cell is close to, but not exactly orthogonal. The magic words and magic number can be traced also in reciprocal space, where the reflections with  $k = 0(\text{mod } 3)$  reveal the symmetry principle on which a polytype is built, and the reflections with  $k \neq 0(\text{mod } 3)$  permit the identification of the stacking sequence.

The existence of a multiple cell with a metric pseudo-symmetry higher than the structural symmetry, together with the trigonal pseudo-symmetry of the planes of the basal oxygen atoms, is also the geometrical reason of the extensive occurrence of twinning in micas. Although polytypism and twinning can be reduced to relatively simple common geometrical bases, the development of general criteria to recognize the presence of twinning from the diffraction pattern took a long time, and still many questions remain open.

The purpose of this chapter is to give a general overview of the factors, in terms of lattice geometry and of symmetry, which are responsible for polytypism and twinning in micas, and to provide general and simple criteria to be applied in the experimental practice of polytype and twin identification. For this reason, micas are hereafter regarded as built by *layer archetypes*, i.e. idealized layers where most of the structural distortions are not taken into account. The true atomic structure of the mica layer influences mainly the intensities but not the geometry of the diffraction pattern, and is discussed in detail in Ferraris and Ivaldi (this volume) and in Brigatti and Guggenheim (this volume).

Rigorous mathematical demonstrations are not given here: readers wishing to acquire a deeper knowledge are invited to consult the original publications, quoted hereinafter, where those demonstrations are given in detail. The crystallographic terminology follows Wondratschek (2002).

## NOTATION AND DEFINITIONS

The geometrical description of mica polytypes is given in terms of the OD theory developed by Dornberger-Schiff (e.g., 1964) and her successors. OD stands for “Order-Disorder” and indicates that the stacking of layers may produce both periodic (“ordered”) and non-periodic (“disordered”) structures. It has no relation with the chemical order-disorder phenomena. The OD theory emphasizes particularly the role of polytypes which involve pairs, triples, quadruples etc. of geometrically equivalent layers, or, when this is not possible, the smallest number of kinds of triples, quadruples etc. of layers. These polytypes are termed *Maximum Degree of Order* (MDO) polytypes. The layer-group notation adopted here is the one developed by Dornberger-Schiff (1959), in which the direction of missing periodicity is indicated by parentheses. For example,  $C12/m(1)$  indicates a monoclinic holohedral  $C$ -centered layer, having  $(a,b)$  as the layer plane (for details see Merlino 1990).

The *indicative* symbols for polytypes were introduced by Ramsdell (1947) and are written as  $NS_n$ , where  $N$  is the number of layers,  $S$  indicates the symmetry and  $n$  is a sequence number, often (but not always) indicating the order in which polytypes have been discovered. Ramsdell’s symbolism is actually a mixed symbolism, since  $S$  (nowadays given with a single uppercase letter according to the IUCr *Ad-Hoc* committee

recommendations: Guinier et al. 1984) is used to indicate the six crystal families, the trigonal syngony (syngony = crystal system) and the rhombohedral Bravais system:  $A$  = anorthic (triclinic),  $M$  = monoclinic,  $O$  = orthorhombic,  $Q$  = quadratic (tetragonal),  $T$  = trigonal,  $R$  = rhombohedral,  $H$  = hexagonal,  $C$  = cubic. This mixed symbolism is nowadays preserved for historical reasons and its use is accepted only for indicating polytypes.  $Q$ ,  $R$  and  $C$  cannot appear in micas (Takeda 1971).

To classify, but also to identify experimentally, mica polytypes, the relations between a lattice and its derivative lattices (superlattices, sublattices) are of fundamental importance. Different authors have given contrasting definitions. Here, we adopt the definition in terms of the group-subgroup relations, in agreement with the *International Tables for Crystallography*, Vol. A, 5<sup>th</sup> ed., in press (Th. Hahn, pers. comm.). *Sublattice* is termed a derivative lattice obtained from an original lattice by taking a subgroup of translations: its unit cell is larger than that of the original lattice. In contrast, *superlattice* is termed a lattice obtained from an original lattice by taking a supergroup of translations: its unit cell is smaller than that of the original lattice. Because the derivative lattice obtained from the original one by taking a subgroup (supergroup) of translations has a larger (smaller) unit cell, in some publications the terms *superlattice* and *sublattice* are defined in the opposite way. The superlattice-sublattice character of a derivative lattice is inverted when going from one space to its dual (i.e. from direct to reciprocal, or vice versa).

The notations most often used in the following are summarized here for ease of consultation:

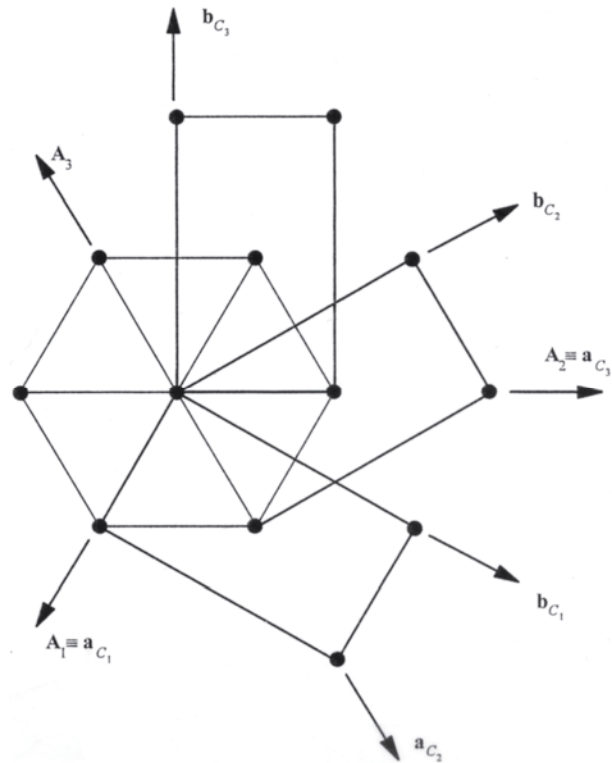
### The mica layer and its constituents

- $T$ : tetrahedral sheet =  $O_b$ -Z- $O_a$  or  $O_a$ -Z- $O_b$
- $O$ : octahedral sheet =  $O_a$ -Y- $O_a$
- $I$ : plane of the interlayer cations (also: these cations as such).
- $O_b$ : plane of the basal oxygen atoms of the tetrahedra
- $O_a$ : plane of the apical oxygen atoms of the tetrahedra; this plane, contains approximately also OH groups and, depending on the kind of mica, F and, less frequently, Cl and S.
- $T1, T2$ : the two translationally independent tetrahedral sites within a  $T$  sheet
- $M1, M2, M3$ : the three translationally independent octahedral sites within an  $O$  sheet
- $Ma, Me, Mi$ : average cations occupying the three translationally independent octahedral sites ( $Ma$  = Maximal;  $Me$  = Medium;  $Mi$  = Minimal, with reference to their scattering power)
- $\delta(Ma), \delta(Me), \delta(Mi)$ : X-ray scattering power of the (average) cations  $Ma, Me, Mi$
- $Z$ : plane of the tetrahedral cations
- $Y$ : plane of the octahedral cations (whose coordination polyhedra are however not regular octahedra but rather trigonal antiprisms).
- Tet: tetrahedral OD layer =  $O_{au}$ -Z- $O_b$ -I- $O_b$ -Z- $O_{al}$  ( $l$  = lower,  $u$  = upper; see text)
- Oc: octahedral OD layer =  $O_{al}$ -Y- $O_{au}$
- $p_{2j}$ : OD packet pointing up =  $Tet_{2j}/2 + Oc_{2j+1}/2$
- $q_{2j+1}$ : OD packet pointing down =  $Oc_{2j+1}/2 + Tet_{2j+2}/2$
- $M$ : the entire mica layer ( $T$ - $O$ - $T$ ). There are two types:  $M1$  and  $M2$  depending on the location ( $M1$  vs.  $M2/M3$ ) of the origin of the  $O$  sheet. Standard character “ $M$ ” indicates layer, italics “ $M$ ” indicates cation sites.

### Axial settings, indices and lattice parameters

- $a, b, c$ : monoclinic crystallographic axes in the space-fixed reference (in italics)  
 $a_{1\sim6}, b_{1\sim6}, c$ : monoclinic crystallographic axes in the crystal-fixed reference (in italics)  
 $A_1, A_2, A_3, c$ : hexagonal crystallographic axes (in italics)  
 $A_{F1}, A_{F2}, A_{F3}, C_F$ : hexagonal crystallographic axes of the family structure (in italics)  
 $\mathbf{a}, \mathbf{b}, \mathbf{c} / \mathbf{a}_{1\sim6}, \mathbf{b}_{1\sim6}, \mathbf{c} / \mathbf{A}_1, \mathbf{A}_2, \mathbf{A}_3, \mathbf{c} / \mathbf{A}_{F1}, \mathbf{A}_{F2}, \mathbf{A}_{F3}, \mathbf{C}_F$ : crystallographic basis vectors (in bold)  
 $C_1, C_2, C_3$ : the three orthohexagonal cells (Fig. 1; cf. Arnold 2002)  
 $\mathbf{c}_n$ : the (001) projection of the of the  $\mathbf{c}$  basis vector  
 $c_0$ : vertical distance between two interlayer cations on the opposite sides of an M layer ( $c_0 = c_1 \cos \beta^*$ )  
 $c^*_1$ : parameter along  $c^*$  of the simplest polytype (1M): it corresponds to about  $0.1 \text{ \AA}^{-1}$   
 $HK.L$ : diffraction indices expressed in hexagonal axes  
 $hkl$ : diffraction indices expressed in orthohexagonal axes  
 $l_{C_1}$ :  $l$  index in the  $C_1$  setting  
 $l_T$ :  $l$  index in the twin setting  
 $\omega$ : obliquity of the twin, divided into a component within the (001) plane ( $\omega_{\parallel}$ ) and a component normal to the (001) plane ( $\omega_{\perp}$ )  
 $\varepsilon$ : angular deviation from orthohexagonality of the (001) plane  
 $\eta$ : linear deviation from orthohexagonality of the (001) plane  
 $t_{(hkl)}$ : trace of the plane ( $hkl$ ) onto the (001) plane  
 ${}^n t_{(hkl)}$ : normal to  $t_{(hkl)}$  in the (001) plane

**Figure 1.** Relation between the hexagonal cell  $P$  and the three orthohexagonal cells  $C_1, C_2, C_3$  (cf. Arnold 2002).



### Symbols

- $N$ : number of layers in the conventional cell  
 $N'$ : number of layers in the unit cell of the (pseudo)-orthohexagonal setting:  $N' = N$  for orthogonal polytypes,  $N' = 3N$  for non-orthogonal polytypes  
 $T_i$ : character ("0"~"5") indicating the mica OD packet orientation

- $v_{2j,2j+1}$ : character (“0”~“5”) indicating the displacement between two adjacent mica OD packets  $p_{2j}$  and  $q_{2j+1}$
- $\langle v \rangle$ : the vector assigned to the character  $v$
- $\Sigma v$ : character (“0”~“5”, “\*”, “+”, “-”) indicating vector sum of  $v_{2j,2j+1}$  over a complete polytype period and corresponding to the projection of the  $c$  axis onto the (001) plane
- $RS_i^P$ :  $i$ -th Rotational Sequence of the polytype “P”
- $R_i$ :  $i$ -th translationally independent reciprocal lattice row parallel to  $c^*$  of the single individual ( $1 \leq i \leq 9$ ).
- $C_i$ :  $i$ -th “composite row”: translationally independent reciprocal lattice row parallel to  $c^*$  of the twin ( $1 \leq i \leq 9$ ).
- $I_j$ : symbol identifying the “node features” of a row of the reciprocal lattice parallel to  $c^*$ .  $I$  is the number of reflections in the  $c^*_1$  repeat,  $j$  a sequence number.

### Symmetry and symmetry operations

- $\lambda$ -symmetry: the symmetry proper of an individual layer ( $\lambda$ -operation: a symmetry operation transforming a layer into itself; the set of  $\lambda$ -operations constitute a *layer-group*)
- $\sigma$ -symmetry: the symmetry of a layer pair ( $\sigma$ -operation: a coincidence operation transforming a layer into the adjacent one)
- $\tau$ -operations: symmetry or coincidence operations which do not change the sign of the coordinate in the layer stacking direction. They are labeled  $\lambda$ - $\tau$  or  $\sigma$ - $\tau$  if they refer to  $\lambda$ - or  $\sigma$ -operations, respectively
- $\rho$ -operations: symmetry or coincidence operations which change the sign of the coordinate in the layer stacking direction and thus turn a layer or a stack of layers upside down. They are labeled  $\lambda$ - $\rho$  or  $\sigma$ - $\rho$  if they refer to  $\lambda$ - or  $\sigma$ -operations, respectively. Evidently,  $\tau.\tau = \tau$ ,  $\tau.\rho = \rho$ ,  $\rho.\tau = \rho$  and  $\rho.\rho = \tau$ .

### THE UNIT LAYERS OF MICA

The conventional layer of mica is described in details in Ferraris and Ivaldi (this volume). Here we recall only those definitions that are referred to in the following.

The conventional layer (also termed *TOT* layer or 2:1 layer) is constructed of seven atomic planes:  $O_{bl}$ ,  $Z_l$ ,  $O_{al}$ ,  $Y$ ,  $O_{au}$ ,  $Z_u$ ,  $O_{bu}$ , where “ $l$ ” and “ $u$ ” stand for “lower” and “upper” respectively. Interlayer cations occur between two successive layers in the  $I$  plane. This layer is referred as the “M layer” and is subdivided into two kinds of sheets:  $T$  ( $T_l$ :  $O_{bl}$ ,  $Z_l$ ,  $O_{al}$ , and  $T_u$ :  $O_{au}$ ,  $Z_u$ ,  $O_{bu}$ ), and  $O$  ( $O_{al}$ ,  $Y$ ,  $O_{au}$ ). On the basis of the occupation of the three octahedral sites, three *families* of micas exist: *homo-octahedral* (all three sites are occupied by one type of cation), *meso-octahedral* (one site is occupied differently from the other two), and *hetero-octahedral* (all three sites are occupied differently). In these three families the idealized  $\lambda$ -symmetry of the  $O$  sheet is  $H(3)1m$ ,  $P(\bar{3})1m$ , and  $P312$  respectively (Dornberger-Schiff et al. 1982). Two models were introduced to describe the  $\lambda$ -symmetry of the  $T$  sheet: the *Pauling model* (Pauling 1930), which neglects all the distortions and assumes  $\lambda$ -symmetry  $P(6)mm$ ; and the *Trigonal model*, which considers only the ditrigonal rotation of tetrahedra and assumes  $\lambda$ -symmetry  $P(3)1m$ . Both these models neglect the distortions occurring in the  $O$  sheet. Although the Trigonal model may seem still rather abstract, it is sufficient to describe the diffraction features useful for polytype and twin identification, whereas the Pauling model is too abstract. In fact, the main influence on the conditions for a reflection comes from the ditrigonal rotation of the tetrahedra. The other distortions, not taken into account by the Trigonal model, are quantitatively less relevant; they influence mainly the diffraction

intensities, and to a much lesser degree the geometry of the diffraction pattern; for this reason they can be neglected, in the first approximation.

The stagger of the two *T* sheets reduces the  $\lambda$ -symmetry of the M layer to monoclinic. Depending on whether the origin of the *O* sheet (which must be taken at the site with the point symmetry corresponding to the  $\lambda$ -symmetry of the sheet) is in *M1* (trans) or in *M2/M3* (cis), the layer itself is termed M1 or M2 respectively, and the highest  $\lambda$ -symmetry for these two layers is *C12/m*(1) and *C12*(1) respectively (for details see Ferraris and Ivaldi, this volume). The preliminary stage of the experimental study of a mica sample, such as the identification of the polytypic stacking sequence, is normally performed by assuming that the structure is homo-octahedral, and thus in the hypothesis of all M1 layers. For this assumption Nespolo et al (1999d), following a suggestion by S. Āuroviĉ (pers. comm.), introduced the term *homo-octahedral approximation*.

### Alternative unit layers

Besides the M layer, other unit layers were introduced, in most cases to simplify the description of some features, such as the diffraction pattern.

***Amelincks-Dekeyser's unit layer***. Amelinckx and Dekeyser (1953) pioneered the study of the spiral growth of micas. They also introduced the first vectorial and symbolic representation of the stacking sequence of layers in mica polytypes. These authors used a unit cell having the apical oxygen atoms and (OH/F) groups at the boundaries (Fig. 2). In this way, the unit cell is orthogonal and the monoclinic symmetry is achieved by stacking successive cells along three directions making 120°. Although this cell has nowadays no practical importance, it represents the first description alternative to Pauling's (1930) model and the precursor of the TS unit layers described below.

***Franzini and Schiaffino's A and B layers***. Franzini and Schiaffino (1963a,b) assumed that the ditrigonal rotation of the tetrahedra was mainly not related to the misfit of the *a* and *b* parameters of the tetrahedral and octahedral sheets, but to an intrinsic tendency of the potassium to assume an octahedral (actually antiprismatic) coordination. Those authors concluded that, with a single type of layer, rotations of  $(2n+1)\times 60^\circ$  were not possible for K-micas. To explain "polymorphs" and twins in which such rotations appear, Franzini and Schiaffino (1963a) introduced two kinds of monolayers, called A and B, in which the antiprismatic coordination for the interlayer cation is preserved for all the six rotations. These two layers differ for the orientation of the octahedral sheet with respect to the tetrahedral sheets: in practice, the slant of the octahedra is reversed in the two layers<sup>1</sup>. The ordered repetition of layers of the same kind (both A or both B) produces *1M*, *2M<sub>1</sub>* and *3T* "polymorphs", while the alternate repetition of both A and B layers produces *2O*, *2M<sub>2</sub>* and *6H* "polymorphs", however preserving the antiprismatic coordination for the interlayer cation. The co-existence of A and B layers was however regarded as highly improbable (Franzini 1966; 1969). The starting assumption of this theory, namely the impossibility of trigonal prismatic coordination for the interlayer cation, is not correct (Sartori et al. 1973), and the Franzini and Schiaffino theory lost its importance.

Despite that, the terms *Franzini-type A and B* have found their way into the literature. As Franzini (1969) noted, owing to ditrigonalization, the basal-oxygen atoms in the type A *approach* the cations in the adjacent octahedral sheet, whereas they *move*

<sup>1</sup> Griffen (1992) described the direction of the ditrigonalization of the *T* sheets with respect to the triangular bases of the octahedra in terms of the rotations "O" (opposite, corresponding to Franzini-type A of layer) and "S" (same, corresponding to Franzini-type B of layer). This terminology, borrowed from pyroxenes, is commonly not adopted for micas.

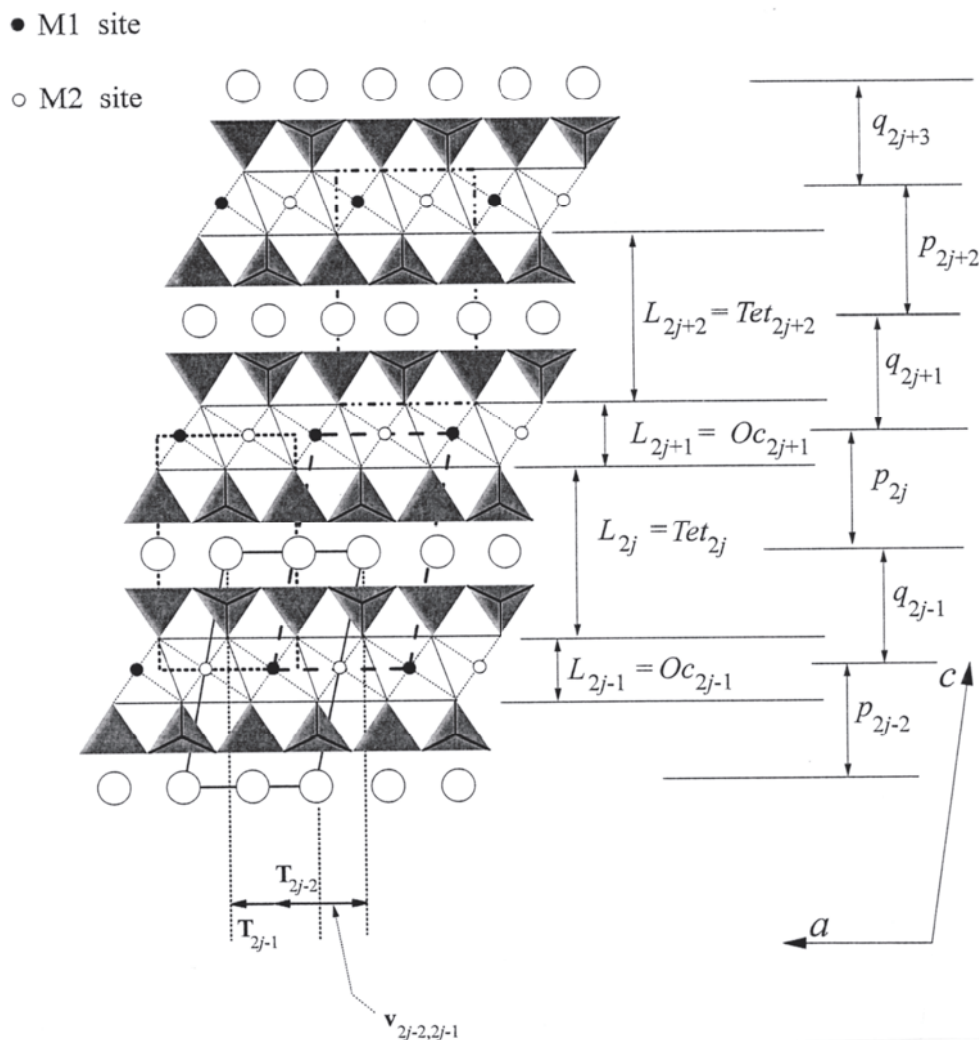


**Figure 2.** Schematic representation of a slab  $b/4$  thick, showing three layers of the 1M polytype. Four different unit cells are shown: the M layer (solid lines), the U layer (dashed lines), the TS D layer (dotted lines) and the cell used by Amelinckx and Dekeyser (1953) (dotted-dashed lines). The OD layers and packets are indicated directly in the figure.

apart in type B layers, if compared with the Pauling model. This holds also for phyllosilicates other than micas. Whereas in mica structures refined to date only the type A has been found, the type B has been encountered in some 1:1 phyllosilicates and in some chlorites, where the energetic handicap of the type B is balanced by a more favorable arrangement of hydrogen bonds elsewhere in the structure.

**The U layer.** The origin of the entire M layer is in the  $I$  plane. By shifting the origin into the  $O$  sheet, the  $U$ -layer (Fig. 2) is obtained and, inside it, a smaller portion, called the  $u$ -layer, which does not represent a unit layer but consists of two tetrahedral sheets and the interlayer cations between. These layers were used as a tentative interpretation of the crystallographic transformation of biotites by means either of crystallographic slips (CS) of cation or oxygen planes corresponding to cation-to-cation or oxygen-to-coplanar-oxygen distance (CS of the first sort) or of co-operative slip movements of two atomic planes (oxygen-oxygen or oxygen-cation) in a single octahedral sheet (CS of the second

sort) (Takéuchi 1971; Takéuchi and Haga 1971). A CS of the first sort probably occurs during polytype formation when a strengthening of the interlayer bonding is accompanied by a destabilization of the *O* sheet (Nespolo 2001).

**The TS layers.** Similarly to the choice of Amelinckx and Dekeyser (1953), Sadanaga and Takeda (1969) and Takeda and Sadanaga (1969) described the structure of micas by means of orthogonal unit layers. Whereas Amelinckx and Dekeyser (1953) had chosen the origin in the  $O_a / OH / F$  plane, Sadanaga and Takeda (1969) and Takeda and Sadanaga (1969) defined their TS unit layers between two octahedral sheets of successive M layers and preserved the origin in the plane of the *I* cations (Fig. 2). TS unit layers are defined within the Trigonal model and consist of four layers, labeled D, D\*, T and T\*, with  $\lambda$ -symmetry  $P(3)1m$  (D and D\*) and  $P(6)2m$  (T and T\*). D is related to D\* and T to T\* by an  $180^\circ$  rotation about  $c^*$  (see Fig. 2,3). Because of their trigonal  $\lambda$ -symmetry, which is higher than the monoclinic  $\lambda$ -symmetry of the M layer, four kinds of unit layers are necessary to describe all possible polytypes. These layers are related by only translations, without rotations, and next layers are staggered  $\pm a/3$  along one of the three hexagonal axes  $A_1, A_2, A_3$  in the plane of the layer. As shown by Nespolo et al (1999d), the TS unit layers represent the most suitable geometrical description for a simple computation of the PID function (see below). The letters D and T indicate a “ditrigoal” or “trigoal” coordination of the *I* cation respectively for the two kinds of layer. Actually, D/D\* layers have the *I* cation in antiprismatic coordination, whereas in the T/T\* layers the *I* cation is in prismatic coordination. In both cases, the coordination polyhedron is trigonal where only the nearest-neighbor oxygen atoms are considered, whereas it becomes ditrigoal by considering also the next-nearest-neighbor oxygen atoms. A symbolism like A/A\* (for “antiprismatic”) and P/P\* (for “prismatic”) instead of D/D\* and T/T\* respectively would perhaps had been more appropriate. The TS layers are constructed by half-pairs of M1 layers in the homo-octahedral approximation and, as shown hereafter, their use is in the calculation of the Periodic Intensity Distribution function to solve an unknown stacking sequence.

**The OD layers and the OD packets .** The OD interpretation presupposes that any polytype of a given polytypic substance may be considered as consisting of *disjunct* parts periodic in two dimensions, called *OD layers*, whose pairs remain geometrically equivalent in any polytype of the same family. The OD layers do not necessarily coincide with the layers commonly chosen on the basis of the chemical identity and/or cleavage properties. In other words, the layers by which a polytypic substance is most commonly described from the crystal-chemical point of view are not always the most suitable layers to describe the geometrical equivalence of layer pairs. Furthermore, the choice of the OD layers in general is not absolute (Grell 1984); their purpose is not to *explain* but to *describe* and/or *predict* polytypism of a substance based on symmetry.

Micas are considered to consist of two kinds of OD layers. The octahedral OD layer (Oc) corresponds to the sequence  $O_{al}-Y-O_{au}$ , and the tetrahedral OD layer (Tet) to the sequence  $O_{au}-Z-O_b-I-O_b-Z-O_{al}$ , with the  $O_{al}$  and the  $O_{au}$  planes ( $au$  = apical upper;  $al$  = apical lower) half belonging to neighboring OD layers (Fig. 2). By denoting an OD layer with the general letter L, Tet and Oc OD layers are  $L_{2j}$  and  $L_{2j+1}$  respectively, where  $j$  is a running integer. Another useful unit is the *OD packet*, which corresponds to half of the M layer plus half the plane of the *I* cations, and constitutes the smallest continuous part, periodic in two dimensions, representing fully the chemical composition of a polytype (Āuroviĉ 1974). OD packets are by definition polar and lie within one side or the other pointing alternatively along  $+c$  and  $-c$ : they are indicated with the letters p and q:  $p_{2j} = Tet_{2j}/2 + Oc_{2j+1}/2$ ;  $q_{2j+1} = Oc_{2j+1}/2 + Tet_{2j+2}/2$  (Fig. 2). All mica packets within the same family are geometrically equivalent and their symmetry is  $P(3)1m$  (homo-octahedral



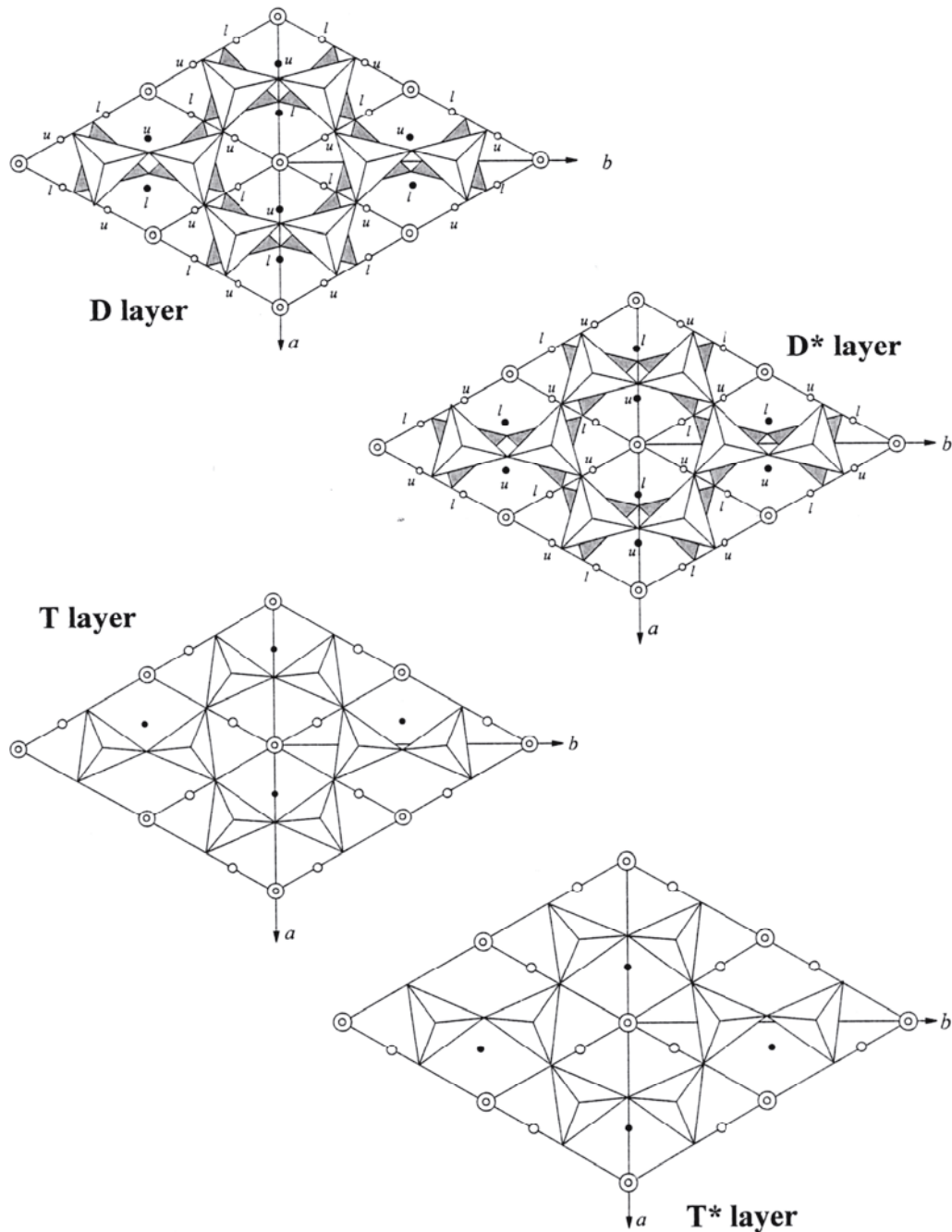


**Figure 3.** The four TS unit layers.  $a$ ,  $b$ : orthohexagonal axes. Black and open small circles represent  $M1$  and  $M2$  sites respectively. Double circles represent interlayer cations and OH/F groups, which are overlapped in the (001) projection.  $u$  and  $l$  indicate octahedral cations with  $z = +1/2$  and  $z = -1/2$  respectively, overlapped in (001) projection for T and T\* layers (modified after Nespolo et al. 1999d).

family),  $C1m(1)$  (meso-octahedral family) or  $C1$  (hetero-octahedral family) (Dornberger-Schiff et al. 1982; Backhaus and Đurovič 1984; Đurovič, et al. 1984). This reduces the problem of handling *two* kinds of OD layers to that of *one* kind of OD packet and this facilitates, among others, also the systematic derivation of MDO polytypes (see below).

Furthermore, both M1 and M2 mica layers within the same family consist of the same kind of OD packet.

### MICA POLYTYPES AND THEIR CHARACTERIZATION

The crystal chemical reason for polytypism is that adjacent layers (two-dimensionally-periodic units) can be linked to each other in many translationally non-equivalent ways. However, the nearest-neighbor relationships remain preserved. Translated into the language of symmetry, this means that the pairs of adjacent layers remain geometrically equivalent in all polytypes of the same family.

The geometrical equivalence must be fulfilled not necessarily by the real layers, but by their *archetypes*, i.e. the (partially) idealized layers to which the real layers can be reduced by neglecting some distortions occurring in the true structure. The notion of polytypism becomes thus unequivocal only when it is used in an *abstract* sense to indicate a structural type with specific geometrical properties. In micas, these archetypes are the layers described by the Trigonal model. Of the several kinds of layers presented in the previous section, the OD layers, and the OD packets, are the most suitable ones to both show and exploit the geometrical equivalence.

#### Micas as OD structures

If the position of a layer is uniquely defined by the position of the adjacent layers and by the so-called *vicinity condition* ( $VC$ )<sup>2</sup>, which states the geometrical equivalence of layer pairs, the resulting structure is *fully ordered*. If, on the other hand, more than one position is possible that obeys the VC, the resulting structure is an OD structure and the layers are OD layers. *VC structures* may thus be either fully ordered structures or OD structures (Dornberger-Schiff 1964, 1966, 1979; see also Āuroviĉ 1999). All OD structures are polytypic; the reverse may or may not be true (see the arguments in Zvyagin 1993). Equivalency depends on the choice of OD layers and also on the definition of polytypism (see below).

In each of the three mica families, the packet pairs  $p_{2j}q_{2j+1}$  and  $q_{2j+1}p_{2j+2}$  are geometrically equivalent through a  $\rho$ -operation of the  $Oc_{2j+1}$  OD layer and of the  $Tet_{2j+2}$  OD layer, respectively. These operations are denoted as  ${}_{2j,2j+1}[\rho^{(i)}]$  and  ${}_{2j+1,2j+2}[\rho^{(i)}]$  respectively. The resulting polytype depends on the kind of these operations (they follow from the  $\lambda$ -symmetry of  $Oc$  or  $Tet$ ) and on their sequence in the polytype. Since  $\rho \cdot \rho = \tau$  and, particularly for OD structures, a product like  ${}_{kl}[\rho^{(i)}] \cdot {}_{mn}[\rho^{(i)}]$  is allowed only if  $l=m$ , each even number of such products, e.g.,

$${}_{01}[\rho^{(1)}] \cdot {}_{12}[\rho^{(2)}] \cdot {}_{23}[\rho^{(3)}] \cdot {}_{34}[\rho^{(4)}] \cdot \dots \cdot {}_{2n-1,2n}[\rho^{(2n)}]$$

yields a  ${}_{0,2n}[\tau]$ -operation. This operation can be either a translation, a glide operation or a screw rotation, whose translation component is the so-called *repeat unit*. The  $\tau$ -operation can be *continued*, i.e. continuously repeated, and then it *generates* a periodic polytype. The operation is thus *global (total)* for the polytype obtained. Of special importance are the  ${}_{02}[\tau]$ -operations which play a decisive role in the derivation of MDO polytypes, as shown below. If the distribution of subsequent  $\rho$ -operations is completely random so that no generating  $\tau$ -operation can be found, the polytype is disordered. Disordered polytypes have been reported as  $2n \times 60^\circ$  rotations only (e.g., Ross et al. 1966; let us indicate them as  $1M_{d-A}$ , where “A” stands for “subfamily A”) and with both  $2n \times 60^\circ$  and  $(2n+1) \times 60^\circ$  rotations (Kogure and Nespolo 1999a; let us indicate them as  $1M_{d-M}$ , where “M” stands

<sup>2</sup> The vicinity condition (e.g., Dornberger-Schiff 1979) consists of three parts. **VC  $\alpha$** : VC layers are either geometrically equivalent or, if not, they are relatively few in kind; **VC  $\beta$** : translation groups of all VC layers are either identical or they have a common subgroup; **VC  $\gamma$** : equivalent sides of equivalent layers are faced by equivalent sides of adjacent layers so that the resulting pairs are equivalent.

for “mixed-rotation”), whereas no examples with  $(2n+1)\times 60^\circ$  rotations only (let us indicate them as  $1M_{a-B}$ , where “B” stands for “subfamily B”) have been reported to date. Note that in periodic polytypes some  $\rho$ -operations also become global, whereas the remaining ones are valid only in a subspace of the crystal space. Note also that, alone, a  $\rho$ -operation could not be used to construct a polytype, because its repeated application leads back to the area of the starting layer or packet. For more details concerning the OD interpretation of mica structures, see Dornberger-Schiff et al (1982); for the derivation of MDO mica polytypes see Backhaus and Durovič (1984); for the classification and abundance of MDO mica polytypes see Āurovič et al (1984).

The set of all the operations valid in the whole crystal space and in a subspace of the crystal space constitutes a space *groupoid* (Dornberger-Schiff 1964; Fichtner 1965, 1977, 1980). The theory of groupoids was introduced in mathematics by Brandt (1927) and applied in crystallography in Germany by the OD school (Dornberger-Schiff 1964, 1966), and in Japan by the school of Ito and Sadanaga, with special emphasis on those groupoids, termed *twinned space groups*, which are necessary to explain the existence of polysynthetic structures (e.g., Ito 1935, 1938, 1950; Ito and Sadanaga 1976; Sadanaga 1978; Sadanaga et al. 1980). The OD school used the terms *total* for a space-group operation, *local* or *partial* (as synonyms) for a symmetry operation valid in a subspace of the crystal space, and *coincidence operation*, represented by a single transformation matrix, for a non-symmetry operation that corresponds – approximately – to a one-way movement in the structure, i.e. an operation without the corresponding inverse operation. Sadanaga and Ohsumi (1979) and Sadanaga et al (1980) used instead *global*, *local* and *partial* in the same way the OD school used *total*, *local/partial* and *coincidence* respectively. To avoid any possible confusion, hereafter the word “partial” is not adopted, and the term “local” is used to indicate a symmetry operation valid in a subspace of the crystal space.

Within the Pauling model, an isolated Tet layer has  $\lambda$ -symmetry  $P(6/m)mm$ , with 12  $\tau$ -operations and 12  $\rho$ -operations. Within a group, the three axial and the three inter-axial directions are symmetry-related and thus one entry for each of these two sets in the conventional Hermann-Mauguin symbol suffices to characterize the corresponding symmetry operations. However, in the OD structures, any of these operations can play a specific role and this is why Dornberger-Schiff (1964 p. 44 ff; 1966 p. 54) introduced extended Hermann-Mauguin symbols consisting of *seven* entries: . . . (.) . . . where the unique direction is in parentheses, the three entries to the left refer to the three axial directions  $A_1, A_2, A_3$  (Fig. 1; cf. Fig. 4) and the three entries to the right refer to the three inter-axial directions  $B_1, B_2, B_3$  where  $B_i \perp A_i$ . Such an extended Hermann-Mauguin symbol for the layer-group  $P(6/m)mm$  reads:  $P\ 2/m\ 2/m\ 2/m\ (6/m)\ 2/m\ 2/m\ 2/m$

Within the Trigonal model, this  $\lambda$ -symmetry reduces to trigonal. The extended Hermann-Mauguin symbols, depending on which of the two maximal non-isomorphic subgroups is preserved (either  $P(\bar{3})1m$  or  $P(\bar{6})2m$ , become:  $P\ 1\ 1\ 1\ (\bar{3})\ 2/m\ 2/m\ 2/m$  and  $P\ 2\ 2\ 2\ (6)\ m\ m\ m$ .

The individual operations in each of these two groups can be characterized either by the extended Hermann-Mauguin (H-M) symbols (as usual in the OD literature), or with reference to the orthogonal (ORT) axes. Although indexing in the orthohexagonal setting is unequivocal, the correspondence between H-M symbols and ORT symbols depends on which cell is adopted ( $C_1$  vs.  $C_2$ ; see Fig. 1). In Table 1, all correspondences are shown.

The two  $\lambda$ -symmetries of the Tet layer correspond to  $2n\times 60^\circ$  and  $(2n+1)\times 60^\circ$  rotations, respectively, of successive M layers about  $c^*$ . Each family of polytypes is defined in terms of the  $\lambda$ -symmetry of the Oc layer, which is the same as that of the O

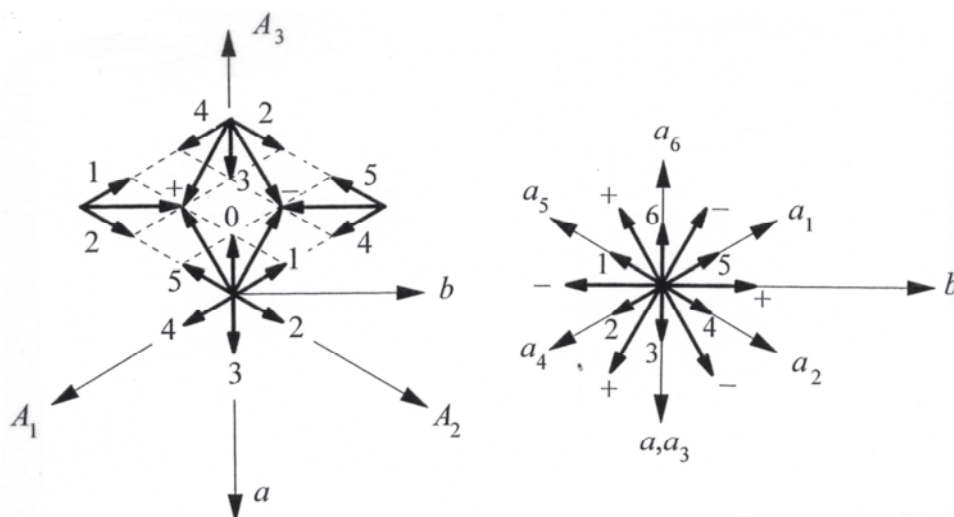
**Table 1.** Extended Hermann-Mauguin (H-M) symbols and corresponding operations indexed in orthogonal (ORT) axes for the two  $\lambda$ -symmetries of the Tet layer within the Trigonal model. The extended H-M symbols consist of *seven* entries:  $\dots (\cdot) \dots$  where the unique direction is in parentheses, the three entries to the left refer to the three axial directions  $A_1, A_2, A_3$  and the three entries to the right refer to the three inter-axial directions  $B_1, B_2, B_3$  ( $B_i \perp A_i$ ). The corresponding orthogonal indices are given with reference to both the  $C_1$  and the  $C_2$  cells.

$P(\bar{3})1m$					
$\tau$ -operations			$\rho$ -operations		
H-M	ORT ( $C_1$ )	ORT ( $C_2$ )	H-M	ORT ( $C_1$ )	ORT ( $C_2$ )
1	1	1	$\bar{1}$	$\bar{1}$	$\bar{1}$
$(3)^{-1}$	$3^{-1}_{[001]}$	$3^{-1}_{[001]}$	$(\bar{3})^{-1}$	$\bar{3}^{-1}_{[001]}$	$\bar{3}^{-1}_{[001]}$
$(3)^1$	$3^1_{[001]}$	$3^1_{[001]}$	$(\bar{3})^1$	$\bar{3}^1_{[001]}$	$\bar{3}^1_{[001]}$
$[\dots (\cdot) m \dots]$	$m_{(010)}$	$m_{(110)}$	$[\dots (\cdot) 2 \dots]$	$2_{[010]}$	$2_{[310]}$
$[\dots (\cdot) \cdot m \cdot]$	$m_{(110)}$	$m_{(1\bar{1}0)}$	$[\dots (\cdot) \cdot 2 \cdot]$	$2_{[310]}$	$2_{[3\bar{1}0]}$
$[\dots (\cdot) \dots m]$	$m_{(1\bar{1}0)}$	$m_{(010)}$	$[\dots (\cdot) \dots 2]$	$2_{[3\bar{1}0]}$	$2_{[010]}$

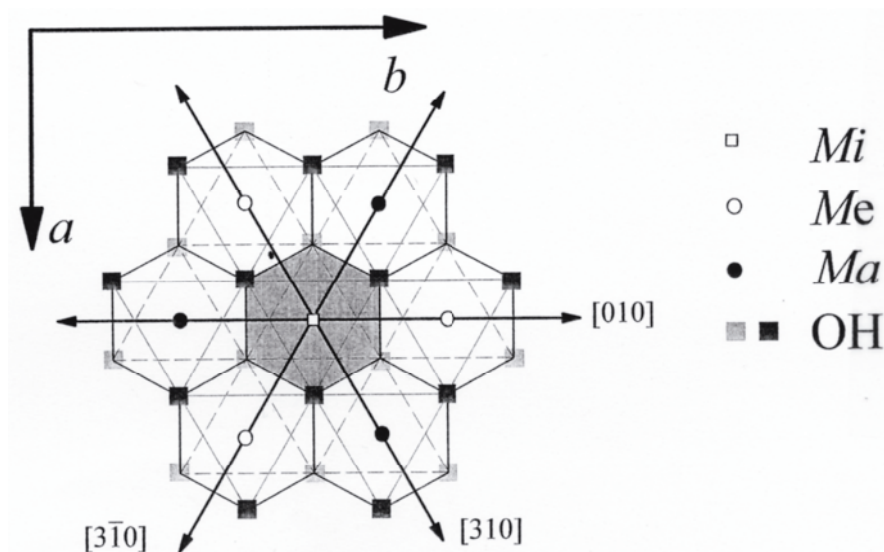
  

$P(\bar{6})2m$					
$\tau$ -operations			$\rho$ -operations		
H-M	ORT ( $C_1$ )	ORT ( $C_2$ )	H-M	ORT ( $C_1$ )	ORT ( $C_2$ )
1	1	1	$(\bar{2})^1$	$m_{(001)}$	$m_{(001)}$
$(3)^{-1}$	$3^{-1}_{[001]}$	$3^{-1}_{[001]}$	$(\bar{6})^{-1}$	$\bar{6}^{-1}_{[001]}$	$\bar{6}^{-1}_{[001]}$
$(3)^1$	$3^1_{[001]}$	$3^1_{[001]}$	$(\bar{6})^1$	$\bar{6}^1_{[001]}$	$\bar{6}^1_{[001]}$
$[m \dots (\cdot) \dots]$	$m_{(100)}$	$m_{(1\bar{3}0)}$	$[2 \dots (\cdot) \dots]$	$2_{[100]}$	$2_{[1\bar{1}0]}$
$[m \cdot (\cdot) \dots]$	$m_{(1\bar{3}0)}$	$m_{(130)}$	$[\cdot 2 \cdot (\cdot) \dots]$	$2_{[1\bar{1}0]}$	$2_{[110]}$
$[\dots m (\cdot) \dots]$	$m_{(130)}$	$m_{(100)}$	$[\dots 2 (\cdot) \dots]$	$2_{[110]}$	$2_{[100]}$

sheet (see Table 2 in Ferraris and Ivaldi, this volume), and is then divided into two subfamilies on the basis of the Tet  $\lambda$ -symmetry: *subfamily A* for  $P(3)1m$ , and *subfamily B* for  $P(\bar{6})2m$ . We suggest for the polytypes where Tet layers with both  $P(3)1m$  and  $P(\bar{6})2m$   $\lambda$ -symmetries co-exist, the term *mixed-rotation polytypes* (see also Nespolo 1999). Both subfamily A and subfamily B polytypes are OD structures, because the layer stacking obeys the VC. However, the layer stacking in the mixed-rotation polytypes with the geometry of the Trigonal model violates the VC: *these polytypes are OD structures only within the Pauling model*, i.e. for a null ditrigonal rotation of the tetrahedra (Backhaus and Āuroviĉ 1984).



**Figure 4.** The nine possible displacements in the structure of polytypes of phyllosilicates. Left: the OD symbols and corresponding vectors, within the primitive hexagonal unit cell (modified after Durovic 1999). The sum of any two vectors is indicated, and the result of the summation of any number of vectors should be taken modulo primitive hexagonal cell. The individual vectors are designated by their conventional numerical characters and signs “+” and “-”, whereas the zero displacement “\*” is not indicated. The “+” and “-” vectors do not explicitly occur in micas. However, in *Class b* polytypes the total displacement, obtained as vector sum of the packet-to-packet displacements ( $\mathbf{v}_{2j,2j+1}$ , second line of the full OD symbol) corresponds to “-”, namely  $\mathbf{c}_n = (0, \bar{1}/3)$ . Right: the corresponding Z vectors (modified after Zvyagin et al. 1979) (cf. Table 4). In the publications by Zvyagin and his school, the coordinate system is oriented so that the orthogonal *a* axis points up and the *b* axis to the left. Here we follow instead the conventions of the *International Tables for Crystallography*: the space-fixed references, and consequently the Z vectors, are rotated by 180° with respect to their orientation in the original publications.



**Figure 5.** An isolated hetero-octahedral Oc layer, with the three two-fold axes in the plane of the layer ( $\rho$ -operations).

In Figure 5 an isolated Oc layer is shown. Depending on whether *Ma*, *Mi* and *Me* are all equal, two different or all different the Oc layer is homo-, meso- or hetero-octahedral respectively, and the  $\lambda$ -symmetry is  $H(\bar{3})1m$ ,  $P(\bar{3})1m$  and  $P(3)12$  respectively. In the

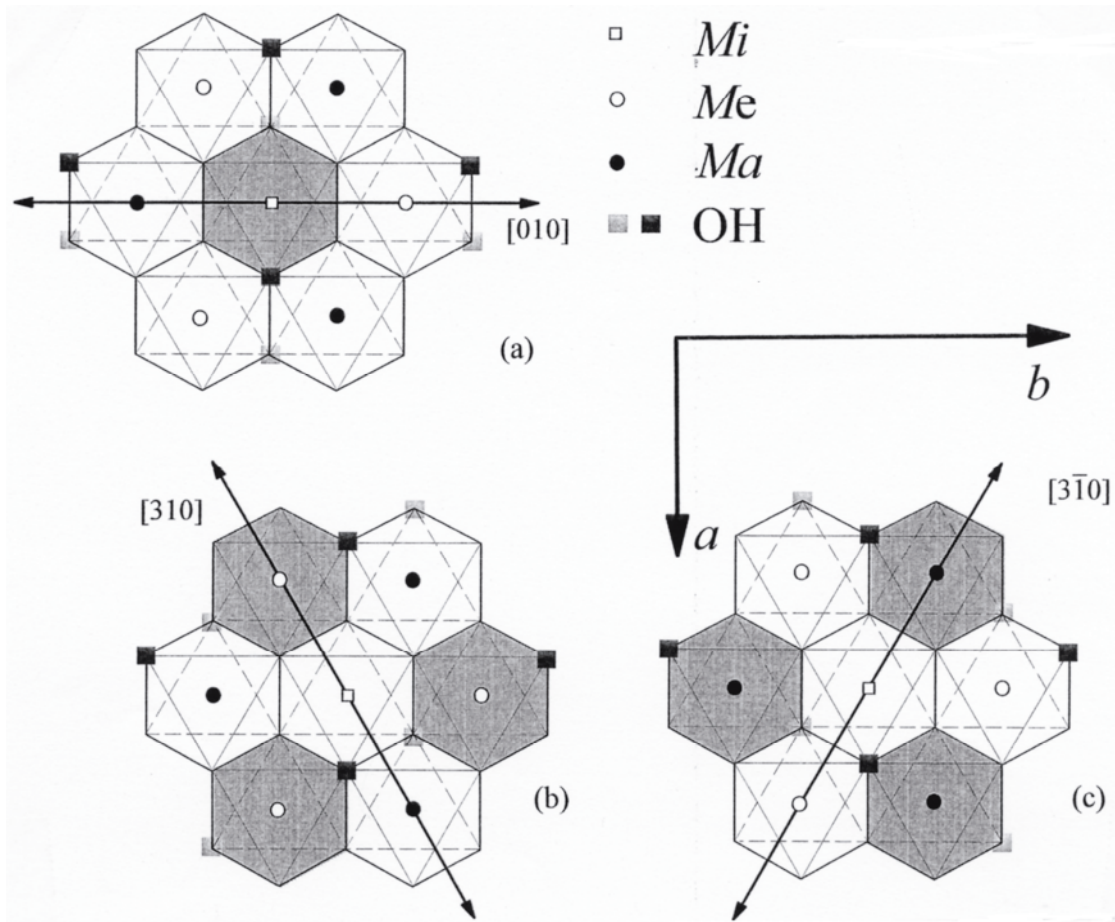


**Figure 6.** The hetero-octahedral Oc layer shown in Figure 5 after substitution of 2/3 of the OH/F groups with  $O_a$  from the upper and lower tetrahedra. Only one of the three  $\rho$ -operations remains, defining the relation between the type of site ( $M1$ ,  $M2$ ,  $M3$ ) and its occupation ( $Ma$ ,  $Me$ ,  $Mi$ ). (a)  $\rho$ -operation  $2_{[010]}$ ,  $Mi$  cation in the  $M1$  site, layer type  $M1$ . (b)  $\rho$ -operation  $2_{[310]}$ ,  $Me$  cation in the  $M1$  site, layer type  $M2$ . (c)  $\rho$ -operation  $2_{[3\bar{1}0]}$ ,  $Ma$  cation in the  $M1$  site, layer type  $M2$ .

meso-octahedral family Oc includes six  $\tau$ -operations ( $1$ ,  $3^+_{[001]}$ ,  $3^-_{[001]}$ ,  $m_{(010)}$ ,  $m_{(110)}$ ,  $m_{(1\bar{1}0)}$ ) and six  $\rho$ -operations ( $2_{[010]}$ ,  $2_{[310]}$ ,  $2_{[3\bar{1}0]}$ ,  $1$ ,  $3^+_{[001]}$ ,  $3^-_{[001]}$ ); these numbers in the homo-octahedral family have, in fact, to be multiplied by three, owing to the  $H$  centering, whereas for the hetero-octahedral family Oc includes three  $\tau$  and three  $\rho$ -operations (the first three of each set). In Figure 6 the same projection is given, but with the positions of the OH/F groups remaining after the substitution with  $O_a$  are indicated. This substitution destroys two-thirds of the  $\lambda$ -operations, leaving one (hetero-octahedral) or two (homo- and meso-octahedral)  $\tau$ -operations (the identity and one  $m$  reflection) and one or two  $\rho$ -operations (one of the two-fold rotations in the plane of the layer, and the inversion). For meso- and hetero-octahedral Oc layer, for the sake of simplicity and without loss of generality, let us assume that  $\delta(Mi) < [\delta(Ma), \delta(Me)]$ . The origin of the Oc layer is then, according to the convention described in Ferraris and Ivaldi (this volume), at the  $Mi$  average cation. In Figure 6a, one of the  $\rho$ -operations (the only one for hetero-octahedral Oc layer) is the two-fold rotation along  $[010]$ , and the  $M1$  (trans) site contains the  $Mi$  average cation. The M layer is thus of the type  $M1$ . Instead, in Figure 6b and 6c the  $\rho$ -operation is the two-fold rotation along  $[310]$  and  $[3\bar{1}0]$  respectively: the  $M1$  site contains the  $Me$  or the  $Ma$  cation respectively, and in both cases the M layer is of type  $M2$ .

**MDO polytyps** . Polytypes in which not only the pairs of layers, but also the triples,



quadruples *etc.* are geometrically equivalent, or, when this is not possible, contain the smallest number of kinds of triples, quadruples *etc.*, are termed *Maximum Degree of Order* (MDO) polytypes. This definition originates in a simple philosophy: if a certain configuration (say a triple of layers) is energetically favorable, it will be repeated again and again and will not be intermixed with other, less favorable configurations.

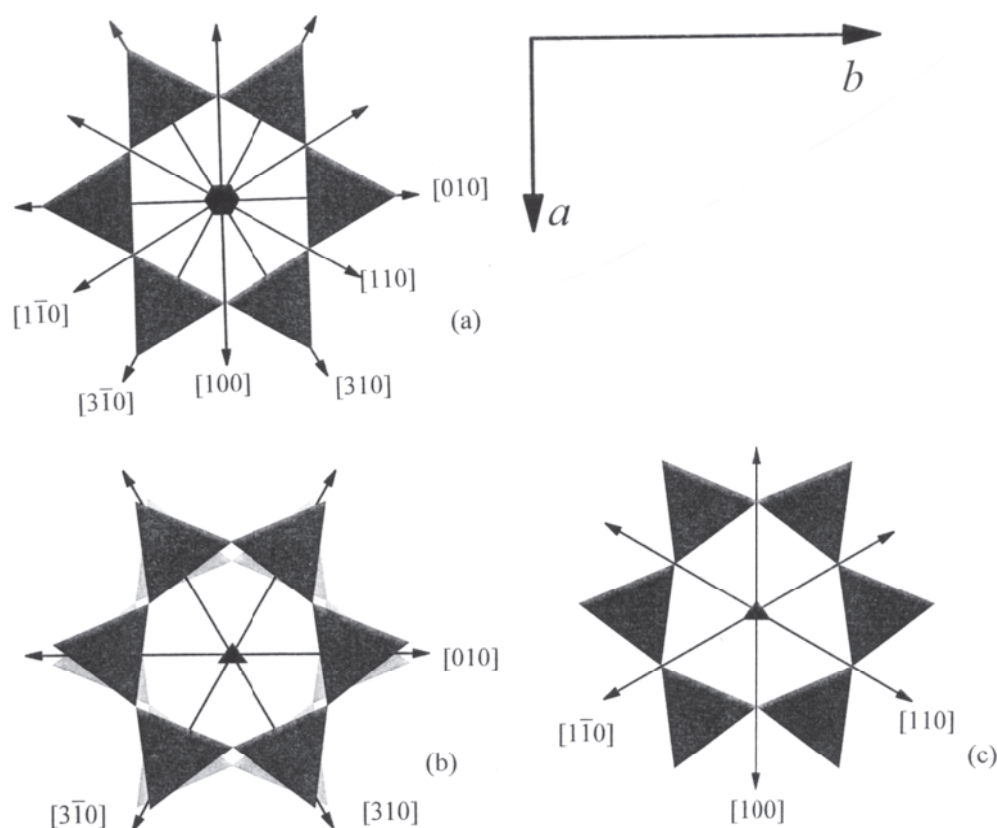


**Figure 7.** The (001) projections of a Tet layer (the *I* cation, not shown, takes place in the hole between the two rings of tetrahedra). The two-fold axes in the plane of the layer (half of the  $\rho$ -operations of the Tet layer) are indicated. (a) The configuration corresponding to the Pauling model, with zero ditrigonal rotation. The symmetry of the Tet layer is  $P(6/m)mm$ . (b) The configuration corresponding to subfamily A in the Trigonal model. The symmetry of the Tet layer is  $P(3)1m$ . (c) The configuration corresponding to subfamily B in the Trigonal model. The symmetry of the Tet layer is  $P(6)2m$ .

MDO polytypes of the subfamily A [ $P(3)1m$   $\lambda$ -symmetry of the Tet layer] are more favorable than MDO polytypes of the subfamily B [ $P(6)2m$   $\lambda$ -symmetry of the Tet layer], probably because of the different (staggered *vs.* eclipsed) configuration of the facing  $O_b$  atoms (Fig. 7). The most common polytypes are indeed MDO subfamily A. Of the MDO subfamily B, only  $2M_2$  is relatively common in Li-rich trioctahedral micas, where an important structural role of the fluorine atoms has been proposed (Takeda et al. 1971).  $2O$  has been found in its ideal space group in a fluor-phlogopite (Ferraris et al. 2001) and in the brittle mica anandite (Giuseppetti and Tadini 1972; Filut et al. 1985): the structure refinement of anandite indicates that it cannot be described in terms of an orthohexagonal *C*-centered cell, its space-group type being  $Pn\bar{m}n$ .  $2O$  was also obtained synthetically in fluor-phlogopite (Sunagawa et al. 1968; Endo 1968), and identified from direct

observation of the growth spirals on the surface, but no diffraction study has been performed. Several non-MDO subfamily A polytypes have been reported, as well as some mixed-rotation polytypes, but their number is far smaller than MDO polytypes. The abundance of MDO subfamily A polytypes shows that the geometrical equivalence of OD layers is an important factor even when considering the real structures. The occurrence of non-MDO polytypes is easily understood when considering that the MDO concept specifically refers to a layer-by-layer growth. In all the environments where crystals grow in a fluid phase, the spiral-growth mechanism, to which the MDO criteria apply less strictly, becomes dominant as soon as the supersaturation decreases below a certain critical value (Sunagawa 1984). As a matter of fact, the appearance of long-period polytypes in micas has precise structural reasons. In polytypes based on the close-packed arrangement of atoms, such as SiC, CdI<sub>2</sub> etc., the layer thickness is only a few Å and the long-range interactions are not negligible. In micas the layer is about 10Å thick and the long-range interactions are thus less relevant. The probability of the occurrence of non-MDO polytypes, as well as of non-periodic (disordered) polytypes, depends in general on how close are the layers to their archetypes (i.e. how close is the real symmetry to the ideal OD symmetry). The more a layer deviates from its archetype, the less valid are the equivalencies between adjacent layers. The consequence is that when the pairs of adjacent layers are not geometrically equivalent, they are also not energetically equivalent and the ambiguity in the stacking of layers is lost.

The first derivation of the predecessors of the MDO polytypes dates back to Smith and Yoder (1956), who theoretically described the six non-equivalent polytypes (termed “*simple polymorphs*” by them) that can be obtained by stacking the M1 layer with the same rotation (in the two possible directions) between adjacent layers. All other polytypes were collectively termed *complex polymorphs*. The term *polymorphism* was also used by Zvyagin (1962) and by Franzini and Schiaffino (1963a,b), whereas the word *polytypism* when referring to micas was used for the first time probably by Amelinckx and Dekeyser (1953). The adjectives *simple* and *complex* used by Smith and Yoder (1956) represent a qualitative description, as well as the word *standard* used by Bailey (1980a). Zvyagin et al (1979) (see also Zvyagin 1988) introduced the notion of “condition of homogeneity<sup>3</sup>”, which identifies polytypes in which the position of any layer relative to the others and the transition from it to the adjacent ones, are the same or equivalent for all layers. These polytypes are called *homogeneous polytypes*; the remaining ones are called *inhomogeneous polytypes*. The condition of homogeneity is similar to the condition of the Maximum Degree of Order, but with less emphasis on chemical variations, and thus also on the symmetry distinguishing the three families. The main difference is that Zvyagin applies his condition to the entire crystal-chemical layer, whereas the algorithms for the derivation of MDO polytypes (Dornberger-Schiff et al. 1982, Dornberger-Schiff and Grell 1982) apply to OD layers or OD packets: the latter in micas roughly correspond to half-layers. Within the homo-octahedral approximation in micas, the procedures for the derivation of “simple”, “standard”, “homogeneous”, “MDO”, yield identical results (Table 2): this is however, in general, not true for other compounds, because the algorithms for the derivation of MDO polytypes are considerably different from those employed to derive “homogeneous” or “simple” polytypes. The difference becomes evident when considering that there are only 6 “simple” or “standard” polytypes (that become 8 when considering the non-congruent polytypes, i.e. counting separately each member of an enantiomorphous pair), but they simply correspond to homo-octahedral MDO polytypes. There are then 14 non-equivalent

---

<sup>3</sup> In some texts, the Russian term “однородность” is translated as “uniformity” instead of “homogeneity”. Here we adopt the latter translation, closer to the original meaning.



**Table 2.** Comparative classification of mica polytypes in the homo-octahedral approximation.

<i>Relative rotations between successive M layers</i>			
1M: 0°; 2M <sub>1</sub> : 120° and 240°; 3T: 120° or 240°	2O: 180°; 2M <sub>2</sub> : 60° and 300°; 6H: 60° or 300°	2n×60° (2n+1)×60°	Both 2n×60° and (2n+1)×60°
Subfamily A MDO <sup>a</sup>	Subfamily B MDO <sup>a</sup>	Subfamily A non-MDO <sup>a</sup>	Mixed-rotation <sup>b</sup>
All triples of OD packets within a given polytype equivalent	More than one type of triple within a given polytype	More than one type of triple of OD packets within a given polytype	More than one type of triple of OD packets within a given polytype
<i>OD structures</i>			
Homogeneous with all octahedra parallel <sup>c</sup>	Homogeneous with octahedra parallel and anti-parallel regularly alternating <sup>c</sup>	Inhomogeneous with all octahedra parallel <sup>c</sup>	Inhomogeneous with mixed (parallel and antiparallel) and randomly alternating orientation of octahedra <sup>c</sup>
All triples of M layers within a given polytype equivalent	More than one kind of triples of M layers within a given polytype	More than one kind of triples of M layers within a given polytype	>1 kind of triples of M layers within a given polytype
Standard, group I <sup>d</sup>	Standard, groups I & II alternating	Non-standard, group I <sup>d</sup>	Non-standard, groups I & II mixed, non-alternating
<i>Simple<sup>e</sup></i>			
Ternary <sup>f</sup>	Senary <sup>f</sup>	Ternary <sup>f</sup>	Senary <sup>f</sup>
<i>Complex<sup>e</sup></i>			

<sup>1</sup>These are OD structures if the ditrigonal rotation of the tetrahedra is zero.<sup>a</sup>Durovic et al (1984); <sup>b</sup>Nespolo (1999); <sup>c</sup>Zvyagin et al (1979) and Zvyagin (1988); <sup>d</sup>Bailey (1980a); <sup>e</sup>Smith and Yoder (1956); <sup>f</sup>Ross et al (1966).

“MDO” stands for “Maximum Degree of Order”.

(22 non-congruent) polytypes in the meso-octahedral family, and 36 non-equivalent (60 non-congruent) polytypes in the hetero-octahedral family, which obey the condition of Maximum Degree of Order. Zvyagin's "condition of homogeneity" applies to homo- and meso-octahedral polytypes, but not to the hetero-octahedral family.

The reason for the derivation of the polytypes mentioned above is to single out, from the theoretically infinite number of periodic polytypes within a given family, those with relatively short periods in the stacking direction, which are most likely to be encountered in investigated specimens. To calculate theoretical single-crystal diffraction patterns is easy, provided that the structure of the single layer is known, and the distribution of intensities can then be used for their identification by simple visual comparison with patterns obtained experimentally (Weiss and Wiewióra 1986). Thus, it is irrelevant which set of polytypes as derived by different authors/schools is used, provided it fulfils its purpose, namely it allows the identification of the polytype. Identification of long-period (non-MDO) polytypes requires special algorithms exploiting the periodicity of the intensity distribution, and this is treated at the end of this chapter.

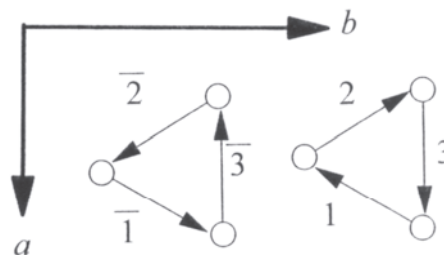
### SYMBOLIC DESCRIPTION OF MICA POLYTYPES

The *indicative* symbolism developed by Ramsdell (1947) is not sufficiently informative for polytypes with more than 2-3 layers in the repeat unit. Because of the rapid increase of the number of possible polytypes with the number of layers in the repeat unit (Mogami et al. 1978; McLarnan 1981) the Ramsdell notation needs augmentation with another, *descriptive* symbolism, from which the structure, including its symmetry, can be reconstructed when the structure of the individual layer is known. Note that a *symbol*, which describes the stacking mode in an individual polytype, consists of a string of *characters*. *Symbolism* is a set of rules governing the construction of symbols. The symbols introduced to describe the stacking mode in mica polytypes can be broadly divided into two types, orientational (giving the absolute orientation of layers with respect to a space-fixed reference) and rotational (giving the relative rotations between pairs of layers).

#### 1) Orientational symbols

1A) **DA symbols.** The first symbolic description is from Dekeyser and Amelinckx (1953), who used a set of vectors and numerical symbols to indicate the *complete* stagger of the layer, defined as the (001) projection of the vector connecting two (OH/F) sites on the two sides of the octahedral sheet. Six characters  $n = 1, 2, 3, \bar{1}, \bar{2}, \bar{3}$  represent the stagger of the layer with respect to a space-fixed reference (Fig. 8). These symbols apply to the homo-octahedral approximation only and therefore cannot correctly describe polytypes containing M2 layers.

**Figure 8.** Symbols used by Dekeyser and Amelinckx (1953) to indicate the orientation of a whole M layer. These symbols can be considered the predecessors of OD and Z symbols (cf. Fig. 4). With respect to the original figure in Dekeyser and Amelinckx (1953), the  $b$  and  $c$  axes have been taken in the opposite direction ( $b$  left instead of right, and  $c$  coming out from the plane instead of into) in accordance with the conventions of the *International Tables for Crystallography*.



1B) **Z symbols.** Zvyagin (1962) introduced a numerical/vectorial description giving the stacking of half-layers, as defined by the interlayer cations and the origin of the  $O$  sheet. This choice made Zvyagin's symbols more general than the symbols introduced previously and also suitable for some other phyllosilicates. However,

Zvyagin changed the notation three times. At first (Zvyagin 1962) he adopted the letters A, B, C, A, B, C to indicate the absolute orientation of the entire layer. He then adopted the characters  $\sigma_i$  and  $\tau_i$  to indicate the intra- and inter-layers displacement of half-layers (Zvyagin 1967). Later (Zvyagin et al. 1979) the Greek letters were abandoned in favor of the corresponding Roman ( $s_i$  and  $t_i$ ) and with a sign inversion between  $\tau_i$  and  $t_i$ , to make homogeneous the definitions of  $s_i$  and  $t_i$ . Finally, the “s” and “t” letters were dropped, leaving only their numerical subscripts as orientation characters (Zhukhlistov et al. 1990). These most recent symbols, and the vectors they represent, are here termed Z symbols and Z vectors. As for DA symbols, Z symbols are oriented symbols linked to a space-fixed, orthohexagonal reference with ( $a$ ,  $b$ ) axes in (001) plane (see also Zvyagin 1985). For non-orthogonal  $N$ -layer polytypes, the period along the  $c$  axis of this reference corresponds to  $3N$  layers (Fig. 9). The vector connecting the origin of the octahedral sheet with the nearest interlayer site and vice versa, always looking at the sequence of layers in the same direction, is called *intralayer displacement*: its projection on the (001) plane has length  $|a|/3$  and corresponds to the vector  $\mathbf{T}_{2j-2}$  (or  $\mathbf{T}_{2j-1}$ , depending on which of the two half-layers is considered) in Figure 2. There are six possible orientations for each half layer, indicated by the six layer-fixed  $a_i$  axes ( $i = 1\sim 6$ ). The projection of the intralayer displacement is indicated by the character  $i = 1, 2, \dots, 6$  when the  $a_i$  axis is parallel to the space-fixed axis  $a$  (Fig. 4). The *interlayer displacement* is the vector giving the relative displacement between two adjacent layers: it can take any of the six orientations 1~6 described for the intralayer vector, and in some other phyllosilicates, also two *independent* orientations corresponding to  $\pm b/3$  (indicated as “+” and “-” respectively), but it can also be a zero vector (indicated as “0”). In micas, owing to the presence of interlayer cations, only the 0 interlayer displacement occurs. The ( $a$ ,  $b$ ) components ( $s_x$ ,  $s_y$ ) of Z vectors are given

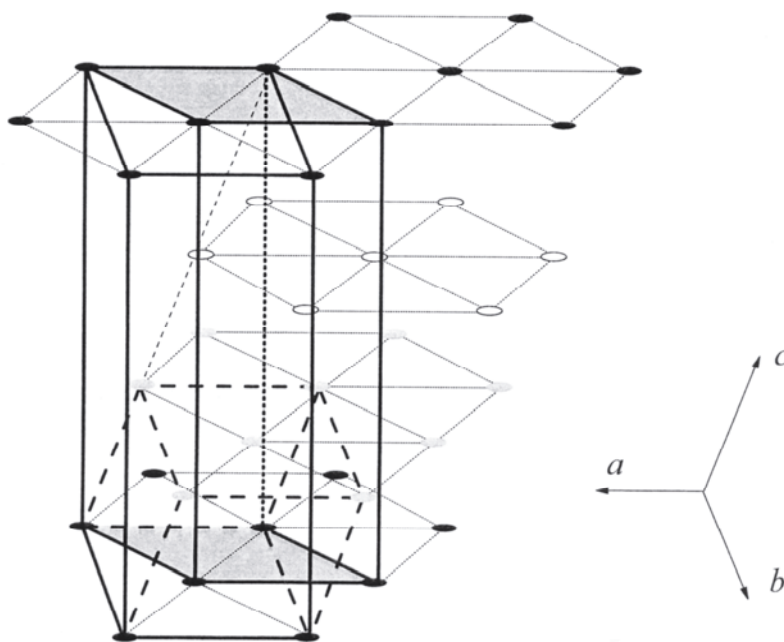


**Figure 9.** The conventional monoclinic cell (dashed lines), the (pseudo)-orthohexagonal cell (solid lines), and the (pseudo)hexagonal cell [(001) base shaded] built overlapping three conventional cells. The scale along  $c$  is compressed (modified after Nespolo et al. 2000a).

**Table 3.** OD symbols and Z symbols and the  $(a, b)$  components of the corresponding orientation vectors.

<i>OD symbol</i>	<i>Z symbol</i>	$(s_x, s_y)$
3	3	(1/3, 0)
2	4	(1/6, 1/6)
1	5	(-1/6, 1/6)
0	6	(-1/3, 0)
5	1	(-1/6, -1/6)
4	2	(1/6, -1/6)
+	+	(0, 1/3)
-	-	(0, -1/3)
0	*	(0, 0)

in Table 3. The complete symbolism, giving the stacking sequence of half layers, is  $ij0kl0mn0\dots$ . For micas containing only M1 layers,  $i=j, k=1, m=n$  etc.; the character 0 can be omitted and a shortened symbol IKM... is obtained (Zhukhlistov et al. 1990). M2 layers always correspond to intralayer displacement of the same parity; opposite parity would in fact produce a trigonal prismatic coordination for the Y cations. The Z vector for each layer corresponds to the (001) projection of a pair of intralayer displacement vectors and it is obtained by summing their  $(s_x, s_y)$  components. For micas built by M1 layers only, this is equivalent to twice the components, namely  $(2s_x, 2s_y)$  (Table 3). Z vectors are thus twice as long as DA stacking vectors (and also SY vectors, described below), and directed in the opposite way. Since  $\pm 2/3$  is translationally equivalent to  $\mp 1/3$ , in practice the  $(a, b)$  components of the Z vectors are the same as those of the intralayer displacements, but with the signs interchanged. The DA and SY stacking vectors are the (001) projections of vectors not passing through a cationic site in the O sheet. On the other hand, Z vectors are the (001) projections of vectors passing through that cationic site. As a consequence, Z vectors can distinguish between M1 and M2 layers, whereas the other two cannot. The latter simply correspond to the vector sum of Z vectors.

The fundamental merit of Z symbols is that they can describe also meso-octahedral polytypes. Their shortcoming is that the symbols describing homo-octahedral mica polytypes are identical with those describing meso-octahedral polytypes consisting of M1 layers, and additional information must be given also. Moreover, in their present form, they cannot handle hetero-octahedral polytypes.

1C) **OD symbols.** The OD school, inspired by Z symbols, derived the most general symbols to describe mica polytypes (Āuroviĉ and Dornberger-Schiff 1979; Dornberger-Schiff et al. 1982; Backhaus and Āuroviĉ 1984; Āuroviĉ et al. 1984; Weiss and Wiewi3ra 1986). These symbols consist of a sequence of characters referring to one period, placed between vertical bars; two lines of characters are used; the first line indicates the packet *orientations*, and the second line the packet-to-packet *displacements*. A dot “.” separating the orientational characters for packets  $p_{2j}$  and  $q_{2j+1}$  indicates the position of Oc layer. The OD symbols are thus expressed:

$$\left| \begin{array}{cccccc} T_0 & \cdot & T_1 & T_2 & \cdot & T_3 & \dots \\ v_{0,1} & & * & & v_{2,3} & * & \dots \end{array} \right|$$

where  $T_j = 0\sim 5$ ,  $v_{2j,2j+1} = T_{2j} + T_{2j+1}$  ( $v$ ,  $T$  are the vectors corresponding to  $v$  and  $T$  characters, and the vector sum is taken *modulo* primitive hexagonal cell), and \* indicates null vector (no displacement) (Fig. 4). Note that the parity of the orientational characters is necessarily opposite to that of the displacement characters. The vector sum of  $v_{2j,2j+1}$  over a complete polytype period (hereafter indicated as  $\Sigma v$ , for shortness) corresponds to the  $c_n$  projection of the  $c$  axis onto the (001) plane and gives the total displacement, which can correspond to the characters "0"~"5", "\*", "+", and "-" (see Tables 3 and 4). In the meso-octahedral family, the  $v_{2j,2j+1}$  characters in the second line are redundant because they follow unequivocally from the  $T_{2j} \cdot T_{2j+1} \cdots$  characters in the first line: simplified symbols  $|T_0 \cdot T_1 \cdot T_2 \cdot T_3 \dots|$  can also be used. In the hetero-octahedral family the chirality of the packets is taken into account: right- and left-handed packets are indicated by a prime (') or double prime ("), respectively, *substituting* the dot, where the chirality is conventionally determined by the direction connecting  $Ma$  to  $Mi$  (Fig. 10) (Durovič et al. 1984). Also in this case the  $v_{2j,2j+1}$  characters in the second line are redundant, and simplified symbols  $T_{2j}' \cdot T_{2j+1}$  or  $T_{2j}'' \cdot T_{2j+1}$  for the individual packet pairs can be used. Although the  $v_{2j,2j+1}$  displacement characters are redundant in both these families, their vector sum  $\Sigma v$ , as shown in the next section, allows the classification of mica polytypes in terms of their reticular features: the complete two-line symbols yield thus additional information. Finally, in the homo-octahedral family, there are only two distinguishable orientations of the packets. This follows from the fact that the Oc layer here is  $H$  centered and it can be attached to the Tet layer so that its *three* equivalent origins can be reached *simultaneously* by the three  $T$  vectors with *even*- or *odd* (*uneven*)- numbered characters, respectively. These two orientations of a packet, differing by a  $180^\circ$  rotation, are indicated by orientational characters  $e$  and  $u$ , respectively. In this case, the first line of characters is redundant and simplified symbols consisting just of the line of *displacement*  $v_{2j,2j+1}$  characters may be sufficient (Dornberger-Schiff et al. 1982).

The OD symbols for the packet orientations were defined with respect to hexagonal axes  $A_1, A_2, A_3$  as indicated in Figure 4. In Table 3 they are described in terms of the  $(a, b)$  orthohexagonal identity periods. The orthohexagonal cell used in the OD literature corresponds to the  $C_2$  setting (Fig. 1). In practice, for the meso-octahedral family, the OD symbols correspond to  $(6-Z)(\text{mod } 6)$ , where  $Z$  are Zvyagin's characters. For the hetero-octahedral family the same numerical relation holds, but the chirality of the packets is considered. For the homo-octahedral family, Zvyagin uses *one* of the three  $e$ - or  $u$ -vectors as representative: 6 or 3, respectively. Going from 0 to 5 instead than from 1 to 6, the OD symbols obey the closure property of the *mod* function. The corresponding OD vectors are disposed in a clockwise sequence, whereas  $Z$  vectors are defined counter-clockwise (Fig. 4), but their crystal chemical basis is the same.

1D) **TS symbols** (Sadanaga and Takeda 1969; Takeda and Sadanaga 1969) give the relative positions of the TS unit layers and are written as a sequence of  $N$  symbols  $L_j(\Delta X_j, \Delta Y_j)$ ,  $j = 1-N$ , where  $L_j$  is the type of layer and  $N$  is the number of layers in the polytype period. Considering two successive repeats of  $N$  layers,  $(\Delta X_j, \Delta Y_j)$  are the  $(a, b)$  components of the vector connecting the origin of the last ( $N$ -th) layer of a repeat and the origin of the  $j$ -th layer of the next repeat (Fig. 2). These symbols respect only the homo-octahedral approximation.

## 2) Rotational symbols

2A) **SY vectors**. Smith and Yoder (1956) described the stacking sequence in a way similar to Dekeyser and Amelinck (1953). The stacking vectors are defined as the (001) projection of the vector connecting two nearest interlayer cations on the two

**Table 4.** Table of vector sums for the nine possible displacement vectors appearing in the structure of most common phyllosilicates. The individual vectors  $\langle v \rangle$  are represented by their respective characters “ $v$ ” and the result of summation should be taken modulo primitive hexagonal cell (*cf.* Fig. 4). These nine vectors form a translation group with vector addition as the group operation.

	OD									Z									
	0	1	2	3	4	5	*	+	-	6	5	4	3	2	5	0	+	-	
0	3	-	1	*	5	+	0	2	4	6	3	-	5	0	1	+	6	4	2
1	-	4	+	2	*	0	1	3	5	1	1	2	+	4	0	6	5	3	1
2	1	+	5	-	3	*	2	0	4	4	2	5	+	1	3	0	4	6	2
3	*	2	-	0	+	4	3	5	1	3	0	4	-	6	+	2	3	1	5
4	5	*	3	+	1	-	4	2	0	4	1	0	3	+	5	-	2	4	6
5	+	0	*	4	-	2	5	1	3	5	+	6	0	2	2	4	1	5	3
*	0	1	2	3	4	5	*	+	-	0	6	5	4	3	2	1	0	+	-
+	4	3	0	5	2	1	+	-	*	+	2	3	6	1	4	5	+	-	0
-	2	5	4	1	0	3	-	*	+	-	4	1	2	5	6	3	-	0	+

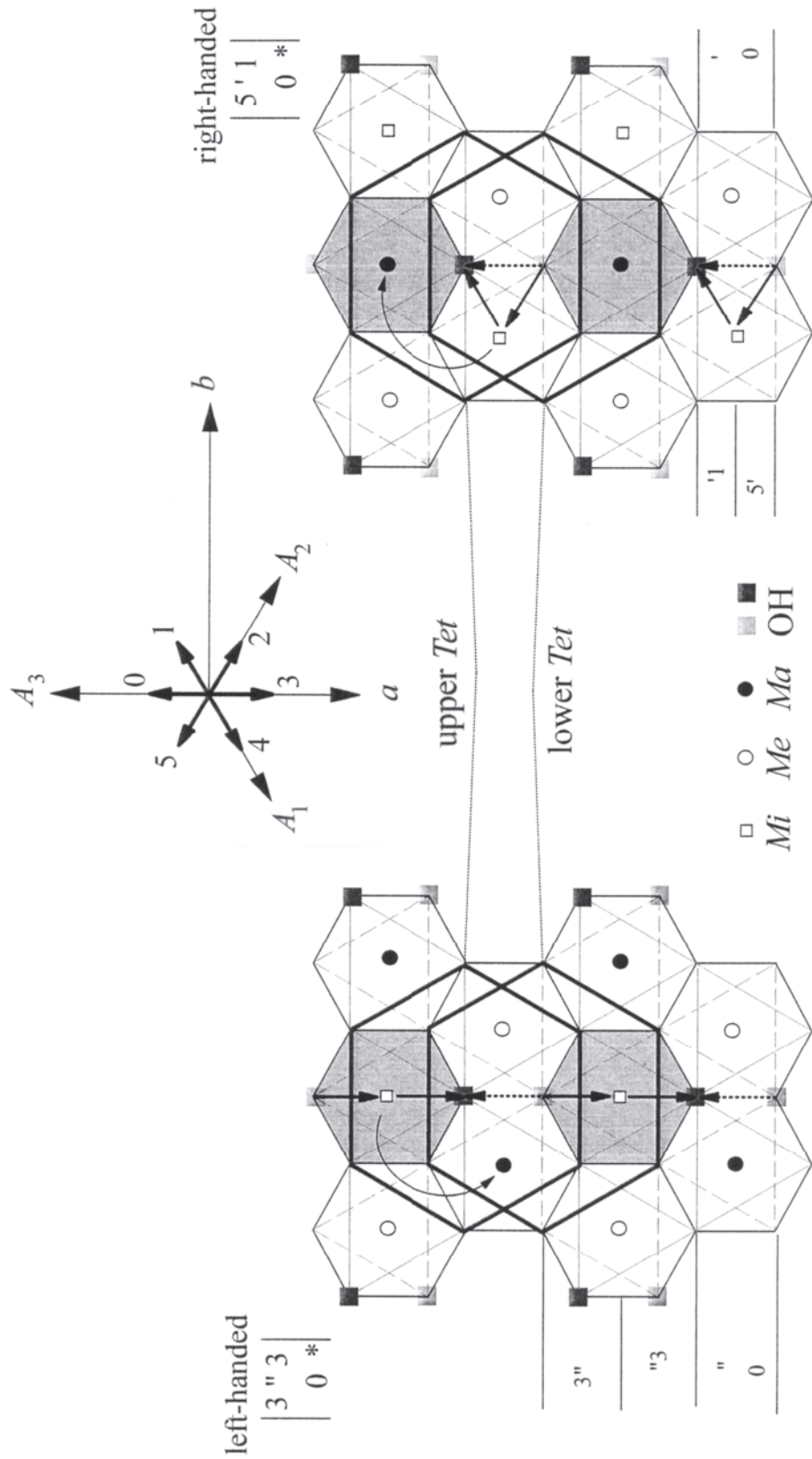


**Figure 10.** Construction of the stacking symbol for hetero-octahedral mica polytypes demonstrated on two one-layer (two-packet) polytypes, through the (001) projection of the Oc layer. Gray squares indicate the position of OH groups (coinciding in the projection to the interlayer cations). Shaded octahedra contain M1 (trans) sites. Thick hexagons are drawn through the lower and upper apical oxygen atoms, as in Durovic et al. (1984, Fig. 5). Thick solid arrows are orientational vectors  $T_{2j}$  and  $T_{2j+1}$ , thick dotted arrows are displacement vectors  $v_{2j,2j+1}$ . The chirality (enantiomorphous hand) is determined by the curved arrow leading from Mi to Ma around the upper OH group: clockwise = right-handed, counter-clockwise = left-handed. Mi and Ma stand for octahedral sites with (Mi)minimal and (Ma)aximal average X-ray scattering power, respectively (modified after Durovic et al. 1984).

sides of a layer. Because interlayer cations and (OH, F) groups overlap in the (001) projection, in practice the methods of Dekeyser and Amelinckx (1953) and of Smith and Yoder (1956) are equivalent; however, Smith and Yoder (1956) did not adopt a symbolic notation. Also these vectors are correct only in the homo-octahedral approximation and cannot thus describe correctly polytypes containing M2 layers.

2B) **RTW symbols.** Ross et al (1966) introduced a numerical description (RTW symbols) giving the relative rotations between successive stacking vectors representing a sequence of M1 layers. This description is the most immediate, although not the most general (it applies to the homo-octahedral approximation only), to describe the mica-polytype stacking mode and to derive all possible mica polytypes with a given number of M1 layers (Takeda 1971; Mogami et al. 1978; McLarnan 1981). However, the method cannot distinguish between M1 and M2 layers. RTW symbols are orientation-free, rotational symbols written as a sequence on  $N$  characters  $A_j = 0, \pm 1, \pm 2, 3$ , the  $j$ -th character giving the rotation angle between  $j$ -th and  $(j+1)$ -th layers as integer multiple of  $60^\circ$ . A RTW symbol corresponds to the difference, with sign inverted, between pairs of displacement OD characters [ $A_j = - (v_{2j,2j+1} - v_{2j-2,2j-1})$ ] or to the difference between pairs of Z characters corresponding to successive M1 layers [ $A_j = +(Z_{2j+1} - Z_{2j-1})$ ]. The opposite sign between OD and Z symbols originates from the fact that Z and RTW symbols are defined counterclockwise, whereas OD symbols are defined clockwise. The closure of the periodicity after  $N$  layers is expressed by the condition (Takeda 1971):

$$\sum_{j=1}^N A_j = 0 \pmod{6} \quad (1)$$

2C) **Thompson's symbols.** Thompson (1981) introduced an operatorial description of mica stacking, in which operators  $N_1$  and  $N_{-1}$  ( $N = 1, 6$ ) produce  $2\pi/N$  counterclockwise ( $N_1$ ) or clockwise ( $N_{-1}$ ) rotation of the M layer. These operators are divided into *dot* [ $N = 1 \pmod{2}$ ] and *cross* operators [ $N = 0 \pmod{2}$ ].

Bailey (1980a,b) gave an alternative description of the polytypism of the micas, by classifying the six possible directions of the stagger of the tetrahedral sheets within a layer (positive and negative directions of the three hexagonal axes in the plane of the layer). The six possible positions of octahedral cations with respect to a space-fixed reference were divided into two groups, labeled I (negative stagger) and II (positive stagger). The first layer of each polytype was kept with tetrahedral stagger along  $-a_1$  (octahedral cation positions I): as a consequence, the axial setting used to derive the polytypes was not the most suitable to identify polytypes from their diffraction pattern, and a final axial transformation is necessary. Subfamily A, subfamily B and mixed-rotation polytypes correspond to sequences of octahedral cations belonging to group I only, to groups I and II alternating, and to groups I and II mixed non-alternating. Bailey's notation cannot distinguish between M1 and M2 layers and is not adopted here. We instead make reference to OD and Z (collectively termed "orientational symbols" when referring to both, for shortness) and to RTW symbols.

### RETICULAR CLASSIFICATION OF POLYTYPES: SPACE ORIENTATION AND SYMBOL DEFINITION

Mica polytypes can belong to five symmetries:  $H$ ,  $T$ ,  $O$ ,  $M$  and  $A$  (Takeda 1971). In both the Pauling and the Trigonal models, the lattice of triclinic polytypes is metrically monoclinic, and the (001) projection of the  $c$  axis, labeled  $\mathbf{c}_n$ , can take three values:  $0$ ,  $|a|/3$ ,  $|b|/3$ , on the basis of which mica polytypes are classified into orthogonal, *Class a* and *Class b* respectively. The number  $N$  of layers building a polytype can be expressed as:



$$N = 3^n(3K+L) \quad (K \text{ and } n \text{ non-negative integers; } L=1 \text{ or } 2) \quad (2)$$

where  $n$  defines the *Series* and  $L$  the *Subclass*;  $K$  is a constant entering in the transformation matrices relating axial settings (Nespolo et al. 1998).

The structural model of each polytype, as described by the stacking vectors, has six possible orientations with respect to the space-fixed ( $a$ ,  $b$ ) axes, each  $60^\circ$  apart. These orientations correspond to one sequence of characters in the RTW symbols, but to six different sequences of orientational symbols, and are in general non-equivalent. The  $\mathbf{c}_n$  projection may correspond to  $\Sigma\mathbf{v} = \langle * \rangle$  (orthogonal polytypes),  $\Sigma\mathbf{v} = \langle 0 \rangle \sim \langle 5 \rangle$  (*Class a* polytypes), or to  $\Sigma\mathbf{v} = \langle + \rangle$  or  $\langle - \rangle$  (*Class b* polytypes), i.e. to  $\mathbf{c}_n = (0, 0)$ ,  $(\pm 1/3, [0, \pm 1/3])$  and  $(0, \pm 1/3)$  respectively. For non-orthogonal polytypes,  $\mathbf{c}_n$  can be reduced to  $(1/3, 0)$  (*Class a*) or  $(0, 1/3)$  (*Class b*) by means of the  $C$ -centering vectors and by rotating the structural model around  $c^*$ . These six orientations can be grouped in the following way (Nespolo et al. 1999d).

1. *Class a polytypes*. Each orientation corresponds to a different  $\mathbf{c}_n$  projection, i.e. to a different character of  $\Sigma\mathbf{v}$ , from  $\langle 0 \rangle$  to  $\langle 5 \rangle$ . Among these, there is only one that corresponds to the  $b$ -unique setting with an obtuse  $\beta$  angle: that with  $\Sigma\mathbf{v} = \langle 0 \rangle$ , i.e.  $\mathbf{c}_n = (1/3, 0)$ .
2. *Class b polytypes*. Three orientations correspond to  $\Sigma\mathbf{v} = \langle + \rangle$ , i.e.  $\mathbf{c}_n = (0, 1/3)$  (acute  $\alpha$  angle) and three others to  $\Sigma\mathbf{v} = \langle - \rangle$ , i.e.  $\mathbf{c}_n = (0, 1/3)$  (obtuse  $\alpha$  angle). The three orientations with the same  $\Sigma\mathbf{v}$  ( $\mathbf{c}_n$ ) are equivalent for triclinic polytypes, but not for monoclinic cases. The symmetry elements are oriented according to an  $a$ -unique setting with  $\alpha$  obtuse. Only one of the three orientations leading to  $\Sigma\mathbf{v} = \langle - \rangle$  agrees with such a requirement.
3. *Orthogonal polytypes*. The six orientations correspond to  $\Sigma\mathbf{v} = \langle * \rangle$ , i.e.  $\mathbf{c}_n = (0, 0)$ , and they are equivalent for hexagonal, trigonal and triclinic polytypes, whereas for orthorhombic and monoclinic polytypes only two orientations, related by  $180^\circ$  rotation around  $c = c^*$  axis, lead to the correct orientation of the symmetry elements.

Because both the reticular features and the OD character are based on the geometry of the layer stacking in polytypes, some relations between the OD and the reticular classifications can be established (Backhaus and Đurovič 1984; Nespolo 1999).

1. **Subfamily A**. These polytypes are described by orientational symbols with characters of the same parity, i.e. by all-even characters in the RTW symbol. They include the three most common MDO polytypes ( $1M$ ,  $2M_1$ ,  $3T$ ) and the great majority of non-MDO polytypes found so far. Successive layers are related by  $2n \times 60^\circ$  rotations; the  $x$  component of the stacking vector of each packet (half-layer) is either always  $+1/3$  (odd orientational parity of characters in the orientational symbols) or always  $-1/3$  (even orientational parity of characters in the orientational symbols). As a consequence, in *Series* 0 [ $n = 0$  in Equation (2), i.e. polytypes with the number of layers not a multiple of 3] the  $x$  component of  $\mathbf{c}_n$  cannot be 0 and these polytypes belong to *Class a*. In *Series* higher than 0, the number of layers building the polytypes is a multiple of 3 and thus  $\Sigma\mathbf{v}$  is  $\langle * \rangle$ ,  $\langle + \rangle$  or  $\langle - \rangle$  (the  $x$  component of  $\mathbf{c}_n$  is always 0). Therefore, these polytypes cannot belong to *Class a*.
2. **Subfamily B**. These polytypes are described by orientational symbols with characters of alternating parity, i.e. by all-odd characters in the RTW symbol. Successive layers are related by  $(2n+1) \times 60^\circ$  rotations. Only polytypes with an even number of layers appear in this subfamily. In addition, because layers with different orientational parity have an opposite  $x$  component of the stacking vector,  $\Sigma\mathbf{v}$  is  $\langle * \rangle$ ,  $\langle + \rangle$  or  $\langle - \rangle$  and it is not possible to have a *Class a* polytype.
3. **Mixed-rotation polytypes**. These polytypes correspond to orientational symbols with

character of different, non-alternating parity and to mixed parity of the characters in the RTW symbol. Because there is no definite rule for the layer orientational parity sequence, the three kinds of polytypes (orthogonal, *Class a*, *Class b*) are possible.

### LOCAL AND GLOBAL SYMMETRY OF MICA POLYTYPES FROM THEIR STACKING SYMBOLS

The main purposes of descriptive stacking symbols are: 1) to uniquely identify a polytype; 2) to enable the reconstruction of the structure of the polytype once the structure of the layer is known; 3) to enable a symmetry analysis of the polytype, not only for the systematic derivation of MDO polytypes but also to determine the symmetry (local and global) of a polytype from its symbol in a purely analytical way – without the need to draw auxiliary pictures (although these may be quite useful to visualize the stacking sequence); and 4) to calculate the Fourier transform of the polytype. It is thus necessary to know how the individual point operations influence the individual characters in the symbol. For mica polytypes, there are 24 point operations constituting the point group  $6/mmm$ . The effect of each of them on the six vectors corresponding to the orientational symbols can be expressed in a general form, e.g., a  $60^\circ$  clockwise rotation converts an OD vector  $\langle j \rangle$  into  $\langle j+1 \rangle$ , or a Z vector  $\langle j \rangle$  into  $\langle j-1 \rangle$ , but as a “working tool” it is more convenient to compile a *table of conversions* to give the results explicitly. Note that the vectors given in Figure 2 and 4 are actually the (001) projections of the intralayer stacking vectors that give the absolute orientations of packets (half-layers in Zvyagin’s concept). The transformation of these projections is almost trivial for  $\tau$ -operations, whereas it must be combined with an inversion for  $\rho$ -operations because the stacking vector must always to point in the same direction, namely along  $+c$ . For example, a  $180^\circ$  rotation around the  $b$  axis (H-M: [ . . . (.) . . 2], ORT :  $2_{[010]}$  in Table 5a) converts a vector  $\langle 0 \rangle$  into vector  $\langle 3 \rangle$  but such a vector would point along  $-c$ . The corresponding vector directed along  $+c$  is  $\langle 0 \rangle$ . It follows that the  $2_{[010]}$  rotation applied to a packet  $p_{2j} = \langle 0 \rangle$  yields a packet  $q_{2j+1} = \langle 0 \rangle$ . Tables 5a and 5b give the conversion rules for OD symbols and Z symbols, respectively. Moreover, a  $\tau$ -operation leaves unchanged the order of the sequence of characters in the orientational symbol, whereas a  $\rho$ -operation inverts it. The effect of the 24 point operations of the point group  $6/mmm$  on the entire orientational symbol is given in Table 6.

#### Derivation of MDO polytypes

The derivation of MDO polytypes for homo-, meso-, and hetero-octahedral micas were described in detail by Backhaus and Āuroviĉ (1984). Therefore, only basic ideas are given here.

The first step is to construct all packet triples compatible with the crystal chemistry. The use of meso-octahedral micas demonstrates the procedure. Let us take an M1 layer and begin with the packet  $p_0$  in the orientation 0 (any other initial orientation could be used). The packet  $q_1$  must then be also in the orientation 0 to preserve M1 layer. The packet-

pair is then  $\left| \begin{array}{c} 0.0 \\ 3 \end{array} \right|$  because the sum of the two orientational vectors  $\langle 0 \rangle + \langle 0 \rangle = \langle 3 \rangle$ , where

$\langle 3 \rangle$  is the displacement vector (*cf.* Fig. 4). A single meso-octahedral packet has the symmetry  $C1m(1)$  but in the following we shall not consider the translations of the layer group. The point group  $m$  has the order 2 and consists of two operations: the identity (an operation of the first sort, whose transformation matrix has determinant +1) and the reflection (an operation of the second sort, whose transformation matrix has determinant -1). Therefore, any transformation of such a packet consists always of *two* operations with

**Table 5a.** Conversion of characters appearing in the OD symbols of mica polytypes. The individual operations are characterized by their extended Hermann-Mauguin (H-M) symbols and by the corresponding operations indexed in orthogonal (ORT)  $C_2$ -setting axes. Cf. Table 1 and Backhaus and Durovic (1984).

$\tau$ -point operations		Character conversion by point operation	$\rho$ -point operations	
H-M	ORT		H-M	ORT
1	1	j: 0 1 2 3 4 5 e u *	$\bar{1}$	$\bar{1}$
$(6)^{-1}$	$(6)^{-1}$	1+j: 1 2 3 4 5 0 u e *	$(\bar{6})^{-1}$	$(\bar{6})^{-1}$
$(3)^{-1}$	$(3)^{-1}$	2+j: 2 3 4 5 0 1 e u *	$(\bar{3})^{-1}$	$(\bar{3})^{-1}$
$(2)^1$	$(2)^1$	3+j: 3 4 5 0 1 2 u e *	$(\bar{2})^1 = m_{(001)}$	$(\bar{2})^1 = m_{(001)}$
$(3)^1$	$(3)^1$	4+j: 4 5 0 1 2 3 e u *	$(\bar{3})^1$	$(\bar{3})^1$
$(6)^1$	$(6)^1$	5+j: 5 0 1 2 3 4 u e *	$(\bar{6})^1$	$(\bar{6})^1$
'_''	'_''		'_''	'_''
"_''	"_''		"_''	"_''
$\tau$ -point operations		Character conversion by point operation	$\rho$ -point operations	
H-M	ORT		H-M	ORT
$[m \dots (\dots)]$	$m_{(1\bar{3}0)}$	5-j: 5 4 3 2 1 0 u e *	$[2 \dots (\dots)]$	$2_{[1\bar{1}0]}$
$[\dots (\dots) m \dots]$	$m_{(1\bar{1}0)}$	4-j: 4 3 2 1 0 5 e u *	$[\dots (\dots) 2 \dots]$	$2_{[3\bar{1}0]}$
$[\dots m (\dots) \dots]$	$m_{(100)}$	3-j: 3 2 1 0 5 4 u e *	$[\dots 2 (\dots) \dots]$	$2_{[100]}$
$[\dots (\dots) m \dots]$	$m_{(110)}$	2-j: 2 1 0 5 4 3 e u *	$[\dots (\dots) 2 \dots]$	$2_{[310]}$
$[\dots m (\dots) \dots]$	$m_{(130)}$	1-j: 1 0 5 4 3 2 u e *	$[\dots 2 (\dots) \dots]$	$2_{[110]}$
$[\dots (\dots) \dots m]$	$m_{(010)}$	-j: 0 5 4 3 2 1 e u *	$[\dots (\dots) \dots 2]$	$2_{[010]}$
'_''	'_''		'_''	'_''
"_''	"_''		"_''	"_''

**Table 5b.** Conversion of characters appearing in the Zvyagin symbols of mica polytypes. The individual operations are characterized by their extended Hermann-Mauguin (H-M) symbols and by the corresponding operations indexed in orthogonal (ORT)  $C_2$ -setting axes. Cf. Table 1 and Zvyagin (1997).

$\tau$ -point operations		Character conversion by point operation	$\rho$ -point operations	
H-M	ORT		H-M	ORT
1	1	j: 6 5 4 3 2 1 0	$\bar{1}$	$\bar{1}$
$(6)^{-1}$	$(6)^{-1}$	5+j: 5 4 3 2 1 6 0	$(\bar{6})^{-1}$	$(\bar{6})^{-1}$
$(3)^{-1}$	$(3)^{-1}$	4+j: 4 3 2 1 6 5 0	$(\bar{3})^{-1}$	$(\bar{3})^{-1}$
$(2)^1$	$(2)^1$	3+j: 3 2 1 6 5 4 0	$(\bar{2})^1 = m_{(001)}$	$(\bar{2})^1 = m_{(001)}$
$(3)^1$	$(3)^1$	2+j: 2 1 6 5 4 3 0	$(\bar{3})^1$	$(\bar{3})^1$
$(6)^1$	$(6)^1$	1+j: 1 6 5 4 3 2 0	$(\bar{6})^1$	$(\bar{6})^1$
$[m \dots (\dots)]$	$m_{(1\bar{3}0)}$	1-j: 1 2 3 4 5 6 0	$[2 \dots (\dots)]$	$2_{[1\bar{1}0]}$
$[\dots (\dots) m \dots]$	$m_{(1\bar{1}0)}$	2-j: 2 3 4 5 6 1 0	$[\dots (\dots) 2 \dots]$	$2_{[3\bar{1}0]}$
$[\dots m (\dots) \dots]$	$m_{(100)}$	3-j: 3 4 5 6 1 2 0	$[\dots 2 (\dots) \dots]$	$2_{[100]}$
$[\dots (\dots) m \dots]$	$m_{(110)}$	4-j: 4 5 6 1 2 3 0	$[\dots (\dots) 2 \dots]$	$2_{[310]}$
$[\dots m (\dots) \dots]$	$m_{(130)}$	5-j: 5 6 1 2 3 4 0	$[\dots 2 (\dots) \dots]$	$2_{[110]}$
$[\dots (\dots) \dots m]$	$m_{(010)}$	-j: 6 1 2 3 4 5 0	$[\dots (\dots) \dots 2]$	$2_{[010]}$

**Table 6.** Transformation rules for OD and Z symbol under the effect of the  $\lambda$ -symmetry operations of the hexagonal syngony.  $\langle i' \rangle, \langle j' \rangle, \dots, \langle p' \rangle$  (OD symbols) and  $\langle i \rangle, \langle j \rangle, \dots, \langle p \rangle$  (Z symbols) are the original symbols. The individual operations are characterized by their extended Hermann-Mauguin (H-M) symbols and by the corresponding operations indexed in orthogonal (ORT)  $C_2$ -setting axes. Cf. Table 1 (modified after Nespolo et al. 1999).

$\tau$ -point operation		effect on OD symbol sequence	effect on Z-symbol sequence
H-M	ORT		
1	1	$\langle i' \rangle, \langle j' \rangle, \dots, \langle p' \rangle$	$\langle i \rangle, \langle j \rangle, \dots, \langle p \rangle$
$(6)^{-1}$	$(6)^{-1}$	$\langle 1+i' \rangle, \langle 1+j' \rangle, \dots, \langle 1+p' \rangle$	$\langle 5+i \rangle, \langle 5+j \rangle, \dots, \langle 5+p \rangle$
$(3)^{-1}$	$(3)^{-1}$	$\langle 2+i' \rangle, \langle 2+j' \rangle, \dots, \langle 2+p' \rangle$	$\langle 4+i \rangle, \langle 4+j \rangle, \dots, \langle 4+p \rangle$
$(2)^1$	$(2)^1$	$\langle 3+i' \rangle, \langle 3+j' \rangle, \dots, \langle 3+p' \rangle$	$\langle 3+i \rangle, \langle 3+j \rangle, \dots, \langle 3+p \rangle$
$(3)^1$	$(3)^1$	$\langle 4+i' \rangle, \langle 4+j' \rangle, \dots, \langle 4+p' \rangle$	$\langle 2+i \rangle, \langle 2+j \rangle, \dots, \langle 2+p \rangle$
$(6)^1$	$(6)^1$	$\langle 5+i' \rangle, \langle 5+j' \rangle, \dots, \langle 5+p' \rangle$	$\langle 1+i \rangle, \langle 1+j \rangle, \dots, \langle 1+p \rangle$
$[m \dots (\cdot) \dots]$	$m_{(1\bar{3}0)}$	$\langle 5-i'' \rangle, \langle 5-j'' \rangle, \dots, \langle 5-p'' \rangle$	$\langle 1-i \rangle, \langle 1-j \rangle, \dots, \langle 1-p \rangle$
$[\dots (\cdot) \dots m \dots]$	$m_{(1\bar{1}0)}$	$\langle 4-i'' \rangle, \langle 4-j'' \rangle, \dots, \langle 4-p'' \rangle$	$\langle 2-i \rangle, \langle 2-j \rangle, \dots, \langle 2-p \rangle$
$[\dots m (\cdot) \dots]$	$m_{(100)}$	$\langle 3-i'' \rangle, \langle 3-j'' \rangle, \dots, \langle 3-p'' \rangle$	$\langle 3-i \rangle, \langle 3-j \rangle, \dots, \langle 3-p \rangle$
$[\dots (\cdot) m \dots]$	$m_{(110)}$	$\langle 2-i'' \rangle, \langle 2-j'' \rangle, \dots, \langle 2-p'' \rangle$	$\langle 4-i \rangle, \langle 4-j \rangle, \dots, \langle 4-p \rangle$
$[m \dots (\cdot) \dots]$	$m_{(130)}$	$\langle 1-i'' \rangle, \langle 1-j'' \rangle, \dots, \langle 1-p'' \rangle$	$\langle 5-i \rangle, \langle 5-j \rangle, \dots, \langle 5-p \rangle$
$[\dots (\cdot) \dots m]$	$m_{(010)}$	$\langle -i'' \rangle, \langle -j'' \rangle, \dots, \langle -p'' \rangle$	$\langle -i \rangle, \langle -j \rangle, \dots, \langle -p \rangle$

$\rho$ -point operation		effect on OD symbol sequence	Effect on Z-symbol sequence
H-M	ORT		
$\bar{1}$	$\bar{1}$	$\langle p'' \rangle, \dots, \langle j'' \rangle, \langle i'' \rangle$	$\langle p \rangle, \dots, \langle j \rangle, \langle i \rangle$
$(\bar{6})^{-1}$	$(\bar{6})^{-1}$	$\langle 1+p'' \rangle, \dots, \langle 1+j'' \rangle, \langle 1+i'' \rangle$	$\langle 5+p \rangle, \dots, \langle 5+j \rangle, \langle 5+i \rangle$
$(\bar{3})^{-1}$	$(\bar{3})^{-1}$	$\langle 2+p'' \rangle, \dots, \langle 2+j'' \rangle, \langle 2+i'' \rangle$	$\langle 4+p \rangle, \dots, \langle 4+j \rangle, \langle 4+i \rangle$
$(\bar{2})^1 = m_{(001)}$	$(\bar{2})^1 = m_{(001)}$	$\langle 3+p'' \rangle, \dots, \langle 3+j'' \rangle, \langle 3+i'' \rangle$	$\langle 3+p \rangle, \dots, \langle 3+j \rangle, \langle 3+i \rangle$
$(\bar{3})^1$	$(\bar{3})^1$	$\langle 4+p'' \rangle, \dots, \langle 4+j'' \rangle, \langle 4+i'' \rangle$	$\langle 2+p \rangle, \dots, \langle 2+j \rangle, \langle 2+i \rangle$
$(\bar{6})^1$	$(\bar{6})^1$	$\langle 5+p'' \rangle, \dots, \langle 5+j'' \rangle, \langle 5+i'' \rangle$	$\langle 1+p \rangle, \dots, \langle 1+j \rangle, \langle 1+i \rangle$
$[2 \dots (\cdot) \dots]$	$2_{[1\bar{1}0]}$	$\langle 5-p' \rangle, \dots, \langle 5-j' \rangle, \langle 5-i' \rangle$	$\langle 1-p \rangle, \dots, \langle 1-j \rangle, \langle 1-i \rangle$
$[\dots (\cdot) \dots 2 \dots]$	$2_{[3\bar{1}0]}$	$\langle 4-p' \rangle, \dots, \langle 4-j' \rangle, \langle 4-i' \rangle$	$\langle 2-p \rangle, \dots, \langle 2-j \rangle, \langle 2-i \rangle$
$[\dots 2 (\cdot) \dots]$	$2_{[100]}$	$\langle 3-p' \rangle, \dots, \langle 3-j' \rangle, \langle 3-i' \rangle$	$\langle 3-p \rangle, \dots, \langle 3-j \rangle, \langle 3-i \rangle$
$[\dots (\cdot) \dots 2 \dots]$	$2_{[310]}$	$\langle 2-p' \rangle, \dots, \langle 2-j' \rangle, \langle 2-i' \rangle$	$\langle 4-p \rangle, \dots, \langle 4-j \rangle, \langle 4-i \rangle$
$[2 \dots (\cdot) \dots]$	$2_{[110]}$	$\langle 1-p' \rangle, \dots, \langle 1-j' \rangle, \langle 1-i' \rangle$	$\langle 5-p \rangle, \dots, \langle 5-j \rangle, \langle 5-i \rangle$
$[\dots (\cdot) \dots 2]$	$2_{[010]}$	$\langle -p' \rangle, \dots, \langle -j' \rangle, \langle -i' \rangle$	$\langle -p \rangle, \dots, \langle -j \rangle, \langle -i \rangle$

the above properties. Accordingly, in the packet pair  $\left| \begin{smallmatrix} 0,0 \\ 3 \end{smallmatrix} \right|$  the two packets are related simultaneously with two  $\rho$ -operations, and a look at Table 5a shows that these, converting 0. into .0 and 3 into itself are  $[. . . (.) . . 2] \equiv 2_{[010]}$  and an inversion. The packet pair has thus the point symmetry  $2/m$ .

The packet triples  $p_0q_1p_2$  compatible with the Trigonal model in the subfamily A are  $\left| \begin{smallmatrix} 0,0,0 \\ 3^* \end{smallmatrix} \right|$ ,  $\left| \begin{smallmatrix} 0,0,2 \\ 3^* \end{smallmatrix} \right|$  plus its enantiomorphous  $\left| \begin{smallmatrix} 0,0,4 \\ 3^* \end{smallmatrix} \right|$ . The two  $0_2\tau$ -operations converting  $p_0$  into  $p_2$  are in the first case (Table 5a) a translation (isogonal with the identity) and a glide operation (isogonal with  $[. . . (.) . m_{(010)}]$ ). A continuation of any of these  $\tau$ -operations leads to the same string  $\dots \begin{smallmatrix} 0,0 & 0,0 & 0,0 & 0,0 \\ 3^* & 3^* & 3^* & 3^* \end{smallmatrix} \dots$  because any of them converts also displacement characters 3 in the same way. This string has modulus  $\left| \begin{smallmatrix} 0,0 \\ 3 \end{smallmatrix} \right|$ , the vector  $\langle 3 \rangle$  is the interlayer vector of this one-layer monoclinic polytype. However, because  $\langle 3 \rangle = +\mathbf{a}/3$  (acute  $\beta$  angle), it must be re-oriented by a rotation of  $180^\circ$  around  $\mathbf{c}^*$  to bring it into the standard, second setting (obtuse  $\beta$  angle). Evidently, this can be made (Table 5a) by adding 3 to all characters, thus  $\left| \begin{smallmatrix} 3,3 \\ 0 \end{smallmatrix} \right|$  is obtained. The basis vectors of this  $1M$  polytype with symmetry  $C12/m1$ , are  $\mathbf{a}$ ,  $\mathbf{b}$ ,  $\mathbf{c}_0 - \mathbf{a}/3$ , where  $\mathbf{c}_0$  is a vector perpendicular to the layer planes with length corresponding to the "layer width" (e.g., a distance between two closest planes of interlayer cations).

The two  $0_2\tau$ -operations for the triple  $\begin{smallmatrix} 0,0,2 \\ 3^* \end{smallmatrix}$  are (Table 5a) a clockwise three-fold screw rotation (first sort operation, isogonal with  $(3)^{-1} \equiv 3_{[001]}$ ) and a glide operation (second sort operation, isogonal with  $[. . . (.) m . .] \equiv m_{(110)}$ ). A continuation of the  $(3)^{-1}$ , through a step-by step application onto the characters in the starting triple, converts  $0 \rightarrow 2$ , then  $2 \rightarrow 4$  and  $4 \rightarrow 0$  but also  $3 \rightarrow 5$ ,  $5 \rightarrow 1$  and  $1 \rightarrow 3$ , which closes the period. The resulting symbol  $\left| \begin{smallmatrix} 0,0 & 2,2 & 4,4 \\ 3^* & 5^* & 1^* \end{smallmatrix} \right|$  characterizes a three-layer, trigonal  $3T$  polytype with symmetry  $P3_212$  and basis vectors  $\mathbf{a}_1$ ,  $\mathbf{a}_2$ ,  $3\mathbf{c}_0$ . A continuation of  $[. . . (.) m . .] \equiv m_{(110)}$  converts  $0 \rightarrow 2$  but then  $2 \rightarrow 0$ , and  $3 \rightarrow 5$ ,  $5 \rightarrow 3$  which closes the period. The symbol  $\left| \begin{smallmatrix} 0,0 & 2,2 \\ 3^* & 5^* \end{smallmatrix} \right|$  describes a two-layer monoclinic polytype (glide operation is the global operation here) with an interlayer vector equal to the sum of the two displacement vectors  $\langle 3 \rangle + \langle 5 \rangle = \langle 4 \rangle$  (cf. Fig. 4). Also this polytype must be clockwise rotated by  $120^\circ$ , by adding 2 to all characters, to bring it into the standard setting. The final form is  $\left| \begin{smallmatrix} 2,2 & 4,4 \\ 5^* & 1^* \end{smallmatrix} \right|$ , the  $2M_1$  polytype with symmetry  $C12/c1$  and basis vectors  $\mathbf{a}$ ,  $\mathbf{b}$ ,  $2\mathbf{c}_0 - \mathbf{a}/3$ .

The packet triple  $\begin{smallmatrix} 0,0,4 \\ 3^* \end{smallmatrix}$ , enantiomorphous to the previous example, yields analogous results. The continuation of the  $(3)^1$  gives string  $\left| \begin{smallmatrix} 0,0 & 4,4 & 2,2 \\ 3^* & 1^* & 5^* \end{smallmatrix} \right|$ , a  $3T$  polytype with symmetry  $P3_112$ , the enantiomorphous counterpart to  $P3_212$ . The continuation of  $[. . . (.) . m . .] \equiv m_{(\bar{1}\bar{1}0)}$  gives a preliminary symbol  $\left| \begin{smallmatrix} 0,0 & 4,4 \\ 3^* & 1^* \end{smallmatrix} \right|$  and, after re-orientation by an anti-clockwise rotation by  $120^\circ$ ,  $\left| \begin{smallmatrix} 4,4 & 2,2 \\ 1^* & 5^* \end{smallmatrix} \right|$ , which is the same  $2M_1$  polytype, just with another choice of origin on the glide plane.

This example is instructive: from a pair of packet triples which are enantiomorphous to each other, we obtain, in general, *three* non-congruent MDO polytypes. Two of them, generated by first-sort operations, contain only packet triples of the one or of the other kind, and these two polytypes form an enantiomorphous pair. The third polytype, generated by second-sort operations, contains both kinds of packet triples, regularly alternating, and it is thus obtained twice in the process of the derivation of MDO



The inversions valid for each packet pair  $p_{2j} q_{2j+1}$  are only local operations. If a string of characters corresponds to a centrosymmetric polytype, then this string, starting and ending with the same character(s), read forwards and backwards, must remain the same. This is not the case in polytype  $3T$ .

Let us now consider the meso-octahedral MDO polytype  $2M_1$  derived above, already in the standard orientation  $\left| \begin{smallmatrix} 4.4 & 2.2 \\ 1 & * 5 * \end{smallmatrix} \right|$ . The only non-trivial  $\tau$ -operation here is the glide operation isogonal with  $[\dots(\dots)m]$ , the local mirror reflections hold only for individual  $M_1$  layers as in the previous case, and also other  $\tau$ -operations are local. On the other hand, this polytype is centrosymmetric. This becomes evident if we write down an extended string of characters so that it will contain an *odd* number of packet pairs  $pq$ .

$$\dots \begin{array}{cccccccc} 4.4 & 2.2 & 4.4 & 2.2 & 4.4 & 2.2 & 4.4 & \dots \\ 1 & * & 5 & * & 1 & * & 5 & * & 1 \end{array} \dots$$

This symbolism remains the same when read forwards and backwards. In a way similar to the above, also all the two-fold rotations  $[\dots(\dots)2]$  can convert any  $q_{2j+1}$  into  $p_{2j+2}$  and are global:  $2 \rightarrow 4$ ,  $4 \rightarrow 2$ ,  $5 \rightarrow 1$ ,  $1 \rightarrow 5$ . The other two-fold rotations, converting any  $p_{2j}$  into  $q_{2j+1}$ , remain local. The space-group type of this polytype is thus  $C12/c1$ , taking into account the  $C$ -centering with respect to the orthogonal axes  $a$ ,  $b$ .

As an example of a polytype containing also  $M_2$  layers, we consider the meso-octahedral polytype identified by the OD symbol  $|2.4 \ 0.0|$  ( $Z$  symbol 420660). The extended string of characters containing an odd number of packet pairs is:

$$\dots \begin{array}{cccccccc} 2.4 & 0.0 & 2.4 & 0.0 & 2.4 & 0.0 & 2.4 & \dots \\ 3 & * & 3 & * & 3 & * & 3 & * & 3 \end{array} \dots$$

from which it clearly appears that the polytype is non-centrosymmetric. The only global  $\tau$ -operation is the trivial  ${}_{04}\tau$  translation (and its multiples) corresponding to the identity period. The packet pair  $\left| \begin{smallmatrix} 2.4 \\ 3 \end{smallmatrix} \right|$  has no local  $\tau$ -operations, but  ${}_{01}[\dots(\dots)2] \equiv 2_{[010]}$  as a local  $\rho$ -operation. The  $\lambda$ -symmetry is  $C12(1)$  and the pair of packets corresponds to an  $M_2$  layer. Instead, as seen in the example of  $3T$ , the packet pair  $\left| \begin{smallmatrix} 0.0 \\ 3 \end{smallmatrix} \right|$  has  $[\dots(\dots)m] \equiv m_{(010)}$  as a local  $\tau$ -operation, and  ${}_{23}[\bar{1}]$  and  ${}_{23}[\dots(\dots)2] \equiv 2_{[010]}$  as local  $\rho$ -operations. The  $\lambda$ -symmetry is  $C12/m(1)$  and the pair of packets corresponds to a  $M_1$  layer. The only global  $\rho$ -operation for the polytype is  $[\dots(\dots)2] \equiv 2_{[010]}$  located at both the  $Oc$  layers. The space-group type is  $C2$ .

The complete analysis for the 8 meso-octahedral polytypes of *Class a* with period up to 2 layers is given in Table 8.





Table 7 (continued).

Homomorphic MDO group	subfamily A			subfamily B			
	Ramsdell symbol	OD symbol		Ramsdell symbol	OD symbol		
		Homo	Hetero		Homo	Meso	Hetero
V					$\begin{pmatrix}  0.0.5.5 & 4.4 & 3.3 & 2.2 & 1.1  \\  3 * 2 * 1 * 0 * 5 * 4 *  \end{pmatrix}$	$\begin{pmatrix}  0^{\circ}0.1^{\circ}1^{\circ}2^{\circ}2.3^{\circ}3.4^{\circ}4.5^{\circ}  \\  0^{\circ}5^{\circ}5^{\circ}4^{\circ}4.3^{\circ}3.2^{\circ}2.1^{\circ}1^{\circ}  \end{pmatrix}$	
					$\begin{pmatrix}  0.0.1.1 & 2.2 & 3.3 & 4.4 & 5.5  \\  3 * 4 * 5 * 0 * 1 * 2 *  \end{pmatrix}$	$\begin{pmatrix}  0^{\circ}0.1^{\circ}1^{\circ}2^{\circ}2.3^{\circ}3.4^{\circ}4.5^{\circ}  \\  0^{\circ}5^{\circ}5^{\circ}4^{\circ}4.3^{\circ}3.2^{\circ}2.1^{\circ}1^{\circ}  \end{pmatrix}$	
					$\begin{pmatrix}  4.2.3.1 & 2.0 & 1.5 & 0.4 & 5.3  \\  3 * 2 * 1 * 0 * 5 * 4 *  \end{pmatrix}$	$\begin{pmatrix}  4^{\circ}2.3^{\circ}1^{\circ}2^{\circ}0.1^{\circ}5^{\circ}0^{\circ}4.5^{\circ}3^{\circ}  \\  (2^{\circ}4.3^{\circ}5^{\circ}4^{\circ}0^{\circ}5^{\circ}1^{\circ}0^{\circ}2.1^{\circ}3^{\circ})  \end{pmatrix}$	
			6H	$\begin{pmatrix}  e.e.u.u & e.e.u.u & e.e.u.u  \\  3 * 2 * 1 * 0 * 5 * 4 *  \end{pmatrix}$	$\begin{pmatrix}  e.e.u.u & e.e.u.u & e.e.u.u  \\  3 * 4 * 5 * 0 * 1 * 2 *  \end{pmatrix}$	$\begin{pmatrix}  2.4.1.3 & 0.2 & 5.1 & 4.0 & 3.5  \\  3 * 2 * 1 * 0 * 5 * 4 *  \end{pmatrix}$	$\begin{pmatrix}  2^{\circ}4.1^{\circ}3^{\circ}0^{\circ}2.5^{\circ}1.4^{\circ}0.3^{\circ}5^{\circ}  \\  (4^{\circ}2.5^{\circ}3^{\circ}0^{\circ}4.1^{\circ}5^{\circ}2^{\circ}0.3^{\circ}1^{\circ})  \end{pmatrix}$
					$\begin{pmatrix}  4.2.5.3 & 0.4 & 1.5 & 2.0 & 3.1  \\  3 * 4 * 5 * 0 * 1 * 2 *  \end{pmatrix}$	$\begin{pmatrix}  4^{\circ}2.5^{\circ}3^{\circ}0^{\circ}4.1^{\circ}5^{\circ}2^{\circ}0.3^{\circ}1^{\circ}  \\  (4^{\circ}2.5^{\circ}3^{\circ}0^{\circ}4.1^{\circ}5^{\circ}2^{\circ}0.3^{\circ}1^{\circ})  \end{pmatrix}$	
			Non-MDO		$\begin{pmatrix}  4.2.1^{\circ}3.2^{\circ}0.5^{\circ}1.0^{\circ}4.3^{\circ}5^{\circ}  \\  (2^{\circ}4.5^{\circ}3.4^{\circ}0.1^{\circ}5^{\circ}0^{\circ}2.3^{\circ}1^{\circ})  \end{pmatrix}$	$\begin{pmatrix}  4^{\circ}2.1^{\circ}3.2^{\circ}0.5^{\circ}1.0^{\circ}4.3^{\circ}5^{\circ}  \\  (2^{\circ}4.5^{\circ}3.4^{\circ}0.1^{\circ}5^{\circ}0^{\circ}2.3^{\circ}1^{\circ})  \end{pmatrix}$	

**Table 8.** The analysis of the local (see Tables 5a and 5b) and global (see Table 6) symmetry of the eight Class *a* meso-octahedral polytypes with period up to two layers. For the derivation of the independent polytypes see Backhaus and Durovič (1984) and Zvyagin (1997). The corresponding Ramsdell symbols apply to the homo-octahedral polytypes obtainable from the relation of homomorphy. The layer groups and space-group types are given in the Trigonal model: the possibility of symmetry reduction to a subgroup in the real structures should always be taken into account.

OD-Symbol (#) = MDO	3.3 0 * (#)	5.1 0 * (#)	2.4 4.2 3 * 3 * (#)	2.4 0.0 3 * 3 * (#)	4.4 2.2 1 * 5 * (#)	0.2 4.0 1 * 5 * (#)	4.0 2.0 5 * 1 * (#)	2.0 2.2 1 * 5 * (#)
Z-Symbol	330	150	420240	420660	220440	640260	260460	460440
$P_{2n}Q_{2n+1}$ $\sigma$ - $\rho$ -operation	$2_{[010]}$ , $\bar{1}$	$2_{[010]}$ , $\bar{3}^{-1(a)}$	$2_{[010]}$ , $\bar{3}^{-1(a)}$	$2_{[010]}$ , $\bar{3}^{-1(a)}$	$2_{[310]}$ , $\bar{1}$	$2_{[310]}$ , $\bar{3}^{-1(a)}$	$2_{[310]}$ , $\bar{3}^{-1(a)}$	$2_{[310]}$ , $\bar{3}^{1(a)}$
$P_{2n}$ $\tau$ -operation	$m_{(010)}$	$m_{(1\bar{1}0)}$	$m_{(1\bar{1}0)}$	$m_{(1\bar{1}0)}$	$m_{(110)}$	$m_{(010)}$	$m_{(110)}$	$m_{(1\bar{1}0)}$
$Q_{2n+1}$ $\tau$ -operation	$m_{(010)}$	$m_{(110)}$	$m_{(110)}$	$m_{(110)}$	$m_{(110)}$	$m_{(1\bar{1}0)}$	$m_{(010)}$	$m_{(010)}$
$P_{2n}Q_{2n+1}$ type of layer	M1	M2	M2	M2	M1	M2	M2	M2
$P_{2n}Q_{2n+1}$ $\lambda$ -symmetry	$C12/m(1)$	$C12(1)$	$C12(1)$	$C12(1)$	$C12/m(1)$	$C12(1)$	$C12(1)$	$C12(1)$
$P_{2n+2}Q_{2n+3}$ $\sigma$ - $\rho$ -operation	$C12/m(1)$	$2_{[010]}$ , $\bar{3}^{1(a)}$	$2_{[010]}$ , $\bar{3}^{1(a)}$	$2_{[010]}$ , $\bar{1}$	$2_{[310]}$ , $\bar{1}$	$2_{[310]}$ , $\bar{3}^{-1(a)}$	$2_{[310]}$ , $\bar{3}^{1(a)}$	$2_{[310]}$ , $\bar{1}$
$P_{2n+2}$ $\tau$ -operation		$m_{(110)}$	$m_{(110)}$	$m_{(010)}$	$m_{(1\bar{1}0)}$	$m_{(110)}$	$m_{(1\bar{1}0)}$	$m_{(1\bar{1}0)}$
$Q_{2n+3}$ $\tau$ -operation		$m_{(1\bar{1}0)}$	$m_{(1\bar{1}0)}$	$m_{(010)}$	$m_{(1\bar{1}0)}$	$m_{(010)}$	$m_{(010)}$	$m_{(1\bar{1}0)}$
$P_{2n+2}Q_{2n+3}$ type of layer		M2	M2	M1	M1	M2	M2	M1
$P_{2n}Q_{2n+1}$ $\lambda$ -symmetry		$C12(1)$	$C12(1)$	$C12/m(1)$	$C12/m(1)$	$C12(1)$	$C12(1)$	$C12/m(1)$
Global $\rho$ -operation	$2_{[010]}$ , $\bar{1}$	$2_{[010]}$	$2_{[010]}$ , $\bar{1}$	$2_{[010]}$	$2_{[010]}$ , $\bar{1}$	$2_{[010]}$	-----	-----
Location	$P_{2n}Q_{2n+1}$ $Q_{2n+1}P_{2n+2}$	$P_{2n}Q_{2n+1}$ $Q_{2n+1}P_{2n+2}$	$P_{2n}Q_{2n+1}(2_{[010]})$ $P_{2n+2}Q_{2n+3}(2_{[010]})$ $Q_{2n+1}P_{2n+2}(\bar{1})$ $Q_{2n+1}P_{2n+3}(\bar{1})$	$P_{2n}Q_{2n+1}$ $P_{2n+2}Q_{2n+3}$	$Q_{2n+1}P_{2n}$ $Q_{2n+1}P_{2n+2}$	$Q_{2n+1}P_{2n}$ $Q_{2n+1}P_{2n+2}$	-----	-----
Global $\tau$ -operations	$m_{(010)}$ , $02t$	$02t$	$C_{(010)}$ , $04t$	$04t$	$C_{(010)}$ , $04t$	$04t$	$C_{(010)}$ , $04t$	$04t$
Space-group type	$C2/m$	$C2$	$C2/c$	$C2$	$C2/c$	$C2$	$Cc$	$C1$
RTW symbol <sup>(a)</sup>	0							$\bar{2}2$
Ramsdell symbol <sup>(b)</sup>	1M							$2M_1$

<sup>(a)</sup> These  $\sigma$ - $\rho$  operations are coincidence operations (one-way movement) and not local symmetry operations.

<sup>(b)</sup> Symbols for the homo-octahedral polytypes homomorphic to the meso-octahedral polytypes listed in this table.

### RELATIONS OF HOMOMORPHY AND CLASSIFICATION OF MDO POLYTYPES

Polytypes are usefully classified not only within the same family, but also between different families. On the basis of the number of layers and of the parity of the corresponding characters in the orientational symbols, several meso-octahedral polytypes can be related to one homo-octahedral polytype; similarly, taking into account the chirality of the packets, several hetero-octahedral polytypes can be related to one meso-octahedral polytype. In mathematics, a  $n \rightarrow 1$  relation is a homomorphism, of which the  $1 \rightarrow 1$  relation (isomorphism) is a special case: the  $n \rightarrow 1$  relation of polytypes of different families is hence termed *relations of homomorphy*.

The recognition of such relations is also of practical importance. For instance, if during the refinement of a mica structure the homo-octahedral model fails, only the choice between the related meso- or hetero-octahedral models has to be made. All such polytypes have *the same framework of all atoms except those octahedrally coordinated*. Therefore, they have identical or very similar basis vectors, and the space-group type of the homo-octahedral polytype is their common supergroup. Also their diffraction patterns are closer to one another than to those of other polytypes: the geometry in reciprocal space is virtually the same and also the distribution of intensities is very similar owing to the fact that the framework of non-octahedral atoms in an “average” mica represents about 70 % of the total diffraction power.

The relations of homomorphy can be easily revealed by analyzing the OD symbols (Ďurovič et al. 1984):

- 1) by substituting the primes (') or double primes (") in the symbols of hetero-octahedral polytypes with dots (.), the corresponding meso-octahedral polytypes are obtained;
- 2) by substituting the  $T_j$  orientational characters in the symbols of meso-octahedral polytypes with “e” (for “even”) or “u” (for “uneven”), the corresponding homo-octahedral polytypes are obtained;
- 3) the relation of homomorphy between hetero- and homo-octahedral polytypes is obtained by combining steps 1) and 2);
- 4) some of the hetero-octahedral MDO polytypes are in relation of homomorphy with non-MDO meso-octahedral polytypes, but the further homomorphy to the homo-octahedral family yields again MDO polytypes (for details, see Ďurovič et al. 1984).

Note that the relations of homomorphy can, in some cases, make two or more sub-periods identical although they are different in the original polytype: as a result, polytypes with a *different periodicity* can be in homomorphy. As an example, let us consider the meso-octahedral polytypes of *Class a* given in Table 8. Of the six 2-layer polytypes, the following four are homomorphous with the homo-octahedral  $2M_1$  polytype.

$$\left| \begin{array}{cc} 4.4 & 2.2 \\ 1 & * 5 * \end{array} \right|, \left| \begin{array}{cc} 0.2 & 4.0 \\ 1 & * 5 * \end{array} \right|, \left| \begin{array}{cc} 4.0 & 2.0 \\ 5 & * 1 * \end{array} \right|, \left| \begin{array}{cc} 2.0 & 2.2 \\ 1 & * 5 * \end{array} \right|$$

In fact, the relation of homomorphy gives for each:  $\left| \begin{array}{ccc} e & e & e \\ 1 & * & 5 * \end{array} \right|$ , for which the shortened symbol is |15|. The other two polytypes ( $\left| \begin{array}{ccc} 2.4 & 4.2 \\ 3 & * & 3 * \end{array} \right|$  and  $\left| \begin{array}{ccc} 2.4 & 0.0 \\ 3 & * & 3 * \end{array} \right|$ ), however, are

homomorphous with  $\begin{vmatrix} e & e & e & e \\ 3 & * & 3 & * \end{vmatrix}$ . In the homo-octahedral family, this polytype has 1-layer periodicity, with a shortened symbol  $|3|$ , and this corresponds to  $1M$  rotated by  $180^\circ$  about  $c^*$  (Fig. 11). This apparent reduction of periodicity occurs whenever: 1) the sequence of  $\mathbf{v}_{2j,2j+1}$  displacement vectors of a meso-octahedral polytype contains two or more identical sub-periods, which are different for  $\mathbf{T}_{2j}, \mathbf{T}_{2j+1}$  orientations of the packets; 2) the sequence of  $\mathbf{T}_{2j}, \mathbf{T}_{2j+1}$  orientation vectors of a hetero-octahedral polytype contains two or more sub-periods which differ only in the chirality of the packets.

The relations of homomorphy in mica structures are summarized in Table 7. Full symbols are given for homo- and meso-octahedral polytypes, shortened symbols (the line of orientational characters) – for hetero-octahedral polytypes. The reason for the somewhat unusual layout of this table is related to the fact that two out of the six homo-octahedral MDO polytypes,  $1M$  and  $2O$ , have *the same projection normal to*  $[010]$  (YZ projection). Thus, for the framework of the non-octahedral atoms in the homo-octahedral MDO polytypes (and also for the corresponding homo-octahedral approximations), there exist *five* different YZ projections labeled by Roman numbers I to V in the first column of Table 7. The significance of the YZ projections will be explained below in the section “Identification of MDO polytypes”.

As an example for the relations of homomorphy, let us take the hetero-octahedral polytype  $\begin{vmatrix} 2'4 & 0'2 & 4'0 \\ 3 & * & 1 * 5 * \end{vmatrix}$  (subfamily A). This polytype is homomorphous to the meso-octahedral polytype  $\begin{vmatrix} 2.4 & 0.2 & 4.0 \\ 3 & * & 1 * 5 * \end{vmatrix}$  and this, in turn, is homomorphous to the homo-octahedral polytype  $3T \begin{vmatrix} e & e & e & e & e & e \\ 3 & * & 1 * 5 * \end{vmatrix}$ : all belong to the MDO group I. The two polytypes in the hetero- and meso-octahedral families are constructed of M2 layers. However, in the homo-octahedral family, the distinction between M1 and M2 layers becomes meaningless: the information about the type of layer is thus lost when applying the relation of homomorphy down to the homo-octahedral family.

From the examples above it is evident that: 1) the homo-octahedral approximation corresponds to applying to a polytype the relation of homomorphy; 2) in micas, the classical Ramsdell notation rigorously applies to homo-octahedral polytypes only.

### BASIC STRUCTURES AND POLYTYPOIDS. SIZE LIMIT FOR THE DEFINITION OF “POLYTYPE”

The term *polytype* implies that there is a *family* of structures to which the polytype belongs. The original idea of Baumhauer (1912, 1915), who introduced the term *polytypism*, was that the individual members of a family consist of identical layers and differ only in their stacking mode.

Since that time, different views concerning the notion of polytypism were expressed, but the present official definition recommended by the *Ad-hoc* Committee on the Nomenclature of Disordered, Modulated and Polytype Structures (Guinier et al. 1984) is very close to the original concept of Baumhauer. According to this definition, “... an element or compound is polytypic if it occurs in several structural modifications, each of which can be regarded as built up by stacking layers of (nearly) identical structure and composition, and if the modifications differ only in their stacking sequence. Polytypism is a special case of polymorphism: the two-dimensional translations within the layers are essentially preserved”. The *Ad-hoc* Committee, however, admitted that this definition is

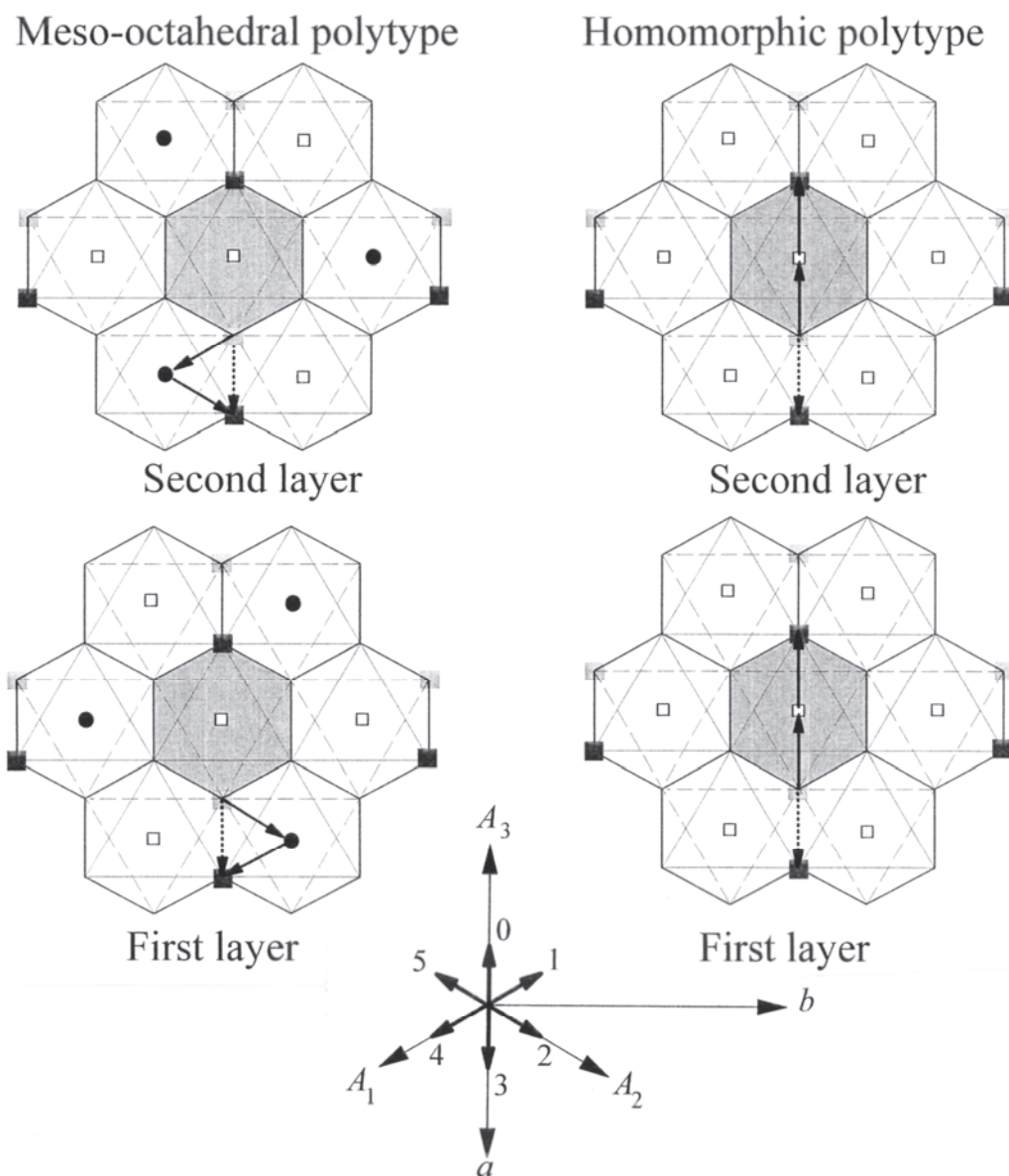


**Figure 11.** Relation of homomorphy between the two-layer meso-octahedral

$\left| \begin{smallmatrix} 2 & 4 & 4 & 2 \\ 3 & * & 3 & * \end{smallmatrix} \right|$  polytype (left) and the one-layer homo-octahedral  $\left| \begin{smallmatrix} e & e \\ 3 & \end{smallmatrix} \right|$  polytype (right),

illustrated by showing separately the two Oc layers. Solid vectors: packet orientation; dotted vectors: packet-to-packet displacements. Solid circles and open squares represent two different average cations. In the meso-octahedral polytype (left), the two Oc layers have the origin in either of the two *cis*-sites, where the different average cation is located: they correspond to M2 layers. The packet orientations, given by the vectors connecting the interlayer/OH sites (overlapped in projection) to the origin of the Oc layer, are 2 (packets  $p_0$  and  $q_3$ ) and 4 (packets  $q_1$  and  $p_2$ ). For both packet pairs, the vector sum (packet-to-packet displacement) is in orientation 3. By applying the relation of homomorphy, i.e., by making identical the content of the three octahedral cation sites, and obtaining the corresponding homo-octahedral polytype (right), both layers are transformed into the type M1, and the packet orientations change into  $e$  for both packets. The packet-to-packet displacements do not change. As a consequence, the two layers in the homo-octahedral polytype have the same orientational vectors, but the periodicity is halved. The  $\Sigma_V$ , now coinciding with  $v_{0,1}$ , corresponds to “3” (acute  $\beta$  angle), but can be transformed into “0” (obtuse  $\beta$  angle) by rotating the polytype by 180° about the normal to the layer.

too wide because – except for the two-dimensional periodicity of layers – it imposes no restrictions on the sequence and stacking mode of layers.

The fact that the definition is not sufficiently geometric prompted Āuroviĉ (1999) to suggest that the layers and their stacking must be limited by the *vicinity condition* (VC, see the section “Micas as OD structures”), and that a *family* can encompass only those polytypes which are built on the same structural and symmetry principle, i.e. only those which belong to the same OD groupoid family. This idea was in principle supported also by Makovicky (1997) who, at the same time, proposed to distinguish between *proper polytypes*, belonging to the same OD groupoid family, and *improper polytypes*, which cannot be interpreted as such. Recently, Christiansen *et al.* (1999) suggested a more detailed classification concept related to this subject. Makovicky also accepted the term polytypoids for polytypic substances in which more than 0.25 atoms per formula unit differ in at least one component as proposed by the IMA-IUCr Joint Committee on Nomenclature (Bailey *et al.* 1977). This term was applied also by Bailey (1980b) for the specific case of micas, and recommended also by the *Ad-hoc* Committee, as discussed above.

### Abstract polytypes

The experience gathered over years with refined periodic structures of polytypic substances indicate that, *sensu stricto*, each such polytype is an individual polymorph with its own stability field, although the energy differences between polytypes of the same compounds are very small. This is caused by desymmetrization, i.e. by changes in the atomic coordinates of individual layers imposed by the influence of the neighboring layers and it is different for different stacking modes. Thus, even layers in different polytypes of the same substance are not identical. A prominent example in micas (1M and 2M1 polytypes of biotite with the same composition) was given by Takeda and Ross (1975), who not only found significant differences in the constituent layers of the polytypes but also postulated that these differences are "directly related to the atomic and geometric constraints imposed by the adjacent unit layers varying with the relative orientation of the adjacent layers". Desymmetrization occurs even in such less pliable structures as SiC, as convincingly reported by researchers at the former Leningrad Electrotechnical Institute (Sorokin *et al.* 1982a,b; Tsvetkov 1982; see also Tairov and Tsvetkov 1983) who showed that also the chemical composition (the ratio of Si/C) varies from polytype to polytype grown under (nearly) the same conditions. If these facts were taken absolutely at the face value, the notion of polytypism would lose its unifying significance. In order to overcome these difficulties, the concept of a *polytype* is often considered an *abstract notion* referring to a *structural type* with relevant geometric properties, belonging to an abstract family whose members consist of layers with identical structure and with identical bulk compositions. Such an abstract notion lies at the root of all systematization and classification schemes of polytypes.

In micas (as well as in many other phyllosilicates) the Pauling model and also the homo-octahedral approximation are abstractions which are very useful, among others, for didactic purposes to gain first knowledge, but also for the calculation of identification diagrams of MDO polytypes, and for the calculation of PID functions, described in sections about experimental identification of mica polytypes below. A better approximation, but still an abstraction, is the Trigonal model, which is important for the explanation of subfamilies and for some features in the diffraction patterns. Also, when speaking of a specific polytype, a characteristic sequence of abstract mica layers is intended rather than deviations from stoichiometry, distribution of cations within octahedral sheets, distortion of coordination polyhedra, etc.

## Basic structures

Owing to the fact that the energy difference between polytypes of the same substance is very small, the occurrence of different polytypes should be influenced mostly by the kinetics of crystal growth, and the frequency of occurrence of different polytypes is, in principle, directly related to the number of layers in the period. However, this statement is contradicted by the existence of a certain degree of *structural control* (Smith and Yoder 1956; Güven 1971) that governs the frequency of occurrence of polytypes as a function of the crystallization environment and of the crystal chemistry. As firstly noted by Ross et al (1966), a portion of the stacking sequence of the non-MDO mica polytypes coincides with the stacking sequence of one of the MDO subfamily A polytypes, similarly to what happens in SiC polytypes. The remaining portion represents a deviation from the sequence. For this reason, Baronnet and Kang (1989) introduced the term *basic structures* to indicate these three MDO polytypes, as well as  $2M_2$  and  $1M_{d-A}$ . The non-MDO polytypes are thus said to belong to one *structural series*: the three structural series  $1M$ ,  $2M_1$  and  $3T$  were defined (Ross et al. 1966; Baronnet 1978; Takeda and Ross 1995). A structural series based on  $2M_2$  has not been found, but its existence cannot be excluded in principle. The causes of the existence of a stacking memory in the basic structures are not well understood. Energy differences between two polytypes of the same family are small. However, the real structures are constructed not by layer archetypes, but by, more or less, desymmetrized layers: the corresponding energy differences may be sufficient to control the original stacking sequence.

However, also when the crystal chemistry is practically identical, a certain degree of structural control exists, as shown by the fact that a few polytypes are clearly dominant, with the others appearing with much lower frequency. A general trend towards a relation between the formation environment, the crystal chemistry and the polytype frequency exists also (Nespolo 2001). The three basic structures may thus be not truly polytypic, even when the crystal chemistry is identical.

## HTREM observations and some implications

The application of the High Resolution Transmission Electron Microscopy (HRTEM) (Iijima and Buseck 1978) has made possible the observation of several stacking sequences that would not be revealed by other techniques. At the same time, HRTEM has raised the question of the limits within which an observed stacking sequence should be considered a polytype. Kogure and Nespolo (1999b) stated that the stacking sequences revealed by HRTEM observation can be defined as a polytype only when they are repeated sufficiently to reveal the presence of a memory mechanism reproducing with regularity the stacking sequence; otherwise, they should rather be considered defects. It is questionable whether a sequence repeated only three times, like the 22-layer biotite reported by Konishi and Akai (1990), may be rigorously termed a “polytype”. In such cases it is recommended to speak of “a sequence corresponding to a certain polytype”. In such cases, we described the form as “a sequence corresponding to the polytype XY”. The problem is similar to that of nanocrystals where it is also questionable how many unit cells are necessary to determine a phase.

## IDEAL SPACE-GROUP TYPES OF MICA POLYTYPES AND DESYMMETRIZATION OF LAYERS IN POLYTYPES

The ideal space-group type of a given polytype can be derived from the stacking sequence, as described above. However, three kinds of symmetries are required:

- 1) the *stacking symmetry*, deduced from the sequence of packet orientations and displacements, which gives the space-group type in the Trigonal model;
- 2) the *structural symmetry*, which may be lower than the stacking symmetry because of structural distortions not taken into account by the Trigonal model;
- 3) the *diffractional symmetry*, which may be higher than the structural symmetry. This phenomenon is termed *diffraction enhancement of symmetry* (Ito 1950) and occurs when a crystal is constructed by substructures whose symmetry is higher than that of the crystal itself (e.g., Iwasaki 1972; Matsumoto et al. 1974). In micas, diffraction enhancement of symmetry was observed in the oxybiotite-10A<sub>1</sub> from Ruiz Peak, which gave a monoclinic diffraction pattern, despite both the stacking symmetry and the structural symmetry were triclinic (Sadanaga and Takeda 1968).

The validity of the local symmetry operations is often only approximate, and the atomic coordinates can deviate more or less from the values demanded by the corresponding space groupoid, depending on the stacking of the packets in the investigated crystal, and this is phenomenon known as *desymmetrization* (Āuroviĉ 1979). The  $\lambda$ -symmetry of the M layers can thus be lower than the  $\lambda$ -symmetry of the layer archetypes described by the Trigonal model (see Table 2 in Ferraris and Ivaldi, this volume). The space-group type corresponding to the stacking symmetry in general does not require the highest  $\lambda$ -symmetry compatible with the family (homo-, meso- or hetero-octahedral) and the type of layer (M1 vs. M2). The layer is thus allowed, although not required, to attain a layer-subgroup. The general trend that results from the structure refinements performed on mica polytypes can be summarized as follows (see Table 9, and Tables 1-3 in Brigatti and Guggenheim, this volume):

- 1) 1M polytype has been refined only in the highest space-group types and layer-groups compatible with the type of layer: C2/m and C12/m(1) for the M1 layer; C2 and C12(1) for the M2 layer.
- 2) The highest space-group type for the 2M<sub>1</sub> polytype is C2/c. All but one example of 2M<sub>1</sub> polytypes refined so far belong to the meso-octahedral family and are constructed by M1 layers. Most of these polytypes have been refined in C2/c. This space-group type allows a desymmetrization of the layer-group to C1, which corresponds to the  $\lambda$ -symmetry normally obtained in 2M<sub>1</sub> polytypes (Güven 1971; Zussman 1979; Takeda and Ross 1975). An important exception is oxybiotite-2M<sub>1</sub> refined by Ohta et al (1982), where the highest  $\lambda$ -symmetry C12/m(1) was observed within experimental error; this was also the  $\lambda$ -symmetry of coexisting oxybiotite-1M (Ohta et al. 1982). Three studies of meso-octahedral margarite-2M<sub>1</sub> refined in the space-group type Cc have been reported (Guggenheim and Bailey 1975, 1978; Joswig et al 1983; Kassner et al. 1993), where the reduction of symmetry was related to the Si-Al ordering, that made the two T sheets no longer equivalent. The layer group is only C1, because of the destruction of the center of symmetry. A further reduction of symmetry was observed in the ephesite-2M<sub>1</sub> reported by Slade et al.

**Table 9 (next nine pages)**. Relevant properties of the MDO polytypes. Only polytypes for which the occupancies of the octahedral sites were given in the original papers are reported. Following Āuroviĉ et al (1984), the effective scattering amplitude is taken directly from the original papers, when reported; otherwise it has been calculated assuming half-ionized atoms, even where the structure was refined using electron or neutron diffraction data. Polytypes built by M2 layers are in bold characters. References are given according to the sequence numbers in the tables of the Brigatti and Guggenheim chapter. For polytypes not reported there, the complete reference is given. (e) = electron diffraction data; (n) = neutron diffraction data; otherwise X-ray diffraction data.



Reference	Type of mica	R factor	Space-group type	$\delta(M1)$	$\delta(M2)$	$\delta(M3)$	Full polytype symbol
<b>Subfamily A – 1M polytype</b>							
<i>Homo-trioctahedral</i>							
1-95	Phlogopite	13.1	<i>C2/m</i>	11.0	11.0	11.0	$\left  \begin{array}{c} u . u \\ 0 * \end{array} \right $
1-61	Synthetic iron mica	9.3	<i>C2/m</i>	25.0	25.0	25.0	$\left  \begin{array}{c} u . u \\ 0 * \end{array} \right $
1-97	Synthetic lithian flourphlogopite	7.3	<i>C2/m</i>	10.4	10.4	10.4	$\left  \begin{array}{c} u . u \\ 0 * \end{array} \right $
3-15	Barium mica	7.1	<i>C2/m</i>	8.8	8.8	8.8	$\left  \begin{array}{c} u . u \\ 0 * \end{array} \right $
1-70	Phlogopite (n)	2.0	<i>C2/m</i>	11.7	11.7	11.7	$\left  \begin{array}{c} u . u \\ 0 * \end{array} \right $
1-97	Phlogopite	4.1	<i>C2/m</i>	11.0	11.0	11.0	$\left  \begin{array}{c} u . u \\ 0 * \end{array} \right $
1-72	Fluorophlogopite	6.1	<i>C2/m</i>	11.0	11.0	11.0	$\left  \begin{array}{c} u . u \\ 0 * \end{array} \right $
1-86	Phlogopite (n)	6.6	<i>C2/m</i>	11.9	11.9	11.9	$\left  \begin{array}{c} u . u \\ 0 * \end{array} \right $
1-98	Fluro phlogopite	4.3	<i>C2/m</i>	11.0	11.0	11.0	$\left  \begin{array}{c} u . u \\ 0 * \end{array} \right $
1-104	Synthetic fluormica	3.8	<i>C2/m</i>	9.4	9.4	9.4	$\left  \begin{array}{c} u . u \\ 0 * \end{array} \right $
1-94	Tetraferriphlogopite	4.2	<i>C2/m</i>	10.5	10.5	10.5	$\left  \begin{array}{c} u . u \\ 0 * \end{array} \right $
1-108	Fluoro phlogopite	2.9	<i>C2/m</i>	10.2	10.2	10.2	$\left  \begin{array}{c} u . u \\ 0 * \end{array} \right $
1.108	Tetra germanatian fluoro phlogopite	3.7	<i>C2/m</i>	11.0	11.0	11.0	$\left  \begin{array}{c} u . u \\ 0 * \end{array} \right $
1-69	Silica- and alkali-rich trioctahedral mica	3.0	<i>C2/m</i>	10.6	10.6	10.6	$\left  \begin{array}{c} u . u \\ 0 * \end{array} \right $
1-103	Germanate mica	3.9	<i>C2/m</i>	14.0	14.0	14.0	$\left  \begin{array}{c} u . u \\ 0 * \end{array} \right $
1-102	Germanate mica	5.0	<i>C2/m</i>	19.5	19.5	19.5	$\left  \begin{array}{c} u . u \\ 0 * \end{array} \right $
1-110	Fluoro phlogopite	4.3	<i>C2/m</i>	10.8	10.8	10.8	$\left  \begin{array}{c} u . u \\ 0 * \end{array} \right $
Knurr and Bailey (1986)	Phlogopite	3.1	<i>C2/m</i>	12.1	12.1	12.1	$\left  \begin{array}{c} u . u \\ 0 * \end{array} \right $
3-7	Potassium Kinoshitalite (27)	2.5	<i>C2/m</i>	13.4	13.4	13.4	$\left  \begin{array}{c} u . u \\ 0 * \end{array} \right $
1-82	Cs-ferriannite	5.5	<i>C2/m</i>	25.0	25.0	25.0	$\left  \begin{array}{c} u . u \\ 0 * \end{array} \right $
1-45	Magnesian annite (WA8E)	3.9	<i>C2/m</i>	19.9	19.9	19.9	$\left  \begin{array}{c} u . u \\ 0 * \end{array} \right $
1-60	Cs-tetra-ferri-annite	3.9	<i>C2/m</i>	25.0	25.0	25.0	$\left  \begin{array}{c} u . u \\ 0 * \end{array} \right $

1-87/92	Ferroan phlogopite	3.9	<i>C2/m</i>	17.2	17.2	17.2	$\left  \begin{smallmatrix} u \cdot u \\ 0 \end{smallmatrix} \right ^*$
3-9	Ferrokioshitalite	3.2	<i>C2/m</i>	20.0	20.0	20.0	$\left  \begin{smallmatrix} u \cdot u \\ 0 \end{smallmatrix} \right ^*$
3-8	Kioshitalite	3.35	<i>C2/m</i>	12.0	12.0	12.0	$\left  \begin{smallmatrix} u \cdot u \\ 0 \end{smallmatrix} \right ^*$
<i>Meso-trioctahedral</i>							
Takéuchi and Sadanaga (1966)	Xantophyllite	10.8	<i>C2/m</i>	11.3	11.0	11.0	$\left  \begin{smallmatrix} 3.3 \\ 0 \end{smallmatrix} \right ^*$
1-96	Synthetic fluor-polyolithionite	5.1	<i>C2/m</i>	3.5	6.6	6.6	$\left  \begin{smallmatrix} 3.3 \\ 0 \end{smallmatrix} \right ^*$
1-66	Annite	4.4	<i>C2/m</i>	22.6	22.7	22.7	$\left  \begin{smallmatrix} 3.3 \\ 0 \end{smallmatrix} \right ^*$
1-100	Synthetic Mg <sup>IV</sup> mica	9.2	<i>C2/m</i>	10.7	10.1	10.1	$\left  \begin{smallmatrix} 3.3 \\ 0 \end{smallmatrix} \right ^*$
1-99	Biotite	4.4	<i>C2/m</i>	16.2	16.0	16.0	$\left  \begin{smallmatrix} 3.3 \\ 0 \end{smallmatrix} \right ^*$
1-93	Lepidolite	6.7	<i>C2/m</i>	3.0	8.2	8.2	$\left  \begin{smallmatrix} 3.3 \\ 0 \end{smallmatrix} \right ^*$
1-105	Taeniolite	2.4	<i>C2/m</i>	8.5	8.1	8.1	$\left  \begin{smallmatrix} 3.3 \\ 0 \end{smallmatrix} \right ^*$
1-107	Germanate mica	3.8	<i>C2/m</i>	7.9	8.3	8.3	$\left  \begin{smallmatrix} 3.3 \\ 0 \end{smallmatrix} \right ^*$
1-106	Germanate mica	5.5	<i>C2/m</i>	6.6	10.5	10.5	$\left  \begin{smallmatrix} 3.3 \\ 0 \end{smallmatrix} \right ^*$
Sokolova et al (1979)	Ephesite	11.5	<i>C2/m</i>	3.2	11.4	11.4	$\left  \begin{smallmatrix} 3.3 \\ 0 \end{smallmatrix} \right ^*$
1-62	Lepidolite	3.5	<i>C2/m</i>	3.6	8.2	8.2	$\left  \begin{smallmatrix} 3.3 \\ 0 \end{smallmatrix} \right ^*$
<b>1-128</b>	<b>Lepidolite</b>	<b>6.2</b>	<b>C2</b>	<b>4.7</b>	<b>10.1</b>	<b>4.7</b>	$\left  \begin{smallmatrix} 5.1 \\ 0 \end{smallmatrix} \right ^*$
1-85	Oxybiotite	4.4	<i>C2/m</i>	12.6	15.2	15.2	$\left  \begin{smallmatrix} 3.3 \\ 0 \end{smallmatrix} \right ^*$
1-63	Manganoan phlogopite (1)	5.4	<i>C2/m</i>	15.2	16.1	16.1	$\left  \begin{smallmatrix} 3.3 \\ 0 \end{smallmatrix} \right ^*$
1-64	Barian manganoan phlogopite (5)	3.8	<i>C2/m</i>	12.6	14.9	14.9	$\left  \begin{smallmatrix} 3.3 \\ 0 \end{smallmatrix} \right ^*$
3-10	Clintonite (n)	2.0	<i>C2/m</i>	11.8	11.2	11.2	$\left  \begin{smallmatrix} 3.3 \\ 0 \end{smallmatrix} \right ^*$
3-12	Clintonite (1782/5)	2.1	<i>C2/m</i>	12.1	11.2	11.2	$\left  \begin{smallmatrix} 3.3 \\ 0 \end{smallmatrix} \right ^*$
3-13	Clintonite (94594)	3.9	<i>C2/m</i>	11.6 <sup>+</sup>	11.6 <sup>-</sup>	11.6 <sup>-</sup>	$\left  \begin{smallmatrix} 3.3 \\ 0 \end{smallmatrix} \right ^*$
3-14	Clintonite (105455)	2.1	<i>C2/m</i>	11.5	11.2	11.2	$\left  \begin{smallmatrix} 3.3 \\ 0 \end{smallmatrix} \right ^*$
1-8	Ferroan phlogopite (M14)	3.3	<i>C2/m</i>	18.6	17.8	17.8	$\left  \begin{smallmatrix} 3.3 \\ 0 \end{smallmatrix} \right ^*$
1-9	Ferroan phlogopite (M32)	2.4	<i>C2/m</i>	17.9	17.1	17.1	$\left  \begin{smallmatrix} 3.3 \\ 0 \end{smallmatrix} \right ^*$
1-12	Ferroan phlogopite (M13)	6.2	<i>C2/m</i>	20.4	19.8	19.8	$\left  \begin{smallmatrix} 3.3 \\ 0 \end{smallmatrix} \right ^*$

1-11	Ferroan phlogopite (M73)	2.1	<i>C2/m</i>	19.0	18.2	18.2	$\left  \begin{array}{c} 3.3 \\ 0 * \end{array} \right $
1-10	Ferroan phlogopite (M62)	3.5	<i>C2/m</i>	20.4	19.6	19.6	$\left  \begin{array}{c} 3.3 \\ 0 * \end{array} \right $
1-111	Norrishite	7.8	<i>C2/m</i>	2.5	23.3	23.3	$\left  \begin{array}{c} 3.3 \\ 0 * \end{array} \right $
1-21	Ferroan phlogopite (8)	2.5	<i>C2/m</i>	13.9	15.1	15.1	$\left  \begin{array}{c} 3.3 \\ 0 * \end{array} \right $
1-22	Phlogopite (9)	2.2	<i>C2/m</i>	13.7	14.0	14.0	$\left  \begin{array}{c} 3.3 \\ 0 * \end{array} \right $
1-23	Ferroan phlogopite (10)	2.2	<i>C2/m</i>	16.3	16.5	16.5	$\left  \begin{array}{c} 3.3 \\ 0 * \end{array} \right $
1-24	Ferroan phlogopite (11)	1.9	<i>C2/m</i>	14.7	16.8	16.8	$\left  \begin{array}{c} 3.3 \\ 0 * \end{array} \right $
1-25	Ferroan phlogopite (12)	2.1	<i>C2/m</i>	14.5	16.1	16.1	$\left  \begin{array}{c} 3.3 \\ 0 * \end{array} \right $
1-26	Ferroan phlogopite (15)	2.3	<i>C2/m</i>	17.5	17.0	17.0	$\left  \begin{array}{c} 3.3 \\ 0 * \end{array} \right $
1-27	Ferroan phlogopite (16)	3.0	<i>C2/m</i>	19.0	18.4	18.4	$\left  \begin{array}{c} 3.3 \\ 0 * \end{array} \right $
1-28	Magnesian annite (17)	2.6	<i>C2/m</i>	18.6	18.4	18.4	$\left  \begin{array}{c} 3.3 \\ 0 * \end{array} \right $
1-112	Protolithionite	3.8	<i>C2/m</i>	20.2	19.4	19.4	$\left  \begin{array}{c} 3.3 \\ 0 * \end{array} \right $
1-7	Magnesian annite (MP9)	3.1	<i>C2/m</i>	18.7	20.2	20.2	$\left  \begin{array}{c} 3.3 \\ 0 * \end{array} \right $
1-13	Titanian phlogopite (18)	2.0	<i>C2/m</i>	12.9	15.4	15.4	$\left  \begin{array}{c} 3.3 \\ 0 * \end{array} \right $
1-17	Ferroan phlogopite (19)	3.2	<i>C2/m</i>	17.6	18.1	18.1	$\left  \begin{array}{c} 3.3 \\ 0 * \end{array} \right $
1-14	Aluminian phlogopite (20)	2.7	<i>C2/m</i>	16.1	16.9	16.9	$\left  \begin{array}{c} 3.3 \\ 0 * \end{array} \right $
1-15	Ferrian phlogopite (21)	2.3	<i>C2/m</i>	15.3	16.1	16.1	$\left  \begin{array}{c} 3.3 \\ 0 * \end{array} \right $
1-16	Ferroan phlogopite (22)	3.3	<i>C2/m</i>	16.3	17.1	17.1	$\left  \begin{array}{c} 3.3 \\ 0 * \end{array} \right $
1-18	Ferrian phlogopite (23)	3.4	<i>C2/m</i>	16.2	16.8	16.8	$\left  \begin{array}{c} 3.3 \\ 0 * \end{array} \right $
1-19	Ferrian phlogopite (24)	2.7	<i>C2/m</i>	17.1	17.5	17.5	$\left  \begin{array}{c} 3.3 \\ 0 * \end{array} \right $
1-20	Ferroan phlogopite (25)	2.2	<i>C2/m</i>	16.6	17.7	17.7	$\left  \begin{array}{c} 3.3 \\ 0 * \end{array} \right $
Brigatti & Poppi (1993)	Potassium kinoshitalite (26)	2.6	<i>C2/m</i>	14.3	13.3	13.3	$\left  \begin{array}{c} 3.3 \\ 0 * \end{array} \right $
1-6	Biotite	3.33	<i>C2/m</i>	19.0	18.1	18.1	$\left  \begin{array}{c} 3.3 \\ 0 * \end{array} \right $
1-1	Phlogopite (1a)	2.9	<i>C2/m</i>	13.2	12.9	12.9	$\left  \begin{array}{c} 3.3 \\ 0 * \end{array} \right $
1-2	Phlogopite (1b)	2.8	<i>C2/m</i>	13.4	12.9	12.9	$\left  \begin{array}{c} 3.3 \\ 0 * \end{array} \right $
1-3	Phlogopite (2a)	2.9	<i>C2/m</i>	13.2	12.9	12.9	$\left  \begin{array}{c} 3.3 \\ 0 * \end{array} \right $

1-4	Aluminian phlogopite (3a)	3.0	<i>C2/m</i>	13.3(1)	13.2(1)	13.2(1)	$\left  \begin{smallmatrix} 3.3 \\ 0 \end{smallmatrix} \right  *$
1-5	Phlogopite (4a)	2.5	<i>C2/m</i>	13.0	12.7	12.7	$\left  \begin{smallmatrix} 3.3 \\ 0 \end{smallmatrix} \right  *$
1-36	Phlogopite (Tas27-2Ba)	2.8	<i>C2/m</i>	14.0	13.1	13.0	$\left  \begin{smallmatrix} 3.3 \\ 0 \end{smallmatrix} \right  *$
1-37	Phlogopite (Tas27-2Bb)	2.5	<i>C2/m</i>	13.7	13.3	13.3	$\left  \begin{smallmatrix} 3.3 \\ 0 \end{smallmatrix} \right  *$
1-38	Ferroan phlogopite (Tag15-4)	2.8	<i>C2/m</i>	15.7	15.6	15.6	$\left  \begin{smallmatrix} 3.3 \\ 0 \end{smallmatrix} \right  *$
1-39	Phlogopite (Tag15-3)	2.8	<i>C2/m</i>	14.9	14.8	14.8	$\left  \begin{smallmatrix} 3.3 \\ 0 \end{smallmatrix} \right  *$
1-32	Ferroan phlogopite (Tpg63-2B)	2.3	<i>C2/m</i>	16.8	16.5	16.5	$\left  \begin{smallmatrix} 3.3 \\ 0 \end{smallmatrix} \right  *$
1-29	Phlogopite (Tae23-1a)	2.7	<i>C2/m</i>	13.4	13.3	13.3	$\left  \begin{smallmatrix} 3.3 \\ 0 \end{smallmatrix} \right  *$
1-30	Phlogopite (Tae23-1b)	2.7	<i>C2/m</i>	13.5	13.5	13.5	$\left  \begin{smallmatrix} 3.3 \\ 0 \end{smallmatrix} \right  *$
1-31	Phlogopite (Tae23-1c)	3.0	<i>C2/m</i>	14.0	13.7	13.7	$\left  \begin{smallmatrix} 3.3 \\ 0 \end{smallmatrix} \right  *$
1-40	Phlogopite (Tpq16-4A)	2.8	<i>C2/m</i>	13.8	13.6	13.6	$\left  \begin{smallmatrix} 3.3 \\ 0 \end{smallmatrix} \right  *$
1-35	Phlogopite (Tpt17-1)	2.8	<i>C2/m</i>	13.8	13.4	13.4	$\left  \begin{smallmatrix} 3.3 \\ 0 \end{smallmatrix} \right  *$
1-33	Tetra-ferri phlogopite (Tas22-1a)	3.2	<i>C2/m</i>	12.9	12.8	12.8	$\left  \begin{smallmatrix} 3.3 \\ 0 \end{smallmatrix} \right  *$
1-34	Tetra-ferri phlogopite (Tas22-1b)	3.3	<i>C2/m</i>	13.9	13.1	13.1	$\left  \begin{smallmatrix} 3.3 \\ 0 \end{smallmatrix} \right  *$
1-41	Tetra-ferri phlogopite (Tpq16-6B)	3.1	<i>C2/m</i>	14.6	13.8	13.8	$\left  \begin{smallmatrix} 3.3 \\ 0 \end{smallmatrix} \right  *$
1-42	Tetra-ferri phlogopite (S1)	3.1	<i>C2/m</i>	13.5	13.1	13.1	$\left  \begin{smallmatrix} 3.3 \\ 0 \end{smallmatrix} \right  *$
1-43	Tetra-ferri phlogopite (S2)	2.5	<i>C2/m</i>	13.8	13.5	13.5	$\left  \begin{smallmatrix} 3.3 \\ 0 \end{smallmatrix} \right  *$
Brigatti et al (1997)	Ferroan phlogopite (Tag15-4a)	2.8	<i>C2/m</i>	15.7	15.6	15.6	$\left  \begin{smallmatrix} 3.3 \\ 0 \end{smallmatrix} \right  *$
1-48	Ferroan phlogopite (Tag15-4b)	2.8	<i>C2/m</i>	15.2	15.4	15.4	$\left  \begin{smallmatrix} 3.3 \\ 0 \end{smallmatrix} \right  *$
1-49	Ferroan phlogopite (Tpq16-4Aa)	2.8	<i>C2/m</i>	13.8	13.6	13.6	$\left  \begin{smallmatrix} 3.3 \\ 0 \end{smallmatrix} \right  *$
1-50	Ferroan phlogopite (Tpq16-4Ab)	2.4	<i>C2/m</i>	13.7	13.4	13.4	$\left  \begin{smallmatrix} 3.3 \\ 0 \end{smallmatrix} \right  *$
Brigatti et al (1997)	Ferroan phlogopite (Tpq16-4Ac)	3.0	<i>C2/m</i>	15.9	15.3	15.3	$\left  \begin{smallmatrix} 3.3 \\ 0 \end{smallmatrix} \right  *$
Brigatti et al (1997)	Ferroan phlogopite (Tas22-1c)	3.1	<i>C2/m</i>	13.5	13.1	13.1	$\left  \begin{smallmatrix} 3.3 \\ 0 \end{smallmatrix} \right  *$
3-1	Clintonite (5a)	3.49	<i>C2/m</i>	13.0	12.6	12.6	$\left  \begin{smallmatrix} 3.3 \\ 0 \end{smallmatrix} \right  *$
3-2	Clintonite (7c)	3.73	<i>C2/m</i>	13.4	13.3	13.3	$\left  \begin{smallmatrix} 3.3 \\ 0 \end{smallmatrix} \right  *$

3-3	Clintonite (8a)	3.11	<i>C2/m</i>	13.2	12.9	12.9	$\left  \begin{array}{c} 3.3 \\ 0 \end{array} \right ^*$
3-4	Clintonite (8d)	3.18	<i>C2/m</i>	12.7	13.0	13.0	$\left  \begin{array}{c} 3.3 \\ 0 \end{array} \right ^*$
3-5	Clintonite (9a)	3.29	<i>C2/m</i>	13.0	13.1	13.1	$\left  \begin{array}{c} 3.3 \\ 0 \end{array} \right ^*$
3-6	Clintonite (9b)	2.70	<i>C2/m</i>	12.6	13.0	13.0	$\left  \begin{array}{c} 3.3 \\ 0 \end{array} \right ^*$
1-65	rubidian cesian phlogopite	4.5	<i>C2/m</i>	16.0	15.8	15.8	$\left  \begin{array}{c} 3.3 \\ 0 \end{array} \right ^*$
1-44	Ferroan phlogopite (WA3H)	2.9	<i>C2/m</i>	18.3	18.2	18.2	$\left  \begin{array}{c} 3.3 \\ 0 \end{array} \right ^*$
1-46	Magnesian annite (WA8H)	3.3	<i>C2/m</i>	19.6	19.3	19.3	$\left  \begin{array}{c} 3.3 \\ 0 \end{array} \right ^*$
1-47	Ferroan phlogopite (WA23E)	2.8	<i>C2/m</i>	18.8	18.6	18.6	$\left  \begin{array}{c} 3.3 \\ 0 \end{array} \right ^*$
1-51	Magnesian annite	3.2	<i>C2/m</i>	19.6	18.9	18.9	$\left  \begin{array}{c} 3.3 \\ 0 \end{array} \right ^*$
1-55	Magnesian annite	3.6	<i>C2/m</i>	19.1	18.2	18.2	$\left  \begin{array}{c} 3.3 \\ 0 \end{array} \right ^*$
1-56	Magnesian annite	3.2	<i>C2/m</i>	19.6	18.8	18.8	$\left  \begin{array}{c} 3.3 \\ 0 \end{array} \right ^*$
1-54	Magnesian annite	3.2	<i>C2/m</i>	19.4	18.5	18.5	$\left  \begin{array}{c} 3.3 \\ 0 \end{array} \right ^*$
1-53	Magnesian annite	3.1	<i>C2/m</i>	19.9	19.6	19.6	$\left  \begin{array}{c} 3.3 \\ 0 \end{array} \right ^*$
1-52	Magnesian annite	3.7	<i>C2/m</i>	19.8	19.2	19.2	$\left  \begin{array}{c} 3.3 \\ 0 \end{array} \right ^*$
1-58	Fe-Li rich mica 26	3.3	<i>C2/m</i>	19.6	22.3	22.3	$\left  \begin{array}{c} 3.3 \\ 0 \end{array} \right ^*$
1-59	Fe-Li rich mica 33	3.6	<i>C2/m</i>	23.5	23.9	23.9	$\left  \begin{array}{c} 3.3 \\ 0 \end{array} \right ^*$
1-57	Fe-Li rich mica 120	2.6	<i>C2/m</i>	24.7	24.4	24.4	$\left  \begin{array}{c} 3.3 \\ 0 \end{array} \right ^*$
<b>1-118</b>	<b>Fe-Li rich mica 130(2)</b>	<b>3.86</b>	<b><i>C2</i></b>	<b>12.7</b>	<b>13.0</b>	<b>12.7</b>	$\left  \begin{array}{c} 5.1 \\ 0 \end{array} \right ^*$
<i>Hetero-trioctahedral</i>							
<b>1-129</b>	<b>Zinnwaldite</b>	<b>5.7</b>	<b><i>C2</i></b>	<b>15.0</b>	<b>11.5</b>	<b>13.5</b>	$\left  \begin{array}{c} 5'1 \\ 0 \end{array} \right ^*$
1-113	Lepidolite	7.3	<i>C2</i>	3.7	11.4	11.5	$\left  \begin{array}{c} 3'3 \\ 0 \end{array} \right ^*$
Zhukhlistov et al (1983)	Li-Fe phengite (e)	10.2	<i>C2</i>	8.0	15.1	14.8	$\left  \begin{array}{c} 3''3 \\ 0 \end{array} \right ^*$
<b>1-130</b>	<b>Masutomilite</b>	<b>4.6</b>	<b><i>C2</i></b>	<b>8.5</b>	<b>11.1</b>	<b>8.1</b>	$\left  \begin{array}{c} 1'5 \\ 0 \end{array} \right ^*$
<b>1-117</b>	<b>Fe-Li rich mica 130(1)</b>	<b>2.96</b>	<b><i>C2</i></b>	<b>13.5</b>	<b>12.6</b>	<b>12.8</b>	$\left  \begin{array}{c} 5'1 \\ 0 \end{array} \right ^*$
<b>1-123</b>	<b>Fe-Li rich mica 140(1)</b>	<b>2.89</b>	<b><i>C2</i></b>	<b>13.8</b>	<b>13.0</b>	<b>13.6</b>	$\left  \begin{array}{c} 5'1 \\ 0 \end{array} \right ^*$
<b>1-124</b>	<b>Fe-Li rich mica 140(2)</b>	<b>2.73</b>	<b><i>C2</i></b>	<b>13.3</b>	<b>12.4</b>	<b>13.7</b>	$\left  \begin{array}{c} 5''1 \\ 0 \end{array} \right ^*$

1-120	Fe-Li rich mica 104	3.34	<i>C2</i>	12.0	12.1	11.8	$\begin{vmatrix} 1'5 \\ 0 * \end{vmatrix}$
1-119	Fe-Li rich mica 137	3.63	<i>C2</i>	13.0	13.0	11.3	$\begin{vmatrix} 1'5 \\ 0 * \end{vmatrix}$
1-122	Fe-Li rich mica 177	3.39	<i>C2</i>	13.8	12.7	12.8	$\begin{vmatrix} 5'1 \\ 0 * \end{vmatrix}$
1-121	Fe-Li rich mica 54b	3.78	<i>C2</i>	11.9	11.6	13.0	$\begin{vmatrix} 5''1 \\ 0 * \end{vmatrix}$
1-125	Fe-Li rich mica 24	3.72	<i>C2</i>	14.2	12.3	13.0	$\begin{vmatrix} 5'1 \\ 0 * \end{vmatrix}$
1-115	Fe-Li rich mica 55a	3.74	<i>C2</i>	11.3	12.0	9.4	$\begin{vmatrix} 1'5 \\ 0 * \end{vmatrix}$
1-116	Fe-Li rich mica 55b	3.21	<i>C2</i>	11.3	13.0	9.9	$\begin{vmatrix} 1'5 \\ 0 * \end{vmatrix}$
1-126	Fe-Li rich mica 47	3.31	<i>C2</i>	19.2	15.8	19.4	$\begin{vmatrix} 5''1 \\ 0 * \end{vmatrix}$
1-127	Fe-Li rich mica 103	3.63	<i>C2</i>	16.0	14.3	17.6	$\begin{vmatrix} 5''1 \\ 0 * \end{vmatrix}$
1-114	Fe-Li rich mica 114	3.35	<i>C2</i>	10.2	8.5	12.2	$\begin{vmatrix} 5''1 \\ 0 * \end{vmatrix}$
<i>Meso-dioctahedral</i>							
2-3	Ferrous celadonite (e)	10.8	<i>C2/m</i>	---	21.4	21.4	$\begin{vmatrix} 3.3 \\ 0 * \end{vmatrix}$
2-2	Paragonite (e)	12.1	<i>C2/m</i>	---	10.8	10.8	$\begin{vmatrix} 3.3 \\ 0 * \end{vmatrix}$
4-1	Boromuscovite	3.8	<i>C2/m</i>	---	12.5	12.5	$\begin{vmatrix} 3.3 \\ 0 * \end{vmatrix}$
<i>Hetero-dioctahedral</i>							
2-1	Dioctahedral mica (e)	10.9	<i>C2</i>	---	12.8	11.5	$\begin{vmatrix} 3''3 \\ 0 * \end{vmatrix}$
<b>Subfamily B – 2O polytype</b>							
<i>Homo-trioctahedral</i>							
Ferraris et al (2000)	Fluor-phlogopite	4.5	<i>Ccmm</i>	12.8	12.8	12.8	$\begin{vmatrix} u.u e.e \\ 0 * 3 * \end{vmatrix}$
<i>Meso-trioctahedral</i>							
3-17	Anandite*	6.1	<i>Pnmn</i>				$\begin{vmatrix} 3.3 0.0 \\ 0 * 3 * \end{vmatrix}$
3-18	Anandite*	6.4	<i>Pnmn</i>				$\begin{vmatrix} 3.3 0.0 \\ 0 * 3 * \end{vmatrix}$
<b>Subfamily A – 2M<sub>1</sub> polytype</b>							
<i>Meso-trioctahedral</i>							
1-139	Biotite	5.6	<i>C2/c</i>	15.8	16.3	16.3	$\begin{vmatrix} 4.4 2.2 \\ 1 * 5 * \end{vmatrix}$
Sartori (1977)	Lepidolite	11.3	<i>C2/c</i>	2.3	8.7	8.7	$\begin{vmatrix} 4.4 2.2 \\ 1 * 5 * \end{vmatrix}$
Sokolova et al (1979)	Bityite (e)	11.5	<i>C2/c</i>	2.3	8.7	8.7	$\begin{vmatrix} 4.4 2.2 \\ 1 * 5 * \end{vmatrix}$
1-135	Magnesian annite	4.2	<i>C2/c</i>	19.4	18.6	18.6	$\begin{vmatrix} 4.4 2.2 \\ 1 * 5 * \end{vmatrix}$
1-138	Lepidolite	9.1	<i>C2/c</i>	3.6	7.5	7.5	$\begin{vmatrix} 4.4 2.2 \\ 1 * 5 * \end{vmatrix}$

1-137	Oxybiotite	3.9	<i>C2/c</i>	12.6	15.2	15.2	$\begin{array}{ c} 4.4 & 2.2 \\ 1 * & 5 * \end{array}$
3-76	Li-Be rich mica	3.0	<i>Cc</i>	1.1	11.5	11.5	$\begin{array}{ c} 4.4 & 2.2 \\ 1 * & 5 * \end{array}$
1-141	Ephesite	4.7	<i>C1</i>	2.9	11.5	11.5	$\begin{array}{ c} 4.4 & 2.2 \\ 1 * & 5 * \end{array}$
1-132	Magnesian annite (MP16)	3.7	<i>C2/c</i>	20.8	20.1	20.1	$\begin{array}{ c} 4.4 & 2.2 \\ 1 * & 5 * \end{array}$
1-133	Magnesian annite (MP17a)	2.7	<i>C2/c</i>	17.5	16.8	16.8	$\begin{array}{ c} 4.4 & 2.2 \\ 1 * & 5 * \end{array}$
1-134	Magnesian annite (MP17b)	3.4	<i>C2/c</i>	17.2	16.6	16.6	$\begin{array}{ c} 4.4 & 2.2 \\ 1 * & 5 * \end{array}$
1-131	Biotite	2.72	<i>C2/c</i>	18.8	18.3	18.3	$\begin{array}{ c} 4.4 & 2.2 \\ 1 * & 5 * \end{array}$
1-136	Magnesian annite	2.8	<i>C2/c</i>	19.4	18.4	18.4	$\begin{array}{ c} 4.4 & 2.2 \\ 1 * & 5 * \end{array}$
<i>Hetero-trioctahedral</i>							
<b>1-140</b>	<b>Zinnwaldite</b>	<b>5.8</b>	<b><i>Cc</i></b>	<b>16.2</b>	<b>14.3</b>	<b>17.4</b>	$\begin{array}{ c} 0''2 & 0'4 \\ 1 * & 5 * \end{array}$
<i>Meso-dioctahedral</i>							
Radoslovich (1960)	Muscovite	17.0	<i>C2/c</i>	---	12.3	12.3	$\begin{array}{ c} 4.4 & 2.2 \\ 1 * & 5 * \end{array}$
Takéuchi (1965)	Margarite	16.8	<i>C2/c</i>	---	11.5	11.5	$\begin{array}{ c} 4.4 & 2.2 \\ 1 * & 5 * \end{array}$
2-4	Muscovite	12.8	<i>C2/c</i>	---	12.3	12.3	$\begin{array}{ c} 4.4 & 2.2 \\ 1 * & 5 * \end{array}$
2-36	Muscovite	3.5	<i>C2/c</i>	---	11.8	11.8	$\begin{array}{ c} 4.4 & 2.2 \\ 1 * & 5 * \end{array}$
2-37	Phengite	4.5	<i>C2/c</i>	---	12.3	12.3	$\begin{array}{ c} 4.4 & 2.2 \\ 1 * & 5 * \end{array}$
2-46	Muscovite (n)	2.7	<i>C2/c</i>	---	12.3	12.3	$\begin{array}{ c} 4.4 & 2.2 \\ 1 * & 5 * \end{array}$
Udagawa et al (1974)	Muscovite	14.2	<i>C2/c</i>	---	12.3	12.3	$\begin{array}{ c} 4.4 & 2.2 \\ 1 * & 5 * \end{array}$
3-19	Margarite	4.0	<i>Cc</i>	---	11.5	11.5	$\begin{array}{ c} 4.4 & 2.2 \\ 1 * & 5 * \end{array}$
Sidorenko et al (1977a)	Paragonite (e)	11.1	<i>C2/c</i>	---	11.6	11.6	$\begin{array}{ c} 4.4 & 2.2 \\ 1 * & 5 * \end{array}$
2-39	Paragonite	4.5	<i>C2/c</i>	---	11.9	11.9	$\begin{array}{ c} 4.4 & 2.2 \\ 1 * & 5 * \end{array}$
2-47	Phengite	3.3	<i>C2/c</i>	---	13.2	13.2	$\begin{array}{ c} 4.4 & 2.2 \\ 1 * & 5 * \end{array}$
2-38	Muscovite	2.7	<i>C2/c</i>	---	12.7	12.7	$\begin{array}{ c} 4.4 & 2.2 \\ 1 * & 5 * \end{array}$
2-19/20	Muscovite	4.8 (LT) 6.0 (HT)	<i>C2/c</i>	---	12.1	12.1	$\begin{array}{ c} 4.4 & 2.2 \\ 1 * & 5 * \end{array}$
2-21	Muscovite (n)	4.0	<i>C2/c</i>	---	13.4	13.4	$\begin{array}{ c} 4.4 & 2.2 \\ 1 * & 5 * \end{array}$
4-2	Boromuscovite	3.8	<i>C2/c</i>	---	12.5	12.5	$\begin{array}{ c} 4.4 & 2.2 \\ 1 * & 5 * \end{array}$
2-30	Chromphyllite	4.8	<i>C2/c</i>	---	19.9	19.9	$\begin{array}{ c} 4.4 & 2.2 \\ 1 * & 5 * \end{array}$

2-5	Mg-, Fe-bearing muscovite	2.54	<i>C2/c</i>	0.64	15.5	15.5	$\begin{array}{ c} 4.4 & 2.2 \\ 1 * & 5 * \end{array}$
2-6	Mg-, Fe-bearing muscovite	2.96	<i>C2/c</i>	0.97	13.9	13.9	$\begin{array}{ c} 4.4 & 2.2 \\ 1 * & 5 * \end{array}$
2-7	Mg-, Fe-bearing muscovite	3.58	<i>C2/c</i>	0.46	13.5	13.5	$\begin{array}{ c} 4.4 & 2.2 \\ 1 * & 5 * \end{array}$
2-8	Mg-, Fe-bearing muscovite	2.92	<i>C2/c</i>	0.44	13.7	13.7	$\begin{array}{ c} 4.4 & 2.2 \\ 1 * & 5 * \end{array}$
2-9	Mg-, Fe-bearing muscovite	3.93	<i>C2/c</i>	0.84	15.0	15.0	$\begin{array}{ c} 4.4 & 2.2 \\ 1 * & 5 * \end{array}$
2-10	Mg-, Fe-bearing muscovite	2.89	<i>C2/c</i>	0.32	13.8	13.8	$\begin{array}{ c} 4.4 & 2.2 \\ 1 * & 5 * \end{array}$
2-11	Mg-, Fe-bearing muscovite	2.78	<i>C2/c</i>	0.49	13.7	13.7	$\begin{array}{ c} 4.4 & 2.2 \\ 1 * & 5 * \end{array}$
2-12	Mg-, Fe-bearing muscovite	2.11	<i>C2/c</i>	0.38	13.7	13.7	$\begin{array}{ c} 4.4 & 2.2 \\ 1 * & 5 * \end{array}$
2-13	Mg-, Fe-bearing muscovite	3.87	<i>C2/c</i>	1.73	14.0	14.0	$\begin{array}{ c} 4.4 & 2.2 \\ 1 * & 5 * \end{array}$
2-14	Mg-, Fe-bearing muscovite	3.12	<i>C2/c</i>	0.88	13.6	13.6	$\begin{array}{ c} 4.4 & 2.2 \\ 1 * & 5 * \end{array}$
2-15	Mg-, Fe-bearing muscovite	2.80	<i>C2/c</i>	0.39	13.8	13.8	$\begin{array}{ c} 4.4 & 2.2 \\ 1 * & 5 * \end{array}$
Smyth et al (2000)	Phengite	1.3	<i>C2/c</i>	---	11.6	11.6	$\begin{array}{ c} 4.4 & 2.2 \\ 1 * & 5 * \end{array}$
2-16	Cr-containing muscovite	2.5	<i>C2/c</i>	0.1	13.8	13.8	$\begin{array}{ c} 4.4 & 2.2 \\ 1 * & 5 * \end{array}$
2-17	Cr-containing muscovite	3.1	<i>C2/c</i>	---	13.8	13.8	$\begin{array}{ c} 4.4 & 2.2 \\ 1 * & 5 * \end{array}$
2-18	Cr-containing muscovite	3.3	<i>C2/c</i>	2.1	14.5	14.5	$\begin{array}{ c} 4.4 & 2.2 \\ 1 * & 5 * \end{array}$

**Subfamily B – 2M<sub>2</sub> polytype***Meso-trioctahedral*

1-144	Lepidolite	7.2	<i>C2/c</i>	2.0	8.4	8.4	$\begin{array}{ c} 2.2 & 1.1 \\ 5 * & 4 * \end{array}$
1-143	Lepidolite	9.6	<i>C2/c</i>	3.0	8.2	8.2	$\begin{array}{ c} 2.2 & 1.1 \\ 5 * & 4 * \end{array}$
1-142	Lepidolite	4.8	<i>C2/c</i>	2.5	8.6	8.6	$\begin{array}{ c} 2.2 & 1.1 \\ 5 * & 4 * \end{array}$

*Meso-dioctahedral*

2-50	Dioctahedral mica (e)	11.7	<i>C2/c</i>	---	11.2	11.2	$\begin{array}{ c} 2.2 & 1.1 \\ 5 * & 4 * \end{array}$
2-49	Nanpingite	5.8	<i>C2/c</i>	---	12.9	12.9	$\begin{array}{ c} 2.2 & 1.1 \\ 5 * & 4 * \end{array}$

**Subfamily A – 3T polytype***Hetero-trioctahedral*

<b>1-145</b>	<b>Lepidolite</b>	<b>4.7</b>	<b>P3<sub>1</sub>12</b>	<b>5.2</b>	<b>3.4</b>	<b>10.3</b>	$\begin{array}{ c} 4'2 & 2'0 & 0'4 \\ 3 * & 1 * & 5 * \end{array}$
<b>Pavlishin et al (1981)</b>	<b>Protolithionite</b>	<b>3.8</b>	<b>P3<sub>1</sub>12</b>	<b>18.7</b>	<b>14.3</b>	<b>15.6</b>	$\begin{array}{ c} 2'4 & 0'2 & 4'0 \\ 3 * & 1 * & 5 * \end{array}$
<b>1-146</b>	<b>Protolithionite</b>	<b>3.0</b>	<b>P3<sub>1</sub>12</b>	<b>16.1</b>	<b>14.4</b>	<b>17.6</b>	$\begin{array}{ c} 2''4 & 0''2 & 4''0 \\ 3 * & 1 * & 5 * \end{array}$



		<i>Hetero-dioctahedral</i>					
2-53	Muscovite	2.4	$P3_112$	---	11.5	12.5	$\begin{vmatrix} 0'0 & 4'4 & 2'2 \\ 3 & * & 1 & * & 5 & * \end{vmatrix}$
2-54	Paragonite (e)	13.0	$P3_112$	3.4	9.2	10.3	$\begin{vmatrix} 0'0 & 4'4 & 2'2 \\ 3 & * & 1 & * & 5 & * \end{vmatrix}$
2-51	Phengite (KZ)	3.6	$P3_112$	---	13.4	13.7	$\begin{vmatrix} 0'0 & 4'4 & 2'2 \\ 3 & * & 1 & * & 5 & * \end{vmatrix}$
2-52	Phengite (DM)	4.5	$P3_112$	---	12.5	13.0	$\begin{vmatrix} 0'0 & 4'4 & 2'2 \\ 3 & * & 1 & * & 5 & * \end{vmatrix}$
Pavese et al (1997)	Phengite (n)	7.0 (LT) 5.0 (HT)	$P3_112$	---	11.5	11.1 (LT) 11.2 (HT)	$\begin{vmatrix} 0''0 & 4''4 & 2''2 \\ 3 & * & 1 & * & 5 & * \end{vmatrix}$
Smyth et al (2000)	Phengite	0.9	$P3_112$	---	12.7	13.0	$\begin{vmatrix} 0'0 & 4'4 & 2'2 \\ 3 & * & 1 & * & 5 & * \end{vmatrix}$

\*The structure of anandite-2*O* cannot be described using an orthohexagonal *C*-centered cell and contains four independent octahedral positions. The symbol of this 'polytype' is therefore only an approximation.

- (1987), where a different Si-Al ordering in the four tetrahedral sites reduced the space-group type to *C1*. Only one example of hetero-octahedral  $2M_1$  polytype is known so far: the zinnwaldite refined by Rieder et al (1996). In the hetero-octahedral family, the highest layer-group for both *M1* and *M2* layers is *C12(1)*: correspondingly, the highest space-group type for  $2M_1$  is *Cc*, which is realized in this zinnwaldite- $2M_1$ . This mica is built up by *M2* layers, with local  $\sigma$ - $\rho$  operations  $2_{[310]}$  and  $2_{[3\bar{1}0]}$  for the two layers respectively, as can be easily confirmed by analyzing the OD symbols (Table 9) on the basis of the conversion rules given in Table 5a.
- 3) The highest space-group type for the  $3T$  polytype is  $P3_{1,2}12$ , which is compatible with the highest layer groups in all the three families, namely *C12/m(1)* (homo- and meso-octahedral) and *C12(1)* (hetero-octahedral). We are aware of nine structure refinements of  $3T$  polytypes in which the composition of the *O* sheet was given. All belong to the hetero-octahedral family, and three of them were reconstructed up by *M2* layers. Refinement of meso-octahedral  $3T$  polytypes is desirable to investigate (a) the desymmetrization of the layer group in this polytype; (b) the frequency of occurrence of *M2* layers that, at least in Li-rich micas, seems higher than in other polytypes.
  - 4) The highest space-group type for the  $2M_2$  polytype is *C2/c*, the same as  $2M_1$ . All the polytypes refined so far have this symmetry.
  - 5) The polytype  $2O$  has ideal space-group type *Ccmm*, which was reported only recently in a fluor-phlogopite from the Khibiny massif (Kola Peninsula, Russia) (Ferraris et al 2000). Previously, two examples were reported in anandite (Giuseppetti and Tadini 1972; Filut et al. 1985), where however an unusual crystal chemistry, including tetrahedral  $Fe^{3+}$  and octahedral  $S^{2-}$  and  $Cl^-$ , reduced the space-group type to *Pnmm*, with some indications of further reduction to  $P2_1$ . The anandite- $2O$  cannot be described with the orthohexagonal *C*-centered cell and contains four independent octahedral positions, two of which are on mirror planes. The symbols given in Table 9 for anandite- $2O$  are thus only a rough approximation.

In *C2/c* and  $P3_{1,2}12$  space-group types there are two independent *T* sites and the two independent *M2/M3* sites. The possibility of cation ordering exists in these groups, and it is often verified in the *O* sheet, but more rarely in the *T* sheets (Bailey 1975; 1984; Amisano-Canesi et al. 1994; see also the examples of margarite and ephesite given above). If the  $\lambda$ -symmetry *C12/m(1)* is maintained no ordering occurs, although it is not

prevented by the space-group type. Thus, this is an example of local symmetry being higher than that required by the global symmetry. As shown by Gŭven (1971) and by Zussman (1979), the symmetry in the interlayer is different also, which is  $\bar{1}$  in  $C12/m(1)$   $\lambda$ -symmetry and  $2_{[010]}$  in  $C\bar{1}$  and  $C12(1)$   $\lambda$ -symmetries (for details see Ferraris and Ivaldi, this volume).

### CHOICE OF THE AXIAL SETTING

A non-orthogonal mica polytype forms, besides the conventional (double) monoclinic  $C$ -centered cell, both a pseudo-orthorhombic  $C$ -centered sextuple cell and a pseudo-hexagonal  $P$  triple cell. For hexagonal and trigonal polytypes ( $\omega_{\parallel} = \omega_{\perp} = 0$ ) the triple cell is rigorously hexagonal. For all others, the orthohexagonal relation  $b = a3^{1/2}$  is obeyed only approximately, the deviation being measured either by an angular parameter  $\varepsilon$  (Donnay et al. 1964) or by a linear parameter  $\eta$  (Zvyagin and Drits 1996), which is a function of  $\omega_{\parallel}$  (Fig. 12). For metrically monoclinic polytypes,  $\beta$  (Class  $a$ ) or  $\alpha$  (Class  $b$ ) of the sextuple and triple cells are in general only close to  $90^\circ$ .

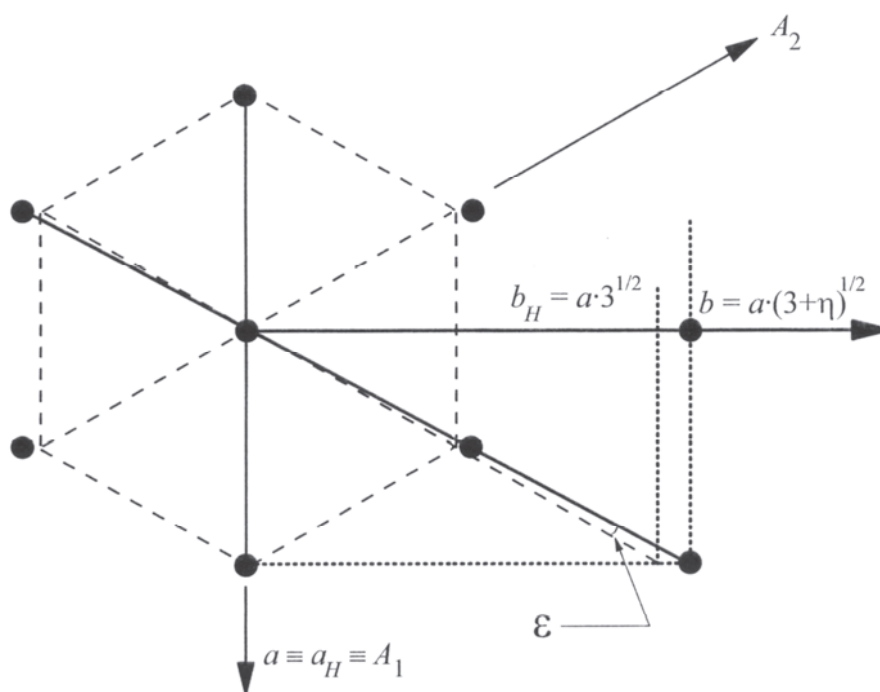


**Figure 12.** A small portion of the (001) two-dimensional  $hp$  lattice of micas.  $\varepsilon$  and  $\eta$  (exaggerated) are the angular and linear deviations from hexagonality.  $A_1, A_2$ : hexagonal axes ( $\varepsilon = 0, \eta = 0$ );  $a_H, b_H$ : orthohexagonal axes ( $\varepsilon = 0, \eta = 0$ ) of the  $C_1$  cell ( $b_H = a_H 3^{1/2}$ );  $a, b$ : pseudo-orthorhombic axes ( $\varepsilon \neq 0, \eta \neq 0$ ). The figure is drawn for the case  $b > b_H$ . Black circles: lattice nodes of the crystal lattice; dashed lines: H cell of the twin lattice; dotted lines:  $C_1$  cell built on the hexagonal and pseudo-hexagonal meshes (modified after Nespolo et al. 2000a).

The monoclinic setting in which, within the Trigonal model,  $\mathbf{c}_n$  is constant and the value of the monoclinic angle changes with the number of layers is labeled  $^a\mathbf{S}$  [Class  $a$ :  $\mathbf{c}_n = (\bar{1}/3, 0)$ ;  $\mathbf{S}$  stands for *Standard*] and  $^b\mathbf{T}$  [Class  $b$ :  $\mathbf{c}_n = (0, \bar{1}/3)$ ;  $\mathbf{T}$  stands for *Transitional*]. The corresponding monoclinic  $l$  indices are labeled  $l^a_{\mathbf{S}}$  and  $l^b_{\mathbf{T}}$  (Nespolo et al. 1997a). The metric equations in both direct and reciprocal space and the relations between  $l$  and  $h, k$  indices are given in Table 10. The  $^b\mathbf{T}$  setting is monoclinic  $a$ -unique

and does not correspond to any of the settings commonly adopted to describe monoclinic crystals. Nevertheless, it facilitates the comparison of the atomic coordinates with other polytypes (Backhaus and Āurovič 1984) and is thus the preferred setting to derive the family structure from a single polytype or vice versa. From  ${}^b\mathbf{T}$  a monoclinic  $b$ -unique setting is obtained through the exchange of axes by  $a \rightarrow -b$ ;  $b \rightarrow -a$ ;  $c \rightarrow -c$ , so that  $a > b$  and  $\beta > 90^\circ$ , as in the Smith and Yoder (1956) definition: this setting is labeled  ${}^b\mathbf{S}$  (Fig. 13). The exchange of axes is adopted when indexing the diffraction pattern (Nespolo et al. 1998; see also Takeda and Ross 1995).

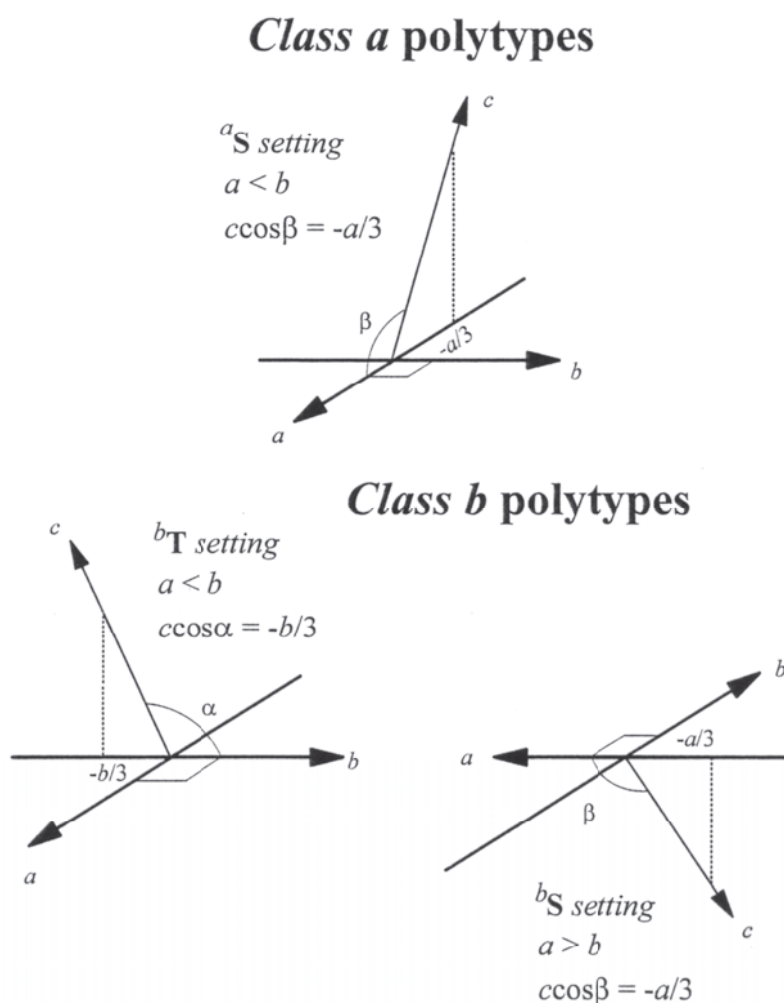


**Figure 13.** Definition of the  ${}^a\mathbf{S}$ ,  ${}^b\mathbf{T}$  and  ${}^b\mathbf{S}$  axial settings of mica polytypes.  ${}^a\mathbf{S}$  and  ${}^b\mathbf{S}$  settings have  $a < b$ ,  ${}^b\mathbf{T}$  setting has  $b < a$  [used by permission of the editor of *Mineralogical Journal*, from Nespolo (1999) Fig. 2, p. 56].

For each *Series* and each *Class*,  $K = 0$  of the *Subclass* 1, see Equation (2), determines the axial setting of the first polytype of the *Series*, which is termed the *Basic axial setting*. All the polytypes belonging to the same *Series* and the same *Class* can be indexed in a setting whose axes are parallel to the axes of the *Basic axial setting* but whose period along  $c$  is  $3K+L$  [Eqn. (2)] times the corresponding period of the *Basic axial setting*. For each *Series* the angle is constant, within the Trigonal model, and the value of  $\mathbf{c}_n$ , non-translationally reduced, changes with the number of layers: this setting is termed *Fixed-angle setting*. For the two *Classes* this setting is symbolized by  ${}^{3^n,a}\mathbf{F}$  and  ${}^{3^n,b}\mathbf{F}$ , which for

Series 0 are shortened in <sup>a</sup>F and <sup>b</sup>F (Nespolo et al. 1997a; 1998) (Fig. 14). This setting is obtained from <sup>a</sup>S and <sup>b</sup>S by means of the transformation:

$$(a \ b \ c)_{3^n, a; 3^n, b, S} \begin{bmatrix} (-1)^{L-1} & 0 & (-1)^L \cdot (K+L-1) \\ 0 & (-1)^{L-1} & 0 \\ 0 & 0 & 1 \end{bmatrix} = (a \ b \ c)_{3^n, a; 3^n, b, F} \quad (3)$$

where *L* (Subclass) and *K* are defined in Equation (2). The choice of a common setting for polytypes belonging to different Series is instead geometrically not possible, because these polytypes are not based on the same Basic axial setting (Fig. 14).

### GEOMETRICAL CLASSIFICATION OF RECIPROCAL LATTICE ROWS

By considering the  $l_{c_1} \pmod 3$  index of reciprocal lattice nodes (Table 10) on rows related by  $n \times 60^\circ$  rotations ( $0 \leq n \leq 5$ ), Nespolo et al (1997b, 2000a) have shown that there are only nine translationally independent rows parallel to  $c^*$  (Fig. 15) indicated as  $R_i$ ,  $1 \leq i \leq 9$ . In each  $R_i$  the same distribution of "present" and "absent" reflections is repeated along  $a^*$  and  $b^*$  with  $3p$  and  $3q$  translations ( $p$  and  $q$  are integers of the same parity).  $R_i$  are defined in terms of  $h$  and  $k$  as:  $[h_i \pmod 3, k_i \pmod 3, l]$  and are distributed along the edges and diagonals of a rhombus-shaped unit, termed *tessellation rhombus* (Fig. 15, solid lines), which can tessellate the entire reciprocal space by  $(3p, 3q)$  translations. A smaller unit, termed *minimal rhombus*, can be drawn (Fig. 15, dotted lines), defined by the same  $R_i$  each taken only once. Opposite edges are different and, contrary to the tessellation rhombus, the minimal rhombus does not represent a translational unit.

The two rhombi have six possible orientations, which represent equivalent descriptions of the same reciprocal lattice: they simply differ in the distribution of the  $R_i$ . Six equivalent rhombi are obtained by applying the five rotations (besides the identity) to the  $h_i, k_i$  indices of each of the nine  $R_i$  of the original rhombus and bringing the resulting  $R_i$  within the area spanned by the original rhombus through a  $(3p, 3q)$  translation between equivalent rows. The rows that can be obtained by rotating the original rhombus are within a star-polygon constructed by the six rhombi with the common origin (Fig. 15). The values of  $p$  and  $q$  to be considered are those connecting rows internal to the star-polygon but external to the original rhombus with rows internal to the original rhombus, i.e.  $(0, \pm 2)$ ,  $(1, \pm 1)$  and  $(2, \pm 2)$ .

**Table 10.** Metric equation in direct and reciprocal space and relation between Miller indices orthogonal and monoclinic settings for the two Classes (after Nespolo 1999).

Class	Metric equations in direct space	Metric equations in reciprocal space	relation between $l_{c_1}$ and $h, k$ indices	relation between orthogonal and monoclinic $l$ indices
<i>a</i>	$c \cos \beta = -a/3$	$a^* \cos \beta^* = c^*/3$	$l_{c_1} = h \pmod 3$	$l_{aS} = (l_{c_1} - h)/3$
<i>b</i>	$c \cos \alpha = -b/3$	$b^* \cos \alpha^* = c^*/3$	$l_{c_1} = k \pmod 3$	$l_{bT} = (l_{c_1} - k)/3$



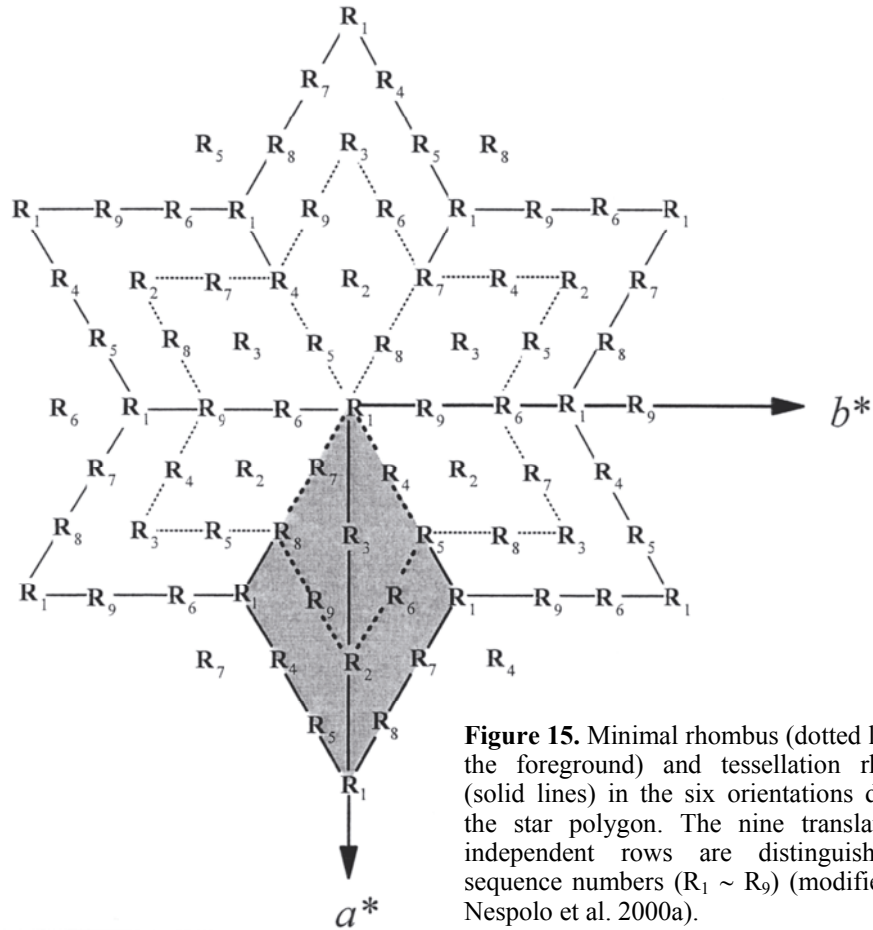


**Figure 15.** Minimal rhombus (dotted lines; in the foreground) and tessellation rhombus (solid lines) in the six orientations defining the star polygon. The nine translationally independent rows are distinguished by sequence numbers ( $R_1 \sim R_9$ ) (modified after Nespolo et al. 2000a).

The geometrical characteristics of the reciprocal lattice rows parallel to  $c^*$ , each taken as a whole, are termed "row features". In the Trigonal model all mica polytypes have the same row features, described by the regular tessellation  $\{3,6\}$  (Takeda and Donnay 1965; see the section "Tessellation of the  $hp$  lattice"), and the nine  $R_i$  were classified into three types (Fig. 16):

1. **S (Single) rows** [ $h = 0(\text{mod } 3)$  and  $k = 0(\text{mod } 3)$ ].
2. **D (Double) rows** [ $h \neq 0(\text{mod } 3)$  and  $k = 0(\text{mod } 3)$ ]. There are two translationally independent D rows, labeled  $D_i$ :  $i = 1, 2$ ;  $h = i(\text{mod } 3)$ ;  $k = 0(\text{mod } 3)$ .
3. **X (seXtuplet) rows** [ $k \neq 0(\text{mod } 3)$ ]. There are six translationally independent X rows, labeled  $X_i$ :  $1 \leq i \leq 6$ ;  $h = i(\text{mod } 3)$ ;  $k = 2 \times (-1)^i(\text{mod } 3)$ .

The nine  $R_i$  rows are thus classified as:  $R_1 = S$ ;  $R_{2-3} = D_{1-2}$ ;  $R_{4-9} = X_{1-6}$ . This classification of  $R_i$  corresponds exactly to the classification in three types of rows introduced by Āurovič (1982), who did not adopt specific names for each type of rows. Each of the three types lies on non-intersecting circular orbits centered on  $c^*$ , of radius  $3h^2 + k^2$  (cf. Table 4 and Fig. 19 in Ferraris and Ivaldi, this volume). Each of these orbits contains only one type of rows (an  $n \times 60^\circ$  rotation overlaps rows belonging to the same type only) and becomes an ellipsis when the incident beam is inclined by a general angle  $\phi$  to the sample. This is the principle on which the *oblique-texture electron diffraction* method (OTED, see Zvyagin 1967) is based, and has been recently applied also to XRD (Rieder and Weiss 1991; for details, see Ferraris and Ivaldi, this volume). Figure 16 shows the orbits of S (solid lines), D (dashed lines), and X (dotted lines). For D and X

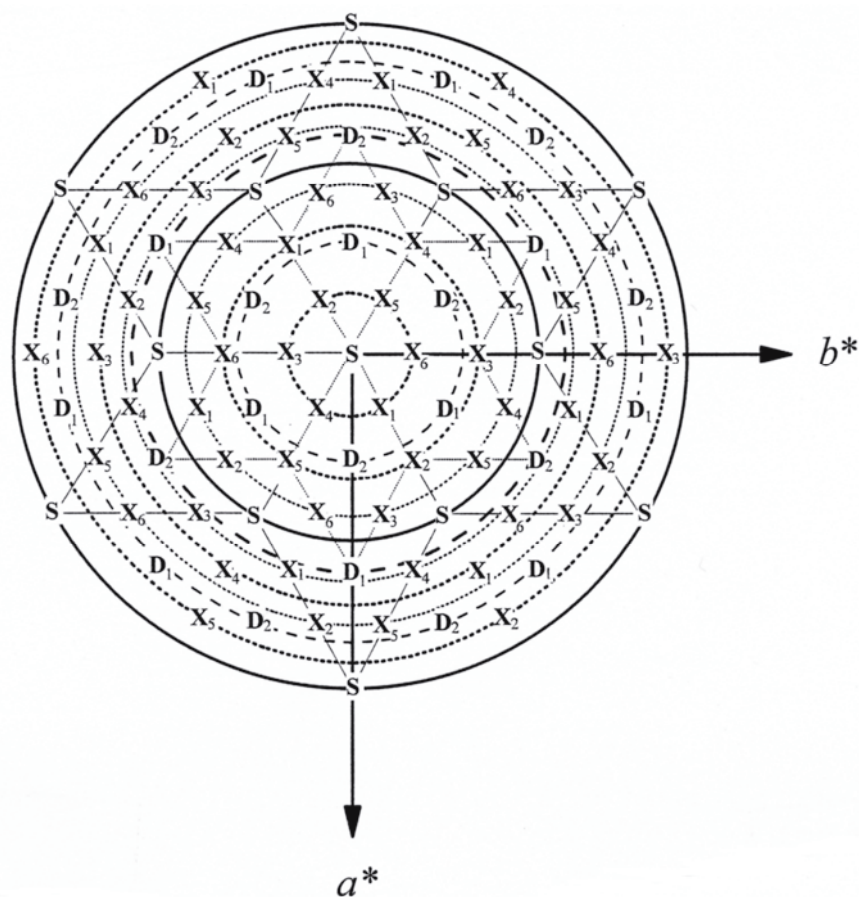


**Figure 16.** Rotational relation between reciprocal lattice rows parallel to  $c^*$ . Because of the pseudo-hexagonal symmetry of the 001 *r.p.*, each type of row (S, D, X) lies on a circular orbit around  $c^*$  with radius  $3h + k$ . Solid, dashed and dotted orbits contain S, D and X rows respectively. D and X orbits are further subdivided into those containing only one set of six rows ( $D_I$  and  $X_I$ , thick orbits) and those containing two sets of six rows ( $D_{II}$  and  $X_{II}$ , thin orbits). The  $n \times 60^\circ$  rotations, which correspond to the relative orientation of twinned mica individuals, relate only rows of the same type and same set (S,  $D_I$ ,  $D_{II}$ ,  $X_I$ ,  $X_{II}$ ), whereas the non-crystallographic rotations typical of plesiotwins relate rows of the same type but of different sets ( $D_I$  and  $D_{II}$ ;  $X_I$  and  $X_{II}$ ) (modified after Nespolo et al. 2000a).

rows, two types of orbits exist: type I ( $D_I$  and  $X_I$  orbits, thick lines) connects one set of six D or X rows, whereas type II ( $D_{II}$  and  $X_{II}$  orbits, thin lines) connects two sets of six D or X rows. The  $n \times 60^\circ$  rotations about  $c^*$  lead to an alternate exchange of the two D-type  $R_i$  located on the long diagonal of the minimal rhombus, and they exchange the six X-type  $R_i$  on the edges of the minimal rhombus in six different ways.

### SUPERPOSITION STRUCTURES, FAMILY STRUCTURE AND FAMILY REFLECTIONS

By superposing two or more identical copies of the same polytype translated by a *superposition vector* (i.e. a vector corresponding to a submultiple of a translation period) a fictitious structure is obtained, which is termed a *superposition structure*. Among the infinitely possible superposition structures, that structure having all the possible positions of each OD layers is termed a *family structure*: it exists only if the shifts between



adjacent layers are rational, i.e. if they correspond to a submultiple of lattice translations. The family structure is common to all polytypes of the same family (Dornberger-Schiff 1964; Āuroviĉ 1994). From a group-theoretical viewpoint, building the family structure corresponds to transforming (“completing”) all the local symmetry operations of a space groupoid into the global symmetry operations of a space-group (Fichtner 1977, 1980). Additional “virtual” atoms are created by the completed operations, and the resulting model may have physically unrealistic interatomic distances: they appear in the superposition structure, which is a purely mathematical construction, as a consequence of the group-theoretical process of completing the local symmetry operations. The group of translations of the polytype reciprocal lattice can be decomposed into a subgroup of translations, which corresponds to the Fourier transform of the family structure (family sublattice), and one or more cosets. The family sublattice is again common to all polytypes of the same family. This means that all polytypes of the same family, normalized to the *same volume of scattering matter*, have a weighted sublattice in common. The diffractions that correspond to the family sublattice are termed *family diffractions* (or, more commonly, *family reflections*). As discussed below, when indexed with respect to the basis vectors of any of the polytypes of the same family, the family sublattice shows several non-space-group absences, which indicate the existence of local symmetry operations. Clearly, the family reflections convey important information, because they reveal the symmetry of the family structure. The family reflections are always sharp, including the case of non-periodic (disordered) polytypes. In fact, the disorder of the stacking concerns the *distribution* of subsequent  $\rho$ -operations. If this distribution is periodic, after a finite even number of steps a period is closed and the product of those  $\rho$ -operations is the generating  $\tau$ -operation (remember that the product of an *even* number of  $\rho$ -operations is a  $\tau$ -operation). If instead the distribution of subsequent  $\rho$ -operations is not periodic, no generating  $\tau$ -operation can be found, and the polytype is disordered. In the family structure the  $\rho$ -operations are completed to global operations: the family structure and its Fourier transform, which consists in the family reciprocal sublattice, are thus common to both periodic and non-periodic polytypes of the same family<sup>4</sup> (Āuroviĉ and Weiss 1986; Āuroviĉ 1997, 1999).

Because the family structure can be deduced from the symmetry principle of the polytype family, it is possible to illustrate its derivation by means of a very simple, hypothetical example, in which the actual atomic arrangement is not taken into account, and geometrical figures with the appropriate  $\lambda$ -symmetry are used instead. Let us consider the three hypothetical polytypes (Āuroviĉ 1999) and their geometric diffraction patterns in Figure 17. The polytypes are constructed by stacking equivalent layers perpendicular to the plane of the drawing, with  $\lambda$ -symmetry  $P(1)m1$ . The stacking direction is  $a$ , and the distance between adjacent layers is  $|\mathbf{a}_0|$ . The  $\lambda$ -symmetry is indicated by isosceles triangles with a mirror plane  $[.m.]$ . The three polytypes can be related to a common orthogonal four-layer cell with  $\mathbf{a} = 4\mathbf{a}_0$ , inside which the cell of the polytype is shown by bold lines (Fig. 17). The first polytype (1A, MDO) has basis vectors  $\mathbf{a}_1 = \mathbf{a}_0 + \mathbf{b}/4$ ;  $\mathbf{b}_1 = \mathbf{b}$ ;  $\mathbf{c}_1 = \mathbf{c}$  and space-group  $P111$ . The only global  $\tau$ -operation is the translation  $\mathbf{a}_0 + \mathbf{b}/4$ . The second polytype (2M, MDO) has basis vectors  $\mathbf{a}_2 = 2\mathbf{a}_0$ ;  $\mathbf{b}_2 = \mathbf{b}$ ;  $\mathbf{c}_2 = \mathbf{c}$  and space-group  $P1a1$ . The global  $\tau$ -operations are the translation  $\mathbf{a} = 2\mathbf{a}_0$  and an  $a$ -glide plane at  $y = 1/8$  and  $7/8$ . The third polytype (4M, non-MDO) has basis vectors  $\mathbf{a}_3 = 4\mathbf{a}_0$ ;  $\mathbf{b}_3 = \mathbf{b}$ ;  $\mathbf{c}_3 = \mathbf{c}$  and space-group  $P1a1$ . The global  $\tau$ -operations are the translation  $\mathbf{a} =$

---

<sup>4</sup> The remaining diffractions, which correspond to the cosets of the weighted reciprocal lattice with respect to the family sublattice, are termed *non-family reflections* and are instead typical of each polytype: they can be sharp or diffuse, depending on whether the polytype is ordered or not, i.e. on whether the distribution of subsequent  $\rho$ -operations is ordered or random.



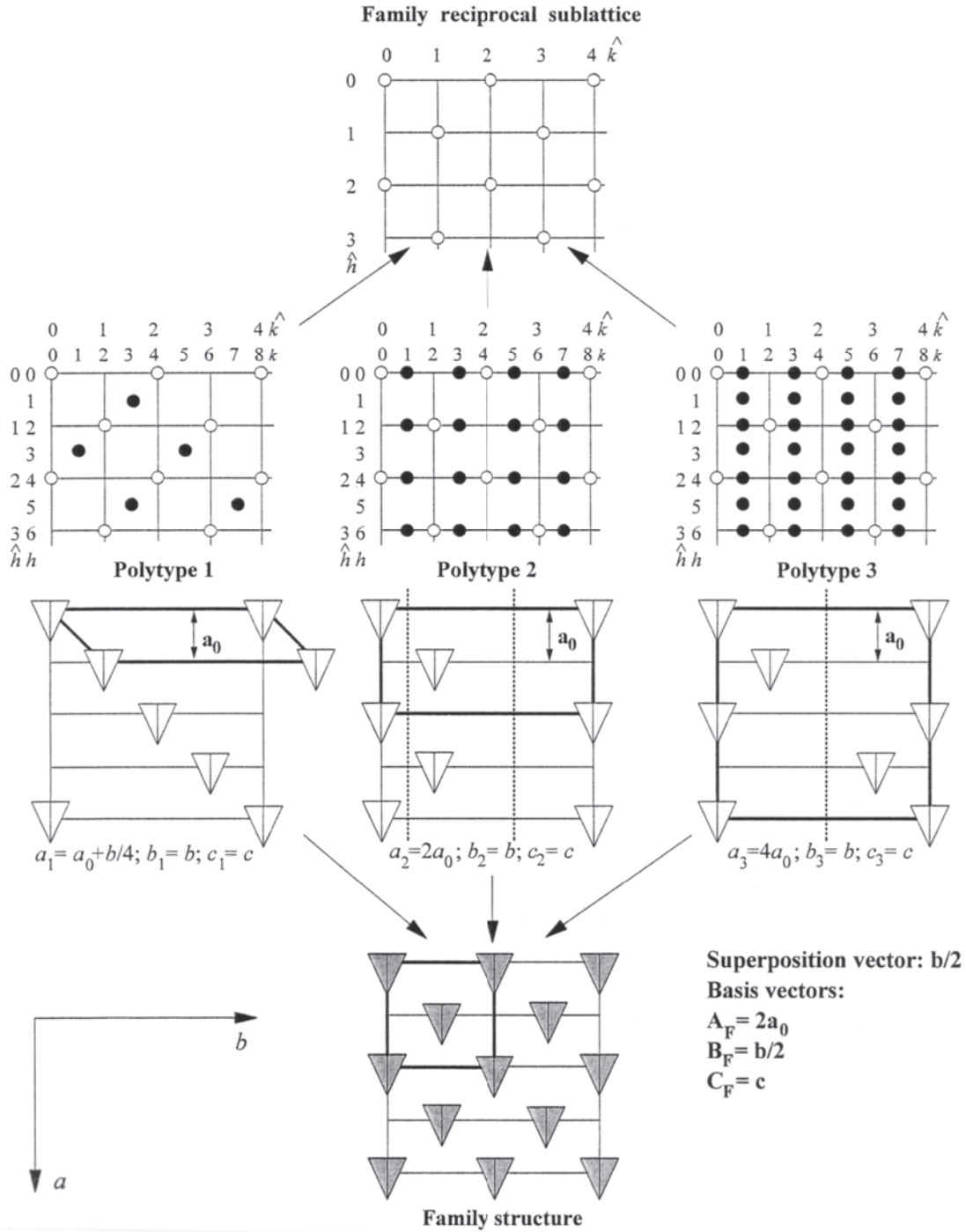


**Figure 17.** Schematic representation of three hypothetical structures belonging to the same family. The layers are perpendicular to the plane of the drawing, and their constituent atomic configurations are represented by isosceles triangles with  $\lambda$ -symmetry [m.]. All structures are related to a common, orthogonal four-layer cell with  $a = 4a_0$ . The family structure is obtained by superposing two identical copies of the same polytype, translated by  $b/4$ , the superposition vector. The diffraction indices refer also to the common cell. Family diffractions correspond to  $k = 2k$  (open circles), and the non-family diffractions, characteristic for individual polytypes, to  $k = 2k+1$  (close circles) (modified after Durovic and Weiss (1986)).

$4\mathbf{a}_0$  and an  $a$ -glide plane at  $y = 0$  and  $y = 1/2$ . The geometric diffraction pattern of each of these polytypes can be divided into two parts:  $\hat{k} = 2k$  (open circles) and  $\hat{k} = 2k+1$  (full circles). The  $\hat{k} = 2k$  are the family reflections, which define the family reciprocal sublattice, common to all the three polytypes. The Fourier transform of this subgroup of diffraction gives the family structure, with space-group  $C1m1$ ,  $\mathbf{a} = 2\mathbf{a}_0$ ,  $\mathbf{b} = \mathbf{b}/2$ : the superposition vector is  $\mathbf{b}/2$ . The non-family reflections are those for which  $\hat{k} = 2k+1$ : the number of reflections along each row in the four-layer reciprocal cell is the same as the number of layers in the period of the polytype.

### Family structure and family reflections of mica polytypes

For micas, the family structure of the Pauling model is nine-fold (the supergroup of translation in direct space has the order nine) and the superposition vectors are  $\pm a/3$  and  $\pm b/3$ ; its symmetry is  $P6/mmm$  (Dornberger-Schiff et al. 1982). To any of the atoms in the layer, eight additional atoms are generated in the family structure, with coordinates  $(x\pm 1/3, y)$ ;  $(x, y\pm 1/3)$  and  $(x\pm 1/3, y\pm 1/3)$ . The family reflections are those with  $h = 0(\text{mod } 3)$  and  $k = 0(\text{mod } 3)$ , and correspond to S rows. The subgroup of translations in reciprocal space has the order nine. Because the layer stagger is  $|a|/3$ , the family vectors of the Pauling model complete the local symmetry operations of space groupoids to global symmetry operations of space groups after one single layer. Therefore, the period along the  $c$  axis of the family structure is  $c_0 = 1/c^*_1 = c_{1M}\sin\beta_{1M}$  and thus corresponds to the vertical distance between two closest interlayer cations. The basis vectors of the family structure are  $A_{F1} = A_1/3$ ,  $A_{F2} = A_2/3$ ,  $C_F = c_0$ . (Backhaus and Āuroviĉ 1984; Āuroviĉ et al. 1984; Āuroviĉ 1994).

In the Trigonal model each of the three families (homo-, meso- and hetero-octahedral) splits into two subfamilies, A and B. For both subfamilies the family structure is three-fold and the superposition vectors are  $\pm b/3$ . To any of the atoms in the layer, two additional atoms are generated in the family structure, with coordinates  $(x, y\pm 1/3)$ . The family reflections are those with  $k = 0(\text{mod } 3)$  and correspond to S and D rows. The subgroup of translation in reciprocal space has the order three. The family vectors complete the local symmetry operations of space groupoids to global symmetry operations of space groups after three layers for subfamily A, but after two layers for subfamily B. The basis vectors for the family structure are thus  $A_{F1} = (A_1+2A_2)$ ,  $A_{F2} = -(2A_1+A_2)$ ,  $C_F$ . For subfamily A,  $C_F = 3c_0$ ; for subfamily B,  $C_F = 2c_0$ . The symmetry of the family structure is  $H_R\bar{3}1m$  (where the subscript  $R$  indicates that the smaller cell is rhombohedral) for subfamily A, and  $H6_3/mcm$  for subfamily B (Āuroviĉ 1994). The adoption of the  $H$ -centered cell allows the description of the family structures and the real structures in the same axes, but additional absences appear in the diffraction pattern (*cf.* Smrĉok et al. 1994, Appendix, for cronstedtite-3T). Mixed-rotation polytypes are OD structures only when the ditrigonal rotation of the tetrahedra is zero. Their family structure and family reflections are those of the Pauling model (S rows).

From the practical viewpoint, as noted by Āuroviĉ (1982), the family reflections of the nine-fold family structure (S rows) are common to all members of a family and are thus not useful for the purpose of distinguishing individual polytypes. D rows instead are characteristic of all members of a subfamily (A or B, in case of micas), permit to distinguish the kind of polytype (subfamily A, subfamily B or mixed-rotation).

The real layers building micas deviate from their archetypes by several distortions, and the shifts between successive layers are in general not exactly rational. The intensities, but not the geometry, of the family reflections differ from polytype to polytype of the same family, and the divergence increases with the deviation of the real layers from their archetypes. Notwithstanding, the concepts of family structure and family reflections are useful in the identification of twins and polytypes, as shown below.

## REFLECTION CONDITIONS

In the diffraction pattern of mica polytypes, systematic non-space-group absences extensively appear. The *International Tables for Crystallography* term this kind of absences *additional reflection conditions* (Hahn and Vos 2002). This definition does not provide anything about the kind of information one can get from these absences. As seen above, the absences along S and D rows derive from the existence of local symmetry operations that relate pairs of packets. These local symmetry operations are not accounted for in the space-group type. In the Trigonal model, any mica polytype of a given family is constructed from layer archetypes in which the atoms in each plane are distributed according to a hexagonal pattern. These atoms are either on special positions, or on positions that, without corresponding to any translation-free symmetry operation of the space-group type, have higher translational symmetry. These positions, under the symmetry operations of a space-group type, define sets of points (*crystallographic orbits*) the eigensymmetry group of which includes additional translations, and are known as *extraordinary orbits of space-groups* (Wondratschek 1976; Matsumoto and Wondratschek; 1979). The corresponding lattice of translation vectors is a proper superlattice of the polytype lattice. In reciprocal space, these vectors correspond to a sublattice, which shows systematic non-space-group absences when indexed with respect to the basis vectors of the polytype. The OD description is based on the existence of local symmetry operations, whereas the description in terms of crystallographic orbits is based on the points on which those local symmetry operations act. In spite of the different languages, the concepts are basically the same. The approach involving crystallographic orbits is not specifically related to VC structures but it is more general. The possible superlattices were however derived for all space-group types *within the same syngony* (Engel et al. 1984). There are no derivations yet for the cases in which the superlattice belongs to a Bravais system higher than that of the entire lattice. The superlattice common to all polytypes of a family (family superlattice, i.e. the lattice of the family structure) corresponds to this latter case (with the exception of trigonal-hexagonal polytypes, of which only *3T* has been reported so far). A general symmetry analysis of mica polytypism in terms of crystallographic orbits is nowadays a completely open task, but the non-space-group absences along S and D rows are interpretable in terms of extraordinary orbits as well. The deviations of layers from their archetypes correspond to the movement of part of the atoms slightly away from the positions of higher translational symmetry, towards general positions. As a consequence, violations of the non-space-group absences appear as faint reflections between pairs of family reflections. These faint reflections can be recorded in dioctahedral micas (Rieder 1968) and, with longer exposure times, in Li-rich trioctahedral micas (Rieder 1970), but they are almost undetectable in Li-poor trioctahedral micas. This sequence is in accordance with the extent of the structural distortions, which decreases in the same order.

The reflection conditions in the two subfamilies were derived by Nespolo (1999). The number and positions of reflections along the D rows reveal the symmetry of the family structure (*H<sub>R</sub>31m*: subfamily A; *H6<sub>3</sub>/mcm*: subfamily B; *P6/mmm*: mixed-rotation). In addition, they are particularly useful in evaluating the possible presence of twins. Taking into account that for non-orthogonal polytypes only one out of three of the orthogonal *l* indices corresponds to integer monoclinic indices, and that subfamily B polytypes necessarily contain an even number of layers, the reflection conditions are (*N* and *N'* are the number of layers in the conventional and orthogonal cell respectively):

1. **S rows** (family reflections of the nine-fold family structure): one reflection out of *N* always occurs, with presence criterion  $l_{C_1} = 0(\text{mod } N)$ .
2. **D rows**: one reflection (family reflection) out of *N* occurs for subfamily A polytypes [presence criterion  $l_{C_1} = (\pm N'h/3)(\text{mod } N)$ , "+" for the obverse setting of the family

structure, “–” for the reverse setting], two (family reflections) for subfamily B [equally spaced, at  $l_{C_1} = 0(\text{mod } N'/2)$ ], and  $N'$  (non-family reflections) for mixed-rotation polytypes.

3. **X rows:**  $N$  reflections appear in the  $c^*_1$  repeat (non-family reflections for all polytypes).

One or more of the  $N$  reflections along X rows (and for mixed-rotation polytypes also along D rows) may be very weak or absent. This non-space-group absence is related not to the symmetry of the family structure, as for family reflections, but to the stacking mode within the polytype.

The family structure of subfamily A polytypes admits a primitive rhombohedral cell, and its lattice (family sublattice) can be overlapped for *all* polytypes belonging to subfamily A only if it is rotated by  $180^\circ$  around the normal to the layer when comparing polytypes built by layers of opposite orientational parity. This is because the rhombohedral primitive cell of the family structure for subfamily A polytypes is in the obverse setting for one orientational parity of the layers (odd orientational parity of the symbols), but in the reverse setting for the other (even orientational parity of the symbols). In *Series 0*, all polytypes belonging to subfamily A are *Class a* polytypes. Polytypes belonging to a different *Subclass* have opposite orientational parity. The “F” setting alternates the directions of  $(a, b)$  and  $(a^*, b^*)$  axes with the *Subclass* (Fig. 14) and is exactly the axial setting leading to the overlap of the sublattice built on family reflections. In higher *Series*, polytypes belonging to subfamily A can be orthogonal or *Class b* polytypes and there is no longer a 1:1 correspondence.

Subfamily B polytypes show two reflections along D rows. However, polytypes of this subfamily either are orthogonal or belong to *Class b*, for which the non-right angle is  $\alpha$  (before the axes interchange) and the  $l_{C_1}$  index of the superlattice nodes does not depend on  $h$ . The reciprocal sublattice in this case matches for all polytypes, which is consistent with the fact that the primitive cell of the family structure is hexagonal.

In mixed-rotation polytypes, the family reflections are only those of the nine-fold family structure and appear along S rows. D rows convey important information, because the different number of reflections along the rows, or their diffuseness, unambiguously reveals the mixed-rotation character of the polytype.

### NON-FAMILY REFLECTIONS AND ORTHOGONAL PLANES

Reciprocal central planes, which have  $c^*$  in common, can be usefully classified, on the basis of the rows they contain, into SD and SX. Here we consider the six densest central planes, which are sufficient for a twin/polytype analysis. The three densest central reciprocal planes (*r.p.*, hereafter) are of type SX:  $0k^*$ ,  $hhl$  and  $\bar{h}hl$ . These planes have the shortest separation between pairs of reciprocal lattice rows parallel to  $c^*$  (about  $0.22\text{\AA}^{-1}$ ), and are followed by the three densest SD central *r.p.*  $h0l$ ,  $h.3h.l$  and  $h.3\bar{h}.l$  (about  $0.38\text{\AA}^{-1}$ ). These six central planes are shown in Figure 18, projected onto the  $(a^*, b^*)$  plane. The three SD central planes are  $60^\circ$  apart each, and the same holds for the three central SX planes. The two kinds of planes are each  $30^\circ$  apart. The SD central planes show the symmetry of the family structure. Then, from the intensities measured along one or more X rows, the stacking sequence can be determined. However, the presence of twinning must be excluded before analyzing the intensity distribution, and for this purpose the analysis of the geometry of the diffraction pattern, in particular the number and type of orthogonal planes, is of primary importance. A plane is orthogonal if the direction  $r^*$  corresponding to the line perpendicular to  $c^*$  and passing through the origin (a direction that belongs to the orthohexagonal cell) contains a node for each row parallel to  $c^*$ .

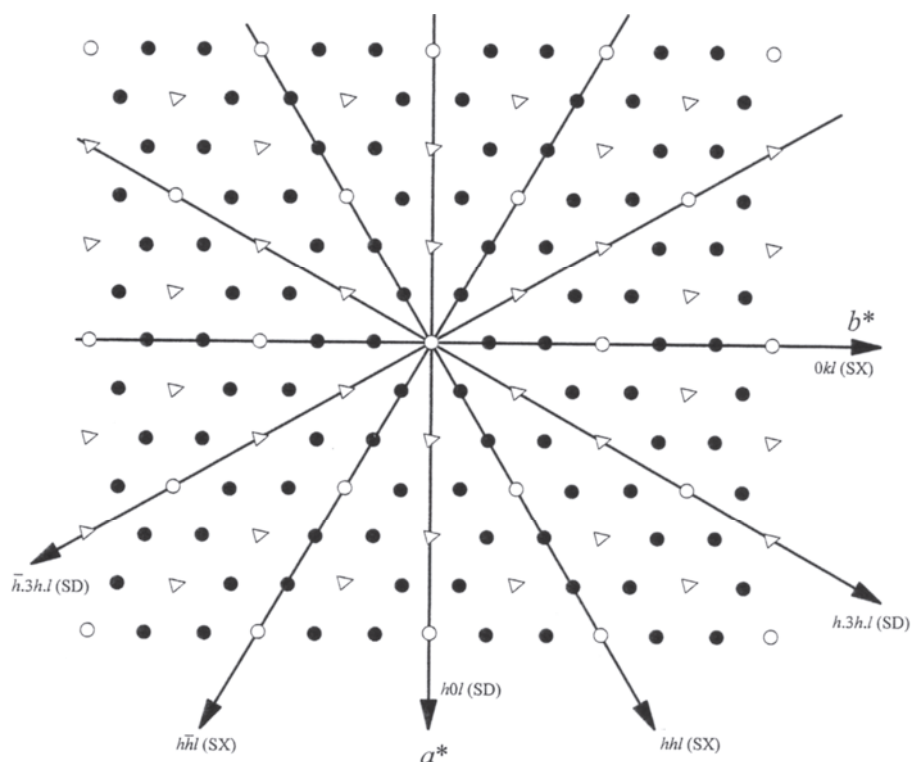


**Figure 18.** (001) projection of mica reciprocal lattice. Open circles: S rows; open triangles: D rows; close circles: X rows. The six central planes (three SD and three SX) that can commonly be recorded by a photographic technique such as precession camera are indicated (modified after Nespolo et al.1999d). Cf. Figure 4 in Sadanaga and Takeda (1969) and Figure 1 in Durovic (1982).

In case of a non-orthogonal plane, no nodes are present on  $r^*$  along the X rows, and the node closest to  $r^*$  is at a height  $\pm c^*_1/3N$ , where  $N$  is the number of layers in the conventional cell. If the node on  $r^*$  or closest to it corresponds to an absent reflection, the orthogonality of the plane must be judged from the position of the two adjacent reflections, whose height is either  $\pm c^*_1/N$  (orthogonal plane) or  $\mp 2c^*_1/3N$  (non-orthogonal plane). For D rows the family character of the reflections should be considered. In subfamily A polytypes, reflections appear at  $\pm c^*_1/3$  (non-orthogonal SD plane); in subfamily B polytypes, reflections appear at 0 and  $c^*_1/2$  (orthogonal SD plane); in mixed-rotation polytypes, the D rows correspond to non-family rows and the same criteria given for X rows hold. Finally, S rows always contain a node on  $r^*$ .

The number and features of the orthogonal planes (as defined above) depend both on the *Class* (lattice features) and on the subfamily (OD character). These are easily obtained by taking into account that polytypes in subfamily B and in subfamily A *Series*  $> 0$  never belong to *Class a*, whereas polytypes in subfamily A *Series* 0 always belong to *Class a*.

1. *Orthogonal polytypes*. In case of subfamily A polytypes, only the three SX central planes are orthogonal, according to the above definition. For subfamily B and mixed-rotation polytypes, all the six central planes are orthogonal.
2. *Class a polytypes*. One SX central *r.p.* is orthogonal:  $0kl$ .
3. *Class b polytypes*. None of the three SX central planes are orthogonal. In subfamily A polytypes (*Series*  $> 0$ ) the SD central planes are non-orthogonal and thus none of the six densest central planes is orthogonal. In subfamily B, the three densest SD

central planes are orthogonal. In mixed-rotation polytypes, D rows correspond to non-family reflections and on these rows, in general,  $N$  reflections occur. On the basis of the relation between  $l$  indices in  ${}^bT$  and in  $C_1$  settings ( $l_{bT}$  and  $l_{C_1}$ ; Table 10), the three SD densest central planes are orthogonal also.

### HIDDEN SYMMETRY OF THE MICAS: THE RHOMBOHEDRAL LATTICE

Takeda (1971) analyzed the symmetry properties of the RTW symbols and showed that the stacking of the mica layers can produce polytypes belonging to five kinds of symmetries:  $A$ ,  $M$ ,  $O$ ,  $T$ ,  $H$ ; it is thus not possible to obtain a polytype belonging to the rhombohedral Bravais system. Notwithstanding, the rhombohedral lattice appears in the geometry of the diffraction pattern and plays an important role in the twinning of the micas. Here the first aspect is briefly analyzed, whereas the effect on twinning is considered below. There are two categories of polytypes in which the rhombohedral lattice represents a kind of “hidden symmetry” for micas.

- 1) *Subfamily A polytypes*. As shown in the section dealing with the family structure, the family structure of subfamily A polytypes has symmetry  $H_R(\bar{3})1m$ , admitting a primitive rhombohedral cell. Within the Trigonal model the family reciprocal sublattice is rhombohedral both in its geometry and intensity distribution. In the real diffraction pattern the intensity distribution deviates from rhombohedral symmetry proportionally to the deviations of the layer from their archetypes described by the Trigonal model, but the geometry remains rhombohedral.
- 2) *Class b polytypes*. Successive lattice planes parallel to (001) are shifted by  $1/3$  of the short (*Class a*) or the long (*Class b*) diagonal of the two-dimensional pseudo-hexagonal mesh built on ( $A_1$ ,  $A_2$ ) axes. For *Class b* polytypes a pseudo-rhombohedral primitive cell can be chosen, having (almost) the same volume of the reduced cell (Fig. 19). The primitive cell is closer to rhombohedral when the layers are closer to

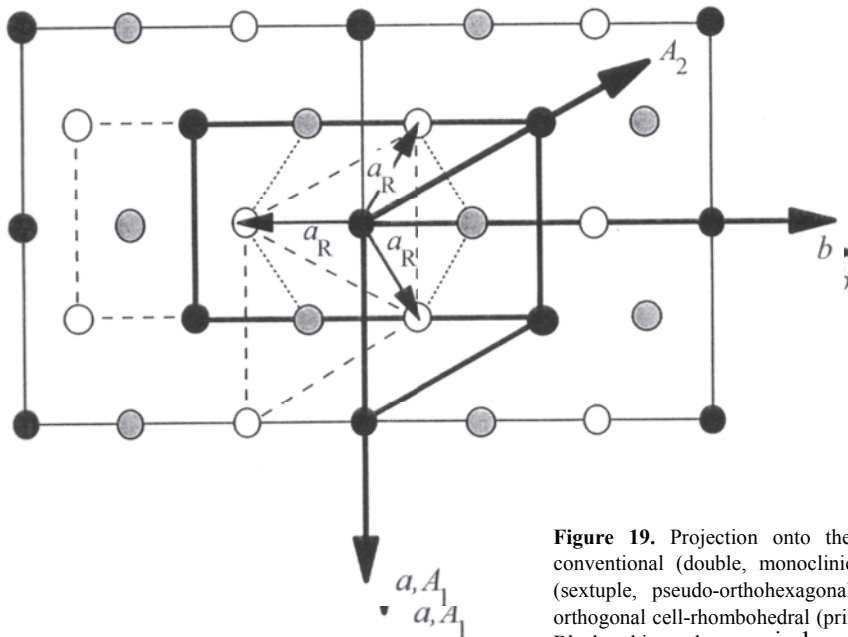


**Figure 19.** Projection onto the (001) plane of the primitive, conventional (double, monoclinic), pseudo-hexagonal (triple),  $C_1$  (sextuple, pseudo-orthohexagonal) and pseudo- $c$  axis of the orthogonal cell-rhombohedral (primitive) cells of *Class b* polytypes. Black, white and gray circles represent lattice nodes at  $z = 0$ ,  $1/3$

and  $2/3$  ( $z$  is referred to  $c$  axis of the orthogonal cells). Thick lines: borders of the  $C_1$  cell and of the pseudo-hexagonal cell. Dashed lines: borders of the upper plane of the conventional and primitive cells (the lower plane is in common with  $C_1$  cell and pseudo-hexagonal cell respectively). The pseudo-rhombohedral cell (dotted lines) is best viewed by means of the pseudo-rhombohedral axes  $a_R$ .  $a$ ,  $b$ : (pseudo)-orthohexagonal axes.  $A_1$ ,  $A_2$ : (pseudo)-hexagonal axes (modified after Nespolo 1999).

their archetypes as described by the Trigonal model. The general reflection conditions for the rhombohedral lattice in hexagonal axes,  $-h+k+l = 3n$ , expressed in the  $C_1$  setting become:  $-3h+k+2l = 6n$ . Taking into account the  $C$  centering condition, the latter equation corresponds to  $l(\text{mod } 3) = k(\text{mod } 3)$ , which is simply an alternative expression of the condition that monoclinic indices are integers, given in Table 10 for the  ${}^bT$  setting (Nespolo 1999).

Because non-orthogonal polytypes of subfamily A *Series*  $> 0$  belong to *Class b*, in this case the “hidden” rhombohedral symmetry appears both in the family sublattice and in the entire polytype lattice.

### TWINNING OF MICAS: THEORY

The definition and classification of twinning is given in Appendix A. The pseudo-symmetries typical of micas made the recognition of the twin laws difficult, and Friedel initially classified mica twins among the “macles aberrantes” (Friedel 1904, p. 222), i.e. oriented crystal associations without either twin plane or twin axis *stricto sensu*. The derivation of the twin laws for mica polytypes must consider the point groups of the twin lattice and of the lattice of the individual, and the point group of the syngony of the individual. The twin operators are the point symmetry operators of the twin lattice not belonging to the point group of the individual and can be obtained by coset decomposition. The decomposition of the twin lattice point group (order  $m$ ) yields one subgroup (the point group of the individual, order  $m' < m$ ) and  $n = m/m'-1$  cosets corresponding to the twin laws. Hereafter the subgroup corresponding to the point group of the individual is always given first, and the twin laws follow as cosets No. 1 to  $n$ . All merohedral polytypes, in any syngony, may undergo twinning by syngonic merohedry: the twin laws depend on the point group of the polytype and should thus be derived case by case (see the example for  $3T$  below). Instead, twins other than by syngonic merohedry can be derived with a general procedure. Hereafter, indexing is given in the (pseudo)orthohexagonal setting of the twin lattice.

- 1) Polytypes of the orthorhombic syngony with a  $hP$  lattice may undergo twinning by metric merohedry, the twin lattice coinciding with the lattice of the individual. The coset decomposition gives two twin laws:

$$\begin{aligned}
 6/mmm = & \left\{ 1, 2_{[010]}, 2_{[001]}, 2_{[100]}, \bar{1}, m_{(010)}, m_{(001)}, m_{(100)} \right\} \cup \\
 & \cup \left\{ 6_{[001]}^+, 6_{[001]}^-, 2_{[110]}, 2_{[1\bar{1}0]}, \bar{6}_{[001]}^+, \bar{6}_{[001]}^-, m_{(130)}, m_{(1\bar{3}0)} \right\} \cup \\
 & \cup \left\{ 3_{[001]}^-, 3_{[001]}^+, 2_{[310]}, 2_{[3\bar{1}0]}, \bar{3}_{[001]}^-, \bar{3}_{[001]}^+, m_{(110)}, m_{(1\bar{1}0)} \right\}.
 \end{aligned} \tag{4}$$

All the operators corresponding to the same twin law are equivalent under the action of the symmetry operators of the orthorhombic syngony. If the lattice is only  $oC$ , twinning is by pseudo-merohedry. The twin lattice ( $hP$ ) does not coincide exactly with the lattice of the individual, because for the latter the orthohexagonal relation  $b = a3^{1/2}$  is only approximated. However, the two lattices have the three orthohexagonal axes parallel. The coset decomposition is the same as given in Equation (4), but the non-zero obliquity ( $\omega = \omega_{\parallel} \neq 0$ ,  $\omega_{\perp} = 0$ ) makes the operators in each of the two cosets not equivalent, as described in detail below.

- 2) Polytypes of the monoclinic and triclinic syngony with an  $hP$  lattice may undergo twinning by metric merohedry. For the monoclinic syngony the coset decomposition gives five twin laws, each with four equivalent twin operators:

$$\begin{aligned}
 6/mmm = & \left\{1, 2_{[010]}, \bar{1}, m_{(010)}\right\} \cup \left\{2_{[001]}, 2_{[100]}, m_{(001)}, m_{(100)}\right\} \cup \\
 & \cup \left\{3_{[001]}^-, 2_{[310]}, \bar{3}_{[001]}^-, m_{(110)}\right\} \cup \left\{6_{[001]}^-, 2_{[110]}, \bar{6}_{[001]}^-, m_{(130)}\right\} \cup \\
 & \cup \left\{3_{[001]}^+, 2_{[\bar{3}\bar{1}0]}, \bar{3}_{[001]}^+, m_{(1\bar{1}0)}\right\} \cup \left\{6_{[001]}^+, 2_{[\bar{1}\bar{1}0]}, \bar{6}_{[001]}^+, m_{(1\bar{3}0)}\right\}
 \end{aligned} \quad (5)$$

whereas for the triclinic syngony the coset decomposition gives eleven twin laws, each with two equivalent twin operators:

$$\begin{aligned}
 6/mmm = & \left\{1, \bar{1}\right\} \cup \left\{2_{[010]}, m_{(010)}\right\} \cup \left\{2_{[001]}, m_{(001)}\right\} \cup \left\{2_{[100]}, m_{(100)}\right\} \cup \\
 & \cup \left\{3_{[001]}^-, \bar{3}_{[001]}^-\right\} \cup \left\{2_{[310]}, m_{(110)}\right\} \cup \left\{6_{[001]}^-, \bar{6}_{[001]}^-\right\} \cup \left\{2_{[110]}, m_{(130)}\right\} \cup \\
 & \cup \left\{3_{[001]}^+, \bar{3}_{[001]}^+\right\} \cup \left\{2_{[\bar{3}\bar{1}0]}, m_{(1\bar{1}0)}\right\} \cup \left\{6_{[001]}^+, \bar{6}_{[001]}^+\right\} \cup \left\{2_{[\bar{1}\bar{1}0]}, m_{(1\bar{3}0)}\right\}.
 \end{aligned} \quad (6)$$

If the lattice of the individual is  $oC$ , the first two cosets in Equation (5) and the first four cosets [Eqn. (6)] correspond to metric merohedry, whereas the others correspond to pseudo-merohedry ( $\omega = \omega_{\parallel} \neq 0$ ,  $\omega_{\perp} = 0$ ). If the lattice of the individual is  $mC$  Class  $a$ , the twin laws in Equations (5) and (6) correspond to reticular pseudo-merohedry. The  $hP$  twin lattice is a sublattice for the individual, with subgroup of translation  $3$ : the twin index is thus  $3$ .

- 3) Monoclinic and triclinic Class  $b$  polytypes with a two-dimensional hexagonal mesh in the (001) plane and a  $c_n$  projection of exactly  $|b|/3$  has a  $hR$  lattice. Twin elements belonging to the  $hR$  lattice but not to the monoclinic or triclinic syngony correspond to the twinning by metric merohedry, whereas twin elements belonging to the  $hP$  sublattice but not to the  $hR$  lattice correspond to twinning by reticular merohedry. The subgroup of translation defining the  $hP$  sublattice is  $3$ , and thus the twin index is  $3$  also. The coset decomposition gives five (monoclinic syngony) or eleven (triclinic syngony) twin laws:

monoclinic syngony:

$$\begin{aligned}
 6/mmm = & \left\{1, 2_{[100]}, \bar{1}, m_{(100)}\right\} \cup \left\{3_{[001]}^-, 2_{[110]}, \bar{3}_{[001]}^-, m_{(130)}\right\} \cup \\
 & \cup \left\{3_{[001]}^+, 2_{[\bar{1}\bar{1}0]}, \bar{3}_{[001]}^+, m_{(1\bar{3}0)}\right\} \cup \left\{2_{[001]}, 2_{[100]}, m_{(001)}, m_{(100)}\right\} \cup \\
 & \cup \left\{6_{[001]}^-, 2_{[310]}, \bar{6}_{[001]}^-, m_{(110)}\right\} \cup \left\{6_{[001]}^+, 2_{[\bar{3}\bar{1}0]}, \bar{6}_{[001]}^+, m_{(1\bar{1}0)}\right\}.
 \end{aligned} \quad (7)$$

triclinic syngony:

$$\begin{aligned}
 6/mmm = & \left\{1, \bar{1}\right\} \cup \left\{2_{[100]}, m_{(100)}\right\} \cup \left\{3_{[001]}^-, \bar{3}_{[001]}^-\right\} \cup \left\{2_{[110]}, m_{(130)}\right\} \cup \\
 & \cup \left\{2_{[\bar{1}\bar{1}0]}, m_{(1\bar{3}0)}\right\} \cup \left\{3_{[001]}^+, \bar{3}_{[001]}^+\right\} \cup \left\{2_{[001]}, m_{(001)}\right\} \cup \left\{6_{[001]}^-, \bar{6}_{[001]}^-\right\} \cup \\
 & \cup \left\{6_{[001]}^+, \bar{6}_{[001]}^+\right\} \cup \left\{2_{[310]}, m_{(110)}\right\} \cup \left\{2_{[010]}, m_{(010)}\right\} \cup \left\{2_{[\bar{3}\bar{1}0]}, m_{(1\bar{1}0)}\right\}.
 \end{aligned} \quad (8)$$



The first two [Eqn. (7)] or four [Eqn. (8)] cosets give the twin laws by metric merohedry, the others give the twin laws by reticular merohedry. Twin operators in each coset are equivalent by the action of the symmetry elements of the syngony.

If the two-dimensional mesh in the (001) plane is not rigorously hexagonal ( $\omega_{\parallel} \neq 0$ ), or if the  $c_n$  projection is not exactly  $|b|/3$  ( $\omega_{\perp} \neq 0$ ), the  $hR$  lattice does not coincide exactly with the lattice of the individual; moreover, the  $hP$  sublattice is only an approximate sublattice for the individual. The twin laws derived in Equations (7) and (8) do not change, but they correspond to pseudo-merohedry and reticular pseudo-merohedry instead of metric merohedry and reticular merohedry respectively. The operators in each coset are no longer equivalent.

### Choice of the twin elements

The twin element that relates a pair of individuals occurs in the morphology of the twin. Micas show two kinds of twin morphologies: rotation twins, with composition plane (001), and reflection twins, with composition plane (almost) normal to (001). As noted by Friedel (1904), the twin axis for rotation twins is within the composition plane, whereas the twin plane for reflection twins coincides with the composition plane.

Whereas the morphological twin operation is unique, the geometrical operations bringing the twin lattice into self-coincidence are in general more numerous, as shown in the previous section. For zero obliquity, the operations within each coset corresponding to a twin law are equivalent, when considering only the lattice, by the action of the symmetry elements of the individual. The morphological twin operation is termed the *representative operation of the coset* (Nespolo and Ferraris 2000). For non-zero obliquity, however, they are no longer equivalent and the correct twin operations are those obeying the law of Mallard, which requires that the twin operations are crystallographic operations. As an example, let us consider the decomposition of the point group of the  $hP$  twin lattice with respect to the point group of the monoclinic syngony in Equation (5). If the monoclinic polytype has a  $hP$  lattice (twinning by metric merohedry) or sublattice (twinning by reticular merohedry) the six two-fold axes in the (001) plane are exactly  $30^\circ$  each apart and each of them is perpendicular to a plane ( $hk0$ ): the four operations in each coset are truly equivalent, when considering only the lattice. Instead, if the lattice or sublattice of the individual is not exactly hexagonal (twinning by pseudo-merohedry and reticular pseudo-merohedry), either  $\omega_{\parallel}$  or  $\omega_{\perp}$  (in general both) is non-zero. For  $\omega_{\parallel} \neq 0$  the  $2_{[310]}$ ,  $2_{[3\bar{1}0]}$ ,  $2_{[110]}$  and  $2_{[1\bar{1}0]}$  are  $(2n+1) \times 30 \pm \varepsilon^\circ$  apart from  $2_{[010]}$  /  $2_{[100]}$  and they are no longer perpendicular to the ( $hk0$ ) planes (Fig. 20). Twin axes and twin planes deviate thus from mutual perpendicularity: rotation twins and reflection twins are no longer equivalent, even for centrosymmetric crystals, and are called *reciprocal twins* (Mügge 1898) or *corresponding twins* (Friedel 1904, 1926). For  $\omega_{\perp} = 0$  the equivalence relations become:

$$\begin{aligned}
 2_{[310]} \cdot 2_{[010]} &= 3_{[001]}^- \pm 2\varepsilon & m_{(110)} \cdot m_{(010)} &= 3_{[001]}^- \mp 2\varepsilon \\
 2_{[3\bar{1}0]} \cdot 2_{[010]} &= 3_{[001]}^+ \pm 2\varepsilon & m_{(1\bar{1}0)} \cdot m_{(010)} &= 3_{[001]}^+ \mp 2\varepsilon \\
 2_{[110]} \cdot 2_{[010]} &= 6_{[001]}^- \pm 2\varepsilon & m_{(130)} \cdot m_{(010)} &= 6_{[001]}^- \mp 2\varepsilon \\
 2_{[1\bar{1}0]} \cdot 2_{[010]} &= 6_{[001]}^+ \pm 2\varepsilon & m_{(1\bar{3}0)} \cdot m_{(010)} &= 6_{[001]}^+ \mp 2\varepsilon \\
 2_{[100]} \cdot 2_{[010]} &= 2_{[001]} & m_{(100)} \cdot m_{(010)} &= 2_{[001]}
 \end{aligned}$$

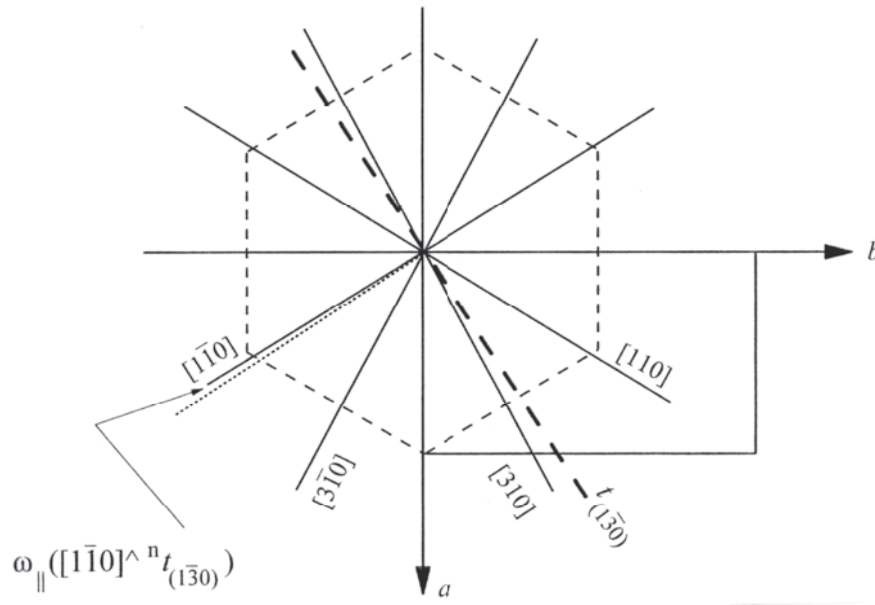


**Figure 20.** Component of the obliquity within the (001) plane of the pseudo-*hp* lattice of micas. The six directions  $[hk0]$  (including the  $a$  and  $b$  axes) in the (001) plane (solid lines) would be equivalent in a hexagonal lattice. The dashed thick line is  $t_{(130)}$ , *i.e.*, the intersection of the (130) plane with the (001) plane, which is almost but not exactly normal to  $[110]$  direction (it would be normal to it in a truly *hp* lattice). The trace of the  $t_{(010)}$  and  $t_{(100)}$  coincide with  $a$  and  $b$  axes respectively ( $\gamma = 90^\circ$ ). To improve the clearness of the figure, the  $t_{(hkl)}$  of the other three planes that would be equivalent in a truly *hp* lattice are not shown, but they can be easily traced (modified after Nespolo and Ferraris 2000).

Only the two-fold rotation about  $c$  of the twin lattice is a correct twin operation, in the sense that it restores the lattice, or a sublattice, of the individuals. If however  $\omega_{\perp} \neq 0$ , the  $c$  axis of the twin lattice is no longer exactly perpendicular to the (001) plane and the above rotations are defined only with respect to  $c^*$  and not to  $c$ : none of them is thus a correct twin operation. The rotations about  $c^*$  give simply the (approximate) relative rotations between pairs of twinned mica individuals, but are not true twin operations. Similar considerations apply also to the rotoinversion operations.  $\varepsilon$  depends upon the obliquity of the twin but, at least in Li-poor trioctahedral micas, is sufficiently small to be neglected for practical purposes (Donnay et al. 1964; Nespolo et al. 1997a,b, 2000a).

In Table 11 the complete scheme developed above is summarized for ease of consultation.

### Effect of twinning by selective merohedry on the diffraction pattern

The above analysis does not consider the case of selective merohedry, which does not appear in the morphology of the twin but influences the diffraction pattern by relating lattice nodes corresponding to present reflections from one individual to nodes corresponding to non-space-group absences from another individual. Twinning by either syngonic or metric merohedry (for the definitions, see Appendix A) does not modify the geometry of the diffraction pattern. Instead, twinning by selective merohedry, *i.e.* when the twin operation belongs to the point group of the twin lattice but not to the point group of the family structure, produces an unusual diffraction pattern. The typical case is that of the  $3T$  polytype orthogonal *Series 1* subfamily A, space-group type  $P3_{1,2}12$ , which has an *hP* lattice. As shown above, the family structure is rhombohedral and the family reflections (S and D rows) obey the presence criterion  $l = N^{\circ}h/3(\text{mod } N^{\circ})$ . With respect to

Table 11. Kind of twinning and twin laws for mica polytypes classified on the basis of the polytype syngony, polytype lattice and twin lattice.

Syngony of the individual	Lattice of the individual	Twin lattice	Kind of twinning	Twin laws	Twin index	Rotation between pairs of individuals*	Polytypes	
<i>O</i>	<i>hP</i>	<i>hP</i>	syngonic merohedry	#	1	#	merohedral polytypes	
	<i>hP</i>	<i>hP</i>	metric merohedry	[310] (110); [310] (110)	1	$\pm(120)^\circ$	all polytypes	
	<i>oC</i>	<i>hP</i>	pseudo-merohedry	[310] (110); [310] (110)	1	$\pm(120\pm 2\varepsilon)^\circ$	all polytypes	
<i>A/M</i>	<i>oC</i>	<i>oC</i>	syngonic merohedry	#	1	#	merohedral polytypes	
	<i>hP</i>	<i>hP</i>	metric merohedry	[310] (110); [310] (110) [110] (130); [110] (130) [100] (100)	1	$\pm(120)^\circ$ $\pm(60)^\circ$ (180) $^\circ$	all polytypes	
	<i>oC</i>	<i>hP</i>	pseudo-merohedry	[310] (110); [310] (110) [110] (130); [110] (130)	1	$\pm(120\pm 2\varepsilon)^\circ$ $\pm(60\pm 2\varepsilon)^\circ$	all polytypes	
<i>M</i>	<i>hR</i>	<i>hR</i>	metric merohedry	[100] (010)	1	(180) $^\circ$	all polytypes	
	(Class <i>b</i> polytypes)	<i>hR</i>	metric merohedry	[110] (130); [110] (130)	1	$\pm(60)^\circ$	all polytypes	
		<i>hP</i>	reticular merohedry	[310] (110); [310] (110) [100] (100)	3	$\pm(60)^\circ$ (180) $^\circ$	all polytypes	
	<i>aC</i> <sup>†</sup> / <i>mC</i> Class <i>b</i>	<i>hR</i>	pseudo-merohedry	[110] (130); [110] (130)	1	$\pm(120\pm 2\varepsilon)^\circ$	all polytypes	
		<i>hP</i>	reticular pseudo-merohedry	[310] (110); [310] (110) [010] (010)	3	$\pm(60\pm 2\varepsilon)^\circ$ (180) $^\circ$	all polytypes	
	<i>aC</i> <sup>†</sup> / <i>mC</i> Class <i>a</i>	<i>hP</i>	reticular pseudo-merohedry	[310] (110); [310] (110) [110] (130); [110] (130) [100] (100)	3	$\pm(120\pm 2\varepsilon)^\circ$ $\pm(60\pm 2\varepsilon)^\circ$ (180) $^\circ$	all polytypes	
		<i>mC</i> Class <i>b</i>	<i>mC</i>	syngonic merohedry	[100] (100)	1	(180) $^\circ$	merohedral polytypes
	<i>A</i>	<i>mC</i> Class <i>a</i>	<i>mC</i>	syngonic merohedry	[010] (010)	1	(180) $^\circ$	merohedral polytypes
		<i>mC</i> Class <i>b</i>	<i>mC</i>	metric merohedry	[100] (100)	1	(180) $^\circ$	all polytypes
	<i>A</i>	<i>mC</i> Class <i>a</i>	<i>mC</i>	metric merohedry	[010] (010)	1	(180) $^\circ$	all polytypes
<i>aC</i> <sup>†</sup> Class <i>b</i>		<i>mC</i>	pseudo-merohedry	[100] (100)	1	(180 $\pm 2\varepsilon$ ) $^\circ$	all polytypes	
<i>aC</i> <sup>†</sup> Class <i>a</i>		<i>mC</i>	pseudo-merohedry	[010] (010)	1	(180 $\pm 2\varepsilon$ ) $^\circ$	all polytypes	
<i>A</i>	<i>aC</i> <sup>†</sup>	<i>aC</i> <sup>†</sup>	syngonic merohedry	1	1	0 $^\circ$	merohedral polytypes	

<sup>†</sup>The unconventional *C* centring of triclinic polytypes is adopted to preserve the same pseudo-orthohexagonal axes (*a*, *b*) used for polytypes of the other Bravais systems. \*Rotations about *c*\*. #Symmetry elements and relative rotations depend on the point group of the individual

the period of the family sublattice,  $1/3c_0$ , one reflection appears in the  $1/c_0$  repeat, with presence criterion  $l = h(\text{mod } 3)$ . The coset decomposition gives three twin laws:

$$6/mmm = \{1, 3_{[001]}^+, 3_{[001]}^-, 2_{[010]}, 2_{[310]}, 2_{[3\bar{1}0]}\} \cup \{2_{[100]}, 2_{[1\bar{1}0]}, 2_{[110]}, 2_{[001]}, 6_{[001]}^-, 6_{[001]}^+\} \cup \{m_{(100)}, m_{(130)}, m_{(1\bar{3}0)}, m_{(001)}, 6_{[001]}^-, 6_{[001]}^+\} \cup \{m_{(010)}, m_{(110)}, m_{(1\bar{1}0)}, \hat{i}, 3_{[001]}^-, 3_{[001]}^+\} \quad (9)$$

By expressing the twin laws through the Shubnikov's two-color group notation (in which the twin elements are dashed: Curien and Le Corre 1958), the three twin laws are:  $6'2'2'$ ;  $6'm'2'$ ;  $3'12/m'$ . The complete twin [i.e. twin by merohedry or reticular merohedry, in which the number of individuals generated from the original individual is equal to the number of possible twin laws (Curien and Donnay 1959)] contains four individuals and has symmetry  $6'/m'' 2'/m''' 2/m''''$ . The  $6'2'2'$  and  $6'm'2'$  twin laws correspond to syngonic selective merohedry class IIA, whereas the  $3'12/m'$  twin law corresponds to syngonic complete merohedry class I (Table A1). In the twins by syngonic selective merohedry, the twin operations do not belong to the point group of the family structure, and the two individuals in the twin are rotated by  $(2n+1) \times 60^\circ$ , whereas layer rotations of subfamily A polytypes are  $2n \times 60^\circ$ . These twin operations produce the complete overlap of the reflections along X rows and S rows, but not of those along D rows. For example, the  $h0l$  family row of one individual is overlapped to the symmetrically independent  $h0l$  family row of the other individual. Because of the presence criterion given above, the two reflections from the two individuals in the  $1/c_0$  repeat along D rows are not overlapped, but are separated by  $1/3c_0$  (Fig. 21). The  $6'2'2'$  and  $6'm'2'$  twin laws, although being twin laws by merohedry according to the classical definition, produce the overlap of only one third of the family reflections (those along S rows), behaving thus as twin laws by reticular merohedry with respect to the family structure.

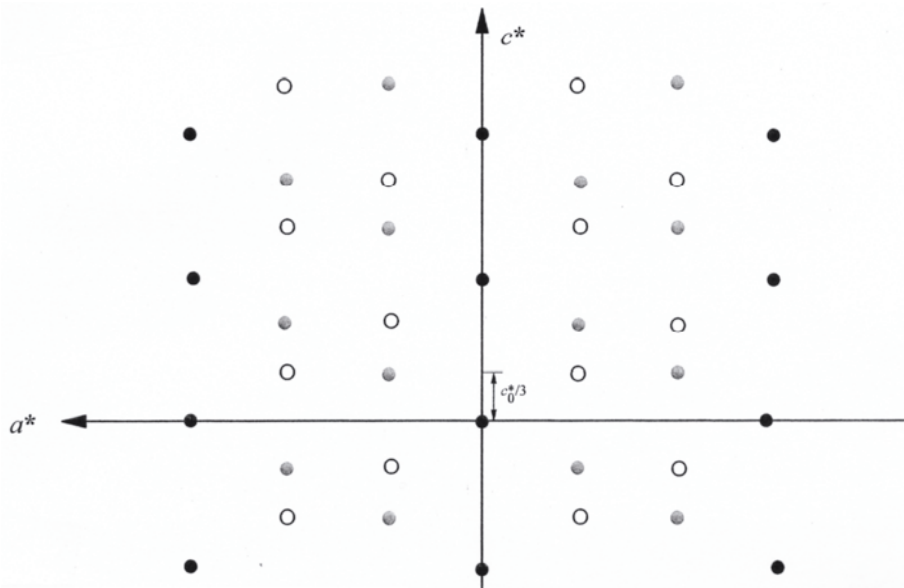


**Figure 21.**  $h0l$  r.p. (SD family plane) of the  $3T$  polytype twinned by selective merohedry. Black circles: family reflections overlapped by the twin operation (common to both individuals). Gray and white circles: family reflections from two individuals rotated by  $(2n+1) \times 60^\circ$ , not overlapped by the twin operation (modified after Nespolo et al. 1999a).

### Diffraction patterns from twins

The twin reciprocal lattice results from the overlap of the reciprocal lattices of the individuals. From each individual, lattice rows of the same type (S, D or X) overlap into a single composite row. The reflections along a composite row are perfectly aligned for  $c_n = |a|/3$  or  $|b|/3$ , but slightly deviate from alignment where  $c_n$  departs from those ideal values. Because of the physical (non-zero) dimension of the reflections, which for micas are commonly broad and oval-shaped, a zigzag disposition of reflections from different individuals can in practice be observed only for significant deviations of  $c_n$ , typical of dioctahedral micas and, to a minor extent, for Li-rich trioctahedral micas (Rieder 1970). The zigzag disposition of the reflections along rows parallel to  $c^*$  is indicative of twinning, but it is normally not noticeable in Li-poor trioctahedral micas. The presence of twinning has thus to be evaluated, in general, from the geometry of the SD and SX central planes.

For non-orthogonal polytypes the metric relations  $lc_1 = h \pmod{3}$  (*Class a*) and  $lc_1 = k \pmod{3}$  (*Class b*) hold (see Table 10). Depending upon the twin law(s) (and thus the relative orientation of twinned individuals), non-family reflections from different individuals may either overlap or occur at positions separated by  $c^*_1/3N$ , where  $N$  is the number of layers in the repeat unit (Table 10). Where two of the three positions in a  $c^*_1/N$  repeat are occupied, the presence of twinning should be suspected. In contrast, where each of the three positions are occupied, the number of reflections in a  $c^*_1$  repeat of a non-orthogonal twinned  $N$ -layer polytype is the same as that of an untwinned  $3N$ -layer polytype. This phenomenon is known as “apparent polytypism” (Takano and Takano 1958). However, twinning in some cases modifies the appearance of the D rows, which, for subfamily A polytypes, may show two reflections at  $1/3$  and  $2/3$  of the  $c^*_1$  repeat, as in case of selective merohedry. The number and the position of reflections along D rows, as well as the number of orthogonal planes, in most cases allows the presence of twinning to be distinguished.

1. Twinning of subfamily A polytypes in which individuals are rotated by  $(2n+1) \times 60^\circ$  corresponds to twinning by reticular pseudo-merohedry. This twinning produces a separation of the single reflection on D rows from each individual into two reflections, corresponding to  $l(c^*_1) = 1 \pmod{3}$  and  $l(c^*_1) = 2 \pmod{3}$ ; no reflection appears corresponding to  $l(c^*_1) = 0 \pmod{3}$ ; this pattern is clearly different from that of a subfamily B polytypes, where two equally spaced reflections appear. In addition, if rotation is by  $\pm 60^\circ$ , for *Series 0* polytypes (*Class a*) the orthogonal plane of one individual necessarily overlaps a non-orthogonal plane of another individual. The composite diffraction pattern has thus two or three SX orthogonal central planes.
2. Twinning of subfamily A polytypes in which individuals are rotated by  $2n \times 60^\circ$  corresponds to twinning by reticular pseudo-merohedry for *Class a* (*Series 0*), but to pseudo-merohedry for *Class b* (*Series > 0*). Twinning produces overlap of the single reflection on D rows from each individual; no reflection appears corresponding to  $l(c^*_1) = 0 \pmod{3}$ . However, for polytypes of *Series 0* (*Class a*) two or three SX planes are orthogonal, depending on the number of individuals. When three such planes appear (three or more twinned individuals), the geometrical features of the diffraction pattern are the same as for orthogonal *Series 1* polytypes. This situation corresponds to the  $3T$  polytype vs. twinned  $1M$ . For dioctahedral micas it is distinguished by careful examination of the appearance of weak reflections violating the reflection conditions (e.g., Nespolo and Kogure 1998), whereas for trioctahedral micas different techniques, such as microscopic observation of the crystal surface, may be necessary (e.g., Nespolo and Kuwahara 2001). If the twin involves only two

individuals, successive reflections along X are unequally separated (1/3 and 2/3) and two SX planes are orthogonal: the presence of twinning is thus easily recognized.

3. Subfamily B polytypes either are orthogonal or belong to *Class b*. In the latter case only three of the five pairs of twin laws correspond to twinning by reticular pseudo-merohedry. However, the corresponding twin operations lead to the overlap of the two reflections on D rows from each individual; no SX plane is orthogonal, whereas the three SD planes are orthogonal. The presence of twinning is not evident.
4. For mixed-rotation polytypes D rows are non-family rows. For *Class a* polytypes, two individuals rotated by 180° share one orthogonal *r.p. Okl*, but reflections are unequally spaced. The presence of twinning is thus evident. In other cases, two or more SX planes are orthogonal, as for subfamily A polytypes of the same *Class*, but no SD plane is orthogonal. The presence of twinning is again evident. For *Class b* polytypes the three SD planes are orthogonal and the presence of twinning is not evident.

In Tables 12a-12c the complete scheme of the identification process is shown. The approximated relative rotations between twinned individuals are given: the corresponding twin laws are easily obtained from Table 11. For *Class a* polytypes (which represent most of the polytypes reported to date) the presence of twinning can be confirmed or excluded by simple inspection of the geometry of the diffraction pattern. Special attention is however needed to distinguish a 3*N*-layer orthogonal polytype from the spiral twinning of three non-orthogonal *N*-layer *Class a* polytypes in which the individuals are rotated by  $2n \times 60^\circ$ . For polytypes of *Class b* subfamily A *Series 1* the presence of reticular pseudo-merohedry twinning is also evident. In the other cases the presence of twinning cannot be confirmed or excluded by analyzing the geometry of the diffraction pattern.

### Allotwinning

The oriented association of two or more crystals differing only in their polytypic character is termed *allotwinning*, from the Greek  $\alpha\lambda\lambda\omicron\varsigma$ , “different”, with reference to the individuals (Nespolo et al. 1999c). Allotwinning differs from twinning in that the individuals are not identical but have a different stacking sequence. Allotwinning differs also from oriented overgrowth (epitaxy: Royer 1928, 1954) and oriented intergrowth (syntaxy: Ungemach 1935) because the chemical composition is (ideally) identical and, because the building layer(s) are the same, at least two of the three parameters – those in the plane of the layer – are identical also. A cell common to the two individuals can always be found, which in general is a multiple cell for both crystals: the parameter not in the plane of the layer is the shortest one common to the cells of both individuals. As in case of triperiodic epitaxy, a three-dimensional common lattice exists (*allotwin lattice*): it may coincide with the lattice of one or more individuals or be a sublattice of it. Whereas a triperiodic epitaxy in general may or may not occur, depending on the degree of misfit of the lattice parameters of the individuals, there is no similar condition in allotwinning, because the individuals have a common mesh in the plane of the layer(s) even in polytypes with a different space-group type.

The allotwin operation is a symmetry operation for the allotwin lattice, which may belong to the point group of one or more individuals also. The allotwin of *N* individuals is characterized by *N* *allotwin indices*: the allotwin index of the *j*-th individual is the order of the subgroup of translation in direct space defining the allotwin lattice with respect to the lattice of the *j*-th individual.

### Tessellation of the *hp* lattice

Assuming the mica two-dimensional lattice in the (001) plane is *hp* [ $\omega_{\parallel} = 0$ ], the lattice can be described through a regular tessellation {3,6}, i.e. an assemblage of equal

**Table 12a.** Classification of diffraction patterns for  $N = 3K+L$ . For the correspondence between the relative rotations of twinned individuals and the twin laws see Table 11 (after Nespolo 1999).

Number of planes with orthogonal appearance	Number of reflections in the $c^*$ repeat along reciprocal lattice rows corresponding to family reflections			N
	1	2		
1 (SX)	$[l_{C_1} \neq 0(\text{mod } 3)]$ Subfamily A Series 0 Class a untwinned polytype	$l_{C_1} = 1(\text{mod } 3)$ and $2(\text{mod } 3)$ -----	$[l_{C_1} = 0(\text{mod } N)$ and $N/2(\text{mod } N)]$ -----	Mixed-rotation Series 0 Class a untwinned polytype
3 (SX)	Subfamily A Series 0 orthogonal polytype untwinned or $\pm 120^\circ$ -twinned	Subfamily A Series 0 orthogonal ( $\pm 60^\circ / 180^\circ$ )-twinned polytype	-----	-----
3 (SD)	-----	-----	Subfamily B Series 0 Class b polytype untwinned or $\pm 120^\circ$ -twinned	Mixed-rotation Series 0 Class b polytype untwinned or $\pm 120^\circ$ -twinned
6 (SX and SD)	-----	-----	Subfamily B Series 0 orthogonal polytype	Mixed-rotation Series 0 orthogonal polytype

**Table 12b.** Classification of diffraction patterns for  $N = 3(3K+L)$ .

Number of planes with orthogonal appearance	Number of reflections in the $c^*_1$ repeat along reciprocal lattice rows corresponding to family reflections			$N$
	1	2		
0	$[l_{c_1} \neq 0(\text{mod } 3)]$ <i>Subfamily A Series 1 Class b</i> polytype untwinned or $\pm 120^\circ$ -twinned	-----	$l_{c_1} = 0(\text{mod } N)$ and $N/2(\text{mod } N)$	-----
1 (SX)	-----	<i>Subfamily A Series 0 Class a</i> polytype $180^\circ$ -twinned	-----	Mixed-rotation <i>Class a</i> : <i>Series 1</i> untwinned polytype <i>Series 0</i> polytype $180^\circ$ -twinned
2 (SX)	<i>Subfamily A Series 0 Class a</i> polytype $\pm 120^\circ$ -twinned (two individuals)	<i>Subfamily A Series 0 Class a</i> polytype $\pm 60^\circ$ -twinned (two individuals)	-----	Mixed-rotation <i>Series 0 Class a</i> polytype ( $\pm 60^\circ / \pm 120^\circ$ )-twinned (two individuals)
3 (SX)	<i>Subfamily A Series 0 Class a</i> polytype $\pm 120^\circ$ -twinned (three individuals) <i>Subfamily A Series 1</i> orthogonal polytype untwinned or $\pm 120^\circ$ -twinned	<i>Subfamily A Series 0 Class a</i> polytype $\pm 60^\circ$ -twinned (three individuals) <i>Subfamily A Series 1</i> orthogonal polytype ( $\pm 60^\circ / \pm 180^\circ$ )-twinned	-----	Mixed-rotation <i>Series 0 Class a</i> polytype ( $\pm 60^\circ / \pm 120^\circ$ )-twinned (three individuals)
3 (SD)	-----	-----	<i>Subfamily B Class b</i> : <i>Series 1</i> polytype untwinned or $\pm 120^\circ$ -twinned <i>Series 0</i> polytype ( $\pm 60^\circ / 180^\circ$ )-twinned	Mixed-rotation <i>Class b</i> : <i>Series 1</i> polytype untwinned or $\pm 120^\circ$ -twinned <i>Series 0</i> ( $\pm 60^\circ / 180^\circ$ )-twinned polytype
6 (SX and SD)	-----	-----	<i>Subfamily B Series 1</i> orthogonal polytype	Mixed-rotation <i>Series 1</i> orthogonal polytype



**Table 12c.** Classification of diffraction patterns for  $N = 3^{n>1}(3K+L)$ . For the correspondence between the relative rotations of twinned individuals and the twin laws see Table 11 (after Nespolo 1999).

Number of planes with orthogonal appearance	Number of reflections in the $c^*_1$ repeat along reciprocal lattice rows corresponding to family reflections		
	1	2	$N$
0	$[l_{C_1} \neq 0(\text{mod } 3)]$ <i>Subfamily A Series n Class b</i> polytype untwinned or $\pm 120^\circ$ -twinned	$l_{C_1} = 1(\text{mod } 3)$ and $2(\text{mod } 3)$ <i>Subfamily A Series n-1 Class b</i> polytype ( $\pm 60^\circ / 180^\circ$ )-twinned	-----
1 (SX)	-----	-----	Mixed-rotation <i>Class a:</i> <i>Series n</i> polytype untwinned <i>Series n-1</i> polytype $180^\circ$ -twinned
2 (SX)	-----	-----	Mixed-rotation <i>Series n-1 Class a</i> polytype ( $\pm 60^\circ / \pm 120^\circ$ )-twinned (two individuals)
3 (SX)	<i>Subfamily A Series n</i> orthogonal polytype untwinned or $\pm 120^\circ$ -twinned	<i>Subfamily A Series n</i> orthogonal polytype ( $\pm 60^\circ / 180^\circ$ )-twinned	Mixed-rotation <i>Series n-1 Class a</i> polytype ( $\pm 60^\circ / \pm 120^\circ$ )-twinned (three individuals)
3 (SD)	-----	-----	Mixed-rotation <i>Class b:</i> <i>Series n</i> polytype untwinned or $\pm 120^\circ$ -twinned <i>Series n-1</i> ( $\pm 60^\circ / 180^\circ$ )-twinned polytype
6 (SX and SD)	-----	-----	Mixed-rotation <i>Series n</i> orthogonal polytype

regular 3-gons (triangles), 6 surrounding each vertex, that covers the two-dimensional plane without overlap or interstices (Schläfli 1950). The tessellation  $\{3, 6\}$  defines the hexagonal mesh; its dual,  $\{6, 3\}$ , gives the  $H$  centering nodes (Coxeter 1973; 1989). If  $(u, v)$  are the coordinates of a node of  $\{3, 6\}$ , which define a vector:

$$\mathbf{r} = u\mathbf{A}_1 + v\mathbf{A}_2 \quad (10)$$

$(\mathbf{A}_1, \mathbf{A}_2, \mathbf{c}; |\mathbf{A}_1| = |\mathbf{A}_2| = a \cong 5.3\text{Å}; \gamma = 120^\circ)$ , the five other nodes produced by  $n \times 60^\circ$  ( $0 \leq n \leq 5$ ) rotations about the origin are:  $(u-v, u)$ ,  $(-v, u-v)$ ,  $(-u, -v)$ ,  $(v-u, -u)$ ,  $(v, v-u)$ . If  $u = v = 1$ , these nodes together with the origin give the  $\{3, 6\}$  regular tessellation. If  $u \neq 1$  or  $v \neq 1$  the *compound tessellation*  $\{3, 6\}[n\{3, 6\}]$  is obtained, whose larger mesh has multiplicity  $n$ :

$$n = u^2 + v^2 - uv \quad (11)$$

(Takeda and Donnay 1965). The length of the vector connecting the origin with a node of coordinates  $(u, v)$  is<sup>5</sup>:

$$r = an^{1/2} \quad (12)$$

and for the regular tessellation ( $u = v = 1$ )  $r/a = 1$ . A single set of six nodes with the same  $r$  exists when either  $u$  or  $v = 0$ ,  $v = u$  or  $v = 2u$ : these nodes lie on the six directions corresponding to the reflection lines in the plane. In all other cases, there are two sets of six nodes with the same  $r$ , which lie outside the six reflection lines. The generating nodes of the two sets are defined as follows:

$$\text{set I: } u_{\text{I}}, v; \text{ set II: } u_{\text{II}}, v; \quad v > u_{\text{II}} = (v - u_{\text{I}}) > u_{\text{I}} > 0 \quad (13)$$

In reciprocal space ( $\gamma = 60^\circ$ ), the relation corresponding to (11a) is given by:

$$\text{set I: } H, K; \text{ set II: } K, H; \quad H = u; \quad K = v - u \quad (14)$$

These are the conditions in reciprocal space given by Zvyagin and Gorshkov (1966) for the regularity of the secondary reflections in hexagonal nets being derivable from only geometrical considerations based on the superposition of the cells of both lattices. Reciprocal lattice nodes of set I correspond to the orbits S, D<sub>I</sub>, X<sub>I</sub>, and those of set II to the orbits D<sub>II</sub> and X<sub>II</sub> in Figure 16.

Because the  $\mathbf{b}$  axis of the  $C_1$  orthohexagonal cell is given by  $\mathbf{b} = \mathbf{A}_1 + 2\mathbf{A}_2$ , the generating node of set I is always between  $\mathbf{b}_{C_1}$  and  $\mathbf{A}_2$  axes, whereas that generating set II is always between  $\mathbf{A}_1$  and  $\mathbf{b}_{C_1}$  axes. Nodes belonging to the same set are still related by  $n \times 60^\circ$  rotations, whereas those belonging to different sets are related by a non-crystallographic angle. These sets are symmetrically disposed with respect to the reflection lines in the plane, which thus bisect the rotation angle (Fig. 22, drawn for  $u_{\text{I}} = 1$ ,  $u_{\text{II}} = 3$ ,  $v = 4$ ). Taking counter clockwise rotations as positive, the angle relating nodes belonging to sets I and II are<sup>6</sup>:

$$\begin{aligned} \varphi' : (\text{I} \rightarrow \text{II})^+ &= (\text{II} \rightarrow \text{I})^- \quad \varphi' = 2 \cos^{-1} \left( \frac{2v - u}{2n^{1/2}} \right) \pmod{60^\circ} \\ \varphi : (\text{I} \rightarrow \text{II})^- &= (\text{II} \rightarrow \text{I})^+ \quad \varphi = 60^\circ - \varphi' \end{aligned} \quad (15)$$

<sup>5</sup> Takéuchi et al (1972) defined the vector  $\mathbf{r}$  as  $\mathbf{r} = u\bar{\mathbf{A}}_1 + v\mathbf{A}_2$ , i.e. with respect to a basis with interaxial angle  $60^\circ$ : correspondingly in the multiplicity of the mesh (Eq. 8) and in the length of the vector (Eq. 9) the term  $uv$  has opposite sign. Their definitions of  $(u, v)$  and  $n$  values correspond to reciprocal lattice values in our treatment.

<sup>6</sup> The definition of the angles  $\varphi$  and  $\varphi'$  is given according to Takéuchi et al (1972).

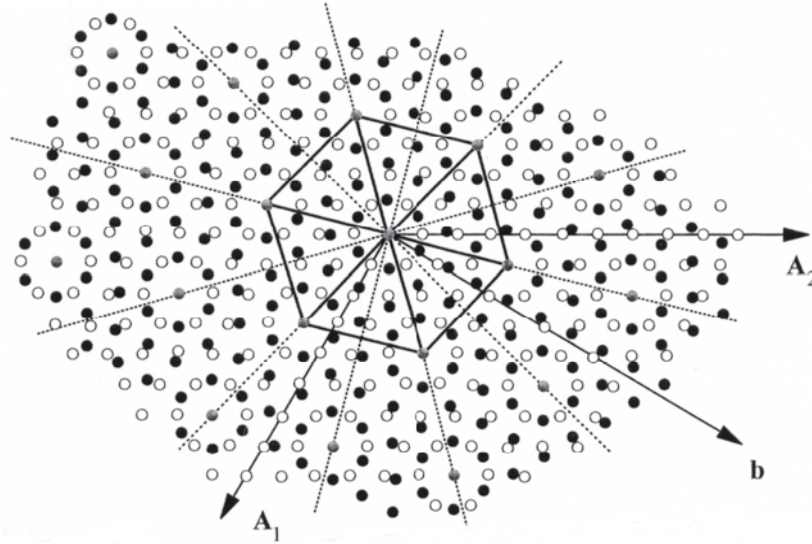


**Figure 22.** Overlap of two *hp* lattices rotated about an axis normal to the plane and passing through the origin by the angle  $\varphi$  of the compound tessellation  $\{3, 6\}[13\{3, 6\}]$ . One node out of 13 is restored. Three hexagonal meshes containing each 13 nodes are also shown.

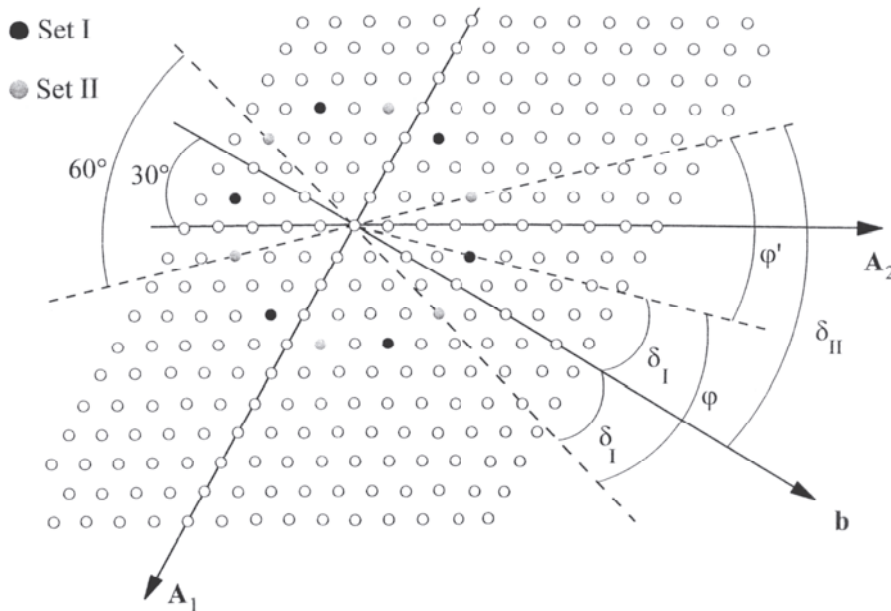


**Figure 23.** Definition of the tessellation angles  $\varphi$ ,  $\varphi'$ ,  $\delta_I$ ,  $\delta_{II}$ . The figure is drawn for the compound tessellation  $\{3, 6\}[13\{3, 6\}]$ .

The relation between  $\varphi$  and  $\varphi'$  is derived taking into account that a node belonging to one set is related to the two nearest nodes of the other set by two reflection lines that intersect at the origin. For the regular tessellation, only one set of six nodes with the same  $r$  exists, each node being  $60^\circ$  apart: in this case  $\varphi = \varphi' = 0^\circ \pmod{60^\circ}$ .

The space-fixed **b** orthohexagonal axis bisects the angle  $\varphi'$  as defined in Equation (15). The angles between **b** and the directions  $(u_I, v)$  ( $\delta_I$ ) and  $(u_{II}, v)$  ( $\delta_{II}$ ) are simply given by (Fig. 23):

$$\delta_I = \varphi/2 = 30^\circ - \varphi'/2 \quad \delta_{II} = -\delta_I \pmod{60^\circ} = \delta_I + \varphi' = 30^\circ + \varphi'/2 \quad (16)$$

In reciprocal space,  $n \times 60^\circ$  rotations relate nodes on the same type of row and of the same set ( $S$ ;  $D_I$ ,  $D_{II}$ ,  $X_I$ ,  $X_{II}$ ); instead, non-crystallographic rotations relate nodes on the same type of row but of different sets ( $D_I$  and  $D_{II}$ ;  $X_I$  and  $X_{II}$ ) and do not restore nodes of the same set (*cf.* Fig. 16).

If  $u$  and  $v$  (and thus also  $h$  and  $k$ ) are not co-prime integers (i.e. they have a common factor), or if  $u+v = 0 \pmod{3}$  [i.e.  $k-h = 0 \pmod{3}$ ], the lattice constructed on the mesh defined by the compound tessellation is multiple. The same lattice is described by a primitive mesh with smaller multiplicity and corresponding to  $u$  and  $v$  co-prime integers and  $u+v \neq 0 \pmod{3}$

Table 13 shows the features of compound tessellations  $\{3, 6\}[n\{3, 6\}]$  to  $r = 100\text{Å}$  [Eqn. (12) assuming  $a = 5.3\text{Å}$ ], each of which describes a coincidence-site lattice (CSL) (Ranganathan 1961): the multiplicity  $n$  of its mesh is termed *coincidence index* or  $\Sigma$  *factor* and corresponds to the order of the subgroup of translation defining the two-dimensional CSL with respect to the  $hp$  lattice. As shown in Table 13, the minimal value of the  $\Sigma$  factor for the  $hp$  lattice is 7 (see also Pleasants et al. 1996).

### Plesiotwinning

If the obliquity is neglected ( $\omega_{\parallel} = \omega_{\perp} = 0$ ), micas have a hexagonal lattice (orthogonal polytypes) or sublattice (non-orthogonal polytypes). The twin lattice coincides with the lattice of the individual (orthogonal polytypes) or with its (pseudo)hexagonal sublattice (non-orthogonal polytypes) and can be described through the regular tessellation  $\{3,6\}$ . A different kind of oriented crystal association occurs, although less frequently, whose lattice is based on one of the compound tessellations  $\{3, 6\}[n\{3, 6\}]$ , and thus has been termed *plesiotwinning*, from the Greek  $\pi\lambda\epsilon\sigma\iota\omicron\varsigma$ , “close to” (Nespolo et al. 1999b). Plesiotwins are characterized by the following features:

- 1) the lattice common to the individuals (plesiotwin lattice) is always a sublattice for any of the individuals; the order of the subgroup of translation (plesiotwin index) is usually higher than in twins;
- 2) the operation relating the individuals corresponds to a symmetry or pseudo-symmetry element of the plesiotwin lattice but not of the individuals, and that element has high indices in the setting of the individuals;
- 3) pairs of individuals are rotated about the normal to the composition plane by a non-crystallographic angle, even neglecting the obliquity.

If  $\Xi$  is the  $hp$  lattice, two identical such lattices  $\Xi_1$  and  $\Xi_2$  with an origin in common can be brought into complete or partial coincidence by keeping  $\Xi_1$  fixed and rotating  $\Xi_2$  about  $c^*$ , producing a two-dimensional CSL. The CSL corresponding to the  $\{3, 6\}[n\{3, 6\}]$  is produced through non-crystallographic rotations of  $\Xi_2$  about  $c^*$ . For orthogonal polytypes the  $c$  axis is normal to  $\Xi$  and in each lattice plane parallel to  $\Xi$  the same two-dimensional CSL is produced. Instead, for non-orthogonal polytypes the  $c$  axis is inclined, with a  $c_n$  projection  $|a|/3$  or  $|b|/3$  (assuming  $\omega_{\perp} = 0$ ). The rotations normal to  $\Xi$  produce an identical CSL every third plane parallel to (001), namely the planes for which the normal to  $\Xi$  passes on a lattice point. The multiple cell containing three lattice planes is (ideally) orthogonal and defines either the twin lattice -  $\{3, 6\}$  tessellation - or the plesiotwin lattice -  $\{3, 6\}[n\{3, 6\}]$  tessellation.

In micas, and more generally in layer compounds, plesiotwinning represents a generalization of the concept of twinning, at least from the lattice viewpoint. In twins the CSL produced in each plane (orthogonal polytypes) or in one plane out of three (non-orthogonal polytypes) has  $\Sigma$  factor 1, whereas in plesiotwins the CSL has  $\Sigma$  factor of  $n > 1$  ( $n \geq 7$  for the  $hp$  lattice). The twin/plesiotwin index is thus 1 (twinning by merohedry)

**Table 13.** Values of  $u$ ,  $v$  ( $\gamma=120^\circ$ ),  $H$ ,  $K$  ( $\gamma=60^\circ$ ) and corresponding angles (mod  $60^\circ$ ) for the compound tessellation  $\{3, 6\}[n\{3, 6\}]$  up to  $r = 100\text{\AA}$  (assuming  $a = 5.3\text{\AA}$ ).

$n$	$r(\text{\AA})$	Set	$(u, v)$	$(H, K)$	$\varphi$	$\varphi'$	$\delta_{\text{I}}$	$\delta_{\text{II}}$
1 <sup>#</sup>	5.3	I, II	(1,1)	(1,1)	0°	0°	0°	0°
7	14.0	I	(1,3)	(1,2)	21°47'	38°13'	10°54'	49°06'
		II	(2,3)	(2,1)				
13	19.1	I	(1,4)	(1,3)	32°12'	27°48'	16°06'	43°54'
		II	(3,4)	(3,1)				
19	23.1	I	(2,5)	(2,3)	13°10'	46°50'	6°35'	53°25'
		II	(3,5)	(3,2)				
31	29.5	I	(1,6)	(1,5)	42°06'	17°54'	21°03'	38°57'
		II	(5,6)	(5,1)				
37	32.2	I	(3,7)	(3,4)	9°26'	50°34'	4°43'	55°17'
		II	(4,7)	(4,3)				
43	34.8	I	(1,7)	(1,6)	44°49'	15°11'	22°25'	37°35'
		II	(6,7)	(6,1)				
49	37.1	I	(3,8)	(3,5)	16°26'	43°34'	8°13'	51°47'
		II	(5,8)	(5,3)				
61	41.4	I	(4,9)	(4,5)	7°20'	52°40'	3°40'	56°20'
		II	(5,9)	(5,4)				
67	43.4	I	(2,9)	(2,7)	35°34'	24°26'	17°47'	42°13'
		II	(7,9)	(7,2)				
73	45.3	I	(1,9)	(1,8)	48°22'	11°38'	24°11'	35°49'
		II	(8,9)	(8,1)				
79	47.1	I	(3,10)	(3,7)	26°00'	34°00'	13°00'	47°00'
		II	(7,10)	(7,3)				
91	50.6	I	(1,10)	(1,9)	49°35'	10°25'	24°47'	35°13'
		II	(9,10)	(9,1)				
		I	(5,11)	(5,6)				
		II	(6,11)	(6,5)				
97	52.2	I	(3,11)	(3,8)	29°25'	30°35'	45°18'	14°42'
		II	(8,11)	(8,3)				
103	53.8	I	(2,11)	(2,9)	40°21'	19°39'	39°50'	20°10'
		II	(9,11)	(9,2)				
109	55.3	I	(5,12)	(5,7)	11°00'	49°00'	54°30'	5°30'
		II	(7,12)	(7,5)				
127	59.7	I	(6,13)	(6,7)	5°05'	54°55'	57°27'	2°33'
		II	(7,13)	(7,6)				
133	61.1	I	(1,12)	(1,11)	51°23'	8°37'	34°18'	25°42'
		II	(11,12)	(11,1)				
		I	(4,13)	(4,9)				
		II	(9,13)	(9,4)				
139	62.5	I	(3,13)	(3,10)	34°32'	25°28'	42°44'	17°16'
		II	(10,13)	(10,3)				
151	65.1	I	(5,14)	(5,9)	18°44'	41°16'	50°38'	9°22'
		II	(9,14)	(9,5)				

<sup>#</sup>Regular tessellation  $\{3,6\}$ .

or  $n$  (plesiotwinning) for orthogonal polytypes, and 3 (twinning by reticular merohedry) or  $3n$  (plesiotwinning). For  $\omega_{\parallel} \neq 0$  or  $\omega_{\perp} \neq 0$  this description is not modified, but the lattice overlap is only approximated and corresponds to pseudo-merohedry ( $n = 1$ ) and reticular pseudo-merohedry ( $n > 1$ ): the rotations normal to  $\Xi$  are  $\varphi \pm 2\varepsilon$ , and do not obey

the law of Mallard. These rotations are useful to describe the CSL and the corresponding twin/plesiotwin indices but, as shown dealing specifically with twins, they are not correct twin/plesiotwin operations: the latter correspond instead to two-fold axes in the (001) plane or reflection planes almost normal to (001). The plesiotwin axes and plesiotwin planes have higher indices than the twin axes (Table 14). Note that plesiotwin planes correspond to crystal faces usually not developed in micas: consequently, reflection plesiotwins have a probability of occurrence lower than rotation plesiotwins.

Table 13, continued

<i>n</i>	<i>r</i> (Å)	Set	( <i>u</i> , <i>v</i> )	( <i>H</i> , <i>K</i> )	φ	φ'	δ <sub>I</sub>	δ <sub>II</sub>																																																																																																																																																																																																																																		
157	66.4	I	(1,13)	(1,12)	52°04'	7°56'	33°58'	26°02'																																																																																																																																																																																																																																		
		II	(12,13)	(12,1)					163	67.7	I	(3,14)	(3,11)	36°31'	23°29'	41°44'	18°16'	II	(11,14)	(11,3)	169	68.9	I	(7,15)	(7,8)	4°25'	55°35'	57°48'	2°12'	II	(8,15)	(8,7)	181	71.3	I	(4,15)	(4,11)	30°09'	29°51'	44°55'	15°05'	II	(11,15)	(11,4)	193	73.6	I	(7,16)	(7,9)	8°15'	51°45'	55°52'	4°08'	II	(9,16)	(9,7)	199	74.8	I	(2,15)	(2,13)	45°54'	14°06'	37°03'	22°57'	II	(13,15)	(13,2)	211	77.0	I	(1,15)	(1,14)	53°10'	6°50'	33°25'	26°35'	II	(14,15)	(14,1)	217	78.1	I	(3,16)	(3,13)	39°41'	20°19'	40°09'	19°51'	II	(13,16)	(13,3)	I	(8,17)	(8,9)	3°53'	56°07'	58°03'	1°57'	II	(9,17)	(9,8)	223	79.1	I	(6,17)	(6,11)	19°16'	40°44'	50°22'	9°38'	II	(11,17)	(11,6)	229	80.2	I	(5,17)	(5,12)	26°45'	33°15'	46°38'	13°22'	II	(12,17)	(12,5)	241	82.3	I	(1,16)	(1,15)	53°36'	6°24'	33°12'	26°48'	II	(15,16)	(15,1)	247	83.3	I	(3,17)	(3,14)	40°58'	19°02'	39°31'	20°29'	II	(14,17)	(14,3)	I	(7,18)	(7,11)	14°37'	45°23'	52°41'	7°19'	II	(11,18)	(11,7)	259	85.3	I	(2,17)	(2,15)	47°39'	12°21'	36°11'	23°49'	II	(15,17)	(15,2)	I	(5,18)	(5,13)	28°47'	31°13'	45°37'	14°23'	II	(13,18)	(13,5)	271	87.2	I	(9,19)	(9,10)	3°29'	56°31'	58°16'	1°44'	II	(10,19)	(10,9)	277	88.2	I	(7,19)	(7,12)	17°17'	42°43'	51°22'	8°38'	II	(12,19)	(12,7)	283	89.2	I	(6,19)	(6,13)	24°01'	35°59'	48°00'	12°00'	II	(13,19)	(13,6)	301	92.0	I	(4,19)	(4,15)	36°58'	23°02'	41°31'	18°29'	II	(15,19)	(15,4)	I	(9,20)	(9,11)	6°37'
163	67.7	I	(3,14)	(3,11)	36°31'	23°29'	41°44'	18°16'																																																																																																																																																																																																																																		
		II	(11,14)	(11,3)					169	68.9	I	(7,15)	(7,8)	4°25'	55°35'	57°48'	2°12'	II	(8,15)	(8,7)	181	71.3	I	(4,15)	(4,11)	30°09'	29°51'	44°55'	15°05'	II	(11,15)	(11,4)	193	73.6	I	(7,16)	(7,9)	8°15'	51°45'	55°52'	4°08'	II	(9,16)	(9,7)	199	74.8	I	(2,15)	(2,13)	45°54'	14°06'	37°03'	22°57'	II	(13,15)	(13,2)	211	77.0	I	(1,15)	(1,14)	53°10'	6°50'	33°25'	26°35'	II	(14,15)	(14,1)	217	78.1	I	(3,16)	(3,13)	39°41'	20°19'	40°09'	19°51'	II	(13,16)	(13,3)			I	(8,17)	(8,9)	3°53'	56°07'	58°03'	1°57'	II	(9,17)	(9,8)	223	79.1	I	(6,17)	(6,11)	19°16'	40°44'	50°22'	9°38'	II	(11,17)	(11,6)	229	80.2	I	(5,17)	(5,12)	26°45'	33°15'	46°38'	13°22'	II	(12,17)	(12,5)	241	82.3	I	(1,16)	(1,15)	53°36'	6°24'	33°12'	26°48'	II	(15,16)	(15,1)	247	83.3	I	(3,17)	(3,14)	40°58'	19°02'	39°31'	20°29'	II			(14,17)	(14,3)	I	(7,18)	(7,11)	14°37'	45°23'	52°41'	7°19'	II	(11,18)	(11,7)	259	85.3	I	(2,17)	(2,15)	47°39'	12°21'	36°11'			23°49'	II	(15,17)	(15,2)	I	(5,18)	(5,13)	28°47'	31°13'	45°37'	14°23'	II	(13,18)	(13,5)	271	87.2	I	(9,19)	(9,10)	3°29'	56°31'	58°16'	1°44'	II	(10,19)	(10,9)	277	88.2	I	(7,19)	(7,12)	17°17'	42°43'	51°22'	8°38'	II	(12,19)	(12,7)	283	89.2	I	(6,19)	(6,13)	24°01'	35°59'	48°00'	12°00'	II	(13,19)	(13,6)	301	92.0	I	(4,19)	(4,15)	36°58'			23°02'	41°31'	18°29'	II	(15,19)	(15,4)	I	(9,20)	(9,11)	6°37'	53°23'	56°42'	3°18'	II
169	68.9	I	(7,15)	(7,8)	4°25'	55°35'	57°48'	2°12'																																																																																																																																																																																																																																		
		II	(8,15)	(8,7)					181	71.3	I	(4,15)	(4,11)	30°09'	29°51'	44°55'	15°05'	II	(11,15)	(11,4)	193	73.6	I	(7,16)	(7,9)	8°15'	51°45'	55°52'	4°08'	II	(9,16)	(9,7)	199	74.8	I	(2,15)	(2,13)	45°54'	14°06'	37°03'	22°57'	II	(13,15)	(13,2)	211	77.0	I	(1,15)	(1,14)	53°10'	6°50'	33°25'	26°35'	II	(14,15)	(14,1)	217	78.1	I	(3,16)	(3,13)	39°41'	20°19'	40°09'	19°51'	II	(13,16)	(13,3)			I	(8,17)	(8,9)	3°53'	56°07'	58°03'	1°57'	II	(9,17)	(9,8)	223	79.1	I	(6,17)	(6,11)	19°16'	40°44'	50°22'	9°38'	II	(11,17)	(11,6)	229	80.2	I	(5,17)	(5,12)	26°45'	33°15'	46°38'	13°22'	II	(12,17)	(12,5)	241	82.3	I	(1,16)	(1,15)	53°36'	6°24'	33°12'	26°48'	II	(15,16)	(15,1)	247	83.3	I	(3,17)	(3,14)	40°58'	19°02'	39°31'	20°29'	II	(14,17)	(14,3)			I	(7,18)	(7,11)	14°37'	45°23'	52°41'	7°19'	II	(11,18)	(11,7)	259	85.3	I	(2,17)	(2,15)	47°39'	12°21'	36°11'	23°49'	II	(15,17)	(15,2)			I	(5,18)	(5,13)	28°47'	31°13'	45°37'	14°23'	II	(13,18)	(13,5)	271	87.2	I	(9,19)	(9,10)	3°29'	56°31'	58°16'	1°44'	II	(10,19)	(10,9)	277	88.2	I	(7,19)	(7,12)	17°17'	42°43'	51°22'	8°38'	II	(12,19)	(12,7)	283	89.2	I	(6,19)	(6,13)	24°01'	35°59'	48°00'	12°00'	II	(13,19)	(13,6)	301	92.0	I	(4,19)	(4,15)	36°58'	23°02'	41°31'	18°29'	II	(15,19)	(15,4)			I	(9,20)	(9,11)	6°37'	53°23'	56°42'	3°18'	II	(11,20)	(11,9)										
181	71.3	I	(4,15)	(4,11)	30°09'	29°51'	44°55'	15°05'																																																																																																																																																																																																																																		
		II	(11,15)	(11,4)					193	73.6	I	(7,16)	(7,9)	8°15'	51°45'	55°52'	4°08'	II	(9,16)	(9,7)	199	74.8	I	(2,15)	(2,13)	45°54'	14°06'	37°03'	22°57'	II	(13,15)	(13,2)	211	77.0	I	(1,15)	(1,14)	53°10'	6°50'	33°25'	26°35'	II	(14,15)	(14,1)	217	78.1	I	(3,16)	(3,13)	39°41'	20°19'	40°09'	19°51'	II	(13,16)	(13,3)			I	(8,17)	(8,9)	3°53'	56°07'	58°03'	1°57'	II	(9,17)	(9,8)	223	79.1	I	(6,17)	(6,11)	19°16'	40°44'	50°22'	9°38'	II	(11,17)	(11,6)	229	80.2	I	(5,17)	(5,12)	26°45'	33°15'	46°38'	13°22'	II	(12,17)	(12,5)	241	82.3	I	(1,16)	(1,15)	53°36'	6°24'	33°12'	26°48'	II	(15,16)	(15,1)	247	83.3	I	(3,17)	(3,14)	40°58'	19°02'	39°31'	20°29'	II	(14,17)	(14,3)			I	(7,18)	(7,11)	14°37'	45°23'	52°41'	7°19'	II	(11,18)	(11,7)	259	85.3	I	(2,17)	(2,15)	47°39'	12°21'	36°11'	23°49'	II	(15,17)	(15,2)			I	(5,18)	(5,13)	28°47'	31°13'	45°37'	14°23'	II	(13,18)	(13,5)	271	87.2	I	(9,19)	(9,10)	3°29'	56°31'	58°16'	1°44'	II	(10,19)	(10,9)	277	88.2	I	(7,19)	(7,12)	17°17'	42°43'	51°22'	8°38'	II	(12,19)	(12,7)	283	89.2	I	(6,19)	(6,13)	24°01'	35°59'	48°00'	12°00'	II	(13,19)	(13,6)	301	92.0	I	(4,19)	(4,15)	36°58'	23°02'	41°31'	18°29'	II	(15,19)	(15,4)			I	(9,20)	(9,11)	6°37'	53°23'	56°42'	3°18'	II	(11,20)	(11,9)																						
193	73.6	I	(7,16)	(7,9)	8°15'	51°45'	55°52'	4°08'																																																																																																																																																																																																																																		
		II	(9,16)	(9,7)					199	74.8	I	(2,15)	(2,13)	45°54'	14°06'	37°03'	22°57'	II	(13,15)	(13,2)	211	77.0	I	(1,15)	(1,14)	53°10'	6°50'	33°25'	26°35'	II	(14,15)	(14,1)	217	78.1	I	(3,16)	(3,13)	39°41'	20°19'	40°09'	19°51'	II	(13,16)	(13,3)			I	(8,17)	(8,9)	3°53'	56°07'	58°03'	1°57'	II	(9,17)	(9,8)	223	79.1	I	(6,17)	(6,11)	19°16'	40°44'	50°22'	9°38'	II	(11,17)	(11,6)	229	80.2	I	(5,17)	(5,12)	26°45'	33°15'	46°38'	13°22'	II	(12,17)	(12,5)	241	82.3	I	(1,16)	(1,15)	53°36'	6°24'	33°12'	26°48'	II	(15,16)	(15,1)	247	83.3	I	(3,17)	(3,14)	40°58'	19°02'	39°31'	20°29'	II	(14,17)	(14,3)			I	(7,18)	(7,11)	14°37'	45°23'	52°41'	7°19'	II	(11,18)	(11,7)	259	85.3	I	(2,17)	(2,15)	47°39'	12°21'	36°11'	23°49'	II	(15,17)	(15,2)			I	(5,18)	(5,13)	28°47'	31°13'	45°37'	14°23'	II	(13,18)	(13,5)	271	87.2	I	(9,19)	(9,10)	3°29'	56°31'	58°16'	1°44'	II	(10,19)	(10,9)	277	88.2	I	(7,19)	(7,12)	17°17'	42°43'	51°22'	8°38'	II	(12,19)	(12,7)	283	89.2	I	(6,19)	(6,13)	24°01'	35°59'	48°00'	12°00'	II	(13,19)	(13,6)	301	92.0	I	(4,19)	(4,15)	36°58'	23°02'	41°31'	18°29'	II	(15,19)	(15,4)			I	(9,20)	(9,11)	6°37'	53°23'	56°42'	3°18'	II	(11,20)	(11,9)																																		
199	74.8	I	(2,15)	(2,13)	45°54'	14°06'	37°03'	22°57'																																																																																																																																																																																																																																		
		II	(13,15)	(13,2)					211	77.0	I	(1,15)	(1,14)	53°10'	6°50'	33°25'	26°35'	II	(14,15)	(14,1)	217	78.1	I	(3,16)	(3,13)	39°41'	20°19'	40°09'	19°51'	II	(13,16)	(13,3)			I	(8,17)	(8,9)	3°53'	56°07'	58°03'	1°57'	II	(9,17)	(9,8)	223	79.1	I	(6,17)	(6,11)	19°16'	40°44'	50°22'	9°38'	II	(11,17)	(11,6)	229	80.2	I	(5,17)	(5,12)	26°45'	33°15'	46°38'	13°22'	II	(12,17)	(12,5)	241	82.3	I	(1,16)	(1,15)	53°36'	6°24'	33°12'	26°48'	II	(15,16)	(15,1)	247	83.3	I	(3,17)	(3,14)	40°58'	19°02'	39°31'	20°29'	II	(14,17)	(14,3)			I	(7,18)	(7,11)	14°37'	45°23'	52°41'	7°19'	II	(11,18)	(11,7)	259	85.3	I	(2,17)	(2,15)	47°39'	12°21'	36°11'	23°49'	II	(15,17)	(15,2)			I	(5,18)	(5,13)	28°47'	31°13'	45°37'	14°23'	II	(13,18)	(13,5)	271	87.2	I	(9,19)	(9,10)	3°29'	56°31'	58°16'	1°44'	II	(10,19)	(10,9)	277	88.2	I	(7,19)	(7,12)	17°17'	42°43'	51°22'	8°38'	II	(12,19)	(12,7)	283	89.2	I	(6,19)	(6,13)	24°01'	35°59'	48°00'	12°00'	II	(13,19)	(13,6)	301	92.0	I	(4,19)	(4,15)	36°58'	23°02'	41°31'	18°29'	II	(15,19)	(15,4)			I	(9,20)	(9,11)	6°37'	53°23'	56°42'	3°18'	II	(11,20)	(11,9)																																														
211	77.0	I	(1,15)	(1,14)	53°10'	6°50'	33°25'	26°35'																																																																																																																																																																																																																																		
		II	(14,15)	(14,1)					217	78.1	I	(3,16)	(3,13)	39°41'	20°19'	40°09'	19°51'	II	(13,16)	(13,3)			I	(8,17)	(8,9)	3°53'	56°07'	58°03'	1°57'	II	(9,17)	(9,8)	223	79.1	I	(6,17)	(6,11)	19°16'	40°44'	50°22'	9°38'	II	(11,17)	(11,6)	229	80.2	I	(5,17)	(5,12)	26°45'	33°15'	46°38'	13°22'	II	(12,17)	(12,5)	241	82.3	I	(1,16)	(1,15)	53°36'	6°24'	33°12'	26°48'	II	(15,16)	(15,1)	247	83.3	I	(3,17)	(3,14)	40°58'	19°02'	39°31'	20°29'	II	(14,17)	(14,3)			I	(7,18)	(7,11)	14°37'	45°23'	52°41'	7°19'	II	(11,18)	(11,7)	259	85.3	I	(2,17)	(2,15)	47°39'	12°21'	36°11'	23°49'	II	(15,17)	(15,2)			I	(5,18)	(5,13)	28°47'	31°13'	45°37'	14°23'	II	(13,18)	(13,5)	271	87.2	I	(9,19)	(9,10)	3°29'	56°31'	58°16'	1°44'	II	(10,19)	(10,9)	277	88.2	I	(7,19)	(7,12)	17°17'	42°43'	51°22'	8°38'	II	(12,19)	(12,7)	283	89.2	I	(6,19)	(6,13)	24°01'	35°59'	48°00'	12°00'	II	(13,19)	(13,6)	301	92.0	I	(4,19)	(4,15)	36°58'	23°02'	41°31'	18°29'	II	(15,19)	(15,4)			I	(9,20)	(9,11)	6°37'	53°23'	56°42'	3°18'	II	(11,20)	(11,9)																																																										
217	78.1	I	(3,16)	(3,13)	39°41'	20°19'	40°09'	19°51'																																																																																																																																																																																																																																		
		II	(13,16)	(13,3)							I	(8,17)	(8,9)	3°53'	56°07'	58°03'	1°57'	II	(9,17)	(9,8)	223	79.1	I	(6,17)	(6,11)	19°16'	40°44'	50°22'	9°38'	II	(11,17)	(11,6)	229	80.2	I	(5,17)	(5,12)	26°45'	33°15'	46°38'	13°22'	II	(12,17)	(12,5)	241	82.3	I	(1,16)	(1,15)	53°36'	6°24'	33°12'	26°48'	II	(15,16)	(15,1)	247	83.3	I	(3,17)	(3,14)	40°58'	19°02'	39°31'	20°29'	II	(14,17)	(14,3)			I	(7,18)	(7,11)	14°37'	45°23'	52°41'	7°19'	II	(11,18)	(11,7)	259	85.3	I	(2,17)	(2,15)	47°39'	12°21'	36°11'	23°49'	II	(15,17)	(15,2)			I	(5,18)	(5,13)	28°47'	31°13'	45°37'	14°23'	II	(13,18)	(13,5)	271	87.2	I	(9,19)	(9,10)	3°29'	56°31'	58°16'	1°44'	II	(10,19)	(10,9)	277	88.2	I	(7,19)	(7,12)	17°17'	42°43'	51°22'	8°38'	II	(12,19)	(12,7)	283	89.2	I	(6,19)	(6,13)	24°01'	35°59'	48°00'	12°00'	II	(13,19)	(13,6)	301	92.0	I	(4,19)	(4,15)	36°58'	23°02'	41°31'	18°29'	II	(15,19)	(15,4)			I	(9,20)	(9,11)	6°37'	53°23'	56°42'	3°18'	II	(11,20)	(11,9)																																																																						
		I	(8,17)	(8,9)	3°53'	56°07'	58°03'	1°57'																																																																																																																																																																																																																																		
		II	(9,17)	(9,8)					223	79.1	I	(6,17)	(6,11)	19°16'	40°44'	50°22'	9°38'	II	(11,17)	(11,6)	229	80.2	I	(5,17)	(5,12)	26°45'	33°15'	46°38'	13°22'	II	(12,17)	(12,5)	241	82.3	I	(1,16)	(1,15)	53°36'	6°24'	33°12'	26°48'	II	(15,16)	(15,1)	247	83.3	I	(3,17)	(3,14)	40°58'	19°02'	39°31'	20°29'	II	(14,17)	(14,3)			I	(7,18)	(7,11)	14°37'	45°23'	52°41'	7°19'	II	(11,18)	(11,7)	259	85.3	I	(2,17)	(2,15)	47°39'	12°21'	36°11'	23°49'	II	(15,17)	(15,2)			I	(5,18)	(5,13)	28°47'	31°13'	45°37'	14°23'	II	(13,18)	(13,5)	271	87.2	I	(9,19)	(9,10)	3°29'	56°31'	58°16'	1°44'	II	(10,19)	(10,9)	277	88.2	I	(7,19)	(7,12)	17°17'	42°43'	51°22'	8°38'	II	(12,19)	(12,7)	283	89.2	I	(6,19)	(6,13)	24°01'	35°59'	48°00'	12°00'	II	(13,19)	(13,6)	301	92.0	I	(4,19)	(4,15)	36°58'	23°02'	41°31'	18°29'	II	(15,19)	(15,4)			I	(9,20)	(9,11)	6°37'	53°23'	56°42'	3°18'	II	(11,20)	(11,9)																																																																																		
223	79.1	I	(6,17)	(6,11)	19°16'	40°44'	50°22'	9°38'																																																																																																																																																																																																																																		
		II	(11,17)	(11,6)					229	80.2	I	(5,17)	(5,12)	26°45'	33°15'	46°38'	13°22'	II	(12,17)	(12,5)	241	82.3	I	(1,16)	(1,15)	53°36'	6°24'	33°12'	26°48'	II	(15,16)	(15,1)	247	83.3	I	(3,17)	(3,14)	40°58'	19°02'	39°31'	20°29'	II	(14,17)	(14,3)			I	(7,18)	(7,11)	14°37'	45°23'	52°41'	7°19'	II	(11,18)	(11,7)	259	85.3	I	(2,17)	(2,15)	47°39'	12°21'	36°11'	23°49'	II	(15,17)	(15,2)			I	(5,18)	(5,13)	28°47'	31°13'	45°37'	14°23'	II	(13,18)	(13,5)	271	87.2	I	(9,19)	(9,10)	3°29'	56°31'	58°16'	1°44'	II	(10,19)	(10,9)	277	88.2	I	(7,19)	(7,12)	17°17'	42°43'	51°22'	8°38'	II	(12,19)	(12,7)	283	89.2	I	(6,19)	(6,13)	24°01'	35°59'	48°00'	12°00'	II	(13,19)	(13,6)	301	92.0	I	(4,19)	(4,15)	36°58'	23°02'	41°31'	18°29'	II	(15,19)	(15,4)			I	(9,20)	(9,11)	6°37'	53°23'	56°42'	3°18'	II	(11,20)	(11,9)																																																																																														
229	80.2	I	(5,17)	(5,12)	26°45'	33°15'	46°38'	13°22'																																																																																																																																																																																																																																		
		II	(12,17)	(12,5)					241	82.3	I	(1,16)	(1,15)	53°36'	6°24'	33°12'	26°48'	II	(15,16)	(15,1)	247	83.3	I	(3,17)	(3,14)	40°58'	19°02'	39°31'	20°29'	II	(14,17)	(14,3)			I	(7,18)	(7,11)	14°37'	45°23'	52°41'	7°19'	II	(11,18)	(11,7)	259	85.3	I	(2,17)	(2,15)	47°39'	12°21'	36°11'	23°49'	II	(15,17)	(15,2)			I	(5,18)	(5,13)	28°47'	31°13'	45°37'	14°23'	II	(13,18)	(13,5)	271	87.2	I	(9,19)	(9,10)	3°29'	56°31'	58°16'	1°44'	II	(10,19)	(10,9)	277	88.2	I	(7,19)	(7,12)	17°17'	42°43'	51°22'	8°38'	II	(12,19)	(12,7)	283	89.2	I	(6,19)	(6,13)	24°01'	35°59'	48°00'	12°00'	II	(13,19)	(13,6)	301	92.0	I	(4,19)	(4,15)	36°58'	23°02'	41°31'	18°29'	II	(15,19)	(15,4)			I	(9,20)	(9,11)	6°37'	53°23'	56°42'	3°18'	II	(11,20)	(11,9)																																																																																																										
241	82.3	I	(1,16)	(1,15)	53°36'	6°24'	33°12'	26°48'																																																																																																																																																																																																																																		
		II	(15,16)	(15,1)					247	83.3	I	(3,17)	(3,14)	40°58'	19°02'	39°31'	20°29'	II	(14,17)	(14,3)			I	(7,18)	(7,11)	14°37'	45°23'	52°41'	7°19'	II	(11,18)	(11,7)	259	85.3	I	(2,17)	(2,15)	47°39'	12°21'	36°11'	23°49'	II	(15,17)	(15,2)			I	(5,18)	(5,13)	28°47'	31°13'	45°37'	14°23'	II	(13,18)	(13,5)	271	87.2	I	(9,19)	(9,10)	3°29'	56°31'	58°16'	1°44'	II	(10,19)	(10,9)	277	88.2	I	(7,19)	(7,12)	17°17'	42°43'	51°22'	8°38'	II	(12,19)	(12,7)	283	89.2	I	(6,19)	(6,13)	24°01'	35°59'	48°00'	12°00'	II	(13,19)	(13,6)	301	92.0	I	(4,19)	(4,15)	36°58'	23°02'	41°31'	18°29'	II	(15,19)	(15,4)			I	(9,20)	(9,11)	6°37'	53°23'	56°42'	3°18'	II	(11,20)	(11,9)																																																																																																																						
247	83.3	I	(3,17)	(3,14)	40°58'	19°02'	39°31'	20°29'																																																																																																																																																																																																																																		
		II	(14,17)	(14,3)							I	(7,18)	(7,11)	14°37'	45°23'	52°41'	7°19'	II	(11,18)	(11,7)	259	85.3	I	(2,17)	(2,15)	47°39'	12°21'	36°11'	23°49'	II	(15,17)	(15,2)			I	(5,18)	(5,13)	28°47'	31°13'	45°37'	14°23'	II	(13,18)	(13,5)	271	87.2	I	(9,19)	(9,10)	3°29'	56°31'	58°16'	1°44'	II	(10,19)	(10,9)	277	88.2	I	(7,19)	(7,12)	17°17'	42°43'	51°22'	8°38'	II	(12,19)	(12,7)	283	89.2	I	(6,19)	(6,13)	24°01'	35°59'	48°00'	12°00'	II	(13,19)	(13,6)	301	92.0	I	(4,19)	(4,15)	36°58'	23°02'	41°31'	18°29'	II	(15,19)	(15,4)			I	(9,20)	(9,11)	6°37'	53°23'	56°42'	3°18'	II	(11,20)	(11,9)																																																																																																																																		
		I	(7,18)	(7,11)	14°37'	45°23'	52°41'	7°19'																																																																																																																																																																																																																																		
		II	(11,18)	(11,7)					259	85.3	I	(2,17)	(2,15)	47°39'	12°21'	36°11'	23°49'	II	(15,17)	(15,2)			I	(5,18)	(5,13)	28°47'	31°13'	45°37'	14°23'	II	(13,18)	(13,5)	271	87.2	I	(9,19)	(9,10)	3°29'	56°31'	58°16'	1°44'	II	(10,19)	(10,9)	277	88.2	I	(7,19)	(7,12)	17°17'	42°43'	51°22'	8°38'	II	(12,19)	(12,7)	283	89.2	I	(6,19)	(6,13)	24°01'	35°59'	48°00'	12°00'	II	(13,19)	(13,6)	301	92.0	I	(4,19)	(4,15)	36°58'	23°02'	41°31'	18°29'	II	(15,19)	(15,4)			I	(9,20)	(9,11)	6°37'	53°23'	56°42'	3°18'	II	(11,20)	(11,9)																																																																																																																																														
259	85.3	I	(2,17)	(2,15)	47°39'	12°21'	36°11'	23°49'																																																																																																																																																																																																																																		
		II	(15,17)	(15,2)							I	(5,18)	(5,13)	28°47'	31°13'	45°37'	14°23'	II	(13,18)	(13,5)	271	87.2	I	(9,19)	(9,10)	3°29'	56°31'	58°16'	1°44'	II	(10,19)	(10,9)	277	88.2	I	(7,19)	(7,12)	17°17'	42°43'	51°22'	8°38'	II	(12,19)	(12,7)	283	89.2	I	(6,19)	(6,13)	24°01'	35°59'	48°00'	12°00'	II	(13,19)	(13,6)	301	92.0	I	(4,19)	(4,15)	36°58'	23°02'	41°31'	18°29'	II	(15,19)	(15,4)			I	(9,20)	(9,11)	6°37'	53°23'	56°42'	3°18'	II	(11,20)	(11,9)																																																																																																																																																										
		I	(5,18)	(5,13)	28°47'	31°13'	45°37'	14°23'																																																																																																																																																																																																																																		
		II	(13,18)	(13,5)					271	87.2	I	(9,19)	(9,10)	3°29'	56°31'	58°16'	1°44'	II	(10,19)	(10,9)	277	88.2	I	(7,19)	(7,12)	17°17'	42°43'	51°22'	8°38'	II	(12,19)	(12,7)	283	89.2	I	(6,19)	(6,13)	24°01'	35°59'	48°00'	12°00'	II	(13,19)	(13,6)	301	92.0	I	(4,19)	(4,15)	36°58'	23°02'	41°31'	18°29'	II	(15,19)	(15,4)			I	(9,20)	(9,11)	6°37'	53°23'	56°42'	3°18'	II	(11,20)	(11,9)																																																																																																																																																																						
271	87.2	I	(9,19)	(9,10)	3°29'	56°31'	58°16'	1°44'																																																																																																																																																																																																																																		
		II	(10,19)	(10,9)					277	88.2	I	(7,19)	(7,12)	17°17'	42°43'	51°22'	8°38'	II	(12,19)	(12,7)	283	89.2	I	(6,19)	(6,13)	24°01'	35°59'	48°00'	12°00'	II	(13,19)	(13,6)	301	92.0	I	(4,19)	(4,15)	36°58'	23°02'	41°31'	18°29'	II	(15,19)	(15,4)			I	(9,20)	(9,11)	6°37'	53°23'	56°42'	3°18'	II	(11,20)	(11,9)																																																																																																																																																																																		
277	88.2	I	(7,19)	(7,12)	17°17'	42°43'	51°22'	8°38'																																																																																																																																																																																																																																		
		II	(12,19)	(12,7)					283	89.2	I	(6,19)	(6,13)	24°01'	35°59'	48°00'	12°00'	II	(13,19)	(13,6)	301	92.0	I	(4,19)	(4,15)	36°58'	23°02'	41°31'	18°29'	II	(15,19)	(15,4)			I	(9,20)	(9,11)	6°37'	53°23'	56°42'	3°18'	II	(11,20)	(11,9)																																																																																																																																																																																														
283	89.2	I	(6,19)	(6,13)	24°01'	35°59'	48°00'	12°00'																																																																																																																																																																																																																																		
		II	(13,19)	(13,6)					301	92.0	I	(4,19)	(4,15)	36°58'	23°02'	41°31'	18°29'	II	(15,19)	(15,4)			I	(9,20)	(9,11)	6°37'	53°23'	56°42'	3°18'	II	(11,20)	(11,9)																																																																																																																																																																																																										
301	92.0	I	(4,19)	(4,15)	36°58'	23°02'	41°31'	18°29'																																																																																																																																																																																																																																		
		II	(15,19)	(15,4)							I	(9,20)	(9,11)	6°37'	53°23'	56°42'	3°18'	II	(11,20)	(11,9)																																																																																																																																																																																																																						
		I	(9,20)	(9,11)	6°37'	53°23'	56°42'	3°18'																																																																																																																																																																																																																																		
		II	(11,20)	(11,9)																																																																																																																																																																																																																																						

**Table 13, concluded.**

<i>n</i>	<i>r</i> (Å)	Set	( <i>u</i> , <i>v</i> )	( <i>H</i> , <i>K</i> )	$\varphi$	$\varphi'$	$\delta_I$	$\delta_{II}$																																																																		
307	92.9	I	(1,18)	(1,17)	54°20'	5°40'	32°50'	27°10'																																																																		
		II	(17,18)	(17,1)					313	93.8	I	(3,19)	(3,16)	43°07'	16°53'	38°27'	21°33'	II	(16,19)	(16,3)	325	95.5	I	(5,20)	(5,15)	32°12'	27°48'	43°54'	16°06'	II	(15,20)	(15,5)	331	96.4	I	(10,21)	(10,11)	3°09'	56°51'	58°26'	1°34'	II	(11,21)	(11,10)	337	97.3	I	(8,21)	(8,13)	15°39'	44°21'	52°10'	7°50'	II	(13,21)	(13,8)	343	98.2	I	(1,19)	(1,18)	54°38'	5°22'	32°41'	27°19'	II	(18,19)	(18,1)	349	99.0	I	(3,20)	(3,17)	44°01'
313	93.8	I	(3,19)	(3,16)	43°07'	16°53'	38°27'	21°33'																																																																		
		II	(16,19)	(16,3)					325	95.5	I	(5,20)	(5,15)	32°12'	27°48'	43°54'	16°06'	II	(15,20)	(15,5)	331	96.4	I	(10,21)	(10,11)	3°09'	56°51'	58°26'	1°34'	II	(11,21)	(11,10)	337	97.3	I	(8,21)	(8,13)	15°39'	44°21'	52°10'	7°50'	II	(13,21)	(13,8)	343	98.2	I	(1,19)	(1,18)	54°38'	5°22'	32°41'	27°19'	II	(18,19)	(18,1)	349	99.0	I	(3,20)	(3,17)	44°01'	15°59'	38°22'	22°00'	II	(17,20)	(17,3)						
325	95.5	I	(5,20)	(5,15)	32°12'	27°48'	43°54'	16°06'																																																																		
		II	(15,20)	(15,5)					331	96.4	I	(10,21)	(10,11)	3°09'	56°51'	58°26'	1°34'	II	(11,21)	(11,10)	337	97.3	I	(8,21)	(8,13)	15°39'	44°21'	52°10'	7°50'	II	(13,21)	(13,8)	343	98.2	I	(1,19)	(1,18)	54°38'	5°22'	32°41'	27°19'	II	(18,19)	(18,1)	349	99.0	I	(3,20)	(3,17)	44°01'	15°59'	38°22'	22°00'	II	(17,20)	(17,3)																		
331	96.4	I	(10,21)	(10,11)	3°09'	56°51'	58°26'	1°34'																																																																		
		II	(11,21)	(11,10)					337	97.3	I	(8,21)	(8,13)	15°39'	44°21'	52°10'	7°50'	II	(13,21)	(13,8)	343	98.2	I	(1,19)	(1,18)	54°38'	5°22'	32°41'	27°19'	II	(18,19)	(18,1)	349	99.0	I	(3,20)	(3,17)	44°01'	15°59'	38°22'	22°00'	II	(17,20)	(17,3)																														
337	97.3	I	(8,21)	(8,13)	15°39'	44°21'	52°10'	7°50'																																																																		
		II	(13,21)	(13,8)					343	98.2	I	(1,19)	(1,18)	54°38'	5°22'	32°41'	27°19'	II	(18,19)	(18,1)	349	99.0	I	(3,20)	(3,17)	44°01'	15°59'	38°22'	22°00'	II	(17,20)	(17,3)																																										
343	98.2	I	(1,19)	(1,18)	54°38'	5°22'	32°41'	27°19'																																																																		
		II	(18,19)	(18,1)					349	99.0	I	(3,20)	(3,17)	44°01'	15°59'	38°22'	22°00'	II	(17,20)	(17,3)																																																						
349	99.0	I	(3,20)	(3,17)	44°01'	15°59'	38°22'	22°00'																																																																		
		II	(17,20)	(17,3)																																																																						

Plesiotwinning is a macroscopic phenomenon that differs from twinning not only in a geometrical definition but also from a physical viewpoint. Whereas for twins the twin index and the twin obliquity directly influence the probability of twin occurrences, for plesiotwins a similar lattice control is not recognized. In fact, the lowest plesiotwin index for micas is 7, which becomes 21 for non-orthogonal polytypes. The degree of restoration of lattice nodes is too small for a lattice control to be active. The plesiotwin formation is thus structurally controlled. Twins are usually believed to form in the early stages of crystal growth (Buerger 1945), but the formation of twins from macroscopic crystals is also known (e.g., Gaubert 1898; Schaskolsky, and Schubnikow 1933). When two or more nanocrystals interact, they can adjust their relative orientation until they reach a minimum energy configuration, corresponding either to a parallel growth or to a twin. When two macrocrystals interact, the energy barrier to the mutual adjustment is higher, especially at low temperature. If two macrocrystals coalesce or exsolve taking at first a relative orientation corresponding to an unstable atomic configuration at the interface, they tend to rotate until they reach a lower energy configuration. Parallel growth and twinning correspond to minimal interface energy, whereas plesiotwinning corresponds to a less-deep minimum. However, twin orientations are less numerous and are separated by larger angles, whereas plesiotwin orientations are more numerous and separated by smaller angles. In Figure 24 the plot  $\Sigma$  vs.  $\varphi$  for the *hp* lattice is given for  $\Sigma \leq 100$  and  $0^\circ \leq \varphi \leq 60^\circ$ . Between the two extreme values of  $\varphi$  corresponding to crystallographic rotations and to  $\Sigma = 1$ , several discrete values appear, corresponding to  $\Sigma > 1$  and to non-crystallographic rotations. Only limited adjustments may be necessary to reach plesiotwin orientations, which may thus represent a kind of compromise between the original unstable configuration and the too distant, although more stable, configuration of twins. This kind of origin is supported also by experiments of dispersion into a fluid and drying of flakes of crystals with layer structure: the result was simply a physical overlap of pairs of crystals, which however gave the same orientations of plesiotwins (Sueno et al. 1971; Takéuchi et al. 1972).

#### TWINNING OF MICAS. ANALYSIS OF THE GEOMETRY OF THE DIFFRACTION PATTERN

A simple and straightforward method to derive the orientations of the individuals in a mica twin or allotwin is introduced. The following analysis is entirely based on the

**Table 14.** Plesiotwin laws for the  $hP$  lattice. Indices of plesiotwin axes and plesiotwin planes are given with respect to the orthohexagonal  $a$ ,  $b$  axes, in counter clockwise orientation from  $\mathbf{b}$ .  $\delta_I$  and  $\delta_{II}$  are given in Table 13 for the corresponding tessellation. Plesiotwin planes correspond to planes not developed as crystal faces: consequently, reflection plesiotwins have low probability of occurrence.

Compound tessellation. $\{3, 6\}[n\{3, 6\}]$	$n=7$	$n=13$	$n=19$	$n=31$	$n=37$	$n=43$	$n=49$	$n=61$	Rotation about $c^*$
Rotation plesiotwins	$[\bar{1}30]_{\pi}$ $[\bar{5}10]_{\pi}$ $[\bar{2}10]_{\pi}$ $[\bar{1}30]_{\pi}$ $[\bar{5}10]_{\pi}$ $[\bar{2}10]_{\pi}$	$[\bar{1}20]_{\pi}$ $[\bar{7}10]_{\pi}$ $[\bar{5}30]_{\pi}$ $[\bar{1}20]_{\pi}$ $[\bar{7}10]_{\pi}$ $[\bar{5}30]_{\pi}$	$[\bar{1}50]_{\pi}$ $[\bar{4}10]_{\pi}$ $[\bar{7}30]_{\pi}$ $[\bar{1}50]_{\pi}$ $[\bar{4}10]_{\pi}$ $[\bar{7}30]_{\pi}$	$[\bar{2}30]_{\pi}$ $[\bar{1}1.10]_{\pi}$ $[\bar{7}50]_{\pi}$ $[\bar{2}30]_{\pi}$ $[\bar{1}1.10]_{\pi}$ $[\bar{7}50]_{\pi}$	$[\bar{1}70]_{\pi}$ $[\bar{1}1.30]_{\pi}$ $[\bar{5}20]_{\pi}$ $[\bar{1}70]_{\pi}$ $[\bar{1}1.30]_{\pi}$ $[\bar{5}20]_{\pi}$	$[\bar{5}70]_{\pi}$ $[\bar{1}3.10]_{\pi}$ $[\bar{4}30]_{\pi}$ $[\bar{5}70]_{\pi}$ $[\bar{1}3.10]_{\pi}$ $[\bar{4}30]_{\pi}$	$[\bar{1}40]_{\pi}$ $[\bar{1}3.30]_{\pi}$ $[\bar{1}1.50]_{\pi}$ $[\bar{1}40]_{\pi}$ $[\bar{1}3.30]_{\pi}$ $[\bar{1}1.50]_{\pi}$	$[\bar{1}90]_{\pi}$ $[\bar{7}20]_{\pi}$ $[\bar{1}3.50]_{\pi}$ $[\bar{1}90]_{\pi}$ $[\bar{7}20]_{\pi}$ $[\bar{1}3.50]_{\pi}$	$2\delta_I-2\varepsilon$ $120^\circ+2\delta_I-2\varepsilon$ $240^\circ+2\delta_I+2\varepsilon$ $2\delta_{II}-2\varepsilon$ $120^\circ+2\delta_{II}+2\varepsilon$ $240^\circ+2\delta_{II}+2\varepsilon$
Reflection plesiotwins	$(\bar{1}90)$ $(\bar{5}30)$ $(\bar{2}30)$ $(\bar{1}90)$ $(\bar{5}30)$ $(\bar{2}30)$	$(\bar{1}60)$ $(\bar{7}30)$ $(\bar{5}90)$ $(\bar{1}60)$ $(\bar{7}30)$ $(\bar{5}90)$	$(\bar{1}15.0)$ $(\bar{4}30)$ $(\bar{7}90)$ $(\bar{1}15.0)$ $(\bar{4}30)$ $(\bar{7}90)$	$(\bar{2}90)$ $(\bar{1}1.30)$ $(\bar{7}.15.0)$ $(\bar{2}90)$ $(\bar{1}1.30)$ $(\bar{7}.15.0)$	$(\bar{1}21.0)$ $(\bar{1}1.90)$ $(\bar{5}60)$ $(\bar{1}21.0)$ $(\bar{1}1.90)$ $(\bar{5}60)$	$(\bar{5}21.0)$ $(\bar{1}3.30)$ $(\bar{4}90)$ $(\bar{5}21.0)$ $(\bar{1}3.30)$ $(\bar{4}90)$	$(\bar{1}12.0)$ $(\bar{1}3.90)$ $(\bar{1}1.15.0)$ $(\bar{1}12.0)$ $(\bar{1}3.90)$ $(\bar{1}1.15.0)$	$(\bar{1}27.0)$ $(\bar{7}60)$ $(\bar{1}3.15.0)$ $(\bar{1}27.0)$ $(\bar{7}60)$ $(\bar{1}3.15.0)$	$2\delta_I+2\varepsilon$ $120^\circ+2\delta_I+2\varepsilon$ $240^\circ+2\delta_I-2\varepsilon$ $2\delta_{II}+2\varepsilon$ $120^\circ+2\delta_{II}-2\varepsilon$ $240^\circ+2\delta_{II}-2\varepsilon$
Plesiotwin index orthogonal polytypes	7	13	19	31	37	43	49	61	
Plesiotwin index non-orthogonal polytypes	21	39	57	93	111	126	147	183	



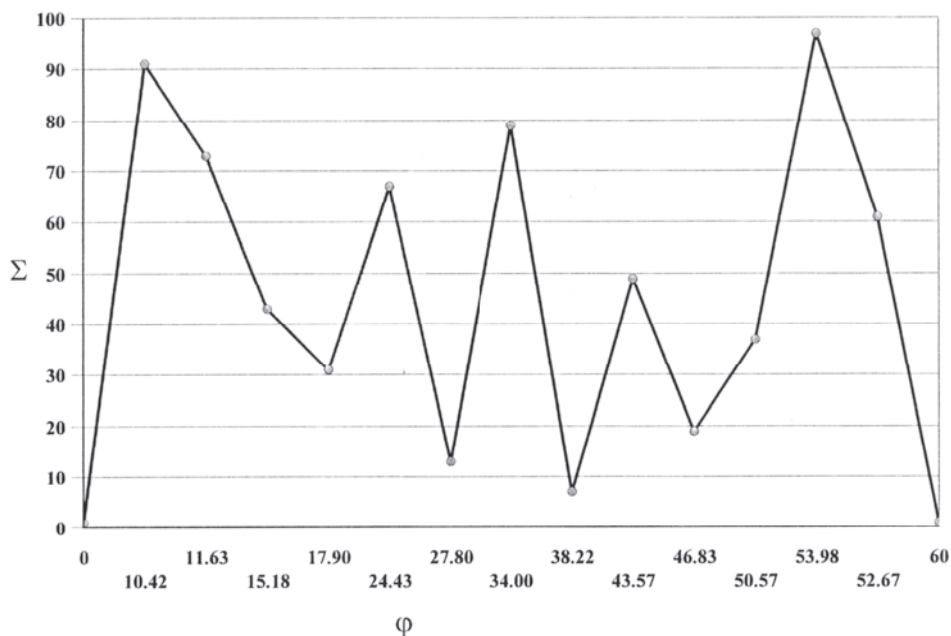


**Figure 24.** The coincidence index ( $\Sigma$  factor) vs.  $\phi$  plot, in case of two-dimensional  $hp$  lattice.  $\phi = 0^\circ$  (parallel growth) and  $\phi = 60^\circ$  (twinning) correspond to  $\Sigma = 1$ . Between these two orientations, a large number of plesiotwin orientations exist, which are shown up to  $\Sigma = 100$ . The plot has been calculated by applying the compound tessellation theory and drawn for counter-clockwise rotations only. Clockwise rotations produce the same  $\Sigma$  in correspondence of  $60^\circ - \phi$  rotations (modified after Nespolo et al. 1999d).

geometry of the diffraction pattern, which is determined by the symmetry of the lattice of the individual, of the twin lattice and of the lattice of the family structure. The diffraction pattern is described within the Trigonal model and in terms of the weighted reciprocal lattice (*w.r.l.*), i.e. the reciprocal lattice (*r.l.*) in which each node has a weight corresponding to the resulting intensity. In particular, a node corresponding to a reflection with zero intensity in the Trigonal model is omitted from the *w.r.l.* The intensities that are actually obtained in a diffraction experiment are clearly influenced by structural deviations from the Trigonal model: two diffraction patterns with the same geometry, and thus considered equivalent hereafter, can thus be different when the actual structure (i.e., with distortions) is taken into account.

### Symbolic description of orientation of twinned mica individuals. Limiting symmetry

As seen in the previous section, rotations between pairs of individuals in a mica twin or allotwin are very close to  $n \times 60^\circ$  about  $c^*$ . The possible orientations of the individuals are thus almost identical to the possible orientations of the layers in a polytype. The absolute orientation of the individuals can be indicated by symbols similar to those used for polytypes. Nespolo et al (2000a) introduced the  $Z_T$  symbols, where "T" indicates "twin", which are derived from the shortened  $Z$  symbols for polytypes. There are four main differences between  $Z$  and  $Z_T$  symbols:

1. Because there cannot be two individuals in a twin oriented in the same way, the sequence of characters in a  $Z_T$  symbol never contains the same character twice.
2. The  $Z$  symbol of polytypes must take into account the space-group type, whereas  $Z_T$  considers only the symmetry of the point group. The orthohexagonal setting of the first individual is taken to coincide with that of the twin lattice: the first individual is

always fixed in orientation  $Z_T = 3$  (Fig. 4), and the orientations of the other individuals are determined by the twin laws.

3. Rotation by  $180^\circ$  of the entire twinned edifice around the  $a$  axis of the space-fixed reference changes the  $Z_T$  symbol  $3IJ\dots P$  into  $(6-P)\dots(6-J)(6-I)3$ ; because the order of the individuals in the twin does not influence the diffraction pattern, this sequence of characters is equivalent to  $3(6-I)(6-J)\dots(6-P)$ , which corresponds to inverting the direction of rotation of the individuals in the twin about the  $c_{C_1}$  axis. Considering the effect on the lattice, the  $3IJ\dots P \rightarrow 3(6-I)(6-J)\dots(6-P)$  transformation corresponds to reflecting the twin lattice across the  $(010)$  plane.
4. For polytypes in which layers are related only by proper motions<sup>7</sup>, like  $3T$ , two twins operations with the same rotational part and differing only for the proper/improper character of the motion produce the same twin lattice. The corresponding two twin laws are however different, and thus an orientation produced by an improper motion is hereafter distinguished by a small black circle ( $\bullet$ ) after the  $Z_T$  symbol.

The number of independent orientations of the *w.r.l.* of an individual is determined by its *limiting symmetry*, i.e. the lower symmetry between the ideal crystal lattice (as described by the Trigonal model) and the family structure. The limiting symmetry is given in Table 15, which is easily understood remembering that: 1) for mixed-rotation polytypes the family structure is defined only within the Pauling model and the limiting symmetry always coincides with the symmetry of the polytype lattice; 2) for orthogonal polytypes, the lattice is (pseudo) hexagonal: for both subfamilies the limiting symmetry coincides with that of the family structure; 3) subfamily B polytypes cannot belong to *Class a*; 4) non-orthogonal subfamily A polytypes belong to *Class a* for *Series 0* but to *Class b* for *Series > 0*.

**Table 15.** Limiting symmetry defining the number of independent lattice orientations. The (idealized) symmetries of the lattice and of the family structure are given. The limiting symmetry corresponds to the lower of the two. For mixed-rotation polytypes the family structure is defined only within the Pauling model and the limiting symmetry by definition coincides with the symmetry of the lattice.

	Orthogonal polytypes ( $hP$ )	<i>Class a</i> polytypes ( $mC$ )	<i>Class b</i> polytypes ( $hR$ )
subfamily A ( $hR$ ) <sup>†</sup>	$hR$	$mC$ ( <i>Series 0</i> )	$hR$ ( <i>Series &gt; 0</i> )
subfamily B ( $hP$ ) <sup>†</sup>	$hP$	----	$hR$
mixed-rotation ( $hP$ ) <sup>‡</sup>	$hP$	$mC$	$hR$

<sup>†</sup>Trigonal model. <sup>‡</sup>Pauling model.

***Class a polytypes*** . Each subfamily A *Series 0* polytypes belong to *Class a*; mixed-rotation polytypes may also belong to *Class a*. In both cases, the limiting symmetry is  $mC$  and the unique axis does not coincide with that of the family structure ( $b$  in the polytypes,  $c$  in the family structure). Each of the six possible orientations of the individuals correspond thus to independent orientations of the *w.r.l.* The possible composite twins are obtained by calculating the sequences of  $Z_T$  symbols for sets of individuals from two to six. The orientation of the first individual is fixed ( $Z_T = 3$ ), and five possible orientations

<sup>7</sup> A “motion” is an instruction assigning uniquely to each point of the point space an ‘image’ whereby all distances are left invariant. A motion is called *proper* (also: “first sort”) or *improper* (also: “second sort”) depending on whether the determinant of the matrix representing it is +1 or -1.

remain where  $m$  individuals ( $1 \leq m \leq 5$ ) must be distributed. The number of twins is then:

$$\sum_{m=1}^5 N_T(m) = \sum_{m=1}^5 \binom{5}{m} = \sum_{m=1}^5 \frac{5!}{m!(5-m)!} = 31 \quad (17)$$

Table 16 gives the 12 sequences of independent  $Z_T$  symbols; the other 19 simply correspond to a rotation of the entire twinned edifice followed by a shift of the origin along  $c$ , eventually coupled with the inversion of the direction of the rotation of the individuals in the twin [reflection of the lattice across (010)], as in  $Z_T = 341$ .

**Class b polytypes**. Non-orthogonal polytypes belong to *Class b* in subfamily A *Series*  $> 0$  and in subfamily B. The unique axis is  $a$  in the polytypes but  $c$  in the pseudo-rhombohedral lattice; the latter coincides with that of the family structure. The limiting symmetry is  $hR$ , which for subfamily A coincides both with the symmetry of the family structure and with the (pseudo) symmetry of the lattice. Only two orientations of the *w.r.l.* of the individual are independent, corresponding to the two parities of  $Z_T$  symbols. A common symbol is thus used for the three equivalent orientations with the same parity, namely “U” (uneven) and “E” (even). Twinning by pseudo-merohedry involves individuals with the same orientation parity of  $Z_T$  symbols and produces complete overlap of the *w.r.l.* of the individual (neglecting the obliquity). The reciprocal lattice of the twin is thus geometrically indistinguishable from the reciprocal lattice of the individual. The three twins  $Z_T = 35$ ,  $Z_T = 31$  and  $Z_T = 351$  are equivalent to the single crystal, when considering the geometry of their lattice, and are thus represented as  $Z_T = U$ . Instead, twinning by reticular pseudo-merohedry involves individuals with an opposite orientation parity of the  $Z_T$  symbols and, considering the lattice only, they are represented as  $Z_T = UE$ .

**Orthogonal polytypes**. In the Trigonal model, the lattice is  $hP$  ( $\omega = 0$ ); in the true structure for orthorhombic polytypes the lattice is normally  $oC$  but pseudo- $hP$  ( $\omega \neq 0$ ). For subfamily B and mixed-rotation polytypes the limiting symmetry is  $hP$  and there is only one independent orientation of the *w.r.l.* Twinning is either by complete merohedry or by pseudo-merohedry and does not modify the geometry of the diffraction pattern.

Subfamily A polytypes have an orthogonal lattice only if they belong to *Series*  $> 0$  and have a 1:1:1 ratio of layers with the three orientations of the same parity (odd or even). The only example reported to date is  $3T$ , which is also the only possible orthogonal polytype in *Series* 1. Other subfamily A orthogonal polytypes may appear in *Series*  $> 1$  but are at present unknown. The limiting symmetry is  $hR$  and the *w.r.l.* has two independent orientations, as for *Class b* polytypes, which correspond to the two settings (obverse/reverse) of the family structure. Twinning is by merohedry ( $\omega = 0$ , either complete or selective, depending on the twin law) or pseudo-merohedry ( $\omega \neq 0$ ).

The  $3T$  polytype has three twin laws, two of which correspond to selective merohedry and invert the parity of the  $Z_T$  symbol, namely  $Z_T = U \rightarrow Z_T = E$  ( $6'2'2$ ) or  $Z_T = E^*$  ( $6'm'2$ ); the third twin law ( $3'12/m'$ ) corresponds instead to complete merohedry and preserves the parity of the  $Z_T$  symbol ( $Z_T = U \rightarrow Z_T = U^*$ ).

### Derivation of twin diffraction patterns

The number and disposition of nodes on the reciprocal lattice rows parallel to  $c^*$  are termed *node features* and are identified by a symbol  $I_j$ , where  $I$  is the number of nodes within the  $c^*_1$  repeat and  $j$  is a sequence number. Nespolo et al (2000a) introduced an orthogonal setting for the analysis of twins in terms of  $I_j$ , which is termed the *twin setting*. When dealing with a single polytype, the twin setting coincides with the  $C_1$  setting, which

**Table 16.** Orientation of the individuals building a twin in *Class a* mica polytype. Angles in parenthesis express the counter clockwise rotations of the whole twinned edifice. “Shift” stands for the shift of the origin along *c*. (010) means reflection of the twin lattice across the (010).plane, which is equivalent to inverting the direction of rotation of the individuals in the twin, *i.e.* to the symbol transformation 3IJ...P  $\rightarrow$  3(6-I)(6-J)...(6-P).

[After Nespolo et al. 2000a]

$Z_T$	Equivalent to	Equivalent to	Equivalent to
34	Unique	-----	-----
35	Unique	-----	-----
36	Unique	-----	-----
31	53(120°)	35(shift)	-----
32	43(60°)	34(shift)	-----
345	Unique	-----	-----
346	Unique	-----	-----
341	325(010)	436(60°)	346(shift)
342	453(60°)	345(shift)	-----
356	134(240°)	341(shift)	346
351	Unique	-----	-----
352	463(60°)	346(shift)	-----
361	634(180°)	346	-----
362	413(60°)	341(shift)	346
312	534(120°)	345(shift)	-----
$Z_T$	Equivalent to	Equivalent to	
3456	Unique	-----	
3451	Unique	-----	
3452	4563(60°)	3456(shift)	
3461	Unique	-----	
3462	Unique	-----	
3412	5634(120°)	3456(shift)	
3561	1345(240°)	3451(shift)	
3562	4613(60°)	3461(shift)	
3512	5134(120°)	3451(shift)	
3612	6345(180°)	3456(shift)	
34561	Unique	-----	
34562	45613(60°)	34561(shift)	
34512	56134(120°)	34561(shift)	
34612	61345(180°)	34561(shift)	
35612	13456(240°)	34561(shift)	
345612	Unique	-----	

is based on the cell of the twin lattice. To compare the geometry of the reciprocal lattice of polytypes with different periods, the twin setting is instead defined to have the shortest period along  $c^*$  in the  $C_1$  setting among all the polytypes considered. The twin setting of the twin lattice is space-fixed and parallel to  $C_1$ , whereas that of the crystal lattice is crystal-fixed for each of the individuals building a twin. Since the first individual of the twin is space-fixed ( $Z_T = 3$  for *Class a*, or  $Z_T = U$  for *Class b* and orthogonal polytypes), its twin setting is parallel to  $C_1$ . The  $l$  index in the twin setting is labeled  $l_T$ .

Rotations between pairs of individuals are taken counter-clockwise in direct space, and thus clockwise in reciprocal space. The  $n \times 60^\circ$  rotations about  $c^*$ , which give the approximate rotations between pairs of individuals, overlap only  $R_i$  belonging to the same type (S, D or X). Each of the  $R_i$  is rotationally related to five other  $R_i$  and along each of them a peculiar sequence of  $l_T$  indices is obtained, which is termed a "Rotational Sequence". Each  $R_i$  generates one rotational sequence, which is shortened to  $RS_i^P(n)$ , where: the superscript P indicates the polytype;  $i$  is the same index defining  $R_i$ ;  $n$  points to each of the six characters of the RS.  $RS_1^P$  corresponds to S rows and thus it is "000000" for all polytypes. The  $n$ -th values of  $RS_i^P$  correspond to the  $l_T$  indices of the nodes on the row which is related to  $R_i$  by  $(n-1) \times 60^\circ$  clockwise rotation. The two  $RS_i^P$  corresponding to D-type rows ( $R_{2-3}$ ) on the one hand, and the six  $RS_i^P$  corresponding to X-type rows ( $R_{4-9}$ ) on the other, can be transformed into each other by cyclic permutations. Since the orientations of the single-crystal lattices and of the twin lattice are fixed and determined by  $Z_T$ , also the starting point of each  $RS_i^P$  is fixed, and the nine  $RS_i^P$  are independent. The node features of the composite rows are obtained from the corresponding  $RS_i^P$  by considering their relation with the  $Z_T$  symbols. A twin of  $N$  individuals ( $2 \leq N \leq 6$ ) is identified by  $N Z_T$  symbols. The  $l_T$  index of the  $q$ -th node coming on  $i$ -th row from the  $j$ -th individual is given by:

$$[l_T(i, j)]_q = [RS_i^P(n)]_q, n = [(Z_T)_j + 4](\text{mod } 6). \quad (18)$$

The node features of composite rows are completely defined by the nine  $RS_i^P$  and  $Z_T$  symbols; therefore, there are only nine independent composite rows, for which the symbol  $C_i$  is adopted.  $R_i$  and  $C_i$  share the same row features and thus the description of the reciprocal lattice in terms of the tessellation rhombus and of the minimal rhombus is the same for both the single-crystal lattice and the twin lattice.

Because of the metric relations (Table 10), the  $l_T$  of both  $C_i$  and  $R_i$  of the same type and belonging to the same central plane are related by:

$$\begin{aligned} [l_T(D_i)]_q &= [6 - l_T(D_{3-i})]_q \\ [l_T(X_i)]_q &= \left\{ 6 - l_T[X_{(9-i)(\text{mod } 6)}] \right\}_q \end{aligned} \quad (19)$$

Knowing the  $l_T$  of one D-type  $C_i / R_i$  and three X-type  $C_i / R_i$ , the  $l_T$  of the remaining four  $C_i / R_i$  can be calculated. There are thus five truly geometrically independent  $C_i / R_i$  (one S-type, one D-type and three X-type), but nine translationally independent  $C_i / R_i$ . The distribution of  $I_j$  on the  $C_i$  of a minimal rhombus is the information necessary to derive and identify the diffraction patterns of mica twins.

A short comparative analysis of the four periodic basic structures ( $1M$ ,  $2M_1$ ,  $2M_2$  and  $3T$ ) is given below. For these four polytypes the twin setting has a period of  $c^*/6$  along  $c^*$ :  $l_T(2M_1, 2M_2) = l_{C_1}(2M_1, 2M_2)$ , but  $l_T(1M, 3T) = 2l_{C_1}(1M, 3T)$ . Table 17 gives the  $C_i$  and  $RS_i^P$ . The definition of  $I_j$  is given in Table 18. The rules for combining  $I_j$ 's of the individuals into composite  $I_j$ 's of the twin are given in Nespolo et al (2000a).

**Table 17.** Composite rows ( $C_j$ ) and Rotational Sequences ( $RS_j^P$ ) for the four basic polytypes (after Nespolo et al. 2000a).

Composite row	Type	$h \pmod{3}$	$k \pmod{3}$	$RS^{1M}$	$RS^{2M_1}$	$RS^{2M_2}$	$RS^{3T}$
$C_1$	S	0	0	000000	000000	000000	000000
$C_2$	$D_1$	1	0	242424	424242	000000 / 333333	242424
$C_3$	$D_2$	2	0	424242	242424	000000 / 333333	424242
$C_4$	$X_1$	1	1	204402	102201 / 435544	121212 / 454545	000000 / 222222 / 444444
$C_5$	$X_2$	2	2	402204	201102 / 534435	212121 / 545454	000000 / 222222 / 444444
$C_6$	$X_3$	0	1	022044	011022 / 344355	121212 / 454545	000000 / 222222 / 444444
$C_7$	$X_4$	1	2	220440	110220 / 443553	212121 / 545454	000000 / 222222 / 444444
$C_8$	$X_5$	2	1	440220	220110 / 553443	121212 / 454545	000000 / 222222 / 444444
$C_9$	$X_6$	0	2	044022	022011 / 355344	212121 / 545454	000000 / 222222 / 444444

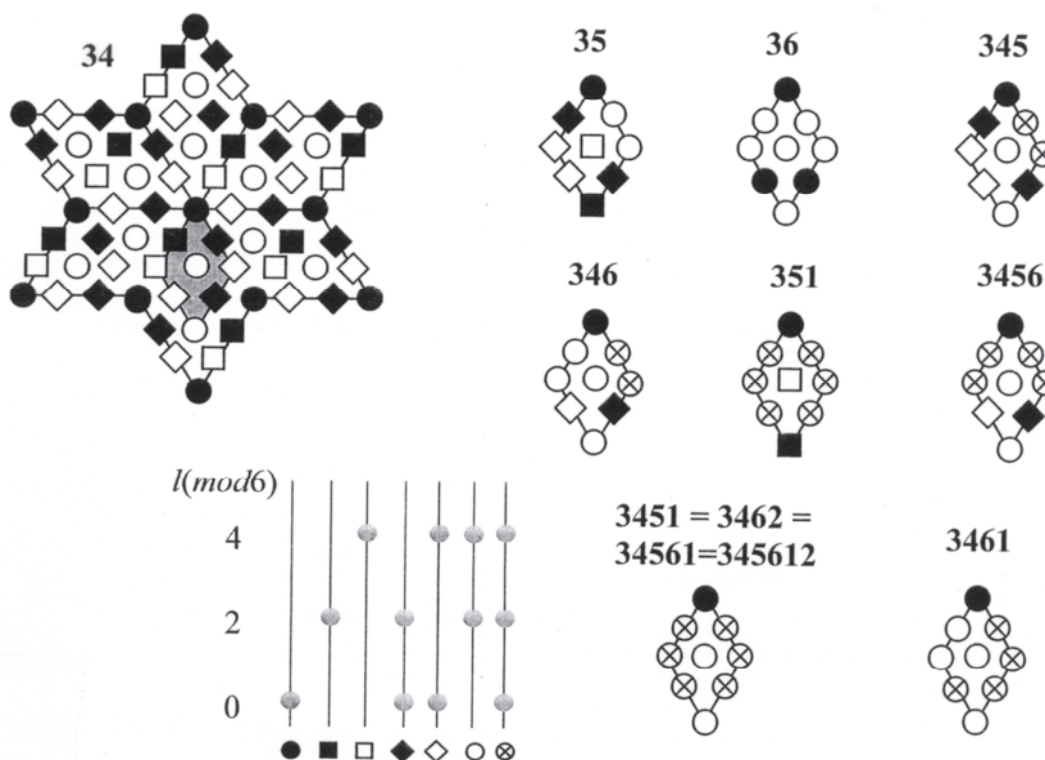
**Table 18.** Definition of the  $J_j$  for the four basic polytypes and their twins. I indicates the number of nodes on the reciprocal lattice row. The subscript  $j$  is a sequential number (after Nespolo et al. 2000a).

$J_j$	$1_1$	$1_2$	$1_3$	$2_1$	$2_2$	$2_3$	$2_4$	$2_5$	$2_6$	$3_1$	$3_2$	$3_3$	$3_4$	$3_5$	$3_6$	$3_7$
$I(\pmod{6})$	0	2	4	0,2	0,4	0,3	1,4	2,5	2,4	0,2,4	0,1,4	0,2,3	0,2,5	0,3,4	1,2,4	2,4,5

$J_j$	$4_1$	$4_2$	$4_3$	$4_4$	$4_5$	$4_6$	$5_1$	$5_2$	$5_3$	$6_1$
$I(\pmod{6})$	0,1,2,4	0,1,3,4	0,2,3,5	0,2,3,4	0,2,4,5	1,2,4,5	0,1,2,3,4	0,1,2,4,5	0,2,3,4,5	0,1,2,3,4,5

**1M polytyp** . The  $c^*_1$  repeat coincides with the polytype period and along each  $R_i$  there is only one node, which obeys the relation  $l_T = 2h(\text{mod } 6)$ . D-type  $R_i$  are either  $1_2$  ( $D_1$ ) or  $1_3$  ( $D_2$ ) and the  $RS_{2,3}^{1M}$  are "242424" and "424242". The  $n \times 60^\circ$  rotations about  $c^*$  produce the overlap of all the reciprocal lattice nodes belonging to D-type  $R_i$  when  $n$  is even, but to their separation when  $n$  is odd. X-type  $RS_{4,9}^{1M}$  are the six cyclic permutations of "220440". On the basis of the relation between  $C_i$  and  $RS_i^{1M}$  (Table 17) seven different  $C_i$  appear in the twin lattice. One or two reflections can appear on D-type  $C_i$  ( $l_T$  is never 0), whereas one, two or three reflections can appear on X-type  $C_i$ . Nine independent 1M twin patterns occur (Fig. 25).



**Figure 25.** The nine independent patterns of 1M twins as expressed through the corresponding minimal rhombi. For the  $Z_T = 34$  twin, the complete star polygon is given, with the minimal rhombus in it shaded. Inset:  $l(\text{mod } 6)$  indices of the nodes on reciprocal lattice composite rows [used by permission of the editor of *Acta Crystallographica A*, from Nespolo et al. (2000a) Fig. 8, p. 143].

When three equally spaced reflections in the  $c^*_1$  repeat occur along non-family rows, in principle the diffraction pattern may correspond either to a 1M twin (apparent polytypism) or to a 3-layer polytype (real polytypism). The distinction is obtained by applying the geometrical criteria given in Tables 12a-12c. However, 1M twins with  $Z_T = 351$  cannot be distinguished geometrically from the 3T polytype (see also Nespolo and Kogure 1998). This ambiguity is removed when weak reflections appear along family rows, which can be expected for dioctahedral and Li-rich trioctahedral micas (Rieder 1968, 1970). The effect of these weak reflections on the twin diffraction pattern is analyzed in Nespolo et al (2000a).

**2M<sub>1</sub> polytyp** . Because the parity of layers is opposite for the 2M<sub>1</sub> polytype ( $Z = 220440$ ,  $T = |4.4 \ 2.2|$ ) with respect to the 1M polytype ( $Z = 330$ ,  $T = |3.3|$ ), the threefold family structure has an opposite setting (reverse / obverse) and the corresponding family rows have different reflection conditions, namely  $k = 0(\text{mod } 3)$ ,  $l_T = 2h(\text{mod } 6)$  for 1M,

but  $k = 0(\text{mod } 3)$ ,  $l_{T_1} = 4h(\text{mod } 6)$  for  $2M_1$  (Nespolo 1999). One reflection occurs in the  $c^*_1$  repeat along family  $R_i$ , but two along non-family  $R_i$ . D-type  $R_i$  are the same as in  $1M$  case, but, because of the opposite parity of the layers in the two polytypes, the two  $RS_{2-3}^{2M_1}$  are inverted. X-type  $R_i$  have the three possible pairs of values of  $l_T(\text{mod } 6)$ : 0 and 3, 1 and 4, 2 and 5. For the X-type  $R_i$  the sequence of  $n \times 60^\circ$  rotations corresponds to a double sequence of  $l_T$  values: 011022 / 344355 or cyclic permutations, producing six independent double  $RS_i^{2M_1}$  (Table 6). As for the  $1M$  polytype, the twelve composite twins produce nine different patterns, none of which can be mistaken for that of a  $1M$  twin (Fig. 26).

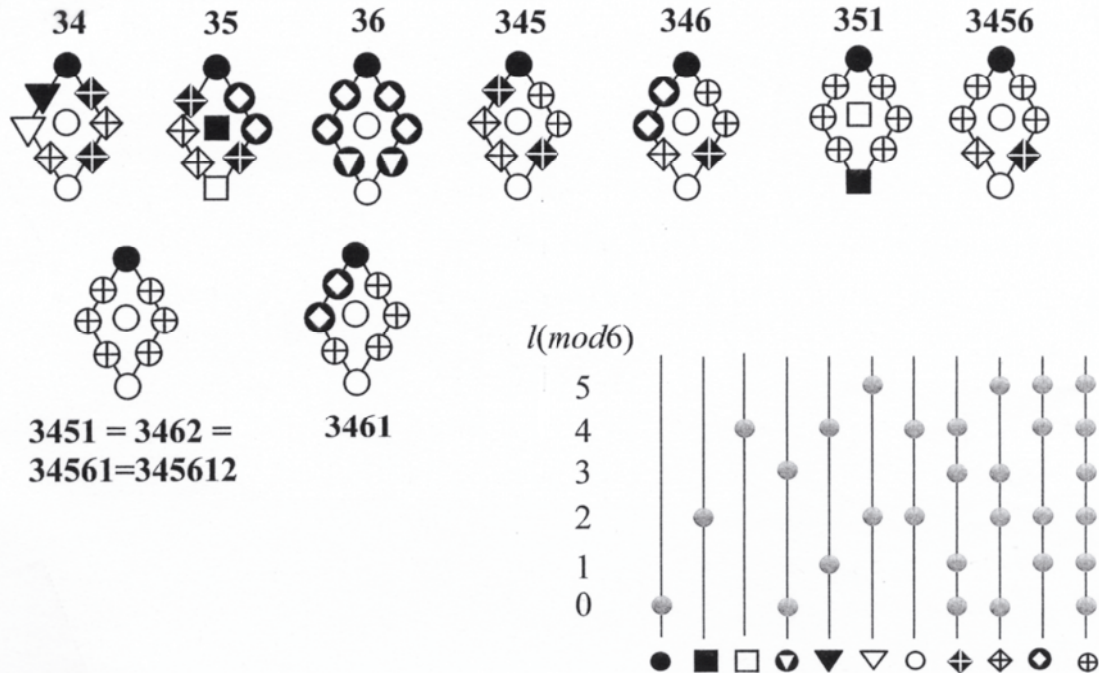


**Figure 26.** The nine independent patterns of  $2M_1$  twins as expressed through the corresponding minimal rhombi. Inset:  $l(\text{mod } 6)$  indices of the nodes on reciprocal lattice composite rows [used by permission of the editor of *Acta Crystallographica A*, from Nespolo et al. (2000a) Fig. 9, p. 144].

**$2M_2$  polytype.** Being a *Class b* polytype,  $2M_2$  has a markedly pseudo-rhombohedral lattice and two of the five pairs of twin laws, namely those corresponding to  $\pm 120^\circ$  rotation about  $c^*$ , correspond to pseudo-merohedry, whereas the remaining three correspond to reticular pseudo-merohedry. Each of the six  $n \times 60^\circ$  rotations belong to the point group of the family structure (subfamily B), and thus the family sublattice of the individuals is always overlapped.  $RS_2^{2M_2}$  and  $RS_3^{2M_2}$  both correspond to the double sequence 000000/333333, whereas  $RS_{4-9}^{2M_2}$  correspond to the cyclic permutations of the double sequence 121212/454545. There are only two kinds of patterns for  $2M_2$  twins. Twinning by pseudo-merohedry gives a pattern geometrically indistinguishable from that of the single crystal ( $Z_T = U$ ). The other pattern corresponds to twinning by reticular pseudo-merohedry ( $Z_T = UE$ ) and differs from the single crystal pattern in the six X-type  $C_i$ , which show four reflections in the  $c^*_1$  repeat (Fig. 27). Neither can be mistaken for any one of the  $1M$  or  $2M_1$  polytypes or twins.

**$3T$  polytype.** The  $3T$  polytype is an orthogonal subfamily A polytype, for which the six orientations of the structural model are equivalent. They can be grouped into two sets of odd or even parity, corresponding to obverse and reverse setting of the family structure



respectively. Taking odd parities, as in Zvyagin (1967), D-type  $R_i$  and  $RS_i^{3T}$  are the same as those of  $1M$  polytype. Taking the even orientation instead, as in Backhaus and Āurovič (1984), D-type  $R_i$  and  $RS_i^{3T}$  are the same as those of  $2M_1$  polytype. In both cases, there is only one triple sequence of X-type  $RS^{3T}$ : 000000/222222/444444. The six orientations of the minimal rhombus are divided into two types, differing for the D-type  $R_i$ . The  $2n \times 60^\circ$  rotations belong to the symmetry of both the individual and the family structure and reproduce the same rhombus. On the other hand,  $(2n+1) \times 60^\circ$  rotations do not belong to either symmetries and thus they exchange the two independent rhombi.

Twinning by complete merohedry ( $Z_T = UU^*$ ) by definition produces a diffraction pattern with the same geometrical appearance as the single crystal, which in its turn may be geometrically identical to the pattern of  $1M$  twinned as  $Z_T = 351$ . In contrast, for twinning by selective merohedry ( $Z_T = UE, UE^*, UU^*E, UU^*E^*, UU^*EE^*$ ), the two D-type  $C_i$  correspond to have two reflections at  $l_T = 2(\text{mod } 6)$  and  $4(\text{mod } 6)$ . This is the same geometrical appearance of  $1M$  twinned as  $Z_T = 3451$ . The distinction between  $1M$  twins and the  $3T$  polytype (twinned or untwinned) requires by very careful examination of the violation of the additional reflection conditions (Nespolo et al. 2000a).

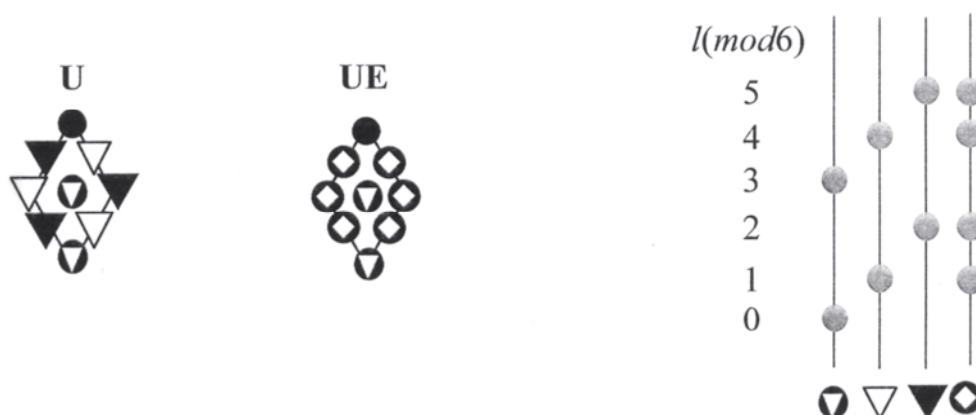


**Figure 27.** The two independent patterns of  $2M_2$  twins as expressed through the corresponding minimal rhombi. Inset:  $l(\text{mod } 6)$  indices of the nodes on reciprocal lattice composite rows.

### Derivation of allotwin diffraction patterns

The allotwin laws include the twin laws for each of the individuals, as well as the symmetry operations of the crystal(s) point group(s). The six rotations about  $c^*$  now must be considered. By indicating the first individual with a superscript and the second one with a subscript, the allotwin  $Z_T = {}^3_3$  must be considered also, whereas the  $Z_T = 33$  twin simply corresponds to a parallel growth. Therefore, the number of possible laws increases and depends upon the number of different polytypes undergoing allotwinning.

Because the geometrical appearance of the diffraction pattern of the  $3T$  polytype and of its twins is ideally the same as  $1M$  twinned as  $Z_T = 351$  or  $3451$ , the contribution from  $3T$  does not produce an independent pattern: it is not considered in the following systematic analysis.

The three basic monoclinic polytypes can produce 3 binary (two-individual) allotwins ( $1M-2M_1$ ;  $1M-2M_2$ ;  $2M_1-2M_2$ ) and 1 ternary (three-individual) allotwin ( $1M-2M_1-2M_2$ ). Binary (AB) and ternary (ABC) allotwins are indicated by  ${}^A_B$  and  ${}^A_{BC}$  respectively, where A, B and C represent the  $Z_T$  symbols for each portion of the allotwin.

These composite allotwins can be described on the following basis:

1. The allotwin is constructed by 2 (binary allotwin) or 3 (ternary allotwin) portions (A, B, C), each consisting only of individuals of the same polytype, which in turn can be twinned;  $1M$  is taken as the first portion (A) of the allotwin; when  $1M$  is not involved (binary allotwin  $2M_1-2M_2$ ), the portion A is  $2M_1$ .
2. Because the individuals building the twin or allotwin are related by point group operations, the A-B-C sequence has no influence on the composite lattice and the two or three portions can be described as juxtaposed and non-mixed; for example,  $Z_T = {}^3_4 {}^5_6$  is equivalent to  $Z_T = {}^{35}_{46}$ .
3. Within each single portion (A, B, C), the restrictions on the possible orientations derived for the twins are retained, but these restrictions are not applicable when comparing individuals belonging to different portions.
4. The first individual of the first portion (A) is fixed in orientation  $Z_T = 3$ , but this restriction is not applicable for the first individual of the other portions. Therefore the number of possible orientations for B and C portions must be multiplied by the number of independent orientations of the minimal rhombus, as determined by the limiting symmetry, namely six for  $2M_1$ , and two for  $2M_2$ .

The minimal rhombi of the allotwins are calculated as combinations of the minimal rhombi of each portion, but the number of minimal rhombi to be considered depends upon the limiting symmetry. Those minimal rhombi of two twins of  $1M$  that are equivalent through an  $n \times 60^\circ$  rotation about  $c^*$  can produce two independent minimal rhombi when combined with a minimal rhombus of  $2M_1$ . Therefore, in the derivation of the reciprocal lattice of  $1M-2M_1$  allotwins, the minimal rhombi of all the thirty-one twins for both polytypes in Table 16 must be considered. To these, the minimal rhombus corresponding to the single crystal must be added. Moreover, keeping fixed the minimal rhombi of  $1M$  (first individual in orientation  $Z_T = 3$ ), the six independent orientations of each of the thirty-two minimal rhombi of  $2M_1$  must be considered. For the  $2M_2$  polytype, there are only two independent orientations of the individual *w.r.l.* ( $Z_T = U$  or  $Z_T = E$ ) and only one for the twin reciprocal lattice ( $Z_T = UE$ ). In deriving the reciprocal lattice of  $1M-2M_2$  or  $2M_1-2M_2$  allotwins, for *Class a* polytypes only the minimal rhombus of the single crystal and the minimal rhombi of the twenty-three twins related by  $(2n+1) \times 60^\circ$  rotations must be combined with the three (U, E, UE) minimal rhombi of  $2M_2$ . The remaining eight minimal rhombi of *Class a* polytypes are related to some of the other twenty-three by  $2n \times 60^\circ$  rotations, which are symmetry operations for the minimal rhombi of  $2M_2$  and cannot produce any further independent allotwin minimal rhombus. Finally, for the ternary allotwins  $1M-2M_1-2M_2$ , the independent minimal rhombi of the binary allotwin  $1M-2M_1$ , and those related by  $(2n+1) \times 60^\circ$  rotations, must be combined with the three minimal rhombi of  $2M_2$ .

For each combination, the composite minimal rhombus obtained in this way, then rotated by  $n \times 60^\circ$  ( $0 \leq n \leq 5$ ), and finally – for each of these rotations – reflected across (010), is compared with those calculated for the previous combinations and, if equivalent, is discarded. The resulting minimal rhombi are given in Nespolo et al (2000a).

## IDENTIFICATION OF MDO POLYTYPES FROM THEIR DIFFRACTION PATTERNS

### Theoretical background

The identification of the stacking mode in an MDO polytype is based on two orthogonal projections, which are sufficient to characterize reliably any structure. For

mica structures (but also for other phyllosilicates) the most suitable projections are the XZ and the YZ projections. A Fourier series calculated with coefficients derived from zonal diffractions only, yields a projection of the structure along the zone axis. It follows that the  $h0l$  and  $0kl$  nets characterize unambiguously the projections XZ and YZ, respectively. The  $h0l$  net contains only the reciprocal rows with family diffractions (S and D rows) and, therefore, this set characterizes the family structure, i.e. the Subfamily. The set of diffractions  $0kl$  contains both S and X rows (not D rows). Whereas the former are common (almost) for all polytypes in both subfamilies and thus useless for identification purposes, the latter are characteristic for any individual polytype and can be used for their identification, unless they are so diffuse that no discernible maxima can be obtained.

Owing to the efficiency of atomic scattering factors as a function of  $\sin\theta/\lambda$ , the diffractions close to the origin of the reciprocal lattice are best suited for identification purposes. Moreover, any family structure in micas is trigonal or hexagonal and from Friedel's law it follows that the reciprocal lattice rows  $20l$ ,  $13l$ ,  $\bar{1}3l$ ,  $\bar{2}0l$ ,  $\bar{1}3l$  and  $\bar{1}\bar{3}l$  carry the same information. Therefore, two reciprocal lattice rows, namely  $20l$  and  $02l$ , suffice to identify the subfamily and the MDO polytype, respectively. The positions of diffraction spots and the distribution of their intensities is so characteristic that a mere visual inspection of the diffraction patterns obtained experimentally with that calculated for a homo-octahedral structure with the expected chemical composition, leads to the solution, provided that the presence of twinning has been ruled out. This procedure was described first by Weiss and Đurovič (1980) and explained in more details by Đurovič (1981) (see also Đurovič 1999, p.761).

The recognition of the significance of the YZ projections (and thus also the five MDO groups given in Table 7), which can be derived also directly from the full polytype symbols (Đurovič et al. 1984), is very important also for the interpretation of HRTEM images (Kogure, this volume).

### Identification procedure

The identification of the stacking mode of an MDO polytype in the homo-octahedral approximation is straightforward. It can be performed by visual inspection of the intensity distribution along two rows (one D and one X), and from visual inspection of the geometry of the diffraction pattern.

1. *Intensity distribution.*
  - a) Calculate  $F^2$  values for each of the six homo-octahedral MDO polytypes given in Table 7 by using average atomic occupations in the octahedral sites, which correspond approximately to the chemical composition of the investigated polytype. Use the space-group type  $P1$  and use a common orthogonal six-layer cell, which can "accommodate" each polytypes. Atomic coordinates from the ideal Pauling model may be used. The  $F^2(0kl)$  values for the  $1M$  and  $2O$  polytypes must be the same (MDO group I, Table 7) and also the  $F^2$  values for the family diffractions must obey the trigonal/hexagonal Laue symmetry. Select the  $20l$  and  $02l$  rows, and construct identification diagrams for the determination of the subfamily (two rows for A and B only) and for the MDO polytype (four rows for the MDO groups I to IV) as indicated in Figure 28, where the size of each circle is proportional to the respective  $F^2$  values. In principle, the MDO V row should be given. However, this group contains only the  $6H$  polytype, which has not been reported to date, and can be unambiguously identified by the geometry of its diffraction pattern, which has six orthogonal planes with two reflections in the  $c^*_1$  repeat along D rows: this geometry cannot be obtained by the twinning of any other polytype. The program DIFK

(Smrčok and Weiss 1993) is very convenient for the calculations of the  $F^2$  values. The program contains a subroutine to produce sequences of the  $F^2$  values along selected reciprocal rows. This program can be obtained free of charge from Smrčok<sup>8</sup>.

- b) Make a set of precession photographs, three from the SX planes and one from an SD plane. Select the  $20l$  and  $02l$  rows, and compare the intensities with the calculated values. Figure 29 and 30 show three examples.

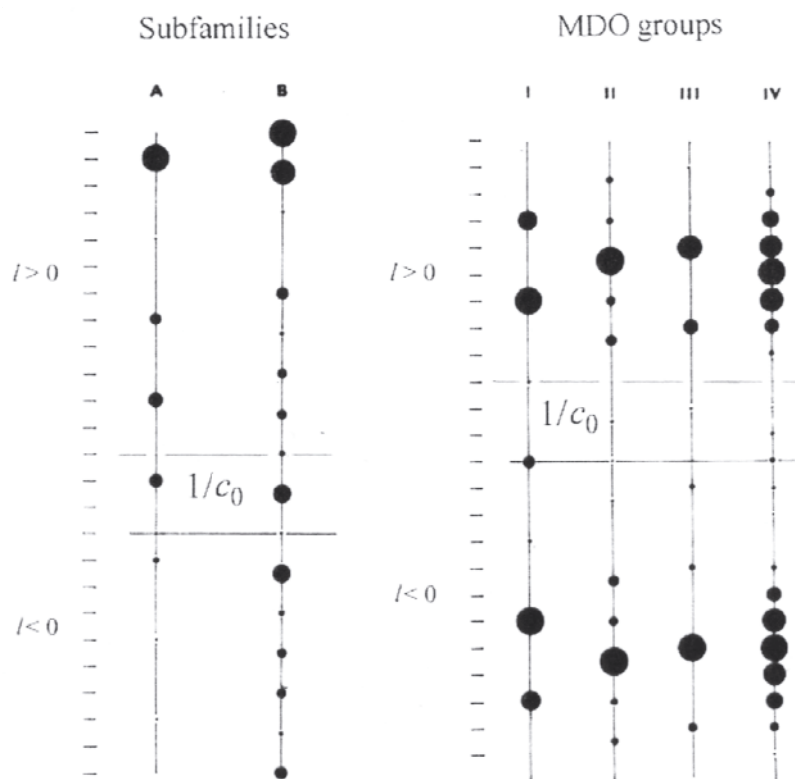


**Figure 28.** Visual representation of calculated intensities of diffractions of MDO polytypes of phlogopite. The indexing refers to the six-layer orthogonal cell ( $C_2$  cell). Left: intensities along  $20l$  (D row, containing family diffractions) reciprocal lattice row and intensity distribution within subfamilies A and B. Right: intensities along  $02l$  (X row, containing non-family diffractions) reciprocal lattice row and intensity distribution within MDO groups I to IV. The strongest intensity of each subfamily (left) or MDO group (right) is drawn as the largest circle (modified after Weiss and Durovic 1989).

## 2. Geometry of the diffraction pattern.

- Reciprocal lattice rows parallel to  $c^*$  in the  $h0l$  *r.p.* have 1 (subfamily A) or 2 (subfamily B) reflections in the  $c^*_1$  repeat;
- Reciprocal lattice rows parallel to  $c^*$  in the  $0kl$  *r.p.* have 1 ( $1M$ ), 2 ( $2M_1$ ,  $2M_2$  or  $2O$ ), 3 ( $3T$ ) or 6 ( $6H$ ) reflections in the  $c^*_1$  repeat;
- $2M_1$  is the only 2-layer subfamily A polytype;  $2M_2$  and  $2O$  are distinguished because the  $0kl$  *r.p.* is orthogonal for the latter but non-orthogonal for the former.

For the determination of the meso- and hetero-octahedral MDO polytypes, a complete structure refinement is necessary, because the occupancy factors of the three

<sup>8</sup> E-mail: uachsmrk@savba.sk

octahedral sites as well as the sizes of the corresponding octahedra must be determined. A complete structure refinement (e.g., using anomalous scattering) is necessary also to distinguish the two members of an enantiomorphous pair.

Our experience shows that the ideal Pauling model is sufficient for identification purposes because the slight deviations from the actual atomic coordinates owing to desymmetrization are not important in these calculations.

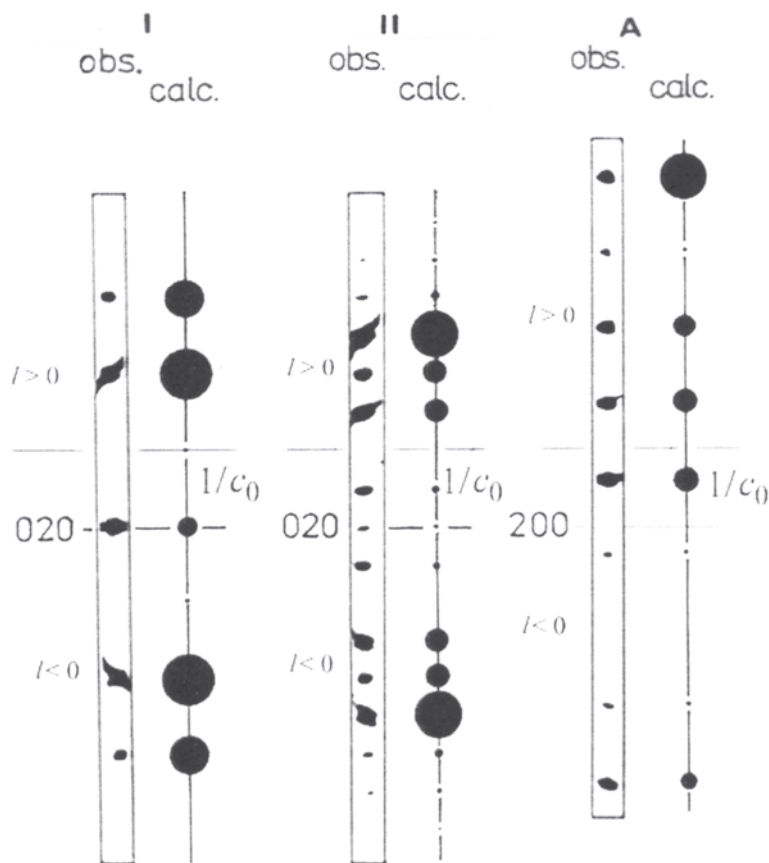


**Figure 29.** Comparison of observed (obs.) and calculated (calc.) intensities along  $02l$  (X row, containing non-family diffractions) and  $20l$  (D row, containing family diffractions) reciprocal lattice rows of zinnwaldites  $1M$  (MDO group I) and  $2M_1$  (MDO group II), which are essential for the identification of MDO groups I, II and of subfamily A, respectively. Observed intensities are taken from  $0kl$  and  $h0l$  precession photographs. The distribution of intensities of  $20l$  diffractions is very similar for both zinnwaldite polytypes, and therefore only the distribution corresponding to the one-layer polytypes is given (modified after Weiss and Durovic 1989).

### IDENTIFICATION OF NON-MDO POLYTYPES: THE PERIODIC INTENSITY DISTRIBUTION FUNCTION

The number of non-MDO polytypes in each family is infinite, and increases dramatically with the number of layers (Mogami et al. 1978; McLarnan 1981). The procedure for the identification of MDO polytypes described in the previous section becomes virtually impossible for non-MDO polytypes with longer periods, which require instead a simplified procedure. This simplified procedure was introduced by Takeda (1967) under the name of Periodic Intensity Distribution (PID). The PID is an

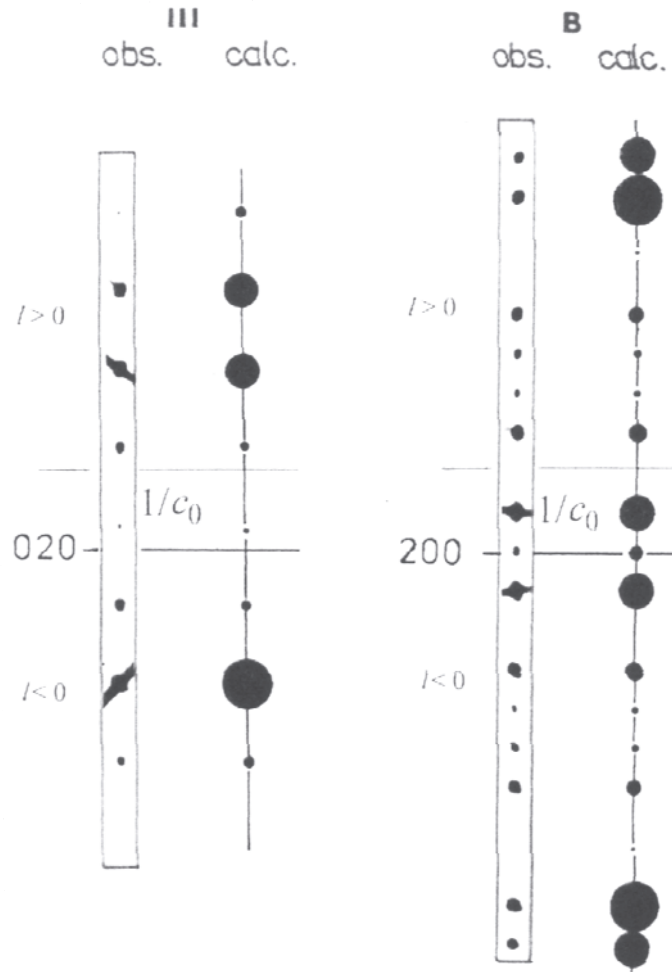


**Figure 30.** Comparison of observed (obs.) and calculated (calc.) intensities along  $02l$  (X row, containing non-family diffractions) and  $20l$  (D row, containing family diffractions) reciprocal lattice rows of lepidolite  $2M_2$  (MDO group III), which are essential for the identification of MDO groups III and subfamily B, respectively. Observed intensities are taken from  $0kl$  and  $h0l$  precession photographs.

approximation of the Fourier transform of the stacking sequence that can be obtained in a simple way from the diffraction intensities: it is defined within the Trigonal model and the homo-octahedral approximation, and gives thus the correct stacking mode for the case of all-M1 layers. If the polytype contains one or more M2 layers, the stacking mode obtained from PID analysis of the diffraction pattern is simply an approximation: for each M2 layer, the characters  $T_{2j} v_{2i,2j+1} T_{2j+1}$  are replaced by the characters  $v_{2j,2j+1}^e$  or  $v_{2i,2j+1}^u$ , depending on the parity of  $T_{2j}$  and  $T_{2j+1}$ , and the displacement character obtained by the PID is simply  $v_{2j,2j+1}$ . No indication can be obtained from the PID that the polytype may belong to the hetero-octahedral family. For the meso- and hetero-octahedral family, as well as for the distinction between the two members of an enantiomorphous pair, a complete structure refinement is required, similarly to the case of MDO polytypes. However, only the structural models corresponding to polytypes homomorphous to the homo-octahedral sequence obtained by PID analysis must be considered.

The Fourier transform of a polytype ( $G^N$ , where  $N$  is the number of layers) is given by the Fourier transform of the stacking sequence, which is a fringe function (Lipson and

Taylor 1958), modulated by the Fourier transform of the layer ( $G_j$ ):

$$G^N(hkl) = \sum_{j=1}^N G_j(hkl) \exp 2\pi i (t_{x,j}h + t_{y,j}k + t_{z,j}l) \quad (20)$$

where  $t_{x,j}$ ,  $t_{y,j}$ ,  $t_{z,j}$  are the ( $x$ ,  $y$ ,  $z$ ) components of the stacking vector relating the  $j$ -th and the  $(j+1)$ -th layers (Takeda 1967). When the shifts between the building layers are rational and the rotations belong to the symmetry of the layer(s), their Fourier transform ( $G_j$ ), which is a continuous function in the direction lacking periodicity, can be factorized from the expression of the structure factor  $G^N$ . Thus,  $G^N$  takes the simple form of the product of the layer transform and of the stacking sequence transform. The second term expresses the periodicity in reciprocal space appearing when a structure is constructed by a translation of subunits. This is the case of polytypes of binary compounds like SiC and ZnS (Tokonami and Hosoya 1965; Tokonami 1966; Farkas-Jahnke 1966; Dornberger-Schiff and Farkas-Jahnke 1970; Farkas-Jahnke and Dornberger-Schiff 1970). In micas, the M layers are instead related by rotations belonging not to the layer symmetry but to the idealized symmetry of the  $O_b$  plane (with the obvious exception of the  $1M$  polytype) and the same simplification is in principle not possible. However the Fourier transform of the M layer in the six possible orientations is almost unmodified in a subspace of the reciprocal space (Takeda 1967). By removing the modulating effect of the layer, the *approximated* Fourier transform of the stacking sequence is obtained. This is known as the *Periodic Intensity Distribution* (PID) function (Takeda 1967; Sadanaga and Takeda 1969; Takeda and Sadanaga 1969). Comparison of calculated and observed PID values along non-family reciprocal lattice rows parallel to  $c^*$  is in principle sufficient to identify any mica polytype (Takeda and Ross 1995; Nespolo et al. 1999d).

### PID in terms of TS unit layers

A single type of non-polar unit layer (the M layer) is sufficient to describe polytypism of micas: the M layer is stacked with both translations along  $c$  and rotations about  $c^*$  which do not belong to the layer symmetry. A different choice, employing more than one type of layers, is more suitable to describe the symmetry of the layer stacking and to simplify the process of identification of the stacking mode. As shown above, two kinds of non-polar OD layers (*Tet* and *Oc*) and one kind of polar OD packet (with two opposite orientations,  $p_{2j}$  and  $q_{2j+1}$ ) are necessary to describe the OD character of mica polytypes. To compute the PID, Sadanaga and Takeda (1969) and Takeda and Sadanaga (1969) introduced the non-polar TS unit layers, which are defined within the Trigonal model. The two layers D and T would be sufficient to describe any mica polytypes if two orientations, related by  $180^\circ$  rotation about  $c^*$ , were permitted. To avoid the use of this rotation, which does not belong to the layer symmetry, four TS layers, including also the  $D^*$  and  $T^*$  layers, are employed. The relative positions of TS unit layers are given by the TS symbols, written as a sequence of  $N$  symbols  $L_j(\Delta X_j, \Delta Y_j)$ ,  $1 \leq j \leq N$ , where  $L_j$  is the kind of layer (D,  $D^*$ , T,  $T^*$ ), and  $(\Delta X_j, \Delta Y_j)$  are the  $(A_1, A_2)$  components in hexagonal axes of the total shift vector between the  $j$ -th TS layer and the  $N$ -th TS layer of the previous repeat (Fig. 2,3). The  $j$ -th TS unit layer is defined by the relation between the  $j$ -th and the  $(j+1)$ -th M layers and corresponds to the pair of packets  $q_{2j-1}p_{2j}$ . D and  $D^*$  layers correspond to  $2n \times 60^\circ$  rotations between  $q_{2j-1}$  and  $p_{2j}$  [i.e. the RTW symbol is  $A_j = 0 \pmod{2}$ ;  $q_{2j-1}$  and  $p_{2j}$  have the same orientation parity], T and  $T^*$  layers correspond to  $(2n+1) \times 60^\circ$  rotations between  $q_{2j-1}$  and  $p_{2j}$  [i.e.  $A_j = 1 \pmod{2}$ ;  $q_{2j-1}$  and  $p_{2j}$  have an opposite orientation parity].

In the homo-octahedral approximation the two OD packets ( $p_{2j}$  and  $q_{2j+1}$ ) describing each layer have the same OD symbol, and the two half-layers of an M layer have the

same  $Z$  symbol. If “u” (*uneven*) and “e” (*even*) are the orientation parities of OD symbols of the OD packets, or of  $Z$  symbols of half  $M$  layers, the following equalities are obtained from Figure 3:

$$D = u0u; \quad D^* = e0e; \quad T = e0u; \quad T^* = u0e \quad (21)$$

The Fourier transform of an  $N$ -layer mica polytype [Eqn. (20)] in terms of TS unit layers in hexagonal axes becomes:

$$G^N(HK.L) = \sum_{j=1}^N G_j(HK.L_R) \exp 2\pi i \left( H\Delta X_j + K\Delta Y_j + \frac{L(j-1)}{N} \right). \quad (22)$$

The Fourier transform of the  $j$ -th TS unit layer,  $G_j(HK.L_R)$ , is two-dimensionally periodic and the reciprocal lattice coordinate in the direction lacking periodicity is not restricted to integral values but is a real variable, labeled  $L_R$ . In Equation (22),  $G_j$  plays a role analogous to that of the atomic scattering factor in the expression of the structure factor.

Because the  $j$ -th and the  $(j+1)$ -th TS layers must connect two packets  $p_{2j}$  and  $q_{2j+1}$  with the same orientation parity (to preserve the octahedral coordination of the  $M$  cations), there are only eight possible pairs of TS unit layers (DD; D\*D\*; TT\*; T\*T; DT\*; D\*T; TD; T\*D\*). In addition, to match the cation positions, the layer stacked over a D or T layer must be shifted by  $-a/3$ , whereas the layer stacked over a D\* or T\* layer must be shifted by  $+a/3$ . Within the Pauling model only the octahedral cations have different coordinates in the four TS unit layers. However, their contribution to the layer Fourier transform becomes identical when the following conditions are satisfied:

$$\begin{aligned} H = 0(\bmod 3), \text{ all } K; H = 1(\bmod 3), K \neq 1(\bmod 3); H = 2(\bmod 3), K \neq 2(\bmod 3) \\ h = 0(\bmod 3), \text{ all } k; h \neq 0(\bmod 3), k \neq 0(\bmod 3) \end{aligned} \quad (23)$$

Consequently,  $G_j$  is identical for all  $j$  ( $G_j = G_0$ ) and the contribution of the Fourier transform of the layer can be extracted from the summation in Equation (22), obtaining the PID function  $S^N$ :

$$S^N(HK.L) \cong \frac{G^N(HK.L)}{G_0(HK.L_R)} = \sum_{j=1}^N \exp 2\pi i \left( H\Delta X_j + K\Delta Y_j + \frac{L(j-1)}{N} \right). \quad (24)$$

Within the Trigonal model also the  $O_b$  atoms have different coordinates, but again their contribution to  $G_j$  in all the four TS unit layers is the same when:

$$\begin{aligned} H = 0, \text{ all } K; K = 0, \text{ all } H; H = -K \\ h = 0, \text{ all } k; h = \pm k \end{aligned} \quad (25)$$

For these reflections,  $G_j = G_0$  and Equation (24) holds again. PID is thus defined in a subspace of the reciprocal space, which narrows from subfamily A polytypes to mixed-rotation polytypes, but always includes at least the three *r.p.*  $0kl$ ,  $hhl$ ,  $hhl$ .

The procedure for computing PID from the stacking mode is illustrated in Appendix B. A concrete example is hereafter analyzed in details for the  $8A_2$  polytype. The PID is computed from the RTW symbols of the stacking sequence with the program PTST98



(Nespolo et al. 1999d). This program can be obtained free of charge from its first author<sup>9</sup>.

### Derivation of PID from the diffraction pattern

The PID analysis of the diffraction pattern can be performed both in XRD and SAED (Selected Area Electron Diffraction) techniques. The experimental PID is easily obtained from the diffraction pattern once the data reduction has been applied. However, a complete data reduction is in general not necessary, because the stacking sequence is determined by the *best* match between the PID obtained from the diffraction pattern and the PID computed for all the homo-octahedral stacking candidates. For polytypes with a limited period, a direct visual comparison of the intensities with the computed PID can reveal the correct homo-octahedral stacking sequence (Ross et al. 1966). The experimental PID function is obtained from the intensities in a  $0.1\text{\AA}^{-1}$  repeat, within which the variation of the experimental factors is small, and the PIDs from several repeats are finally weighted, so that possible uncertainties are further reduced. For example, in general, the improvement in PID obtained by applying the absorption correction is smaller than the approximation of describing the mica structure with the TS layers, which are defined within the Trigonal model. Complete data reduction may improve the quality of the match of the experimental PID with that computed from the correct stacking sequence, but it does not change the sequence of stacking candidates. In other words, the homo-octahedral stacking sequence that best matches the experimental PID is not replaced by a different candidate when a more complete data reduction is applied. Some uncertainties can however be expected for a less complete data reduction in the hypothetical case of a long-period polytype (for which the number of possible stacking sequences is high) with a poor quality of the reflections, and consequently large uncertainties on the experimental PID, if two candidates show relatively close matches with the experimental PID. Such a hypothetical case has not appeared so far, but this is a possibility.

A particularly intriguing case may occur when polytypes with different periodicities are in relation of homomorphy. As shown above, this may happen if a sub-periodicity exists in the sequence of  $\mathbf{v}_{2j,2j+1}$  displacement vectors of meso-octahedral polytypes, or in the sequence of  $\mathbf{T}_{2j}, \mathbf{T}_{2j+1}$  orientation vectors of hetero-octahedral polytypes when the chirality of the packets is neglected. In general, the number of reflections in the  $c^*_1$  repeat corresponds to the number of layers in the full-period polytype. However, when the chemical difference between the family of the full-period polytype and the family of the shorter homomorphous polytype becomes smaller, some of the reflections weaken: if these weak reflections are overlooked, the homo-octahedral stacking sequence obtained from the PID analysis corresponds to an apparent periodicity shorter than the correct one. The visual comparison of the intensities, if performed, involves only the meso-octahedral polytypes homomorphous with the homo-octahedral polytype indicated by the PID, but *with the same number of layers* and the mistake may be overlooked. Special attention is necessary not to miss weak reflections along X rows.

The general guidelines for the PID derivation from the diffraction pattern is summarized as follows:

1. For X-ray diffraction, the effect of the absorption on the PID is normally negligible for the purpose of polytype identification, if a sufficient number (e.g., four or more) of periods along the same row are considered and the corresponding PIDs are weighted. The LP factors are critical, however, if the diffraction pattern is taken with a precession camera, because the Lorentz-polarization effect in the precession motion is severe.

---

<sup>9</sup> E-mail: nespolo@lcm3b.uhp-nancy.fr

2. For electron diffraction, the near-flatness of the Ewald sphere reduces greatly the effect of the experimental factors on the intensities. The pattern is, however, no longer kinematical, and the dynamical effects in general must be taken into account. However, the intensity ratio between adjacent reflections in a reciprocal lattice row can be treated as kinematical, and the PID analysis applies to electron diffraction as well (Kogure and Nespolo 1999b).
3. Equation (24) is based on the approximation of the trigonal distribution of each kind of atom in the layer and  $G_0$  is thus an approximation of the Fourier transform of the layer. In the regions of reciprocal space where  $G_0$  passes through zero and changes sign, the relative error becomes large and Equation (24) is no longer applicable. In the practice of mica-polytype identification, the periods corresponding to  $l$  intervals including those regions should not be used to derive PID from the intensities. These intervals depend on the chemical composition: in the diffraction pattern they include very faint reflections and are easily recognized.
4. The square root of the intensities, partially reduced when necessary, gives an approximant of the structure factors. By dividing these by the Fourier transform of the layer, an un-weighted, un-scaled PID is obtained. The mean value of PID along several period of the same reciprocal lattice row is computed, and the result is brought on the same scale [see Appendix B, Eqn. (B.4)].

### EXPERIMENTAL INVESTIGATION OF MICA SINGLE CRYSTALS FOR TWIN / POLYTYPE IDENTIFICATION

Here we present the general guidelines for the experimental investigation of an unknown mica single crystal. The following represents an ideal outline and note that, depending on the availability and quality of the sample, and on the experimental equipment accessible to the investigator, not all the following steps may be possible. The local-scale investigation by TEM is described in detail by Kogure (this volume) and is thus not discussed here.

#### Morphological study

The first step in the investigation of a mica single crystal consists in a morphological observation under the polarizing microscope. The sample should be observed immersed in a high refractive-index medium (an index oil if available; a natural fluid such as clove oil or glycerin may be used also) and not in air; otherwise the presence of twinning can be easily missed. In case of reflection twins [composition plane (quasi) normal to (001)] a twin results in different extinction positions under crossed polarizers and no complete extinction of light occurs for any orientation of the crystal. Instead, for rotations twins [composition plane parallel to (001)] the presence of twinning may be missed if the sample is observed only on one of the two surfaces, in case the uppermost crystal of a twin is larger than the others. A negative result from the morphological observation should thus be prudently taken as not conclusive about the absence of twinning.

#### Surface microtopography

The second step should possibly involve a surface microtopography, which gives important information on both twinning and polytypism. The microtopography of a mica surface reveals spiral and parallel step patterns on the (001) crystal surfaces. Different techniques have been developed for this kind of investigation, such as phase-contrast microscopy, multiple-beam interferometry (e.g., Tolansky and Morris 1947a,b), surface decoration in TEM (Bassett 1958) and Atomic Force Microscopy. Three kinds of information, useful for the study of polytypism, are obtained by surface microtopography: 1) shape of the spirals; 2) height of the spiral step(s); 3)

presence/absence of interlacing (Sunagawa 1964; Sunagawa and Koshino 1975).

Micas of metamorphic origin are formed by alteration of the original rock and spiral growth is commonly not observed on the surface, which instead presents step systems as a consequence of Ostwald ripening typical of environments in which crystals grow or dissolve *via* a thin film of vapor or solution owing to an interstitial solvent (Sunagawa et al. 1975; Tomura et al. 1979). In contrast, micas formed in magmatic environments invariably show growth spirals on their surfaces, more or less polygonalized depending upon the strength of the solid-fluid interaction (Sunagawa 1977, 1978). A zigzag stacking sequence (i.e. a stacking sequence different from  $1M$ ) appears at the surface with an interlaced pattern: interlacing unambiguously indicates that the crystal under investigation is not  $1M$ . In the case of metamorphic micas, multiple steps split into  $N$  unit layers with rhombic form, where  $N$  is the number of layers in the period of the polytype. In the case of magmatic micas, it is the spiral turn that decomposes into  $N$  unit layers. In both cases, the cause of interlacing is the anisotropy of the advancing rate, which is faster along the stagger direction and slower normal to it (Frank 1951; Verma 1953). No interlacing appears on the surface of the  $1M$  polytype, because all the layers have the same stagger direction. The interlacing pattern of growth spirals is also observed in other phyllosilicates, and was exploited to identify kaolinite (single-layer, no interlacing), dickite (two-layer kaolinite with  $60^\circ$  or  $120^\circ$  rotations) and nacrite (two-layer kaolinite with  $180^\circ$  rotations) of hydrothermal metasomatic origin (Sunagawa and Koshino 1975).

The shape of the growth spirals is controlled by the whole-layer symmetry, rather than by the symmetry of the sheet exposed on the growing surface. Typical growth spirals of trioctahedral micas are five-sided and show the monoclinic metric symmetry of the mica layer (Sunagawa 1964; Sunagawa and Tomura 1976) (Fig. 31). This shape of the growth spirals can be described as deriving from a regular hexagon through elongation and truncation. The growth is more rapid along  $[100]$  (the direction of the stagger) and results in longer sides parallel to the  $a$  axis (perpendicular to  $[010]$ , the direction of slower growth), and the other four shorter edges and more largely spaced sides  $[\pm 310, 3\pm 10]$ , corresponding to faster growth. The two sides  $[310]$  and  $[\bar{3}10]$  are truncated to form a single line, eventually with a denticulated pattern, parallel to  $b$ . Truncation is not observed in 1:1 phyllosilicates, where there is no layer stagger. It is also not observed in dioctahedral micas: the reasons for this difference between trioctahedral and dioctahedral micas are not clear (Sunagawa and Koshino 1975; Sunagawa 1978). Because  $n \times 60^\circ$  rotations are not equivalent when applied to a pentagonal spiral, the relative rotations of each component clearly appear at a surface observation and reveal the direction of stagger of each layer (Fig. 32). For short-period polytypes this information alone is sufficient to determine the stacking sequence. The height of the spiral step can also be directly measured by multiple-beam interferometry (step height as thin as  $2.3\text{\AA}$  were measured in hematite: Sunagawa 1960) and AFM (Kuwahara et al. 1998). In this way, Sunagawa et al (1968) identified polytypes  $1M$ ,  $2M_1$ ,  $2M_2$ ,  $2O$  and  $3T$  in synthetic fluor-phlogopite, and confirmed the presence of polytypes with longer period, whose stacking sequence was however too complex to be identified only on the basis of the surface morphology.

Also the presence of twinning is clearly shown by surface microtopography. Sunagawa and Tomura (1976) reported beautiful examples of five-sided plateau-like patterns on the (001) face of phlogopite. These patterns derive from the agglutination of thin platy crystals, formed in the vapor phase and moving around as “flying magic carpets” while they are growing, onto the surface of a larger crystal, on which they settle with equal probability on any of the  $n \times 60^\circ$  rotations, making thus either a parallel or a

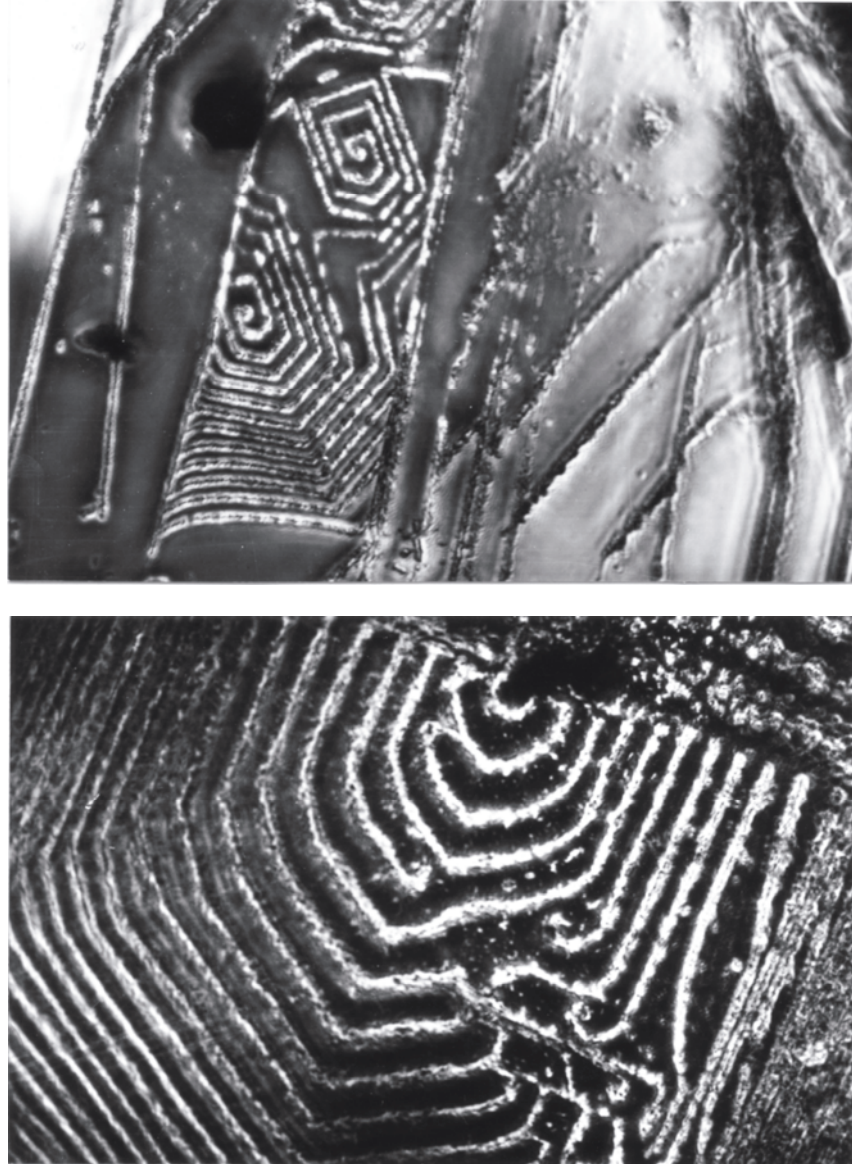


**Figure 31.** The five-fold growth spiral on the surface of the Mutsuré-jima phlogopite-1M, as revealed by multiple-beam interferometry (courtesy of I. Sunagawa) [from Sunagawa (1964) Fig. 1,2 p. 1429].

twin orientation (Fig. 33). Multiple platy crystals may come in contact when they agglutinate on the surface of the same larger crystal. In this case, a composite twin is formed: the platy crystals are twinned on (001) with respect to the substrate, forming a rotation twin, but they reciprocally contact on one of the ( $hk0$ ) [orthohexagonal indexing] planes, thereby forming a reflection twin (Nespolo and Kuwahara 2001).

### Two-dimensional XRD study

The most common two-dimensional technique employs a precession camera, but any technique giving two-dimensional undistorted images of the reciprocal lattice is suitable as well. From these undistorted images, the geometry of the diffraction pattern can be analyzed by simple visual inspection. In the case of a precession camera study, the crystal must be mounted so as to have the (001) plane perpendicular to the goniometer rotation axis. In fact, the stacking of layers in micas is along  $c$  and the periodicity in reciprocal

space appears along  $c^*$ , thus it is necessary to have  $c^*$  in all the images, i.e. to have  $c^*$  aligned with the dial axis. A different mounting would show only one plane containing  $c^*$ , which is insufficient for a twin/polytype analysis. The latter orientation shows diffraction from the (001) plane, with an almost hexagonal geometry. This plane is useless for twin/polytype identification, but is the richest in information for plesiotwins, because the Coincidence-Site Lattice (CSL) produced by the plesiotwin operations is parallel to (001). When the presence of a plesiotwin is suspected in a mica sample, the diffraction from (001) is necessary: it can be easily obtained by mounting the mica crystal so as to have the direction of elongation parallel to the glass fiber.

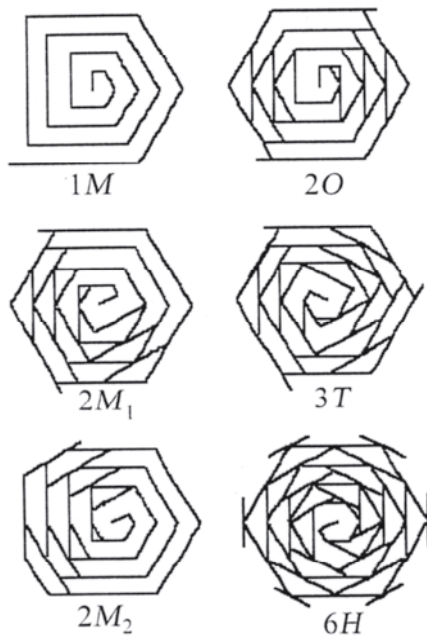


**Figure 32.** Schematic drawing of the interlaced pattern of the six homogeneous polytypes, resulting from the  $n \times 60^\circ$  rotations of the five-fold growth spirals (modified after Endo 1968).

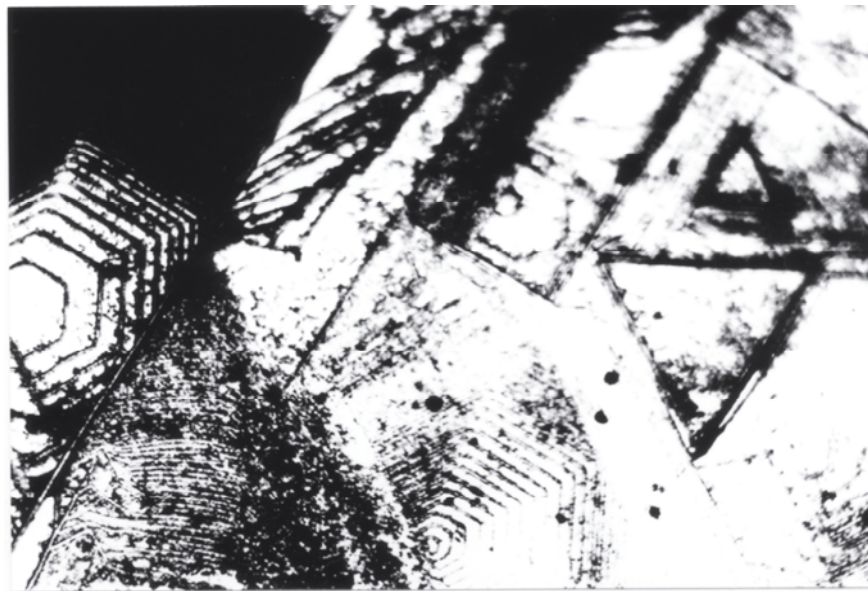


**Figure 33.** Tiny platy crystals agglutinated onto the (001) surface of a larger crystal. The tiny crystals are twinned on (001) with respect to the larger one, but on  $(hk0)$  with respect to each other. Notice the five-fold morphology (courtesy I. Sunagawa).



The radiation to be employed initially can be either a short wavelength (e.g., Mo) or a longer wavelength (e.g., Cu or Fe). Mo is preferable for making easier the orientation of the crystal, but its wavelength is too short for the study of long-period polytypes, or even for twins of polytypes with period longer than three layers, resulting in an insufficient resolution between two successive reflections. Cu or Fe radiation is suitable for longer period polytypes ( $\leq 10$ -12 layers). The separation of the reflections can be improved by increasing the crystal-to-film distance, with slightly longer exposure times. This avoids the weakening of the reflections occurring when employing a longer wavelength. The choice of the radiation to employ initially is thus the result of a compromise between the ease of orienting the crystal (Mo) and the need of proper resolution. With some practice the orientation of a mica crystal on the precession camera becomes routine even with Cu radiation, which can thus be selected as the best compromise. For longer period polytypes, Fe or Cr radiation becomes necessary to obtain sufficient resolution, once the crystal is oriented.

For investigating the possibility of apparent polytypism, one SD plane and three SX central planes must be recorded. From these planes, the geometry of the diffraction pattern is analyzed on the basis of the criteria given in Tables 12a-12c. If the crystal is twinned or allotwinned, the nine translationally independent rows forming a minimal rhombus, obtained from these four planes, allow the determination of the relative rotations between the individuals (see the example of  $Z_T = {}^3_4 1M-2M_1$  allotwin below). If the crystal is not twinned, the stacking sequence in the homo-octahedral approximation can be obtained from the geometry of the diffraction pattern (MDO polytypes) or from the PID obtained along one or more X rows (non-MDO polytypes). This is the final stacking sequence if the polytype is composed of only M1 layers, otherwise it represents the homomorphic equivalent of the correct stacking sequence. In the meso-octahedral family, if the meso-octahedral character is pronounced (large difference between the average cations), the real stacking sequence can in principle be found by comparing the experimental intensities with the intensities computed for all the meso-octahedral polytypes homomorphic to the homo-octahedral polytype obtained by the PID analysis. When the meso-octahedral character is not pronounced, the distinction is much more difficult. Moreover, as discussed in "Derivation of PID from the diffraction pattern", when the sequence of displacement vectors contains one or more sub-periods, weak reflections occur along the X rows, and care must be taken to observe them. In both the meso- and the hetero-octahedral family, the true stacking sequence can be obtained only from a complete structure refinement, because the occupancies of the octahedral sites, and the sizes of the corresponding octahedra, must be refined. Unfortunately, the quality of the sample is often not sufficient to allow a complete data collection, and only the stacking sequence of the homomorphic polytype (PID stacking sequence) can be obtained.

### **Diffraction study**

Once the stacking sequence in the homo-octahedral approximation is determined, if the quality of the crystal permits, the final stage consists of intensity measurements (usually by diffractometric measurement) and a structure refinement. The radiation to be employed is the same used in the preliminary (two-dimensional) study. The strongly anisotropic shape of mica crystals indicates applying an absorption correction through a  $\psi$ -scan procedure, rather than an analytical correction. Knowing the structure of the single layer and the homo-octahedral stacking sequence, the starting model is already very close to the final result, but the presence of one or more M2 layers must be determined. In other words, the meso- and hetero-octahedral stacking sequences, and not only the homomorphic sequence revealed by the PID, should be employed also as starting models, otherwise the presence of M2 layers may be overlooked. For instance, consider a hypothetical  $N$ -layer meso-octahedral polytype with biotitic composition, and suppose,

for simplicity, that there are two Mg and one  $\text{Fe}^{2+}$  ions in the *O* sheet. Suppose also that *n* layers are of M2 type, and the remaining *N* - *n* layers are of M1 type. The occupation of the cation sites in the *O* sheet is described as: M1 layers:  $M1 = (1 - x)\text{Fe} + x\text{Mg}$ ; M2, M3:  $0.5x\text{Fe} + (1 - 0.5x)\text{Mg}$ ; M2 layers:  $M2 = (1 - x)\text{Fe} + x\text{Mg}$ ; M1, M3:  $0.5x\text{Fe} + (1 - 0.5x)\text{Mg}$ . If the value of *x* is far from 2/3, the presence of the M2 layers should, in principle, be revealed even by a structure refinement employing only the homomorphic sequence as starting model. However, with the approach of *x* to 2/3 (where the difference between M1 and M2 disappears), the distinction between *N* layers of type M1 and (*N*-*n*) layers of type M1 plus *n* layers of type M2 becomes difficult. The presence of an M2 layer may be erroneously interpreted for disorder in the cation distribution. The site occupancies in the *O* sheet should be carefully checked; otherwise important information about the nature of the polytype under investigation can be easily overlooked (see also Nespolo 2001).

## APPLICATIONS AND EXAMPLES

### 24 layer Subfamily A Series 1 Class b biotite from Ambulawa, Ceylon

This polytype was found by Hendricks and Jefferson (1939) and is a typical example of how easily an incorrect stacking sequence may be accepted if the presence or absence of twinning is not properly evaluated. In most cases, the possibility of *apparent polytypism* may lead one to assume a longer stacking sequence, simulated by the twinning of a shorter polytype. In the present case, instead, a case *real polytypism* was incorrectly interpreted as apparent polytypism.

Hendricks and Jefferson (1939) were the first to accomplish a systematic X-ray study of a large number (more than 100) of mica crystals, and the first to report the existence of non-MDO polytypes. At those times, the effect of twinning on the diffraction pattern was not understood yet and the authors implicitly assumed that the number of reflections in the  $c^*_1$  repeat invariably corresponds to the number of layers in the polytype. They reported 1,2,3,6 and 24-layer polytypes, but later Smith and Yoder (1956) showed that the 3 and 6-layer polytypes were twins of 1 and 2-layer polytypes respectively. Smith and Yoder also re-analyzed the Weissenberg photographs of the 24-layer polytype, concluding that it could be indexed on an 8-layer unit cell; the  $3n$ -th,  $(3n+1)$ -th and  $(3n+2)$ -th reflections should thus come each from a different individual. Takeda (1969), adopting Smith and Yoder's twin interpretation, performed a PID analysis based on the intensities of each third reflection. He derived a semi-quantitative intensity distribution from the sequence of *w* (*weak*), *m* (*medium*), or *s* (*strong*) given by Hendricks and Jefferson (1939). The best match with the PID values computed from the stacking sequences of all possible 8-layer polytypes corresponded to  $8A_2$  polytype (for details about this polytype see below). Nespolo and Takeda (1999) re-analyzed the geometry of the diffraction pattern, as described in Hendricks and Jefferson's paper, on the basis of the twin identification criteria given in Nespolo (1999) (see Table 12b) and showed that the pattern cannot correspond to a twin of an 8-layer polytype. They found:

- 1) the cell dimension given by Hendricks and Jefferson are:  $a = 5.3\text{\AA}$ ,  $b = 9.2\text{\AA}$ ,  $c = n \times 10\text{\AA}$ ,  $\gamma = 90^\circ$ ,  $\beta = 90^\circ$ ; it was thus a *Class b* polytype;
- 2) reflections  $hkl$  with  $k = 0(\text{mod } 3)$  were the same as the single-layer structure: it was thus a subfamily A polytype;
- 3) the heavy trace of continuous scattering from 060 on an over-exposed photograph did not pass through any 02*l* reflection but, rather it occurred at a distance of about one-third the periodicity from the closest reflection; the 0*kl* *r.p.* was thus not orthogonal and the diffraction pattern is typical of a *Class b* polytype.

An 8-layer subfamily A polytype cannot belong to *Class b*; a twin of an orthogonal or *Class a* polytype cannot produce a diffraction pattern typical of *Class b* polytype. Therefore, the diffraction pattern reported by Hendricks and Jefferson was actually from a 24-layer polytype (*Series 1*), whose stacking sequence has not been resolved, and not a twin of the  $8A_2$  polytype. On the basis of Takeda's (1969) analysis of a subset of reflections, it can be inferred that Hendricks and Jefferson's 24-layer polytype probably possesses a stacking sequence related to that of  $8A_2$ , belonging thus to the  $2M_1$  structural series also.

This example shows the danger of blindly applying a powerful method such as the PID. The direct determination of the polytype stacking sequence is easily obtained through comparison of the PID from the diffraction pattern with the PID computed for all the theoretical candidates, i.e. the polytypes with the same number of layers and the same OD character (subfamily A, subfamily B, or mixed-rotation). The correct stacking sequence corresponds to the best match between the experimental and the theoretical PID. If the presence of twinning is overlooked the experimental PID corresponds to the weighted mean of the PID from each individual, where the weight is the volume of the individuals. In contrast, as in the case of the 24-layer polytype shown here, if twinning is incorrectly assumed, the experimental PID is only a portion of the "true" PID. For a short-period polytype, with a limited number of candidates, the match with the computed PID is probably insufficient, and this should alert the investigator. However, for a longer period polytype a reasonable match may occur by chance, because the difference between the two closest PID decreases with the increase of the number of layers. Because the PID match is evaluated on a relative basis, taking the best match as the correct one, the possibility of a wrong interpretation exists. The presence/absence of twinning must therefore be correctly analyzed before PID analysis is applied to the diffraction pattern.

#### **$8A_2$ (subfamily A *Series 0 Class a*) oxybiotite from Ruiz Peak, New Mexico**

This polytype was identified by Nespolo and Takeda (1999) in the oxybiotite from Ruiz Peak (New Mexico). Figure 34 is the diffraction pattern corresponding to the  $h0l$  (SD) *r.p.*, with the geometry typical of a subfamily A polytype. Figure 35 shows the diffraction pattern corresponding to the  $hhl$  (SX) *r.p.*, which is non-orthogonal and with eight reflections in the  $c^*_1$  repeat along X rows. The diffraction pattern is that of the subfamily A *Series 0 Class a* polytype and thus excludes the possibility of twinning: the crystal is an 8-layer polytype. Out of 9212 possible 8-layer homo-octahedral polytypes, only 94 belong to subfamily A (Ross et al 1966). Comparison of theoretically computed and experimentally recorded PID values was performed only for the 94 subfamily A homo-octahedral polytypes.

In Table 19, the  $l$  indices in the three axial settings ( $C_1$ ,  ${}^a\mathbf{S}$  and  ${}^a\mathbf{F}$ ) and the  $\hat{l} = l \pmod{8}$  index are given, together with the corresponding observed structure factors corrected for the Lorentz and polarization effects, the Fourier transform of the single layer, the ratio of the latter two terms, and the scaled PID [Eqn. (B.4)]. The PID was not computed in the two periods in which the single-layer Fourier transform undergoes a sign change. The PID along the remaining five periods has been assigned weights (Table 20). The stacking sequences of all possible 8-layer homo-octahedral subfamily A polytypes were generated by the PTGR program (Takeda 1971). The PID of each polytype was computed by the PTST98 program (Nespolo et al. 1999d) and the closeness to the observed pattern was evaluated by means of an  $R_{PID}$  index defined by analogy with the reliability index used structure refinements, namely:

$$R_{PID} = \frac{\sum_{j=1}^N |S_j^N(hkl)_o - S_j^N(hkl)_c|}{S_j^N(hkl)_o} \quad (26)$$



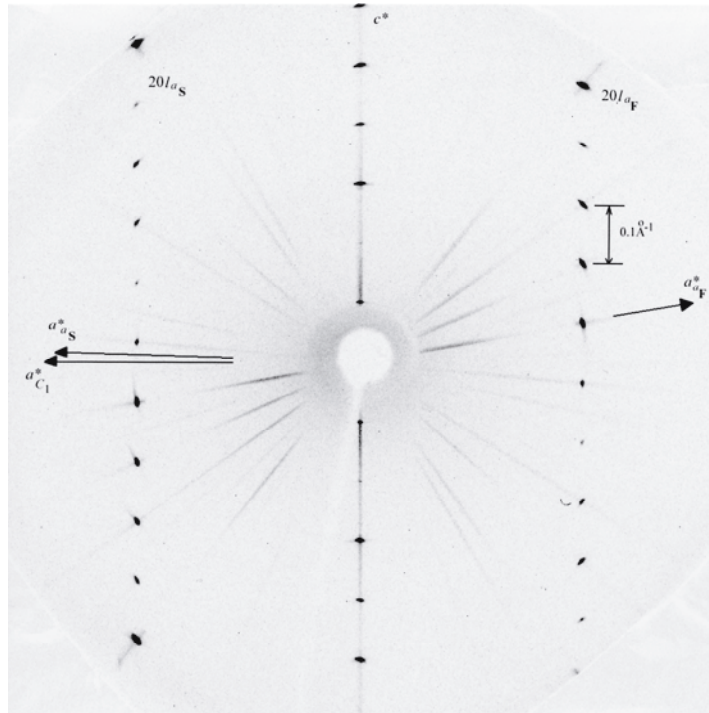


**Figure 34.** Precession diffraction pattern corresponding to the  $h0l$  SD  $r.p.$  of  $8A_2$  polytype ( $Cu K\alpha$ ). The  $a^*$  axes of the three settings,  $C_1$ ,  $^aS$  and  $^aF$ , are shown [used by permission of the editor of *Mineralogical Journal*, from Nespolo and Takeda (1999) Fig. 2, p. 108].

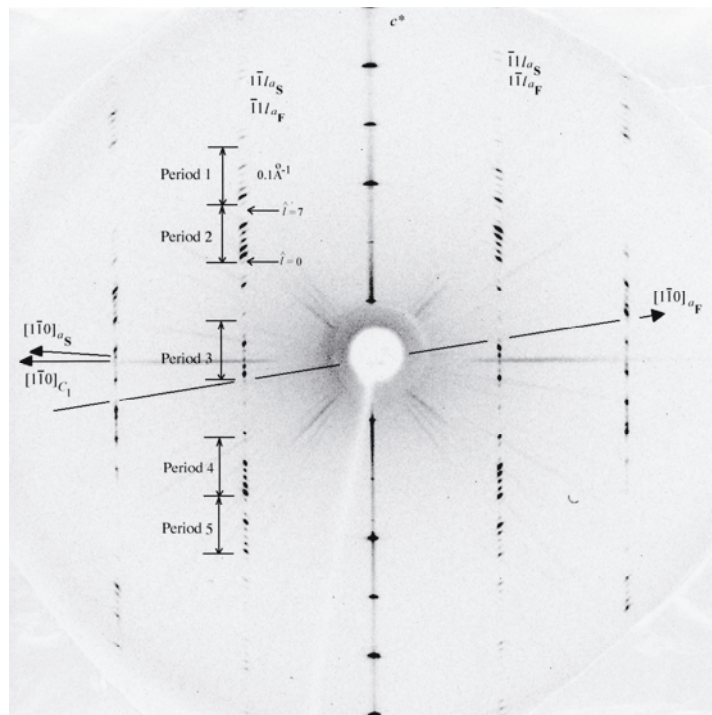


**Figure 35.** Precession diffraction corresponding to the  $\bar{h}hl$  SX  $r.p.$  of  $8A_2$  polytype ( $Cu K\alpha$ ). The  $[\bar{1}\bar{1}0]^*$  directions of the three settings  $C_1$ ,  $^aS$  and  $^aF$  are shown. In  $^aF$  setting the origin of PID is by definition in correspondence of  $l = 0(\text{mod } N)$ . PID has been obtained from the intensities measured along the five periods indicated in the figure [used by permission of the editor of *Mineralogical Journal*, from Nespolo and Takeda (1999) Fig. 3, p. 109].

**Table 19.** Derivation of PID from measured intensities of  $8A_2$  polytype. Observed structure factors ( $F_o$ ) have been obtained from the intensities measured in five periods along the  $11l$  reciprocal lattice row of  ${}^aF$  setting ( $1\bar{1}l$  of  ${}^aS$  setting.). SLFT stands for Single Layer Fourier Transform (after Nespolo and Takeda 1999).

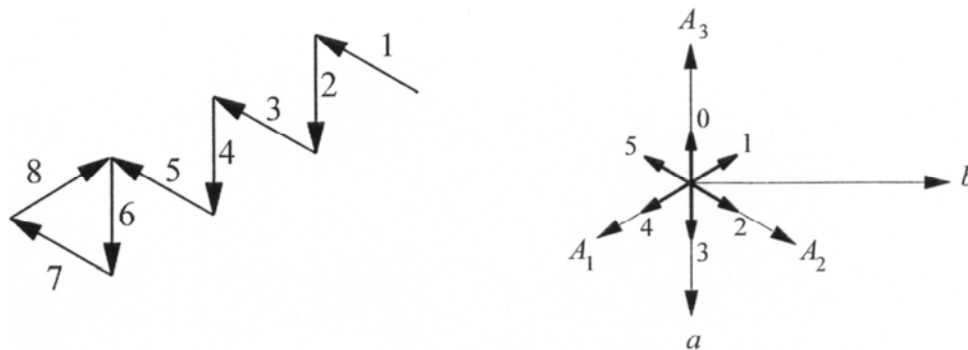
Period	$I(C_1)$	$I({}^aS)$	$I({}^aF)$	$\hat{l}$	$F_o$	SLFT	$F_o/SLFT$	PID
1	85	28	31	7	.25	12.99	.02	.02
	82	27	30	6	.25	16.77	.01	.02
	79	26	29	5	83.33	20.65	4.04	4.44
	76	25	28	4	38.63	24.53	1.574	1.73
	73	24	27	3	47.01	28.28	1.66	1.83
	70	23	26	2	83.00	31.77	2.61	2.87
	67	22	25	1	168.75	34.86	4.84	5.32
	64	21	24	0	40.70	37.43	1.09	1.20
2	61	20	23	7	.22	39.34	.00	.00
	58	19	22	6	30.06	40.51	.74	.57
	55	18	21	5	183.05	40.85	4.48	3.47
	52	17	20	4	76.75	40.31	1.90	1.47
	49	16	19	3	91.39	38.88	2.35	1.82
	46	15	18	2	169.81	36.57	4.64	3.59
	43	14	17	1	246.62	33.46	7.37	5.70
	40	13	16	0	32.92	29.65	1.11	.86
3	13	4	7	7	24.77	12.46	1.99	1.46
	10	3	6	6	33.28	15.41	2.16	1.58
	7	2	5	5	111.86	17.64	6.33	4.65
	4	1	4	4	23.28	19.11	1.21	.89
	1	0	3	3	41.45	19.78	2.10	1.54
	-2	-1	2	2	60.84	19.64	3.10	2.27
	-5	-2	1	1	134.28	18.71	7.18	5.26
	-8	-3	0	0	30.39	16.98	1.79	1.31
4	-35	-12	-9	7	18.80	22.08	.85	.62
	-38	-13	-10	6	20.98	26.78	.78	.57
	-41	-14	-11	5	172.90	30.99	5.58	4.07
	-44	-15	-12	4	89.73	34.58	2.59	1.89
	-47	-16	-13	3	99.68	37.43	2.66	1.94
	-50	-17	-14	2	188.67	39.46	4.78	3.49
	-53	-18	-15	1	288.53	40.59	7.10	5.19
	-56	-19	-16	0	28.74	40.83	.70	.51
5	-59	-20	-17	7	.22	40.21	.00	.01
	-62	-21	-18	6	52.30	38.78	1.34	1.26
	-65	-22	-19	5	172.66	36.64	4.71	4.42
	-68	-23	-20	4	57.59	33.88	1.70	1.59
	-71	-24	-21	3	51.37	30.65	1.68	1.57
	-74	-25	-22	2	86.01	27.06	3.18	2.98
	-77	-26	-23	1	129.75	23.25	5.58	5.23
	-80	-27	-24	0	26.51	19.35	1.37	1.28

**Table 20.** Comparison of measured and computed PID of  $8A_2$  polytype (after Nespolo and Takeda 1999).

$\hat{l}$	Period 1	Period 2	Period 3	Period 4	Period 5	Mean	Calculated
7	.02	.00	1.46	.62	.01	.30	.23
6	.02	.57	1.58	.57	1.26	.89	.90
5	4.44	3.47	4.65	4.07	4.42	3.98	4.07
4	1.73	1.47	.89	1.89	1.59	1.52	1.73
3	1.83	1.82	1.54	1.94	1.57	1.74	1.78
2	2.87	3.59	2.27	3.49	2.98	2.98	3.35
1	5.32	5.70	5.26	5.19	5.23	5.13	5.31
0	1.20	.86	1.31	.51	1.28	1.04	1.00

**Table 21.** OD symbols ( $v_{2j-2,2j-1}$ ) and Z symbols ( $Z_{2j} = Z_{2j-1}$ ) in the homo-octahedral approximation, RTW symbols ( $A_j$ ) and TS symbols [ $L_j(X_j, Y_j)$ ] describing the stacking sequence of  $8A_2$  polytype (after Nespolo and Takeda 1999).

$j$	$v_{2j-2,2j-1}$	$Z_{2j-1}$	$A_j$	$L_j(X_j, Y_j)$
1	5	4	2	D(0,-1)
2	3	6	-2	D(0,-1)
3	5	4	2	D(0,1)
4	3	6	-2	D(0,1)
5	5	4	2	D(0,0)
6	3	6	-2	D(0,0)
7	5	4	-2	D(0,-1)
8	1	2	2	D(0,0)

**Figure 36.** The  $v_{2j,2j+1}$  displacement vectors of the  $8A_2$  polytype in the homo-octahedral approximation, as revealed by PID analysis of the diffraction pattern in Figure 35 (modified after Nespolo and Takeda 1999).

The best match corresponded to  $R_{PID} = 0.04$  (computed PID values for this sequence are in Table 20); the second best match to  $R_{PID} = 0.33$ . This clearly shows that the homo-octahedral stacking sequence has been uniquely identified. By employing the cell dimensions of the refined  $1M$  polytype from the same sample (Ohta et al. 1982), the approximate cell parameters of this polytype was calculated through the axial transformations given in Equation (3) and the results are:  $a = 5.3\text{Å}$ ,  $b = 9.2\text{Å}$ ,  $c = 79.6\text{Å}$ ,  $\alpha = 90^\circ$ ,  $\beta = 91.3^\circ$ ,  $\gamma = 90^\circ$ . The symbols for the homo-octahedral stacking sequence are given in Table 21, and the corresponding vector sequence is in Figure 36. The space-group type is  $C\bar{1}$ , derived by applying the transformation rules given in Table 6.

### **$1M$ - $2M_1$ oxybiotite allotwin $Z_T = {}^3_4$ from Ruiz Peak, New Mexico**

This allotwin was also identified in the Ruiz-Peak oxybiotite and represents an example of apparent polytypism.

Figures 37-40 present the diffraction patterns from three SX planes. The shortest separation between successive reflections along  $c^*$  of X rows is  $c^*/6$ : the apparent period is six layers and thus the  $l$  index of all the reflections are expressed as (mod 6). Figure 40 shows the diffraction pattern from an SD plane of the same sample which, with one reflection for  $c^*_1$  repeat, has the typical appearance of a subfamily A polytype. The presence of twinning is not evident from this plane.

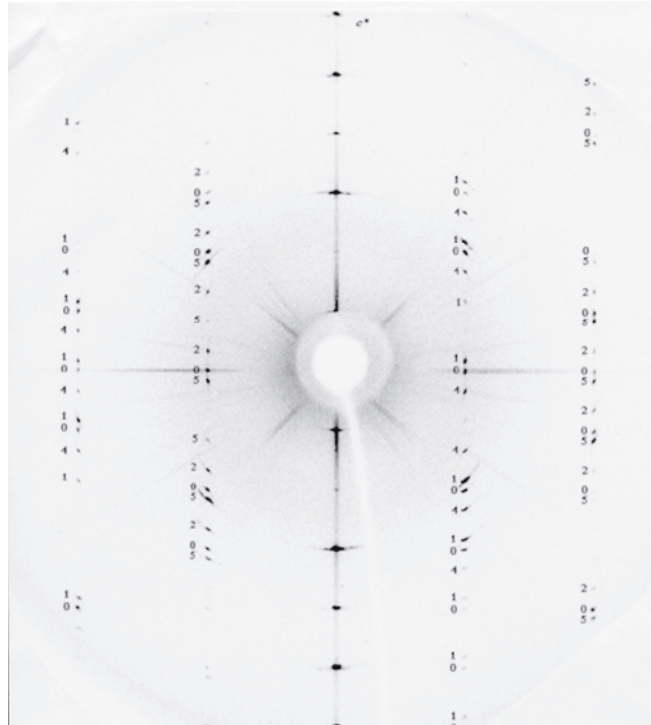
In principle, the investigated sample may be either a six-layer polytype, or a twin or allotwin involving the  $2M_1$  polytype. However, two of the SX planes (Fig. 37 and 38) are orthogonal (i.e. reflections are present at  $l = 0$  of the orthogonal six-layer cell, along each row parallel to  $c^*$ ). This geometry of the reciprocal lattice is impossible for a 6-layer subfamily A polytype, which would belong to *Class b* and should therefore have all the SX planes non-orthogonal (Table 12b). It follows that the sample is a twin or allotwin of the  $2M_1$  polytype.

Figure 41 shows the star polygon, comprised by the six possible orientations of the tessellation rhombus and the minimal rhombus, drawn by reporting the  $l \pmod{6}$  indices of the reflections occurring in the four planes above, and applying the  $(3p, 3q)$  translations between translationally equivalent reciprocal lattice rows. None of the six orientations of the minimal rhombus matches any of the nine independent minimal rhombi which are possible for the  $2M_1$  twins (Fig. 26). The sample is thus an allotwin. The pattern cannot involve a  $3T$  crystal, otherwise three reflections corresponding to  $l = 0 \pmod{6}$ ,  $l = 2 \pmod{6}$  and  $l = 4 \pmod{6}$  would be present along all X rows. The sample is thus a  $1M$ - $2M_1$  allotwin. The shaded minimal rhombus matches the computed minimal rhombus of the  $1M$ - $2M_1$  allotwin with relative rotation of  $60^\circ$  between the two individuals and it corresponds to  $Z_T = {}^3_4$  in Nespolo et al (2000a).

The cell of the allotwin lattice has a period of  $6c_0$  along  $c$  and contains six lattice planes of the  $1M$  polytype and three lattice planes of the  $2M_1$  polytype. Of these, only the plane with  $z = 0 \pmod{6}$  has all the nodes from both polytypes overlapped by the allotwin operation, whereas in all the other lattice planes the nodes from the two polytypes are separated. Consequently, the allotwin index of  $1M$  is 6, and that of  $2M_1$  is 3.

### **$\{3,6\}[7\{3,6\}]$ biotite plesiotwin from Sambagawa, Japan**

Sadanaga and Takéuchi (1961) performed a systematic study of micas of volcanic origin, and reported several examples of  $1M$  twinning, and also one example of  $2M_1$  twinning. Takéuchi et al (1972) foresaw that micas from a different environment, namely metamorphic, could reveal different kinds of “twinning” and investigated by electron diffraction a large number of small biotite crystals from the Sambagawa metamorphic belt in the Besshi area, Japan. They found several twins of the same type reported by



**Figure 37.** Precession diffraction pattern from the first SX plane (SX1) of the allotwin  $Z_T = \frac{5}{4}$ . The  $l$  index of the reflections is expressed (mod 6) [used by permission of the editor of *Acta Crystallographica B*, from Nespolo et al. (2000b) Fig. 7, p. 644].

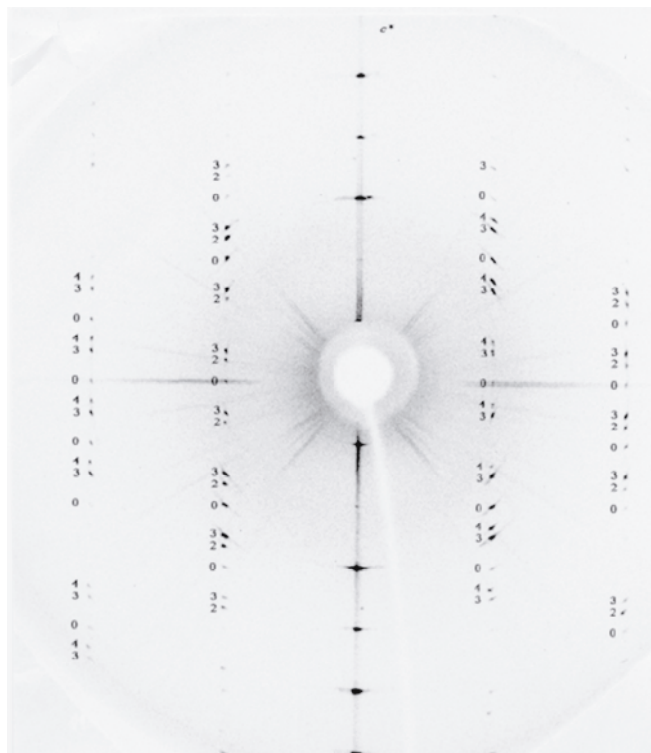


**Figure 38.** Precession diffraction pattern from the second SX plane (SX2) of the allotwin  $Z_T = \frac{3}{4}$  ( $60^\circ$  from SX1).  $l$  index as in Figure 37 [used by permission of the editor of *Acta Crystallographica B*, from Nespolo et al. (2000b) Fig. 8, p. 644].

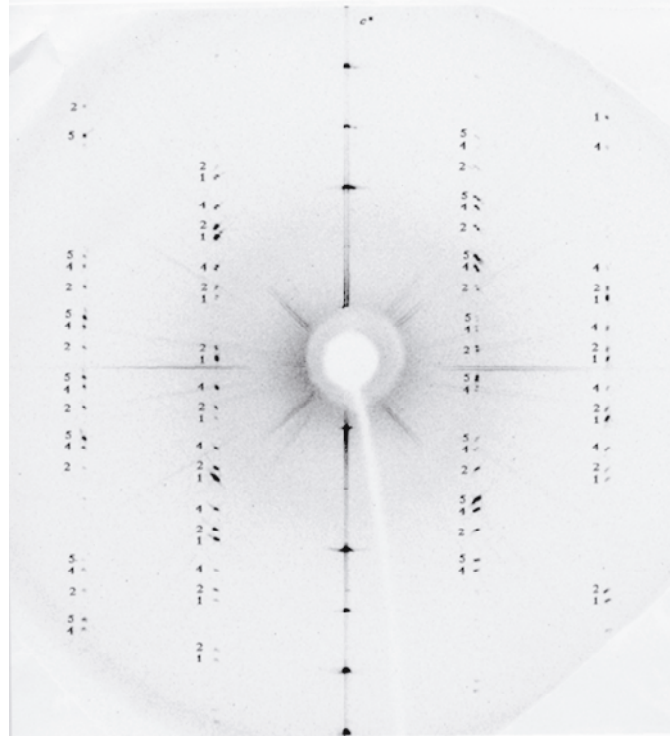


**Figure 39.** Precession diffraction pattern from the third SX plane (SX3) of the allotwin  $Z_T = {}^3_4$  ( $120^\circ$  from SX1).  $l$  index as in Figure 37 [used by permission of the editor of *Acta Crystallographica B*, from Nespolo et al. (2000b) Fig. 9, p. 645].

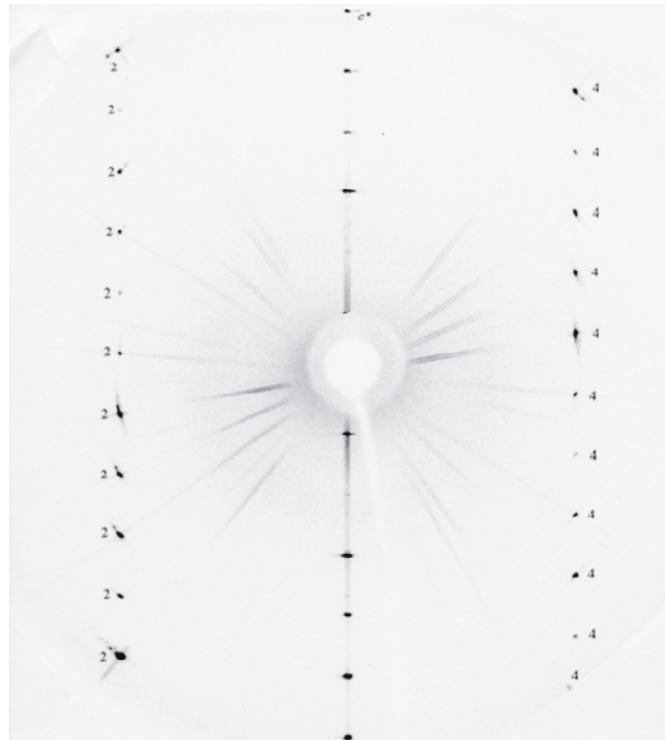


**Figure 40.** Precession diffraction pattern from an SD plane of the allotwin  $Z_T = {}^3_4$  ( $30^\circ$  from SX3).  $l$  index as in Figure 37 [used by permission of the editor of *Acta Crystallographica B*, from Nespolo et al. (2000b) Fig. 10, p. 645].



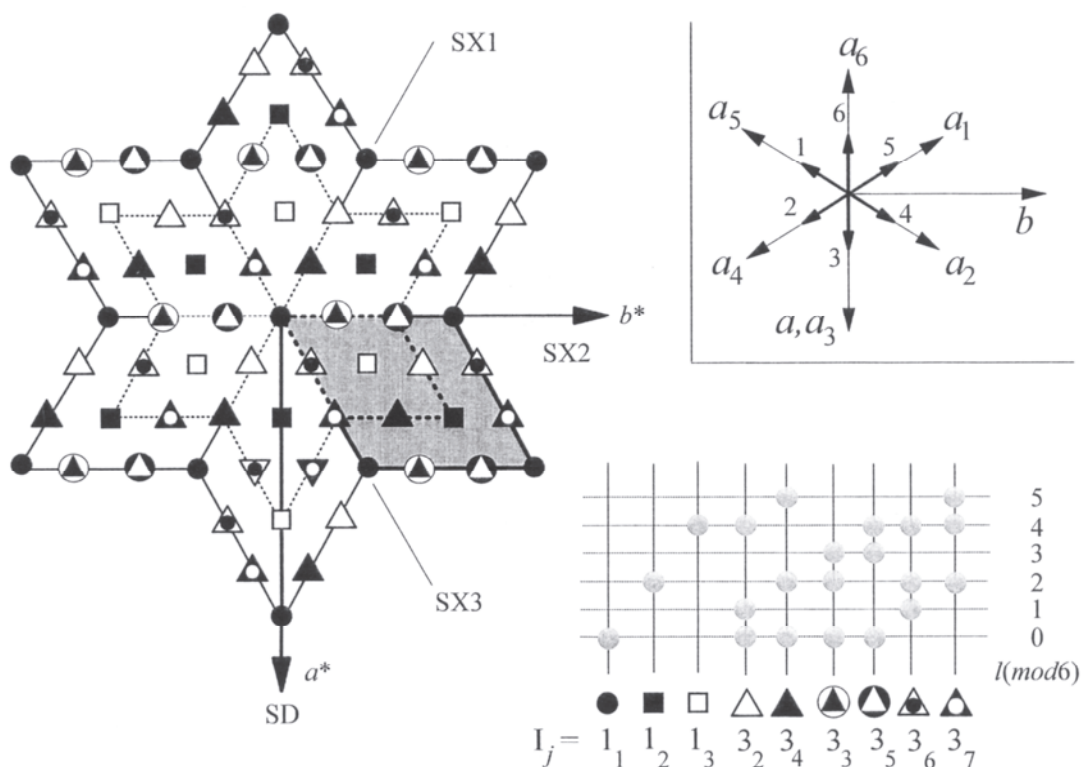


**Figure 41.** Construction of the star polygon corresponding to the diffraction patterns in Figs. 37-40. The SD plane in Figure 40 is taken coincident with the  $(a^*c^*)$  plane, and the three SX planes are reported counter clockwise according to the rotations indicated in Figures 37-40. The star polygon is then obtained by  $(3p, 3q)$  translations of the nine translationally independent rows in those four planes. The minimal rhombus and the tessellation rhombus are indicated in their six possible orientations. The shaded minimal rhombus corresponds to the  $Z_T = {}^3_4$  minimal rhombus tabulated in Nespolo et al. (2000a). Inset on the top-right: axes  $(a, b)$  of the space-fixed reference and of the individual-fixed references in the six possible orientations ( $a_1 - a_6$ ), and corresponding  $Z_T$  symbols ( $b_1 - b_6$  axes are not shown). Inset in the bottom-right:  $l \pmod{6}$  indices of the reflections which are present on the composite rows of the lattice, and symbol of the rows.  $I_j$  is the symbol identifying the composite row, where  $I$  gives the number of reflections in the  $c^*_1$  repeat and  $j$  is a sequence number [used by permission of the editor of Acta Crystallographica B, from Nespolo et al. (2000b) Fig. 11, p. 646].

Sadanaga and Takéuchi (1961), but they also found some flakes which gave a more complex diffraction pattern, and correspond to “plesiotwins” in the later definition introduced by Nespolo et al (1999b). One of these diffraction patterns is shown in Figure 42, where two (001) lattices rotated about the normal and with only one common node out of seven recognized. The angle between two corresponding reflections in the two rotated lattices is  $21.8^\circ$ , very close to the  $21^\circ 47'$  computed for the  $n = 7$  plesiotwin. The slight difference is probably related to the deviation of the (001) plane from hexagonality.

This kind of diffraction pattern is commonly obtained when flakes of layered crystals are suspended in water and dried in air (Sueno et al. 1971; Takéuchi et al. 1972). This process allows the flakes to settle over each other without alignment; the need for reducing the interface energy is not strong, because the flake-to-flake interaction is purely physical and there are no chemical bonds between them. In contrast, plesiotwins are formed by chemical interaction of crystals that have already reached a significant size, or by exsolution. The metamorphic environment, where crystals are less free of moving,

favors the formation of plesiotwins. Plesiotwins, are less probable in a magmatic environment. In the presence of a fluid phase, crystals are more free to move and can overcome the kinetic barrier towards the more stable configuration of twins.

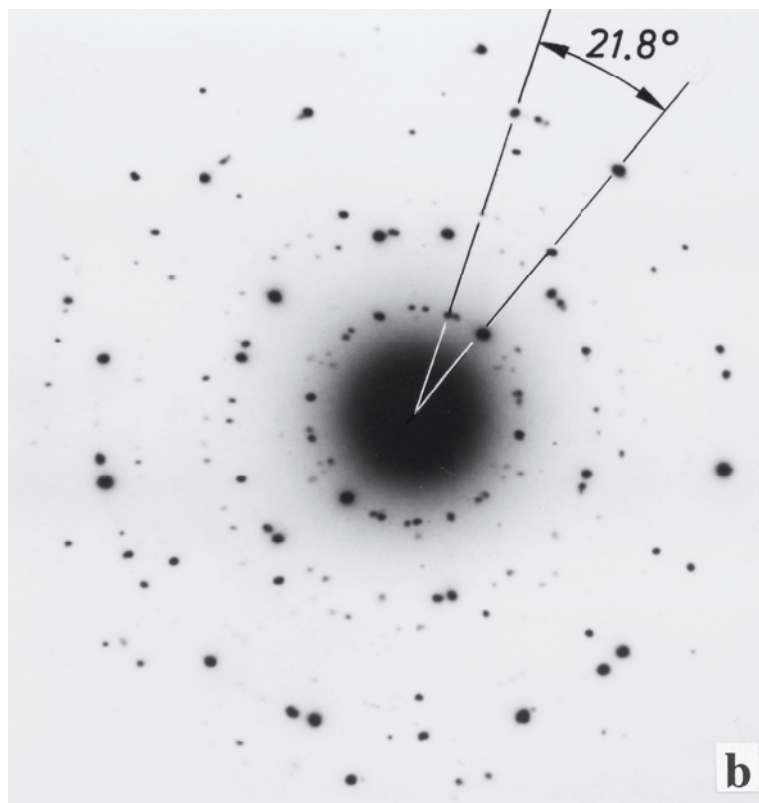
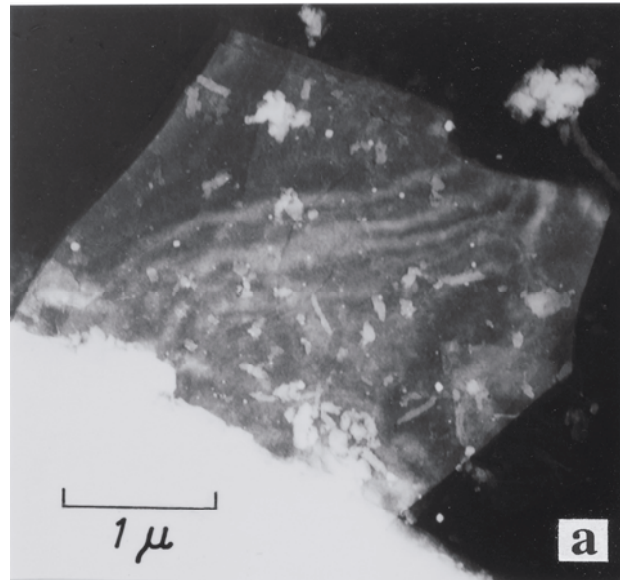


**Figure 42.** Composite diffraction pattern (right) produced by a single flake (left) of metamorphic biotite-1M from the Sambagawa belt (courtesy Y. Takéuchi). Several pseudo-hexagonal lattices are overlapped with different orientation; two of these are rotated by  $21.8^\circ$ , close to the  $21^\circ 47'$  angle corresponding to the  $\{3,6\}[7\{3,6\}]$  composite tessellation. The two crystals to which these lattice belong form a plesiotwin with  $\Sigma$  factor 7 and plesiotwin index 21 [used by permission of the editor of *Zeitschrift für Kristallographie*, from Takéuchi et al (1972) Fig. 6, p. 219].



## APPENDIX A. TWINNING: DEFINITION AND CLASSIFICATION

Twinning is the oriented association of two or more individuals<sup>10</sup> of the same crystalline compound, in which pairs of individuals are related by a geometrical operation termed *twin operation*. The twin operation is a symmetry operation that belongs to a crystallographic point group; it cannot belong to the symmetry of the crystal, otherwise it would produce a parallel growth instead of a twin. The lattice common to the twinned individuals is called *twin lattice*: it can either coincide (exactly or approximately) with the lattice of the individuals, or be a sublattice (exact or approximated) of them. A *Twin element* is a symmetry or pseudo-symmetry element for the twin lattice with respect to which the twin operation is defined. *Twin index* ( $n$ ) is the order of the subgroup of translation in direct space defining the twin lattice, and coincides with the ratio of the number of lattice nodes of the individual to the number of nodes restored, exactly or approximately, by the twin operation. *Twin obliquity* ( $\omega$ ) is the angle, in the crystal setting of the individual, 1) between a twin axis and the normal to the lattice plane which is quasi-normal to the twin axis (rotation twins), or 2) between the normal to a twin plane and the rational direction closest to it (rotation twins).. The point group of the twin has the common symmetry of the individuals, as modified by the twin operation and may be lower, the same or higher than the point group of the single crystal (Friedel 1904, 1926; Buerger 1954).

The French school (Bravais 1851; Mallard 1879; Friedel 1904, 1926) gave a classification of twinning based on the twin index and obliquity, introducing the four categories of *merohedry* ( $n = 1, \omega = 0$ ), *reticular merohedry* ( $n > 1, \omega = 0$ ), *pseudo-merohedry* ( $n = 1, \omega > 0$ ), *reticular pseudo-merohedry* ( $n > 1, \omega > 0$ ). Twinning by merohedry has been further subdivided on the basis of the point groups of the Bravais class of the lattice, of the Bravais class of the space group, of the individual and, for OD structures, of the family structure (Table A1). The kind of merohedry the French school considered is that in which the Bravais class of lattice and the Bravais class of the space group coincide, and it has now been renamed *syngonic merohedry*. The case in which the Bravais class of the lattice is accidentally higher than the Bravais class of the space group includes two kinds of twinning: one is again a syngonic merohedry (the twin operations belong to the point group of the Bravais class of the space group), and the other is termed *metric merohedry* (the twin operations belong to the point group of the Bravais class of the lattice but not to the point group of the Bravais class of the space group) (Nespolo and Ferraris 2000).

For each crystal family except the hexagonal, the “point group of the Bravais class of the space group” is tantamount to say “point group of the syngony”, because there is a 1:1 correspondence between crystal family, syngony and Bravais system, and for this reason the term “syngonic merohedry” was introduced. However, two syngonies (trigonal and hexagonal) and two lattices ( $hR$  and  $hP$ ) correspond to the hexagonal crystal family. A trigonal crystal with lattice  $hR$  twinned within the same crystal family ( $h$ ) may have two kinds of twinning: syngonic merohedry, with twin elements belonging to the  $hR$  lattice (only merohedral crystals) and reticular merohedry, with twin elements belonging to the  $hP$  sublattice of the  $hR$  lattice (twin index 3). Instead, a trigonal crystal with lattice  $hP$  twinned within the same crystal family ( $h$ ) has only one kind of twinning and the twin elements belong to the  $hP$  lattice. This twinning corresponds to a syngonic merohedry.

---

<sup>10</sup> The term “individual” is used to indicate one crystal of a twin, and the term “single crystal” to mean an untwinned crystal. Other authors (e.g., Hahn et al. 1999) use “component” instead of “individual”.

**Table A1.** Classification of twinning.  $p(TL)$  = point group of the Twin Lattice;  $p(BCL)$  = point group of the Bravais Class of the Lattice of the individual;  $p(BCSG)$  = point group of the Bravais Class of the Spae Group of the individual;  $p(La)$  = Laue point group of the individual;  $p(T)$  = Twin point group;  $p(FS)$  = point group of the Family Structure. The point group of the twins has the common symmetry of the individuals, as modified by the twin operation (see Appendix B). Modified after Nespolo et al. (1999a) and Nespolo and Ferraris (2000).

		$p(TL) = p(BCL)$		$p(TL) > p(BCL) \geq p(BCSG)$		
		$p(TL) = p(BCSG) \geq p(T) > p(La)$	$p(TL) \geq p(T) > p(BCSG) \geq p(La)$			
$\omega = 0, n = 1$		$\omega = 0, n = 1$	$\omega = 0, n = 1$	$\omega > 0, n = 1$	$\omega = 0, n > 1$	
Syngonic Merohedry  Class I	Syngonic Merohedry class IIA	TPG $\leq$ FSPG	TPG $>$ FSPG	Metric Merohedry class IIB		
		Syngonic Complete Merohedry	Syngonic Selective Merohedry			TPG $\leq$ FSPG
	Syngonic Merohedry class IIB	TPG $\leq$ FSPG	TPG $>$ FSPG	Metric Complete Merohedry	Metric Selective Merohedry	
		Syngonic Complete Merohedry	Syngonic Selective Merohedry			

Syngonic merohedry is subdivided, on the basis of the ratio between the order of the lattice point group and the order of the individual point group, into hemihedry (order 2), tetartohedry (order 4) and ogdohedry (order 8, possible only for the point group 3).

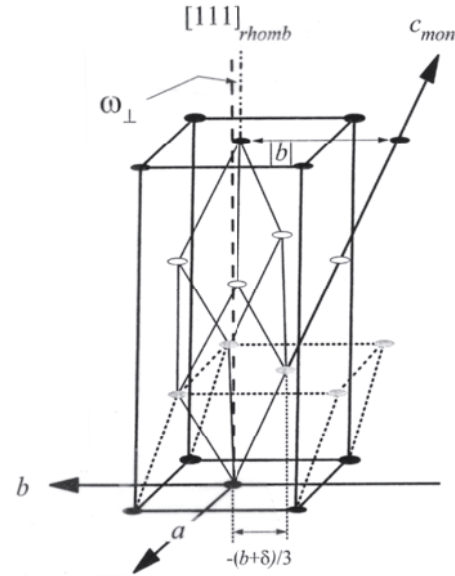
Where the Laue symmetry of the individual is the same as the twin symmetry, the corresponding twins belong to class I. The diffraction pattern does not differ from that of a single crystal, unless anomalous scattering is substantial. The inversion center can always be chosen as a twin operation and the set of intensities collected from a twin is indistinguishable from that collected from a single crystal. Instead, when the Laue symmetry of the crystal is lower than the twin symmetry, the twins belong to class II and are then subdivided into class IIA (syngonic merohedry) and class IIB (metric merohedry). The twin operations relate non-equivalent reflections, and the presence of twinning may hinder a correct derivation of the symmetry from the diffraction pattern. In particular, when the number of individuals coincides with the order of the twin operation and the volumes of the individuals are identical, the symmetry of the diffraction pattern is higher than the Laue symmetry of the individual. An incorrectly chosen space-group type may thus be assumed in the initial stage of the structure refinement (Catti and Ferraris 1976; Nespolo and Ferraris 2000).

In the case of OD structures, class II twins are further subdivided. The family structure may correspond to a Bravais system different from both the crystal lattice and the twin lattice. When the point group of the family structure is a subgroup of the point group of the twin lattice and twinning is by class II merohedry (both IIA and IIB), one or more of the twin laws do not belong to the point group of the family structure. This kind of twin law corresponds to merohedry for the polytype but to reticular merohedry for the family structure. These twin operations produce incomplete overlap of the family reciprocal sublattice; in particular, in terms of the polytype lattice, they overlap some of the nodes with zero weight of an individual to nodes with non-zero weight of another individual, and vice versa. Therefore, peculiar violations of the non-space-group absences along family rows appear in the diffraction pattern, where indexed in terms of the actual structure. This modifies the diffraction pattern, whose geometry no longer corresponds to that of the single crystal. This kind of merohedry, which restores only a part of the family sublattice of OD structures, is termed *selective merohedry*, whereas twinning by merohedry of OD structures in which the twin operation belongs to the point group of the family structure and restores the whole family reciprocal sublattice is termed *complete merohedry* (Nespolo et al. 1999a).

In the case of layer compounds, it is useful to decompose the obliquity into two components, within and outside the plane of the layer, which for micas is (001). Labeling  $t_{(hkl)}$  the “trace” of a plane  $(hkl)$  on the (001) plane, the component of the obliquity within the (001) plane ( $\omega_{\parallel}$ ) corresponds to the angle between the normal  ${}^n t_{(hkl)}$  to  $t_{(hkl)}$  and the direction  $[hk0]$  quasi normal to  $t_{(hkl)}$ , i.e.  $\omega_{\parallel}([hk0] \wedge {}^n t_{(hkl)})$  (Fig. 20). The component normal to the (001) plane ( $\omega_{\perp}$ ) corresponds to the angle between the normal to the (001) plane and the lattice row quasi-normal to (001).  $\omega_{\perp}$  measures the deviation of the  $c$  axis of the triple and sextuple cells of non-orthogonal polytypes from the normal to (001); for *Class b* polytypes it measures also the deviation of the rhombohedral  $[111]$  direction, i.e.  $\omega_{\perp}([111]_R \wedge [001]^*)$  (Fig. B1).  $\omega_{\parallel}$  measures the deviation from hexagonality of the (001) plane and is thus related to  $\varepsilon$ . In both the Pauling and the Trigonal models, non-orthogonal polytypes are metrically monoclinic, because  $\gamma = 90^\circ$ ,  $\omega_{\parallel}([100] \wedge {}^n t_{(100)}) = 0$  and  $\omega_{\parallel}([010] \wedge {}^n t_{(010)}) = 0$ , but  $\omega_{\parallel}$  is non-zero for the other four directions that would be equivalent in a hexagonal lattice. Imposing  $\omega_{\parallel} = 0$  for each of these four directions, the two-dimensional lattice in the (001) plane becomes  $hp$ , but the three-dimensional lattice

is only pseudo- $hP$ , because the  $c$  axis of the triple cell is not exactly perpendicular to (001). Imposing instead  $\omega_{\perp} = 0$ , an  $oC$  lattice is obtained. Finally, imposing both  $\omega_{\parallel} = 0$  and  $\omega_{\perp} = 0$ , the lattice becomes  $hP$ , and for *Class b* polytypes the lattice is centered.

**Figure A1.** Perspective view of the lattice of *Class b* mica polytypes. The monoclinic conventional cell (doubly primitive, thick dotted lines), the pseudo-rhombohedral cell (primitive, solid thin lines) and the pseudo-orthohexagonal cell  $C_1$  (sextuplely primitive, thick solid lines) are shown. Thick dotted-dashed line: [111] row of the pseudo-rhombohedral cell. Thick dotted line: direction normal to (001). Thin dotted lines: directions normal to (001) passing through the  $C$ -centering nodes on two successive lattice planes of the monoclinic conventional cell.  $\omega_{\perp}$  is the component of the obliquity normal to the (01) plane. Black, gray and white circles represent lattice nodes at  $z = 0, 1/3$  and  $2/3$  respectively ( $z$  is referred to  $c$  axis of the  $C_1$  cell). The stagger of the layer at  $z = 1/3$  is  $-(b+\delta)/3$ . For the ideal case  $\delta = 0$ ,  $\omega_{\perp} = 0$  (modified after Nespolo and Ferraris 2000).



## APPENDIX B.

### COMPUTATION OF THE PID FROM A STACKING SEQUENCE CANDIDATE.

The calculation of the PID function requires the following steps.

**Step 1.** Conversion from RTW symbols into “provisional” OD or Z symbols in the homo-octahedral approximation, by simply looking for  $\Sigma \mathbf{v} = “*”, “0”$  or “-” [i.e.  $\mathbf{c}_n = (0, 0), (1/3, 0)$  or  $(0, 1/3)$ ]. This is straightforwardly obtained by means of a simple addition cycle:

$$\begin{aligned} v_{2j,2j+1} &= v_{2j-2,2j-1} - A_j \\ Z_{2j+1} &= Z_{2j-1} + A_j; Z_{2j} = Z_{2j-1} \end{aligned} \quad (\text{B.1})$$

where  $j = 1 \sim N$ . The initial value is fixed as  $v_{0,1} = 3$  or  $Z_1 = 3$ ; if the resulting  $\mathbf{c}_n$  projection does not take one of the three expected values,  $v_{0,1}$  or  $Z_1$  is incremented and Equation (B.1) is recalculated.

**Step 2.** Derivation of the correct homo-octahedral OD or Z symbol, by analyzing the symmetry properties. For orthogonal and *Class b* polytypes the symbols obtained from Equation (B.1) may correspond to an orientation of the symmetry elements not compatible with the space-group type. In such a case, the sequence of characters must be changed, by making  $v_{0,1}$  or  $Z_1$  taking one of the other values with the same parity. This is equivalent to rotating the structural model around  $c^*$  by  $2n \times 60^\circ$ . The correct sequence is found when the characters in the OD or Z symbols are related by symmetry operators located along the lattice directions compatible with the space-group type requirements (Table 5a,b).

**Step 3.** Expression of the *stacking operators*  $r_j$ , which give the displacement between the  $(j-1)$ -th and the  $j$ -th TS layers, as a function of OD or Z symbols and calculation of TS symbols. The relation of the stacking operators  $r_j$  with OD or Z symbols is straightforward for orthogonal polytypes, whereas for non-orthogonal polytypes the

*Subclass* must be taken into account. OD and Z symbols for non-orthogonal polytypes always correspond to  $(1/3, 0)$  (*Class a*) or  $(0, 1/3)$  (*Class b*). The PID is most conveniently expressed in the  $(3^n a, 3^n b)$   $\mathbf{F}$  axial setting, which corresponds to  $\mathbf{c}_n = (1/3, 0)$  or  $(0, 1/3)$  for *Subclass 1* and  $\mathbf{c}_n = (1/3, 0)$  or  $(0, 1/3)$  for *Subclass 2*. It follows that for orthogonal polytypes and *Subclass 1* polytypes the stacking operators simply coincide with OD or Z symbols ( $r_j = v_{2j-2,2j-1}$  or  $r_j = Z_{2j-1}$ ), whereas for *Subclass 2* polytypes they are related by a 180° rotation around  $c^*$  ( $r_j = v_{2j-2,2j-1} + 3$  or  $r_j = Z_{2j-1} + 3$ ).

**Step 4.** Computation of PID ( $S^N$ ) as a function of the  $(a, b)$  components of TS symbols. The components of the  $j$ -th TS layer referred to the  $(a, b)$  axes are indicated as  $(X_j, Y_j)$ , to distinguish from the components in  $(A_1, A_2)$  axes, which were labeled  $(\Delta X_j, \Delta Y_j)$  (Eqn. (22) and (24)).  $(X_j, Y_j)$  are equal to the sum of the  $(x_{r_j}, y_{r_j})$  components of the stacking operators from the first to  $j$ -th stacking operators. However, because the  $c$  axis of the  $(3^n a, 3^n b)$   $\mathbf{F}$  axial setting is displaced  $-1/3^{(n+1)}$  (where  $n$  is the *Series*) along  $a$  or  $b$  (depending upon the *Class*), the additional displacement  $(-j/3^{(n+1)}, 0)$  (*Class a*) or  $(0, -j/3^{(n+1)})$  (*Class b*) must be added to the  $(X_j, Y_j)$  component of the  $j$ -th TS symbol to express the layer stacking of non-orthogonal polytypes with respect to  $(3^n a, 3^n b)$   $\mathbf{F}$  axial setting. In this way, TS symbols for *Series 0* subfamily A polytypes always have  $X_j = 0$  ( $c$  axis passing through the origin of each layer).

$$\left\{ \begin{array}{l} \text{Orthogonal polytypes: } (X_j, Y_j) = \sum_{i=1}^j (x_{r_i}, y_{r_i}) \\ \text{Class a polytypes: } (X_j, Y_j) = \sum_{i=1}^j (x_{r_i}, y_{r_i}) + \left( \frac{-j}{3^{n+1}}, 0 \right) \\ \text{Class b polytypes: } (X_j, Y_j) = \sum_{i=1}^j (x_{r_i}, y_{r_i}) + \left( 0, \frac{-j}{3^{n+1}} \right) \end{array} \right. \quad (\text{B.2})$$

Finally, in *Class b* the axes exchange  $a \leftrightarrow b$  expresses PID in the  $3^n b$   $\mathbf{F}$  axial setting. The complete TS symbols  $L_j(X_j, Y_j)$  are obtained from Table 5 and Equation (B.2), and the PID function  $S^N$  is:

$$S^N(hkl) = \sum_{j=1}^N S_j^N(hkl) = \sum_{j=1}^N \exp 2\pi i \left( hX_j + kY_j + \hat{l} \frac{j-1}{N} \right) \left[ \hat{l} = l \pmod{N} \right] \quad (\text{B.3})$$

with the normalizing condition:

$$\sum_{j=1}^N \left[ S_j^N(hkl) \right]^2 = N^2 \quad (\text{B.4})$$

### Symmetry of the PID

Nespolo et al (1999d) have analyzed the symmetry of the PID in relation to the kind of polytype present. The results are briefly summarized here: for details, refer to the original paper.

For *Series 0* polytypes there is a well-determined relation between the PID sequences along rows related by  $2n \times 60^\circ$ :

$$S^N(2h, 2k, \hat{l}) = S^N(h, k, N - \hat{l}) \quad (\text{B.5})$$

which, for the reciprocal lattice rows commonly used in the PID analysis, become:

$$S^N(04\hat{l}) = S^N(02, N - \hat{l}); \quad S^N(22\hat{l}) = S^N(11, N - \hat{l}); \quad S^N(\bar{2}2\hat{l}) = S^N(\bar{1}1, N - \hat{l}) \quad (\text{B.6})$$

For all OD polytypes (both subfamilies A and B) of *Series 0*, the PID has also a translational symmetry reminiscent of that relation between pairs of translationally equivalent rows defining a minimal rhombus:

$$S^N(h + 3N, k + 3N, \hat{l}) = S^N(hk\hat{l}). \quad (\text{B.7})$$

For subfamily A of *Series 0* PID values have a trigonal symmetry:

$$S^N(0, 2k, \hat{l}) = S^N\left(\begin{smallmatrix} \pm \\ k \end{smallmatrix} k \hat{l}\right) = S^N\left(\begin{smallmatrix} \pm \\ k \end{smallmatrix} k, N - \hat{l}\right). \quad (\text{B.8})$$

which, for the reciprocal lattice rows commonly used in PID analysis, is expressed as:

$$S^N(02\hat{l}) = S^N(\bar{1}\bar{1}\hat{l}) = S^N(1\bar{1}\hat{l}) = S^N(0\bar{2}, N - \hat{l}) = S^N(11, N - \hat{l}) = S^N(\bar{1}1, N - \hat{l}) \quad (\text{B.9})$$

For *Series* > 0, subfamily A polytypes either are orthogonal or belong to *Class b*; in the latter case the symmetry of the PID must take into account a shift of the origin. *Class b* polytypes have a pseudo-rhombohedral primitive lattice, which thus allows three equivalent orientations, related by  $2n \times 60^\circ$  rotations about  $c^*$ . For monoclinic polytypes, only one of the three orientations leading to  $\mathbf{c}_n = (0, 1/3)$  corresponds to a correct disposition of the symmetry elements (*a*-unique setting for  $a < b$ ). Instead, for triclinic polytypes these three orientations are truly equivalent. Z, OD and TS symbols are different for the three orientations, but they describe three equivalent orientations of the structural model. PID values expressed for a given reciprocal lattice row in a certain orientation of the structural model correspond to a different row in another orientation. For *Series* > 0 the *c* axis of the  $(3^a, 3^b)\mathbf{F}$  setting is displaced by  $1/3^n$  for each layer and the length of the axis displacement is a *submultiple* of the layer stagger: therefore, the origin of the PID is not the same in the three orientations of the structural model. An example is given for the  $3A_1$  polytype in Table 14 of Nespolo et al (1999d). The existence of a similar ambiguity in chlorite was reported by Brindley et al (1950).

### ACKNOWLEDGMENTS

We wish to acknowledge Prof. Giovanni Ferraris (Torino University), Prof. Hiroshi Takeda (Chiba Institute of Technology), Prof. Yoshio Takéuchi (Nihon University, Tokyo), Prof. Takeo Matsumoto (Kanazawa University), Prof. Ichiro Sunagawa (Yamanashi Institute of Gemology and Jewelry Arts), Prof. Boris B. Zvyagin (IGEM – Russian Academy of Sciences, Moscow) and Prof. Theo Hahn (RWTH, Aachen) for several profitable discussions; Prof. Maria Franca Brigatti (Modena University) and Prof. S. Guggenheim (University of Illinois at Chicago) for letting us obtain the tables of their chapter while this manuscript was in preparation. The manuscript was reviewed by Prof. Stefano Merlini (University of Pisa) and Prof. Stephen. Guggenheim (University of Illinois at Chicago), to whom we express our gratitude.

### REFERENCES

- Amelinckx S, Dekeyser W (1953) Le Polytypisme des Minéraux Micacés et Argileux. Première partie: observations et leurs interprétations. C R XIX Congr Geol Int'l, Comité International pour l'Étude des Argiles, Alger, fascicule XVIII, 1-22
- Amisano-Canesi A, Chiari G, Ferraris G, Ivaldi G, Soboleva SV (1994) Muscovite- and phengite-3T: crystal structure and conditions of formation. Eur J Mineral 6:489-496
- Arnold H (1996) Transformations in crystallography. Sect. 5 in International Tables for Crystallography Vol. A, 5<sup>th</sup> edition. Th Hahn (ed) Dordrecht / Boston / London: Kluwer Academic Publishers (in press)
- Backhaus K-O, Āuroviĉ S (1984) Polytypism of micas. I. MDO polytypes and their derivation. Clays Clay Minerals 32:453-463
- Bailey, SW (1975) Cation Ordering and Pseudosymmetry in Layer Silicates. Am Mineral 60:175-187

- Bailey SW (1980a) Classification and Structures of the Micas. *Rev Mineral* 13:1-12
- Bailey SW (1980b) Crystal chemistry of true Micas. *Rev Mineral* 13:13-60
- Bailey SW (1984) Review of cation ordering in micas. *Clays Clay Miner* 32:81-92
- Bailey SW, Frank-Kamenetskii A, Goldsztaub S, Kato A, Pabst A, Schulz H, Taylor HFW, Fleischer M, Wilson AJC (1977) Report of the International Mineralogical Association (IMA) - International Union of Crystallography (IUCr) Joint Committee on Nomenclature. *Acta Crystallogr* A33:681-684
- Baronnet A (1978) Some aspects of polytypism in crystals. *In Progr Crystal Growth Charact Vol. 1*, Pergamon Press, p 151-111
- Baronnet A, Kang ZC (1989) About the origin of mica polytypes. *Phase Trans* 16/17:477-493
- Bassett G (1958) A new technique for decoration of cleavage and slip steps on ionic crystal surface. *Phil Mag* 3:1042-1043
- Baumhauer H. (1900) Über die Kristallform des Muscovit. *Z Kristallogr* 32:164-176
- Baumhauer H (1912) Über die Kristalle des Carborundums. *Z Kristallogr* 50:33-39
- Baumhauer H. (1915) Über die verschiedenen Modifikationen des Carborundums und die Erscheinung der Polytypie. *Z Kristallogr* 55:249-259
- Brandt H (1927) Über eine Verallgemeinerung des Gruppenbegriffes. *Mathematische Annalen* 96:360-366
- Bravais M (1851) Etudes cristallographiques. Troisième partie. Des macles et des hémitropies. *J Ecole Polytechn* XX (XXXIV) 248-276
- Brigatti MF, Guggenheim S (2001) Mica crystal chemistry and influence of intensive variables on atomistic models (this book)
- Brigatti MF, Poppi L (1993) Crystal chemistry of Ba-rich trioctahedral micas-1M. *Eur J Mineral* 5:857-871
- Brigatti MF, Lalonde AE, Medici L (1997) Crystal chemistry of <sup>IV</sup>Fe<sup>3+</sup>-rich phlogopites: A combined single-crystal X-ray and Mössbauer study. *Proc. 11<sup>th</sup> Int. Clay Conf. Ottawa, Canada*, 317-327
- Brindley GW, Oughton BM, Robinson K (1950) Polymorphism of the chlorites. I. Ordered structures. *Acta Crystallogr* 3:408-416
- Brooke HJ, Miller WH (1852) An elementary introduction to mineralogy, by the late William Phillips. London: Longman, Brown, Green, and Longmans, XI+700 p
- Buerger MJ (1945) The genesis of twin crystals. *Am Mineral* 30:469-482
- Buerger MJ (1954) The diffraction symmetry of twins. *Anais de Acad Bras de Ciencias* 26:111-12
- Catti M, Ferraris G (1976) Twinning by merohedry and X-ray crystal structure determination. *Acta Crystallogr* A32:163-165
- Christiansen CC, Makovicky E, Johnsen O (1999) Homology and typism in heterophyllosilicates: An alternative approach. *N Jb Miner Abh*, 175:153-189
- Coxeter HSM (1973) Regular polytopes, 3<sup>rd</sup> edition. Dover Publication Inc. New York
- Coxeter HSM (1989) Introduction to Geometry, 2<sup>nd</sup> edition. John Wiley and Sons New York
- Curien H, Donnay JDH (1959) The Symmetry of the Complete Twin. *Am Mineral* 44:1067-1070
- Curien H, Le Corre Y (1958) Notations des macles à l'aide du symbolisme des groupes de couleurs de Choubnikov. *Bull Soc franç Minér Crist* 81:126-132
- Dekeyser W, Amelinckx S (1953) Le Polytypisme des Minéraux Micacés et Argileux. Deuxième partie: discussion et extension. *Comptes Rendus de la XIX session Congrès Géologique International, Comité International pour l'Étude des Argiles, Alger, fascicule XVIII*
- Des Cloizeaux A (1862) Manuel de Mineralogie, vol. 1. Paris
- Donnay G, Morimoto N, Takeda H, Donnay JDH (1964) Trioctahedral One-Layer Micas. I. Crystal Structure of a Synthetic Iron Mica *Acta Crystallogr* 17:1369-1373
- Dornberger-Schiff K (1959) On the nomenclature of the 80 plane groups in three dimensions. *Acta Crystallogr* 12:173
- Dornberger-Schiff K (1964) Grundzüge einer Theorie von OD-Strukturen aus Schichten. *Abh dtsh Akad Wiss Berlin, Kl f Chem* 3:107 p
- Dornberger-Schiff K (1966) Lehrgang über OD-strukturen. Berlin: Akademie-Verlag 135p
- Dornberger-Schiff K (1979) OD Structures, - a Game and a Bit more. *Kristall und Technik* 14:1027-1045
- Dornberger-Schiff K, Backhaus K-O, Đurovič S (1982) Polytypism of micas: OD-Interpretation, stacking symbols, symmetry relations. *Clays Clay Miner* 30:364-374
- Dornberger-Schiff K, Farkas-Jahnke M (1970) A direct method for the determination of polytype structures. I. Theoretical Basis. *Acta Crystallogr* A26:24-34
- Dornberger-Schiff K, Grell H (1982) Geometrical properties of MDO polytypes and procedures for their derivation. II. OD families containing OD layers of M > 1 kinds and their MDO polytypes. *Acta Crystallogr* A38:491-498
- Đurovič S (1974) Notion of "packets" in the theory of OD structure of M>1 kinds of layer. Examples: Kaolinites and MoS<sub>2</sub>. *Acta Crystallogr* B30:76-78
- Đurovič S (1979) Desymmetrization of OD structures. *Kristall und Technik* 14:1047-1053

- Āuroviĉ S (1981) OD-Charakter, Polytypie und Identifikation von Schichtsilikaten. *Fortschr Mineral* 59:191-226
- Āuroviĉ S (1982) Ordered and disordered polytypes of sheet silicates and their diffraction pattern assuming ideal ditrigonalization of tetrahedral sheets. 9th Conf on Clay Mineralogy and Petrology, Zvolen, 127-134
- Āuroviĉ S (1994) Significance of superposition structures in the polytypism of phyllosilicates. In *Aperiodic '94 Proceedings of the International Conference on Aperiodic Crystals*. G Chapuis, W Paciorek (ed) World Scientific, Singapore / New Jersey / London / Hong Kong, p 595-599
- Āuroviĉ S (1997) Fundamentals of OD theory. In *Modular aspects of minerals / EMU Notes in Mineralogy*, vol. 1. S Merlini (ed) Eötvös University press, Budapest, p 1-28
- Āuroviĉ S (1999) Layer stacking in general polytypic structures. Sect. 9.2.2 in *International Tables for Crystallography, Vol. C* (Ed. ACJ Wilson, E Prince) Dordrecht / Boston / London: Kluwer Academic Publishers, 752-765
- Āuroviĉ S, Dornberger-Schiff K (1979) New fully descriptive polytype symbols for basic polytypes of clay minerals. *Eighth Conference on Clay Mineralogy and Petrology*, Teplice, 19-25
- Āuroviĉ S, Weiss Z (1986) OD structures and polytypes. *Bull Minéral* 109:15-29
- Āuroviĉ S, Weiss Z, Backhaus K-O (1984) Polytypism of micas. II. Classification and abundance of MDO polytypes. *Clays Clay Miner* 32:454-474
- Endo Y (1968) Growth Spirals and Polytypism of Fluor-phlogopite. *J Mineral Soc Jpn* 8, Spec. issue 2:39-41 (in Japanese)
- Engel P, Matsumoto T, Steinmann G, Wondratschek H (1984) The non-characteristic orbits of the space groups. *Z Kristallogr Supplement Issue No. 1*
- Farkas-Jahnke M (1966) Direct method for the determination of polytype structures. *Acta Crystallogr* 21:A173
- Farkas-Jahnke M, Dornberger-Schiff K (1970) A Direct Method for the Determination of Polytype Structures. II. Determination of a 66R Structure. *Acta Crystallogr* A26:35-41
- Ferraris G, Gula A, Ivaldi G, Nespolo M, Sokolova E, Uvarova Yu, Khomyakov AP (2001) First structure determination of an MDO-2O mica polytype associated with a 1M polytype. *Eur J Miner* 13: 1013-1023
- Fichtner K (1965) Zur Existenz von Gruppoiden verschiedener Ordnungsgrade bei OD-Strukturen aus gleichartigen Schichten. *Wiss Z TU Dresden* 14:1-13
- Fichtner K (1977) Zur Symmetriebeschreibung von OD-Kristallstrukturen durch Brandtsche und Ehresmannsche Gruppoide. *Beitr z algebra u Geometrie* 6:71-99
- Fichtner K (1980) On groupoid in crystallography. *MATCH, commun math comput chem* 9:21-40
- Filut MA, Rule AC, Bailey SW (1985) Crystal structure refinement of anandite-2Or, a barium- and sulfur-bearing trioctahedral mica. *Am Mineral* 70:1298-1308
- Frank FC (1951) The growth of carborundum; dislocations and polytypism. *Phil Mag* 42:1014-1021
- Franzini M (1966) Nuovi dati sulla struttura delle miche triottaedriche. *Atti Soc Tosc Sci Nat, Mem Ser A* 73:620-631
- Franzini M (1969) The A and B mica layers and the crystal structure of sheet silicates. *Contrib Mineral Petrol* 21:203-224
- Franzini M, Schiaffino L (1963a) Polimorfismo e leggi di geminazione delle biotiti. *Atti Soc Tosc Sci Nat, Mem Ser A* 70:60-98
- Franzini M, Schiaffino L (1963b) On the crystal structure of biotite. *Z Kristallogr* 119:297-309
- Friedel G (1904) Étude sur les groupements cristallins. Extrait du Bulletin de la Société de l'Industrie minière, Quatrième série, Tomes III e IV. Saint-Étienne, Société de l'Imprimerie Thèolier J. Thomas et C., 485 p
- Friedel G. (1926) *Leçons de Cristallographie*, Berger-Levrault, Nancy, Paris, Strasbourg, 602 p
- Gaubert P (1896) Sur la production artificielle de la macle des spinelles dans les cristaux d'azotate de plomb. *Bull Soc franç Minér* 19:431-434
- Giuseppetti G, Tadini C (1972) The Crystal Structure of 2O brittle mica: Anandite. *Tschermaks Mineral Petrol Mitt* 18:169-184
- Goldschmidt V (1918) *Atlas der Krystallformen*, band IV. Heidelberg: Carl Winters Universitätsbuchhandlung
- Grell H (1984) How to choose OD layers. *Acta Crystallogr* A40:95-99
- Griffen DT (1992) *Silicate Crystal Chemistry*. Oxford University Press, Oxford
- Guggenheim S, Bailey SW (1975) Refinement of the margarite structure in subgroup symmetry. *Am Mineral* 60:1023-1029
- Guggenheim S, Bailey SW (1978) The refinement of the margarite structure in subgroup symmetry: corrections, further refinement and comments. *Am Mineral* 63:186-187
- Guinier A, Bokij GB, Boll-Dornberger K, Cowley JM, Āuroviĉ S, Jagodzinski H, Khrišna P, DeWolff PM, Zvyagin BB, Cox DE, Goodman P, Hahn Th, Kuchitsu K, Abrahams SC (1984) Nomenclature of



- Polytype Structures. Report of the International Union of crystallography Ad-Hoc Committee on the Nomenclature of Disordered, Modulated and Polytype Structures Acta Crystallogr A40:399-404
- Güven N (1971) Structural Factors Controlling Stacking Sequences in Dioctahedral Micas. *Clays Clay Miner* 19:159-165
- Hahn Th, Vos A (2002) Reflection conditions. Sect. 2.13 in *International Tables for Crystallography*, Vol. A 5<sup>th</sup> edition. Th Hahn (ed) Dordrecht / Boston: London: Kluwer Academic Publishers (in press)
- Hahn T, Janovec V, Klapper H (1999) Bicrystals, twins and domain structures – A Comparison. *Ferroelectrics* 222:11-21
- Hendricks SB, Jefferson ME (1939) Polymorphism of the micas with optical measurements. *Am Mineral* 24:729-771
- Iijima S, Buseck PR (1978) Experimental study of disordered mica structure by high-resolution electron microscopy. *Acta Crystallogr* A34:709-719
- International Tables for Crystallography* Vol. A. (2002) 5<sup>th</sup> edition. Th Hahn (ed) Dordrecht / Boston / London: Kluwer Academic Publishers (in Press)
- Ito T (1935) On the symmetry of rhombic pyroxenes. *Z Kristallogr* 90:151-162
- Ito T (1938) Theory of twinned space groups. *J Japan Assoc Mineral Petr Econ Geol* 20:201-210 (in Japanese)
- Ito T (1950) X-ray studies on polymorphism. Maruzen Co., Tokyo, 231 pp
- Ito T, Sadanaga R (1976) On the crystallographic space groupoids. *Proc Jpn Acad* 52:119-121
- Iwasaki H (1972) On the diffraction enhancement of symmetry. *Acta Crystallogr* A28:253-261
- Jackson WW, West J (1931) The crystal structure of muscovite  $KAl_2(AlSi_3)O_{10}(OH)_2$ . *Z Kristallogr* 76:211-227
- Joswig W, Takéuchi Y, Fuess H (1983) Neutron-diffraction study on the orientation of hydroxyl groups in margarite. *Z. Kristallogr* 165:295-303
- Kassner D, Baur WH, Joswig W, Eichhorn K, Wendschuh-Josties M, Kupčik V (1993) A test of the importance of weak reflections in resolving a space-group ambiguity involving the presence or absence of an inversion centre. *Acta Crystallogr* B49:646-654
- Kogure T, Nespolo M (1999a) First occurrence of a disordered stacking sequence including ( $\pm 60^\circ$  180 $^\circ$ ) in Mg-rich annite. *Clays Clay Miner* 48:784-792
- Kogure T, Nespolo M (1999b) A TEM study of long-period mica polytypes: determination of the stacking sequence of oxybiotite by means of atomic-resolution images and Periodic Intensity Distribution (PID) *Acta Crystallogr* B55:507-516
- Kokscharow NV (1875) *Materialen zur Mineralogie Russlands*. Vol. 7. St. Petersburg
- Konishi H, Akai J (1990) HRTEM observation of new complex polytype of biotite from dacites in Higashiyama hills, Niigata, Central Japan. *Clay Science* 8:25-30
- Knurr RA, Bailey SW (1986) Refinement of Mn-substituted muscovite and phlogopite. *Am Mineral* 71:7-16
- Kuwahara Y, Uehara S, Aoki Y (1998) Surface microtopography of lath-shaped hydrothermal illite by tapping-mode<sup>TM</sup> and contact-mode AFM. *Clays Clay Miner* 46:574-582
- Lipson H, Taylor CA (1958) *Fourier Transforms and X-Ray Diffraction*, Bell, London
- Mackovicky E (1997) Modularity – different types and approaches. *In* *Modular aspects of minerals / EMU Notes in Mineralogy*, vol. 1. S Merlino (ed) Eötvös University press, Budapest, p 315-343
- Mallard E (1879) *Traité de Cristallographie geometrique et physique*, Vol. I. Paris: Dunod. 372pp
- Marignac C (1847) *Notices minéralogiques*. Suppl Bibl Universe Genève, arch Sci Phys Nat 6:293-304
- Matsumoto T, Kihara K, Iwasaki H (1974) Conditions for the diffraction enhancement of symmetry of types 1 and 2. *Acta Crystallogr* A30:107-108
- Matsumoto T, Wondratschek H (1979) Possible superlattices of extraordinary orbits in 3-dimensional space. *Z Kristallogr* 150:181-198
- Mauguin MCh (1927) Étude du mica muscovite au moyen des rayons X. *CR Acad Sci Paris* 185:288-291
- Mauguin MCh (1928) Étude de Micas au moyen du rayons X. *Bull Soc franç Minér Crist* 51:285-332
- McLarnan TJ (1981) The number of polytypes in sheet silicates. *Z Kristallogr* 155:247-268
- Merlino S (1990) OD structures in mineralogy. *Per Mineral* 59:69-92
- Mogami K, Nomura K, Miyamoto M, Takeda H, Sadanaga R (1978) On the number of distinct polytypes of mica and SiC with a prime layer-number. *Can Mineral* 16:427-435
- Mügge O (1898) Über Translationen und verwandte Erscheinungen in Krystallen. *N Jb Miner Geol Paläontol* 1:71-158
- Nespolo M (1999) Analysis of family reflections of OD-mica polytypes, and its application to twin identification. *Mineral J* 21:53-85
- Nespolo M (2001) Perturbative theory of mica polytypism. Role of the M2 layer in the formation of inhomogeneous polytypes. *Clays Clay Miner* 49:1-23

- Nespolo M, Ferraris G (2000) Twinning by syngonic and metric merohedry. Analysis, classification and effects on the diffraction pattern. *Z Kristallogr* 215:77-81
- Nespolo M, Kogure T (1998) On the indexing of 3*T* mica polytype. *Z Kristallogr* 213:4-12
- Nespolo M, Kuwahara Y (2001) Apparent polytypism in the Ruiz Peak ferric phlogopite. *Eur J Mineral* 13 (in press)
- Nespolo M, Takeda H (1999) Inhomogeneous mica polytypes: 8-layer polytype of the 2*M*<sub>1</sub> structural series determined by the Periodic Intensity Distribution (PID) analysis of the X-ray diffraction pattern. *Mineral J* 21:103-118
- Nespolo M, Takeda H, Ferraris G (1997a) Crystallography of mica polytypes. In *Modular aspects of minerals / EMU Notes in Mineralogy*, vol. 1. S Merlino (ed) Eötvös University press, Budapest, p 81-118
- Nespolo M, Takeda H, Ferraris G, Kogure T (1997b) Composite twins of 1*M* mica: derivation and Identification. *Mineral J* 19:173-186
- Nespolo M, Takeda H, Ferraris G (1998) Representation of the axial settings of mica polytypes. *Acta Crystallogr A* 54:348-356
- Nespolo M, Ferraris G, Āuroviĉ S (1999a) OD character and twinning – Selective merohedry in class II merohedric twins of OD polytypes. *Z Kristallogr* 214:776-779
- Nespolo M, Ferraris G, Takeda H, Takéuchi Y (1999b) Plesiotwinning: oriented crystal associations based on a large coincidence-site lattice. *Z Kristallogr* 214:378-382
- Nespolo M, Kogure T, Ferraris G (1999c) Allotwinning: oriented crystal association of polytypes – Some warnings on consequences. *Z Kristallogr* 214:1-4
- Nespolo M, Takeda H, Kogure T, Ferraris G (1999d) Periodic Intensity Distribution (PID) of mica polytypes: symbols, structural model orientation and axial settings. *Acta Crystallogr A* 55:659-676
- Nespolo M, Ferraris G, Takeda H (2000a) Twins and allotwins of basic mica polytypes: theoretical derivation and identification in the reciprocal space. *Acta Crystallogr A* 56:132-148
- Nespolo M, Ferraris G, Takeda H (2000b) Identification of two allotwins of mica polytypes in reciprocal space through the minimal rhombus unit. *Acta Crystallogr B* 56:639-647
- Ohta T, Takeda H, Takéuchi Y (1982) Mica polytypism: similarities in the crystal structures of coexisting 1*M* and 2*M*<sub>1</sub> oxybiotite. *Am Mineral* 67:298-310
- Pabst A (1955) Redescription of the single layer structure of the micas. *Am Mineral* 40:967-974
- Pauling L (1930) The structure of micas and related minerals. *Proc Nat Ac Sci* 16:123-129
- Pavese A, Ferraris G, Prencipe M, Ibberson R (1997) Cation site ordering in phengite 3*T* from the Dora-Maira massif (western Alps): a variable-temperature neutron powder diffraction study. *Eur J Mineral* 9:1183-1190
- Pavlishin VI, Semenova TF, Rozhdesvenskaya IV (1981) Protolithionite-3*T*: structure, typomorphism and practical importance. *Mineral Zh* 3:47-60 (in Russian)
- Peacock MA, Ferguson RB (1943) The morphology of muscovite in relation to the crystal lattice. *Univ Toronto, Studies in Mineral* 48:65-82
- Pleasant PA, Baake M, Roth J (1996) Planar coincidences for N-fold symmetry. *J Math Phys* 1029-1058
- Radoslovich EW (1960) The structure of muscovite KAl<sub>2</sub>(Si<sub>3</sub>Al)O<sub>10</sub>(OH)<sub>2</sub>. *Acta Crystallogr* 13:919-932
- Ramsdell LS (1947) Studies on silicon carbide. *Am Mineral* 32:64-82
- Ranganathan S (1966) On the geometry of coincidence-site lattices. *Acta Crystallogr* 21:197-199
- Rieder M (1968) Zinnwaldite: Octahedral ordering in lithium-iron micas. *Science* 160:338-1340
- Rieder M (1970) Lithium-iron micas from the Krušné hory Mountains (Erzgebirge): Twins, epitactic overgrowths and polytypes, *Z Kristallogr* 132:161-184
- Rieder M, Weiss Z (1991) Oblique-texture photographs: more information from powder diffraction. *Z Kristallogr* 197:107-114
- Rieder M, Hybler J, Smrĉok L, Weiss Z (1996) Refinement of the crystal structure of zinnwaldite 2*M*<sub>1</sub>. *Eur J Mineral* 8:1241-1248
- Ross M, Takeda H, Wones DR (1966) Mica polytypes: systematic description and identification. *Science* 151:191-193
- Rieder M, Cavazzini G, D'yakonov YuS, Frank-Kamenetskii VA, Gottardi G, Guggenheim S, Koval' PV, Müller G, Neiva AMR, Radoslovich EW, Robert JL, Sassi FP, Takeda H, Weiss Z, Wones DR (1998) Nomenclature of the micas. *Clays and Clay Miner* 46:586-595
- Royer L (1928) Recherches expérimentales sur l'épitaixie ou orientation mutuelle de cristaux d'espèces différentes. *Bull Soc franç Minér Crist* 51:7-159
- Royer L (1954) De l'épitaixie; quelques remarques sur le problèmes qu'elle soulève. *Bull Soc franç Minér Crist* 77:1004-1028
- Sadanaga R (1978) Complex structures and space groupoids. *Rec Progr Nat Sci Jpn* 3:143-151
- Sadanaga R, Ohsumi K (1979) Basic theorems of vector symmetry in crystallography. *Acta Crystallogr A* 35:115-122

- Sadanaga R, Sawada T, Ohsumi K, Kamiya K (1980) Classification of superstructures by symmetry. *J Jpn Assoc Min Petr Econ Geol, Spec. Issue No. 2*:23-29
- Sadanaga R, Takeda H (1968) Monoclinic diffraction patterns produced by certain triclinic crystals and diffraction enhancement of symmetry. *Acta Crystallogr B24*:144-149
- Sadanaga R, Takeda H (1969) Description of mica polytypes by new unit layers. *J Mineral Soc Japan 9*:177-184 (in Japanese)
- Sadanaga R, Takéuchi Y (1961) Polysynthetic twinning of micas. *Z Kristallogr 116*:406-429
- Sartori F (1977) The crystal structure of a  $2M_1$  lepidolite. *Tschermaks Min Petr Mitt 24*:23-37
- Sartori F, Franzini M, Merlino S (1973) Crystal Structure of a  $2M_2$  Lepidolite. *Acta Crystallogr B29*:573-578
- Schaskolsky M, Schubnikow A (1933) Über die künstliche herstellung gesetzmäßiger kristallverwachsungen des kalialauns. *Z Kristallogr 85*:1-16
- Schläfli L (1950) *Gesammelte mathematische Abhandlungen (Vol. 1)* Birkhäuser, Basel
- Sidorenko OV, Zvyagin BB, Soboleva SV (1975) Crystal structure refinement for  $1M$  dioctahedral mica. *Sov Phys Crystallogr 20*:332-335
- Sidorenko OV, Zvyagin BB, Soboleva SV (1977a) Refinement of the crystal structure of  $2M_1$  paragonite by the high-voltage electron diffraction method. *Sov Phys Crystallogr 22*:554-556
- Sidorenko OV, Zvyagin BB, Soboleva SV (1977b) The crystal structure of  $3T$  paragonite. *Sov Phys Crystallogr 22*:557-560
- Smith JV, Yoder HS (1956) Experimental and theoretical studies of the mica polymorphs, *Mineral Mag 31*:209-235
- Slade PG, Schultz PK, Dean C (1987) Refinement of the Ephesite structure in  $C1$  symmetry. *N Jb Mineral Mh 1987*:275-287
- Smrčok L, Ďurovič S, Petříček V, Weiss Z (1994) Refinement of the crystal structure of cronstedtite- $3T$ . *Clays Clay Miner 42*:544-551
- Smrčok L, Weiss Z (1993) DIFK91: a program for the modelling of powder diffraction patterns on a PC. *J Appl Cryst 26*:140-141
- Smyth JR, Jacobsen SD, Swope RJ, Angel RJ, Arlt T, Domanik K, Holloway JR (2000) Crystal structures and compressibilities of synthetic  $2M_1$  and  $3T$  phengite micas. *Eur J Mineral 12*:955-963
- Sokolova GV, Aleksandrova VA, Drits VA, Bairakov VV (1979) Crystal structures of two brittle Lithia micas. *In Kristallokimiya i Struktura Mineralov. Frank-Kamenetskii VA (ed) Nauka, Moscow, p 55-66 (in Russian)*
- Sorokin ND, Tairov YuM, Tsvetkov VF, Chernov MA (1982a) The laws governing the changes of some properties of different silicon carbide polytypes. *Dokl Akad Nauk SSSR 262*:1380-1383 (in Russian)
- Sorokin ND, Tairov YuM, Tsvetkov VF, Chernov MA (1982b) Crystal-chemical properties of the polytypes of silicon carbide. *Sov Phys Crystallogr 28*:539-542
- Sueno S, Takeda H, Sadanaga R (1971) Two-dimensional regular aggregates of layered crystals. *Mineral J 6*:172-185
- Sunagawa I (1960) Mechanism of crystal growth, etching and twin formation of hematite. *Mineral J 3*:59-89
- Sunagawa I (1964) Growth spirals on phlogopite crystals. *Am Mineral 49*:1427-1434
- Sunagawa I (1977) Natural crystallization. *J Crystal Growth 42*:214-223
- Sunagawa I (1978) Vapour growth and epitaxy of minerals and synthetic crystals. *J Crystal Growth 45*:3-12
- Sunagawa I (1984) Growth of crystal in nature. *In Material Science of the Earth's Interior. I Sunagawa (ed) Terra Publishing Company, Tokyo - D. Reidel Publishing Company, Dordrecht / Boston / Lancaster, p 63-105*
- Sunagawa I, Endo J, Daimon N, Tate I (1968) Nucleation, growth and polytypism of fluor-phlogopite from the vapour phase. *J Crystal Growth 3,4*:751
- Sunagawa I, Koshino Y (1975) Growth Spirals on Kaolin Group Minerals. *Am Mineral 60*:407-412
- Sunagawa I, Koshino Y, Asakura M, Yamamoto T (1975) Growth mechanism of some clay minerals. *Fortschr Miner 52*:217-224
- Sunagawa I, Tomura S (1976) Twinning in phlogopite. *Am Mineral 61*:939-943
- Tairov YuM, Tsvetkov VF (1983) Progress in controlling the growth of polytypic crystals. *In Crystal Growth and Characterization of Polytype Structures. P Krishna (ed) Pergamon Press, Oxford / New York / Toronto / Sydney / Paris / Frankfurt, p 111-162*
- Takano Y, Takano K (1958) Apparent polytypism and Apparent Cleavage of the Micas. *J Mineral Soc Jpn 3*:674-692 (in Japanese)
- Takeda H (1967) Determination of the layer stacking sequence of a new complex mica polytype: A 4-layer Lithium Fluorophlogopite. *Acta Crystallogr 22*:845-853
- Takeda H (1969) Existence of complex mica polytype series based on  $2M_1$  sequence. *Jpn Crystallogr Assoc Autumn Meeting, Iwate, 2-3 (in Japanese)*
- Takeda H (1971) Distribution of mica polytypes among space groups. *Am Mineral 56*:1042-1056

- Takeda H, Donnay JDH (1965) Compound tessellations in crystal structures. *Acta Crystallogr* 19:474-476
- Takeda H, Haga N, Sadanaga R (1971) Structural investigation of polymorphic transition between  $2M_2$ -,  $1M$ -Lepidolite and  $2M_1$  Muscovite. *Mineral J* 6:203-215
- Takeda H, Ross M (1975) Mica polytypism: dissimilarities in the crystal structures of coexisting  $1M$  and  $2M_1$  biotite. *Am Mineral* 60:1030-1040
- Takeda H, Ross M (1995) Mica polytypism: identification and origin. *Am Mineral* 80:715-724
- Takeda H, Sadanaga R (1969) New unit layers for micas. *Mineral J* 5:434-449
- Takéuchi Y (1965) Structures of brittle micas. Proc. 13<sup>th</sup> Natl. Conf. Madison, Wisconsin, 1964, Clays Clay minerals. Pergamon Press, 1-25
- Takéuchi Y. (1971) Polymorphic or polytypic changes in biotites, pyroxenes, and wollastonites. *J Mineral Soc Jpn* 10:Spec. Issue No. 2:87-99 (in Japanese)
- Takéuchi Y, Haga N (1971) Structural Transformation of Trioctahedral Sheet Silicates. Slip mechanism of octahedral sheets and polytypic changes of micas. *Mineral Soc Japan Spec Pap* 1:74-87 (Proc. IMA-IAGOD Meetings '70, IMA Vol.)
- Takéuchi Y, Sadanaga R (1966) Structural studies of brittle micas. I. The structure of xantophyllite refined. *Mineral J* 4:424-437
- Takéuchi Y, Sadanaga R, Aikawa N (1972) Common lattices and image sets of hexagonal lattices, and their application to composite electron-diffraction patterns of biotite. *Z Kristallogr* 136:207-225
- Thompson JB Jr (1981) Polytypism in complex crystals: contrast between mica and classical polytypes. *In* Structure and Bonding vol. II. M O'Keefe, A Navrotsky (ed), Academic Press, San Diego / London / Burlington, p 167-196
- Tokonami M (1966) The structure determination of the 96R polytype of SiC by a direct method. *Mineral J* 4:401-423
- Tokonami M, Hosoya S (1965) A systematic method for unravelling a periodic vector set. *Acta Crystallogr* 18:908-916
- Tolansky S, Morris PG (1947a) An interferometric survey of the mica. *Mineral Mag* 28:137-145
- Tolansky S, Morris PG (1947b) An interferometric examination of synthetic mica. *Mineral Mag* 28:146-150
- Tomura S, Kitamura M, Sunagawa I (1979) Surface microtopography of metamorphic white micas. *Phys Chem Miner* 5:65-81
- Tschermak G (1878) Die Glimmergruppe (I. Theil) *Z Kristallogr* 2:14-50
- Tsvetkov V F (1982) Problems and prospects of growing large silicon carbide crystals. *Izv Leningr Elektrotekh Inst* 302:14-19 (in Russian)
- Udagawa S, Urabe K, Hasu H (1974) The crystal structure of muscovite dehydroxylate. *J Japan Assoc Mineral Petr Econ Geol* 58:381-389 (in Japanese, with English Abstract)
- Ungemach H (1935) Sur la Syntaxie et la Polytypie. *Z Kristallogr* 91:1-22
- Verma AR (1953) *Crystal Growth and Dislocations*. London: Butterworths, 182p
- Weiss Z, Đurovič S (1980) OD interpretation of Mg-vermiculite. Symbolism and X-ray identification of its polytypes. *Acta Crystallogr* A36:633-640
- Weiss Z, Đurovič S (1989) A united classification and X-ray identification of phyllosilicate polytypes. Collected abstracts, 9th International Clay Conference, Strasbourg (France), p. 430
- Weiss Z, Wiewióra A (1986) Polytypism of micas. III. X-ray Diffraction Identification. *Clays Clay Minerals* 34:53-68
- Wondratschek H (1976) Extraordinary orbits of space groups. Theoretical considerations. *Z Kristallogr* 143:460-470
- Wondratschek H (2002) Introduction to space-groups. Sect. 8 in international Tables for Crystallography, Vol. A, 5th edition. The Hahn (ed) Dordrecht / Boston: London: Kluwer Academic Publishers (in press)
- Zhukhlistov AP, Zvyagin BB, Shuriga TN (1983) Electron-diffraction investigation of the crystal structure of di-trioctahedral Li,Fe-phengite  $1M$ . *Sov Phys Crystallogr* 28:518-521
- Zhukhlistov AP, Zvyagin BB, Pavlishin VI (1990) Polytypic 4M modification of Ti-biotite with nonuniform alternation of layers, and its appearance in electron-diffraction patterns from textures. *Sov Phys Crystallogr* 35:232-236
- Zussman J (1979) The crystal chemistry of micas. *Bull Mineral* 102:5-13
- Zvyagin BB (1962) A theory of polymorphism of micas. *Sov Phys Crystallogr* 6:571-580
- Zvyagin BB (1967) Electron diffraction analysis of clay mineral structures. New York: Plenum Press, 364 p
- Zvyagin BB (1985) Polytypism in contemporary crystallography. *Sov Phys Crystallogr* 32:394-399
- Zvyagin BB (1988) Polytypism of crystal structures. *Comput Math Applic* 16:569-591
- Zvyagin BB (1993) A contribution to polytype systematics. *Phase Trans* 43:21-25
- Zvyagin BB (1997) Modular analysis of crystal structures. *In* Modular aspects of minerals / EMU Notes in Mineralogy, vol. 1. S Merlino (ed) Eötvös University press, Budapest, p 345-372
- Zvyagin BB, Drits VA (1996) Interrelated features of structure and stacking of kaolin mineral layers *Clays Clay Miner* 44:297-303

- Zvyagin BB, Gorshkov AI (1966) Effects of secondary diffraction in selected area patterns of mineral crystals superimposed with a relative rotation around the primary beam. Sixth Internat. Congress for Electron Microscopy, Kyoto. *In* Electron Microscopy 1966 Vol. I. R Uyeda (ed) Maruzen, Tokyo, p 603-604
- Zvyagin BB, Vrublevskaya ZV, Zhukhlistov AP, Sidorenko OV, Soboleva SV, Fedotov AF (1979) High-voltage electron diffraction in the study of layered minerals. Moscow: Nauka Press, 224 pp. (in Russian)